MECHANISMS OF SALT TOLERANCE IN THE HALOPHYTE SEASHORE PASPALUM

by

JOHN JAMES SPIEKERMAN

(Under the Direction of Katrien M. Devos)

ABSTRACT

In the coming decades, crop production will need to increase to meet the demands of a burgeoning population. Moreover, climate change-induced drought is predicted to increase irrigation, and in turn, soil salinity. About 20% of irrigated land worldwide is considered saline without any efficient means of removing salt from the soil. Saline soils significantly inhibit plant growth, and thus salt tolerant crops are needed to continue food production in the future. Most salt tolerance research has focused on salt-sensitive glycophytes, including most crop species we rely on. Research on tolerance mechanisms in halophytes, plant species that thrive in salt, is currently limited. We have chosen seashore paspalum (*Paspalum vaginatum*), a halophytic grass closely related to agronomically vital crops in the *Panicoideae*, to better under mechanisms of salt tolerance in halophytes. Seashore paspalum is used as a popular turfgrass due to its ability to be irrigated with brackish water, stemming from its high salt tolerance. Though it has been intensely studied, it has only been done so as a turf. We have grown seashore paspalum in a novel way, without trimming plants, to gain a more accurate understanding of how it copes with elevated salinity. This has been done in comparison with *P. distichum*, a glycophytic sister species that inhabits mostly freshwater habitats. We show that *Paspalum* is tolerant of salt shock

conditions and show that genotypes that are slow-growing under low salt lose less relative biomass under high salt. Furthermore, we provide evidence for a novel mechanism of sodium sequestration in seashore paspalum, whereby sodium is sequestered in leaf papillae, the first known specialized organ for sodium sequestration in the *Panicoideae*. An RNA-seq analysis further illustrates differences between seashore paspalum accession 'HI10' and *P. distichum* accession 'Spence', with 'HI10' being poised to respond to salt stress, while many mechanisms are salt induced in 'Spence'. Collectively, our results lay the groundwork for investigating seashore paspalum as a model halophytic system.

INDEX WORDS: Salt tolerance, Soil salinity, Crop production, Seashore paspalum, Halophyte, Glycophyte, Turfgrass, Sodium sequestration, Salt glands

MECHANISMS OF SALT TOLERANCE IN THE HALOPHYTE SEASHORE PASPALUM

by

JOHN JAMES SPIEKERMAN

B.S. Integrative Biology, University of Illinois at Urbana-Champaign, 2012

A Dissertation Submitted to the Graduate Faculty of The University of Georgia in Partial Fulfillment of the Requirements for the Degree

DOCTOR OF PHILOSOPHY

ATHENS, GEORGIA

2019

MECHANISMS OF SALT TOLERANCE IN THE HALOPHYTE SEASHORE PASPALUM

by

JOHN JAMES SPIEKERMAN

Major Professor:	Katrien Devos
Committee:	Wolfgang Lukowitz
	Chung-Jui Tsai
	Wayne Parrott
	Paul Raymer

Electronic Version Approved:

Suzanne Barbour
Dean of the Graduate School
The University of Georgia
May 2019

Prologue

“Food is the moral right of all who are born into this world”

-Norman Borlaug

“The universe is under no obligation to make sense to you”

-Neil deGrasse Tyson

ACKNOWLEDGEMENTS

I would like to thank my advisor, Dr. Katrien Devos, for her faith and creative freedom granted to me throughout the years. Her support has helped these projects flourish, and I am honored to continue working with her in the coming years. I would also like to thank my family and friends, for whom I have eternal gratitude for their wholehearted love throughout my life and my graduate school career. Acquiring my PhD, or surmounting any other hurdle in life, would quite literally have been impossible without them.

TABLE OF CONTENTS

LIST OF TABLES

Page

LIST OF FIGURES

Page

CHAPTER I

INTRODUCTION AND LITERATURE REVIEW

Salinity: a growing issue

Soil salinity can be caused by natural geological processes such as mineral weathering (primary salinity) as well as human activities (secondary salinity) [1]. One of the main culprits of secondary salinity is irrigation. Persistent irrigation leads to an increase in soil salinity due to dissolved minerals and ions in irrigation mixtures [1], as well as minerals reaching the upper layers of the soil due to a rising of the water table [2]. At present, 70% of withdrawn freshwater worldwide is used for crop irrigation, and this number increases in some developing countries to over 90% [3]. In addition to fertilizer use, increased irrigation is responsible for the large increases in food production seen in past decades, with irrigated agriculture producing over 40% of food worldwide on only 20% of cultivated land [4]. However, the world population has doubled since the 1960s to over 7.5 billion people, and is predicted to reach 9.8 billion by 2050, thus illustrating a dire need to improve food production [4]. In the developed world, 90% of the required increase in crop production will likely be attained by increasing yields and cropping intensity. In the developing world, arable land will need to expand by some 120 million ha [5] which will require bringing lands that suffer from a number of constraints including drought and salinity into cultivation. Unpredictable rainfall patterns caused by climate change will lead to a further increase of irrigation practices, and hence soil salinity [6]. Consequently, the need to produce salt tolerant crops to withstand elevated soil salinity will be vital in the coming decades.

Salt tolerance mechanisms in plants

Sodium chloride (NaCl) is the most widespread, soluble salt on earth and it is highly detrimental to crop production [1]. Soil salinity inhibits several vital growth processes in plants including water uptake, ion homeostasis, turgor maintenance, and photosynthesis [7]. Sodium toxicity also occurs once Na^+ reaches intracellular compartments where it disrupts enzymatic activity in addition to elevating harmful reactive oxygen species (ROS) [8]. Due to the prevalence of NaCl in soils worldwide, plants have evolved a wide assortment of coping mechanisms to survive and sometimes even thrive under salt conditions.

Salt stress occurs in two distinct phases: the osmotic phase and the ionic phase [1]. The osmotic phase is the initial phase that plants experience when inundated with high salt concentrations, and mostly prevents water absorption due to the rapid onset of high external osmotic pressure, which also activates stomatal closure [9, 10]. The osmotic phase thus inhibits plant growth quite quickly and tolerance is accomplished through mechanisms such as limiting stomatal closure and quickly producing osmolytes to balance the osmotic gradient across membranes. Plants also initiate mechanisms to exclude sodium at the root level during this phase. Genetic pathways including the Salt Overly Sensitive (SOS) pathway are initiated to signal downstream factors involved with sodium exclusion and sequestration [11, 12]. The second phase of salt stress, the ionic phase, occurs when sodium reaches high intracellular concentrations and disrupts enzymatic function, which leads to increased leaf senescence [1]. To combat intracellular sodium, plants have evolved mechanisms of sodium sequestration in vacuoles utilizing genes such as NHX sodium antiporters in addition to specialized structures explained in detail below [13, 14].

Salt sensitive and tolerant plants are split between glycophytes (sensitive) and halophytes (tolerant), with halophytes having the ability to complete their life cycle in 200 mM salt conditions [15, 16]. Halophytes use many of the same salt tolerance mechanisms that glycophytes use, including sodium exclusion, sequestration, excretion, and even producing the same osmolytes at higher concentrations [17, 18]. Halophytes also utilize specialized structures not active in glycophytes to sequester and/or secrete sodium including salt glands and bladders [17]. Though halophytes clearly excel at coping with high salt concentrations, the vast majority of research has focused on salt sensitive glycophytes [2].

The Poales order of grasses contains around 8% of all known halophytic plant species, and thus represents an excellent group for studying salt tolerance [19]. Halophytic grass species are highly efficient at excluding sodium from internal tissue [16]. Indeed, several transporters have been identified in halophytic grasses that are thought to enhance sodium exclusion through being highly selective for potassium [20, 21]. Osmolyte production is another mechanism typically found in halophytic grasses, with proline and glycine betaine being the most common for maintaining osmotic balance under salt stress [22, 23]. Salt tolerant grasses have also been shown to produce inositols, such as pinitol in the wild rice species *Porteresia coarctata* [24] and myo-inositol in *Spartina alterniflora* [25]. Their biosynthesis was highly beneficial to *Arabidopsis* under salt stress when overproduced using the myo-inositol biosynthetic enzyme myo-inositol 1-phosphate synthase (*SaINO1*) from S. *alterniflora* [26]. ROS production, stemming from an increased rate of photorespiration under salt stress, is detrimental due to oxidative damage caused to DNA and other cellular components [27], and thus halophytic grasses have evolved ROS detoxification enzymes that are rapidly salt induced. The grasses *Aeluropus lagopoides* and *Panicum antidotale* use the superoxide dismutase (SOD) gene to help

detoxify ROS accumulating in tissue [28, 29]. Overexpression of the transcription factor *ZjZFN1*, thought to be involved with ROS detoxification, from the halophyte *Zoysia japonica* was also shown to increase salt tolerance in *Arabidopsis* [30].

Arguably the most fascinating salt tolerance mechanism found in halophytic grasses is sequestration and secretion of salt using glands as observed in the *Chloridoideae* and *Oryzoideae* grass subfamilies [19, 31]. Salt glands in the *Poaceae* can be unicellular or bicellular, though unicellular glands have only been found in *P. coarctata*, a halophytic rice relative [19, 32]. Interestingly, microhairs similar in structure to the unicellular glands found in *P. coarctata* are found in every grass subfamily except for the *Pooideae* [19, 33], and thus it is possible that unicellular structures found in other grass species may perform similar salt-sequestering/secreting function. Despite structural differences, salt glands in the *Poaceae* accomplish the same task of sodium sequestration and/or secretion as the complex, multicellular salt glands present in dicots [31]. Though much research, including cell type-specific transcriptomic analysis, has been conducted on salt-sequestering structures in dicots like *Limonium bicolor*[34], *Chenopodium quinoa* [35, 36], *Gossypium hirsutum* [37], and *Mesembryanthemum crystallinum* [38], not nearly as much is known about salt sequestering/secreting structures in grasses. Salt gland structure and function have been studied in halophytic grasses like *Spartina alterniflora* [39], *A. lagopoides* [20], and the turfgrasses *Zoysia* [40] and *Sporobolus virginicus* [41], but currently no genetic information on their production nor sequestering/secreting mechanisms exist.

Studying salt tolerance in halophytic grasses has provided beneficial insight into how grasses cope with high salinity. However, more work is required to better understand these mechanisms in species more closely related to cereals in the grass subfamily *Panicoideae*. The

Panicoid grasses include many cereal crops that collectively provide a large proportion of worldwide caloric intake, and thus represents an economically crucial group in which to further examine mechanisms of salt tolerance.

Seashore paspalum: a model halophytic grass species

We have chosen seashore paspalum, a halophytic grass utilized worldwide as a turfgrass due to its high salt tolerance [42], as our study system. Additionally, we have also chosen *P. distichum*, a salt sensitive sister species that inhabits mostly freshwater habitats and differs from seashore paspalum in growth vigor, leaf morphology, and glume pubescence [43], for comparative analyses. Seashore paspalum is native to saline marshes and mudflats, sandy coastal habitats, and intertidal areas in tropical/subtropical geographic regions, and is thus highly salt tolerant [44, 45]. It is a diploid, Panicoid grass that has gained traction as a sustainable turfgrass due to an ability to water it with brackish or reclaimed water. Furthermore, seashore paspalum is closely related to agronomically vital crops including maize and sorghum [44]. It been highly studied for turf quality characteristics, including tolerance to wear [46, 47], low light [48, 49], low temperature [50], drought [51-53], and herbicide resistance [54, 55]. A large body of research in seashore paspalum has also focused on salt tolerance due to its ability to grow in salt concentrations near that of seawater [56].

A comparison of salt tolerance within seashore paspalum and relative to other turfgrasses has indicated that there is high variation in salt tolerance between genotypes [57]. Organic osmolytes including proline and glycine betaine have been shown to increase under salt stress, indicating their role in osmotic adjustment [58, 59]. Compared with other turfgrasses, seashore paspalum also exhibits highly selective potassium uptake, even under high salt stress [60]. The

same study also illustrates seashore paspalum's ability to exclude sodium from leaf tissue while maintaining high leaf potassium levels. It has also been shown to have high SOD enzymatic activity, indicating tolerance to ROS accumulation, relative to bermudagrass[61]. Furthermore, seashore paspalum maintains high photosynthetic levels under salt stress [62] and has been shown to enhance growth as a turf under low salt stress [63], with some genotypes showing higher density and canopy cover in salt conditions [62]. However, the mechanisms behind this halophytic growth enhancement are unknown. Despite the large body of salt tolerance research treating seashore paspalum as a closely trimmed turf, some work suggests that salt tolerance can be improved by increasing the mowing height [64].

There is currently little genetic information available regarding seashore paspalum's high tolerance to salt. Genes from seashore paspalum have been assessed for their ability to confer salt tolerance in a salt sensitive yeast strain using a yeast cDNA expression library [65]. A total of 18 salt-tolerance genes were identified, which were associated with photosynthetic metabolism, antioxidant detoxification, protein modification, iron transport, vesicle traffic, and phospholipid biosynthesis. A transcriptome study identified and further tested two genes, a metallothionein (*PvMET1*) and a UDP-galactose (glucose)-4-epimerase (*PvUGE1*), that were salt-induced in seashore paspalum[66]. When *PvMET1* was transformed into rice, and then backcrossed into a salt-sensitive background, it increased survivability of the *PvMET1*-containing line under salt stress relative to the sensitive parent (Koshihikari). A proteomic analysis yielded several interesting salt-induced proteins including a peroxidase, a cytoplasmic malate dehydrogenase, and an abscorbate peroxidase [67].

Genetic diversity within *Paspalum vaginatum* was recently assessed in the Devos lab [43]. This study also included species belonging to *Paspalum distichum*, a close relative of

seashore paspalum. The germplasm analyzed formed three distinct subpopulations [43]. Two subpopulations consisted of *P. vaginatum* accessions with fine-textured leaves, while the third subpopulation consisted of a mix of *P. vaginatum* and *P. distichum* accessions. Interestingly, while *P. distichum* is typically polyploid, this study identified two diploid accessions, 'Spence' and 'Tropic shore'. To date, only a single transcriptomic dataset is available for seashore paspalum, though the aim of that study was to conduct transcript annotation and was not focused on stress tolerance [68]. Generation of a high-quality genome sequence for seashore paspalum is nearing completion (J. Schnable and J. Schmutz, pers. comm.). Genetic mapping and QTL analyses for salt tolerance are in progress in the Devos lab. Excluding the studies mentioned, not much genetic information associated with salt tolerance exists for seashore paspalum nor for any other species in the *Paspalum* genus.

Despite their close taxonomic relationship, diploid seashore paspalum and *P. distichum* have never been directly compared for their innate level of salt tolerance using untrimmed growth and physiological measurements as well as modern genetic tools such as RNA-Seq. Consequently, studying the physiology and genetics of seashore paspalum in conjunction with *P. distichum* is a beneficial approach to better understand its salt tolerance mechanisms.

Overarching goals

The principal goals of my dissertation research were to identify the physiological and genetic mechanisms by which seashore paspalum grows in high salt conditions. Assessing seashore paspalum's salt tolerance using node-grown ramets, without trimming as a turf, may represent a more accurate means of examining tolerance mechanisms without exposing plants to additional stresses imposed by the recurrent trimming applied to mimic growth as a lawn turf. To

accomplish this task, we have assessed salt tolerance of seashore paspalum and *P. distichum* accessions in Chapter II, where we show that they differ in their growth response under a wide variety of salt concentrations. To investigate seashore paspalum's ability to enhance growth despite accumulating high sodium concentrations, we conducted an in-depth anatomical analysis of leaf tissue in seashore paspalum accession 'HI10' and *P. distichum* accession 'Spence' in Chapter III. Here, we show that 'HI10' and 'Spence' exhibit distinct morphological features on the leaf surface and demonstrate that the adaxial leaf papillae sequester sodium under salt stress. These results provide evidence for the first known specialized salt sequestration structures in the agronomically relevant *Panicoideae* subfamily. To further understand phenotypic differences in growth between 'HI10' and 'Spence' under salt stress, we conducted an RNA-seq experiment using ramets grown in 0 dS/m, 10 dS/m, and 30 dS/m salt, which is presented in Chapter IV. We show that in contrast to 'Spence', 'HI10' seems poised to respond to salt stress by constitutively activating many salt response mechanisms. Together, our results provide the groundwork for studying seashore paspalum as a model halophytic system and illustrate novel mechanisms of salt tolerance in *Paspalum*.

References

1. Munns, R. and M. Tester, *Mechanisms of salinity tolerance*, in *Annual Review of Plant Biology*. 2008, Annual Reviews: Palo Alto. p. 651-681.
2. Munns, R. and M. Gilliham, *Salinity tolerance of crops - what is the cost?* New Phytologist, 2015. **208**(3): p. 668-673.
3. Howell, T.A., *Enhancing water use efficiency in irrigated agriculture.* Agronomy Journal, 2001. **93**(2): p. 281-289.
4. FAO, *World Food and Agriculture Statistical Pocketbook.* 2018.
5. FAO, *High Level Expert Forum - How to Feed the World in 2050: Global agriculture towards 2050.* 2009.
6. Taylor, R.G., et al., *Ground water and climate change.* Nature Climate Change, 2013. **3**(4): p. 322-329.
7. Almeida, D.M., M.M. Oliveira, and N.J.M. Saibo, *Regulation of Na+ and K+ homeostasis in plants: towards improved salt stress tolerance in crop plants.* Genetics and Molecular Biology, 2017. **40**(1): p. 326-345.
8. Flowers, T.J., R. Munns, and T.D. Colmer, *Sodium chloride toxicity and the cellular basis of salt tolerance in halophytes.* Annals of Botany, 2015. **115**(3): p. 419-431.
9. Shavrukov, Y., *Salt stress or salt shock: which genes are we studying?* J Exp Bot, 2012. **64**(1): p. 119-27.
10. Julkowska, M.M. and C. Testerink, *Tuning plant signaling and growth to survive salt.* Trends in Plant Science, 2015. **20**(9): p. 586-594.

11. Shi, H.Z., et al., *The Arabidopsis thaliana salt tolerance gene SOS1 encodes a putative Na+/H+ antiporter.* Proceedings of the National Academy of Sciences of the United States of America, 2000. **97**(12): p. 6896-6901.

12. Qiu, Q.S., et al., *Regulation of SOS1, a plasma membrane Na+/H+ exchanger in Arabidopsis thaliana, by SOS2 and SOS3.* Proceedings of the National Academy of Sciences of the United States of America, 2002. **99**(12): p. 8436-8441.

13. Wu, H.H., *Plant salt tolerance and Na+ sensing and transport.* Crop Journal, 2018. **6**(3): p. 215-225.

14. Barragan, V., et al., *Ion exchangers NHX1 and NHX2 mediate active potassium uptake into vacuoles to regulate cell turgor and stomatal function in Arabidopsis.* Plant Cell, 2012. **24**(3): p. 1127-1142.

15. Rajalakshmi, S. and A. Parida, *Halophytes as a source of genes for abiotic stress tolerance.* Journal of Plant Biochemistry and Biotechnology, 2012. **21**(1): p. S63-S67.

16. Roy, S. and U. Chakraborty, *Salt tolerance mechanisms in Salt Tolerant Grasses (STGs) and their prospects in cereal crop improvement.* Botanical Studies, 2014. **55**: p. 9.

17. Flowers, T.J. and T.D. Colmer, *Salinity tolerance in halophytes.* New Phytologist, 2008. **179**(4): p. 945-963.

18. Grieve, C.M. and E.V. Maas, *BETAINE ACCUMULATION IN SALT-STRESSED SORGHUM.* Physiologia Plantarum, 1984. **61**(2): p. 167-171.

19. Ceccoli, G., et al., *Salt Glands in the Poaceae Family and Their Relationship to Salinity Tolerance.* Botanical Review, 2015. **81**(2): p. 162-178.

20. Sanadhya, P., P. Agarwal, and P.K. Agarwal, *Ion homeostasis in a salt-secreting halophytic grass.* Aob Plants, 2015. **7**: p. 15.

21. Shao, Q., et al., *SsHKT1;1 is a potassium transporter of the C-3 halophyte Suaeda salsa that is involved in salt tolerance.* Functional Plant Biology, 2014. **41**(8): p. 790-802.

22. Marcum, K.B., *Salinity tolerance mechanisms of grasses in the subfamily Chloridoideae.* Crop Science, 1999. **39**(4): p. 1153-1160.

23. Slama, I., et al., *Diversity, distribution and roles of osmoprotective compounds accumulated in halophytes under abiotic stress.* Annals of Botany, 2015. **115**(3): p. 433-447.

24. Sengupta, S., et al., *Inositol methyl tranferase from a halophytic wild rice, Porteresia coarctata Roxb. (Tateoka): regulation of pinitol synthesis under abiotic stress.* Plant Cell and Environment, 2008. **31**(10): p. 1442-1459.

25. Baisakh, N., P.K. Subudhi, and P. Varadwaj, *Primary responses to salt stress in a halophyte, smooth cordgrass (Spartina alterniflora Loisel.).* Functional & Integrative Genomics, 2008. **8**(3): p. 287-300.

26. Joshi, R., M.V. Ramanarao, and N. Baisakh, *Arabidopsis plants constitutively overexpressing a myo-inositol 1-phosphate synthase gene (SaINO1) from the halophyte smooth cordgrass exhibits enhanced level of tolerance to salt stress.* Plant Physiology and Biochemistry, 2013. **65**: p. 61-66.

27. Miller G, S.N., Ciftci-Yilmaz S, Mittler R., *Reactive oxygen species homeostasis and signalling during drought and salinity stresses.* Plant Cell Environ, 2010. **33**(4): p. 453-467.

28. Sobhanian, H., et al., *Salt Stress Responses of a Halophytic Grass Aeluropus lagopoides and Subsequent Recovery.* Russian Journal of Plant Physiology, 2010. **57**(6): p. 784-791.

29. Hussain, T., et al., *Eco-physiological adaptations of Panicum antidotale to hyperosmotic salinity: Water and ion relations and anti-oxidant feedback.* Flora, 2015. **212**: p. 30-37.

30. Teng, K., et al., *Heterologous Expression of a Novel Zoysia japonica C2H2 Zinc Finger Gene, ZjZFN1, Improved Salt Tolerance in Arabidopsis.* Frontiers in Plant Science, 2018. **9**: p. 13.

31. Dassanayake, M. and J.C. Larkin, *Making Plants Break a Sweat: the Structure, Function, and Evolution of Plant Salt Glands.* Front Plant Sci, 2017. **8**: p. 406.

32. Flowers, T.J., et al., *SALT TOLERANCE IN THE HALOPHYTIC WILD RICE, PORTERESIA-COARCTATA TATEOKA.* New Phytologist, 1990. **114**(4): p. 675-684.

33. Liphschitz N., W.Y., *Adaptation of plants to saline environments: salt excretion and glandular structure. In: Sen D.N., Rajpurohit K.S. (eds) Contributions to the ecology of halophytes. Tasks for vegetation science.* Springer, Dordrecht, 1982. **2**.

34. Yuan, F., et al., *Comparative transcriptome analysis of developmental stages of the Limonium bicolor leaf generates insights into salt gland differentiation.* Plant Cell and Environment, 2015. **38**(8): p. 1637-1657.

35. Bohm, J., et al., *Understanding the Molecular Basis of Salt Sequestration in Epidermal Bladder Cells of Chenopodium quinoa.* Current Biology, 2018. **28**(19): p. 3075-+.

36. Kiani-Pouya, A., et al., *Epidermal bladder cells confer salinity stress tolerance in the halophyte quinoa and Atriplex species.* Plant Cell and Environment, 2017. **40**(9): p. 1900-1915.

37. Peng, Z., et al., *Na+ compartmentalization related to salinity stress tolerance in upland cotton (Gossypium hirsutum) seedlings.* Scientific Reports, 2016. **6**: p. 14.

38. Oh, D.H., et al., *Cell type-specific responses to salinity - the epidermal bladder cell transcriptome of Mesembryanthemum crystallinum.* New Phytologist, 2015. **207**(3): p. 627-644.

39. Bradley, P.M. and J.T. Morris, *RELATIVE IMPORTANCE OF ION EXCLUSION, SECRETION AND ACCUMULATION IN SPARTINA-ALTERNIFLORA LOISEL.* Journal of Experimental Botany, 1991. **42**(245): p. 1525-1532.

40. Marcum, K.B., S.J. Anderson, and M.C. Engelke, *Salt gland ion secretion: A salinity tolerance mechanism among five zoysiagrass species.* Crop Science, 1998. **38**(3): p. 806-810.

41. Naidoo, Y. and G. Naidoo, *Sporobolus virginicus leaf salt glands: morphology and ultrastructure.* South African Journal of Botany, 1998. **64**(3): p. 198-204.

42. Lee, G.J., R.N. Carrow, and R.R. Duncan, *Criteria for assessing salinity tolerance of the halophytic turfgrass seashore paspalum.* Crop Science, 2005. **45**(1): p. 251-258.

43. Eudy D, B.B., Harrison ML, Raymer P, Devos KM *Ploidy level and genetic diversity in the genus Paspalum, group Disticha.* Crop Science 2017. **57**: p. 3319-3332.

44. Lonard, R.I., F.W. Judd, and R. Stalter, *Biological Flora of Coastal Dunes and Wetlands: Paspalum vaginatum Sw.* Journal of Coastal Research, 2015. **31**(1): p. 213-223.

45. Maitland, T.D., *The grassland vegetation of the Cameroons Mountain.* Bulletin of Miscellaneous Information (Royal Gardens, Kew), 1932. **9**: p. 417-425.

46. Trenholm, L.E., R.N. Carrow, and R.R. Duncan, *Mechanisms of wear tolerance in seashore paspalum and bermudagrass.* Crop Science, 2000. **40**(5): p. 1350-1357.

47. Trenholm, L.E., R.R. Duncan, and R.N. Carrow, *Wear tolerance, shoot performance, and spectral reflectance of seashore paspalum and bermudagrass.* Crop Science, 1999. **39**(4): p. 1147-1152.

48. Jiang, Y.W., R.R. Duncan, and R.N. Carrow, *Assessment of low light tolerance of seashore paspalum and bermudagrass.* Crop Science, 2003. **44**(2): p. 587-594.

49. Jiang, Y.W., R.N. Carrow, and R.R. Duncan, *Physiological acclimation of seashore paspalum and bermudagrass to low light.* Scientia Horticulturae, 2005. **105**(1): p. 101-115.

50. Cyril, J., et al., *Changes in membrane polar lipid fatty acids of seashore paspalum in response to low temperature exposure.* Crop Science, 2002. **42**(6): p. 2031-2037.

51. Banuelos, J.B., et al., *Deficit Irrigation of Seashore Paspalum and Bermudagrass.* Agronomy Journal, 2011. **103**(6): p. 1567-1577.

52. Shahba, M.A., M.S. Abbas, and S.F. Alshammary, *Drought Resistance Strategies of Seashore Paspalum Cultivars at Different Mowing Heights.* Hortscience, 2014. **49**(2): p. 221-229.

53. Johnson, G.L., T.R. Sinclair, and K. Kenworthy, *Transpiration and Normalized Difference Vegetation Index Response of Seashore Paspalum to Soil Drying.* Hortscience, 2009. **44**(7): p. 2046-2048.

54. Unruh, J.B., et al., *Tolerance of 'Salam' seashore paspalum (Paspalum vaginatum) to postemergence herbicides.* Weed Technology, 2006. **20**(3): p. 612-616.

55. Heckart, D.L., W.A. Parrott, and P.L. Raymer, *Obtaining Sethoxydim Resistance in Seashore Paspalum.* Crop Science, 2010. **50**(6): p. 2632-2640.

56. Uddin, M.K., et al., *Physiological and growth responses of six turfgrass species relative to salinity tolerance.* Scientific World Journal, 2012: p. 10.

57. Lee, G., R.R. Duncan, and R.N. Carrow, *Salinity tolerance of seashore paspalum ecotypes: Shoot growth responses and criteria.* Hortscience, 2004. **39**(5): p. 1138-1142.

58. Marcum, K.B. and C.L. Murdoch, *SALINITY TOLERANCE MECHANISMS OF 6 C(4) TURFGRASSES.* Journal of the American Society for Horticultural Science, 1994. **119**(4): p. 779-784.

59. Lee, G., et al., *Synthesis of organic osmolytes and salt tolerance mechanisms in Paspalum vaginatum.* Environmental and Experimental Botany, 2008. **63**(1-3): p. 19-27.

60. Chen, J.B., et al., *Growth responses and ion regulation of four warm season turfgrasses to long-term salinity stress.* Scientia Horticulturae, 2009. **122**(4): p. 620-625.

61. Kurup, S.S., et al., *Changes In Antioxidant Enzyme Activity In Turfgrass Cultivars Under Various Saline Water Irrigation Levels To Suit Landscapes Under Arid Regions.* Communications in Soil Science and Plant Analysis, 2017. **48**(17): p. 1989-2001.

62. Lee, G., R.N. Carrow, and R.R. Duncan, *Photosynthetic responses to salinity stress of halophytic seashore paspalum ecotypes.* Plant Science, 2004. **166**(6): p. 1417-1425.

63. Pessarakli, M., et al., *Candidate halophytic grasses for addressing land degradation: Shoot responses of Sporobolus airoides and Paspalum vaginatum to weekly increasing NaCl concentration.* Arid Land Research and Management, 2017. **31**(2): p. 169-181.

64. Shahba, M.A., S.F. Alshammary, and M.S. Abbas, *Effects of Salinity on Seashore Paspalum Cultivars at Different Mowing Heights.* Crop Science, 2012. **52**(3): p. 1358-1370.

65. Chen, Y., et al., *Functional Identification and Characterization of Genes Cloned from Halophyte Seashore Paspalum Conferring Salinity and Cadmium Tolerance.* Frontiers in Plant Science, 2016. **7**: p. 16.

66. Endo, N., et al., *Putative UDP-galactose epimerase and metallothioneine of Paspalum vaginalum enhanced the salt tolerance of rice, Oryza sativa L. from transplanting to harvest stages.* Breeding Science, 2005. **55**(2): p. 163-173.

67. Liu, Y.M., et al., *Identification of differentially expressed salt-responsive proteins in roots of two perennial grass species contrasting in salinity tolerance.* Journal of Plant Physiology, 2012. **169**(2): p. 117-126.

68. Jia, X.P., et al., *Characterization of the global transcriptome using Illumina sequencing and novel microsatellite marker information in seashore paspalum.* Genes & Genomics, 2015. **37**(1): p. 77-86.

CHAPTER II

SHORT-TERM SALT RESPONSE OF UNTRIMMED SEASHORE PASPALUM RAMETS

[1] Spiekerman, J. J., Jesperson, D., Raymer, P. L. and K. M Devos. To be submitted to *Crop Science*.

Abstract

Seashore paspalum (*Paspalum vaginatum*) is a halophyte that grows in coastal dunes and marshes. It is widely cultivated as a sustainable turfgrass due to its high salinity tolerance and, consequently, its ability to be irrigated with brackish water. The mechanisms underlying its salinity tolerance have only been investigated while cultivating seashore paspalum as a turf, and its tolerance to salt shock has never been thoroughly investigated. We show that *Paspalum* is tolerant of salt shock when grown as nodally propagated ramets. The ability to increase salt stress quickly instead of stepwise thus enhances the throughput with which seashore paspalum accessions can be screened for salt tolerance. We identified *Paspalum* accessions with a range of physiological responses to salt stress by measuring biomass fractions and leaf ion levels under varying levels of salt stress. The rate of growth under low salt was positively correlated with biomass loss under high salt, and negatively correlated with visual turf quality scores from a traditional salt screen. We also show that leaf proline content may be negatively correlated with biomass production. Collectively, our results provide a basis for understanding *Paspalum's* tolerance to short-term salt stress and salt shock conditions when grown as ramets.

Introduction

Saline soils negatively impact the yield of crop species, the vast majority of which are salt sensitive. For the past 20 years, 2,000 hectares of land on average have been lost each day due to salinization [1]. Though elevated soil salinity can arise from slow, natural geologic processes (primary salinity), the main culprits are urbanization and irrigation (secondary salinity). Salt prevents water uptake by plants and induces tissue-level damage through sodium toxicity, caused by sodium outcompeting potassium for binding sites in vital enzymes. The general control of growth in response to salt stress has been well-studied in plants [2]. Typically, plants experience slowed growth or quiescence upon salt stress, followed by re-initiation of growth, usually at a slower rate [3]. The relative difference in growth rate between control and stress conditions is thus an important measure to assess salt tolerance across accessions. Other traits for assessing salt tolerance include aboveground Na^+ concentration, tissue-level K^+/Na^+ ratio, osmolyte production, Na^+ sequestration, and Na^+ secretion [4]. To date, most research on salt tolerance has been conducted on glycophytes, but there is increasing interest to focus on the mechanisms used by halophytic plants to cope with salt stress [4]. Halophytes are able to complete their life cycle in high salt conditions, and thus represent an excellent resource to mine for salt tolerance mechanisms [5]. Salt tolerance mechanisms in halophytic grasses are of particular interest due to their close genetic relatedness with food crops as well as biofuel crops.

Seashore paspalum (*Paspalum vaginatum*) is a warm-season, halophytic turfgrass widely used in golf courses, sports stadiums, and landscaping projects [6]. It has the ability to grow in salt concentrations near that of seawater [7]. Under salt stress, seashore paspalum is thought to use selective K^+ uptake, osmolyte production, positive turgor maintenance, and sodium exclusion at the root level [8-10]. Seashore paspalum resides in the *Panicoideae*, the second largest grass

subfamily containing the glycophytic cereals maize, sorghum and foxtail millet, and the bioenergy crops switchgrass and miscanthus. Therefore, this halophytic grass represents an excellent model to enhance our understanding of and ultimately increase the salt tolerance of Panicoid grasses. *Paspalum distichum*, a sister species to *P. vaginatum*, inhabits mostly freshwater habitats and is significantly more salt sensitive [11]. The two species make up group Disticha within the genus *Paspalum.* They differ in several key physical characteristics including growth vigor, growth under salt, leaf width, and glume pubescence [12]. An analysis of the genetic diversity within group Disticha combined with flow cytometric analyses showed that that the germplasm analyzed formed three genetic subpopulations [12]. Two subpopulations consisted entirely of *P. vaginatum* accessions with fine to medium leaf texture. The third subpopulation comprised polyploid as well as two diploid *P. distichum* accessions, and a small number of mostly broad-leaved *P. vaginatum* accessions [12]. Because of the close genetic relationship between *P. vaginatum* and *P. distchum*, group Disticha thus represents a useful system to study differences in salt tolerance within *Paspalum.*

Much of the work done on identifying variation for salt tolerance in seashore paspalum germplasm has focused on analyzing plants as turf [9, 13-16]. This involves starting plants from plugs and letting them grow while trimming them to a constant, low height to mimic mowing. Once each accession has filled the pot like a 'lawn', the salt screen is started. Generally, salt stress is introduced slowly at a rate of 2.5-7.5 dS/m every 1-2 days to avoid salt shock [9, 13, 15, 16]. Plants continue to be trimmed regularly for the duration of the experiment. The trimming mimics normal turf maintenance but represents an additional stress (i.e. wounding) that may obscure an accession's innate response to salt. Mowing height directly affects proline content, evapotranspiration, sugar content, and non-structural carbohydrate production in seashore

paspalum under drought stress [17]. It has also been shown that increasing mowing height is beneficial under salt stress [18]. This conforms to the results of studies in tomato where mechanical wounding of tissue drastically altered physiological responses to salt stress [19, 20]. To date, only a single study has assessed salt tolerance in seashore paspalum without trimming [21], though this study compared transgenic lines, and not genotypic differences. We therefore assessed salt tolerance in seashore paspalum ramets without trimming. We also tested the generally accepted paradigm that salt levels need to be slowly increased to avoid salt shock when screening seashore paspalum for salt tolerance. Halophytes encounter widely varying salt concentrations in coastal habitats that can change quickly (*i.e.* seawater flooding, freshwater rainfall, etc.). We therefore hypothesized that seashore paspalum is tolerant of salt shock conditions.

Here, we grow seashore paspalum as replicated ramets, each propagated from a single node, without trimming, in cone-tainers under various salt stress regimes. We test growth under both salt shock conditions and slow salt increases. In addition to more accurately reflecting seashore paspalum's natural growth response under salt, our methodology shows that the duration of traditional salt screens may be reduced by elimination of the salt acclimation step. We also correlate our results with data obtained in an independently conducted acclimatized 'trimmed' screen using the same accessions.

Materials and Methods

Traditional Salt Screen

A traditional salt screen [8] was conducted with 88 *Paspalum* group Disticha accessions. The ploidy level, genetic diversity and genetic subpopulation membership of these accessions

had been analyzed by Eudy et al. [12]. Sources of the accessions are described in Eudy et al. [12]. Experiments were conducted in an environmentally controlled greenhouse during the winter of 2010-2011 and repeated during the summer of 2012. We used four in-house constructed ebb and flow type benches to provide daily sub-irrigation. All irrigation solutions contained soluble fertilizer (Miracle-Gro Professional Excel water soluble fertilizer, 13-2-13 + 6 Ca + 3 Mg plug special, Scotts-Sierra Horticultural Products Company, Marysville, OH 43041). Salt treatments (Instant Oceanic Synthetic Sea Salt, Aquarium Systems, Mentor, OH 44060) were achieved by increasing salt concentration by 6 dS/m at four-day intervals until target concentrations were reached for each bench. Water levels were maintained and salt concentrations were monitored using a portable pH/conductivity meter equipped with a conductivity electrode and adjusted twice weekly for the duration of the experiment.

Each experiment consisted of three replications of 88 accessions that were simultaneously evaluated at salt concentrations of 0, 15, 30 and 45 dS/m. For reference, seawater has a conductivity of around 45-50 dS/m, which corresponds to ~450-500 mM NaCl [22]. Plants for evaluation were grown in washed play sand in 10 cm square pots and were placed on the ebb and flow tables. Plants were irrigated with fertilizer solution for 30 days prior to initiating salt treatments. After the 30 day grow-in period, all plants were clipped to a standard height of 2.5 cm for turf types and 5.0 cm for forage types and salt treatments were started.

At approximately two-week intervals, all plants were scored for turf quality clipped to standard heights to determine top-growth biomass. Turf quality was visually rated on a 0-9 scale with 0= no green tissue and 9=optimum quality.

Salt Screen 1

Based on the results from the traditional screen at the 45 dS/m salt level, six tolerant and six sensitive *P. vaginatum* accessions, and two diploid *P. distichum* accessions [12] were selected for a short-term high salt analysis. Accessions, maintained in 12-inch pots, were used as source plants for nodal propagation into ramets. For all experiments, a soil mixture of 3 parts sand:1part pine bark mix was used. Single nodes with 1.5-2 cm of surrounding stolon tissue were cut from growing stolons (Suppl. Fig. 2.1A). Stolon segments were placed in a tray of soil with the node below the soil line, and after one week, nodes with emerging shoot tissue were transferred to UV stabilized SC-10 (164 mL) Ray Leach Cone-tainers™ (Stuewe and Sons Inc, Tangent, Oregon) (Suppl. Fig. 2.1B). Three to six replicates (plants) were used for each genotype per treatment. The cone-tainers for each genotype were randomly placed in 98-cell racks in ebb & flow irrigation bins consisting of large trays with an inlet and drainage holes connected to large bins containing the irrigation solution (Suppl. Fig. 2.1C). The flood tables were irrigated for a period of 15 minutes six times daily and once nightly using a 500 GPH (gallons per hour) fountain pump on a timer. The irrigation solution contained 2 g/gallon of Excel Plus and Bedding Special (13-2-13) liquid feed fertilizer (G99120 Everris NA Inc, Dublin, OH) and 0.6 g/gallon of magnesium sulfate. After one week of plant establishment, the freshwater irrigation solution was replaced with a 2.5 dS/m salt solution consisting of a sea salt mix (Oceanic 81050) with added fertilizer and magnesium sulfate as described above for two days, then a 5 dS/m salt solution for two days and finally a 10 dS/m salt solution (Suppl. Fig. 2.1D). Seashore paspalum has been reported to grow better at 10 dS/m salt than in freshwater [15, 23]. After two weeks at 10 dS/m, salt stress was initiated. The control bin was left at 10 dS/m while the salt level in the treatment bin was increased in a single step to 70 dS/m. After 48 hours at 70 dS/m, the salt stress

in the treatment bin was reduced to 30 dS/m for three weeks before trait analysis (Suppl. Fig. 1D). Salt level in the control bin was maintained at 10 dS/m throughout the experiment. All experiments were conducted in the University of Georgia Plant Biology Greenhouse under a day/night temperature of 27°/18° C and 14-hr days.

Salt Screen 2

Four *P. vaginatum* accessions ('HI10', '509018-3', 'KC9' and 'Durban') and one *P. distichum* accession ('Spence') were chosen for further analysis based on their growth type and biomass production in salt screen 1. Nodes were propagated and ramets were established for one week in ebb & flow irrigation bins at 0 dS/m as described for salt screen 1. Half of the plants (4-5 individuals per accession) for each of six treatments (0 dS/m, 5 dS/m, 10 dS/m, 30 dS/m, 60 dS/m and 90 dS/m salt) were 'salt-shocked' by increasing salt levels from 0 dS/m to the final salt concentration in one step. The other half of the plants were subjected to a more gradual increase of 2.5 dS/m salt for two days, 5 dS/m for two days, 10 dS/m for five days, and then a single step increase to the final salt concentration. The number of steps depended on the final salt level. For example, if the final salt level was 5 dS/m, plants were grown at 2.5 dS/m for two days and then at 5 dS/m for the remainder of the experiment. Plants were grown for six weeks following the start of the ≥30 dS/m salt treatments before trait analysis in greenhouse conditions as described above.

Salt Screen 3

Accessions 'HI10', '509018-3', 'Durban', 'KC9' and 'Spence' were nodally propagated and salt concentrations were increased gradually as described for salt screen 2. Final salt

concentrations were 0 dS/m, 10 dS/m, and 30 dS/m. Plants were grown for three weeks once the final salt concentration was reached prior to analysis of total biomass and leaf proline concentrations.

Biomass Measurements

Individual plants were rinsed with deionized water and split into stolon, leaf, and root fractions. Organ fractions were placed into paper bags, dried at 65 ^{0}C for 3 days, and weighed. Measurements were averaged across all plants (replicates) per accession per treatment.

Leaf Ion Measurements

After weighing leaf fractions for biomass determination, a subset of each sample was placed into a 2 mL tube containing a metal BB, then put in liquid nitrogen to make the dried samples more brittle, then powdered using a Qiagen TissueLyser II. Ten milligrams of ground tissue was incubated with 1.8 mL 0.5 M nitric acid in a 2 mL Eppendorf tube on a shaker for two days at 25 ^{0}C. Tubes were then centrifuged, and samples were diluted with deionized water for measurements (1:15 for sodium and 1:20 for potassium). Sodium (Na^+) and potassium (K^+) content were measured on a Cole-Parmer single-channel digital flame photometer. Parts per million (ppm) values were calculated by using a standard curve ranging from 2-60 ppm for both Na^+ and K^+. Values were averaged across all plants (replicates) per accession per treatment.

Proline Measurements

Proline content was measured on plants from salt screen 3 using all leaves collected from a single growing stolon from four individual plants per accession (‘HI10’, ‘509018-3’, ‘Durban’,

'KC9' and 'Spence') per treatment using a colorimetric assay [24, 25]. Briefly, 100 mg of fresh leaf tissue was ground to a fine powder in liquid nitrogen and then transferred to a 2 mL eppendorf tube containing 500 μL of 3% sulfosalicylic acid and vortexed. Tubes were centrifuged at 14,000 RPM for five minutes. After centrifugation, 100 μL of the supernatant was transferred to a tube containing 500 μL reaction mixture comprising 100 μL of 3% sulfosalicylic acid, 200 μL glacial acetic acid, and 200 μL acidic ninhydrin. To avoid high pressure during the subsequent incubation step, a single hole was made with a hot needle in the top of each tube. Samples were incubated at 96 ^{0}C for one hour and the reaction was terminated by placing the tubes for five minutes on ice. One milliliter of toluene was added to the chilled reaction mixture, after which samples were vortexed vigorously and left at room temperature for five minutes. Absorbance of the proline-ninhydrin chromophore-containing toluene was read on a spectrometer at 520 nm and concentrations were calculated using a standard curve.

Statistical Analyses

Significant differences between accessions were calculated using type III ANOVA analyses followed by *post-hoc* Tukey's honest significant difference (HSD) tests with multiple comparisons across means. For ANOVA analyses, groups were considered significantly different at a level of $p<0.05$. In salt screen 1, dried weights of the leaves, stolons, and roots (Suppl. Fig. 2.3A-C) were highly correlated (stolon-leaf: $r^2 = 0.7391$, $p<0.00001$; stolon-root: $r^2 = 0.5649$, $p<0.00001$; leaf-root: $r^2 = 0.617$; $p<0.00001$). Therefore, leaf, stolon and root biomass were combined, and total biomass was used in all subsequent analyses. For salt screens 1 and 2, one-way ANOVAs were conducted for each trait at each salt level separately. Two-tailed t-tests were conducted to observe differences between control and salt treatment for each accession in salt

screen 1. Two-tailed t-tests were also conducted on each trait for each accession between non-shock and shock plants at all salt levels in salt screen 2. If significant differences were observed for a trait between non-shock and shock plants with t-tests, those trait values were analyzed separately in the ANOVA. Significance was counted at $p<0.05$ in all t-tests. For salt screen 3, one-way ANOVAs were conducted for each trait at each salt level separately and also split by genotype. Additional one-way and two-way ANOVAs were also conducted to view interaction effects for the salt screen 2 split by salt level. For salt screen 1, results from statistical analyses can be found in Suppl. Table 2.2 (ANOVA analyses for freshwater control plants), Suppl. Table 2.3 (ANOVA analyses for salt-treated plants), and Suppl. Table 2.5 (two-tailed t-tests comparing control and salt-treated plants). For salt screen 2, results from statistical analyses can be found in Suppl. Table 2.7 (Pearson correlations for all measured traits), Suppl. Table 2.8 (two-tailed t-tests comparing nonshock and shock treatments), Suppl. Table 2.9 (ANOVA analyses split by salt treatment), Suppl. Table 2.10 (Pearson correlations split by salt treatment). For salt screen 3, results from statistical analyses can be found in Suppl. Table 2.11 (ANOVA analyses for proline measurements split by salt treatment) and Suppl. Table 2.12 (ANOVA analyses for proline measurements split by genotype).

Results

Salt Screen 1

Biomass and ion data for the fourteen genotypes grown in salt screen 1 are given in Suppl. Fig. 2.2, Suppl. Fig. 2.3, and Suppl. Table 2.1-2.3. Accessions with high biomass production under 10 dS/m salt had a greater reduction in relative biomass when subjected to salt shock treatment ($r^2 = 0.71$; $p=0.003901$) (Fig. 2.1, Suppl. Fig. 2.3E). We compared our biomass

data with turf quality measurements in a traditional salt screen conducted in 2010-11 by Dr. Paul Raymer, UGA, Griffin (Suppl. Table 2.4). Accessions on the high end of the biomass yield spectrum under 10 dS/m in our screen typically had the lowest leaf quality scores in the traditional salt screen when analyzing the final turf quality scores of plants grown for 8 weeks under salt stress (Suppl. Fig. 2.4).

Salt Screen 2

Due to the ability of some *Paspalum* accessions to cope with salt shock conditions in salt screen 1, we investigated growth speed for five accessions ('HI10', '509018-3', 'Durban', 'KC9' and *P. distichum* acc. 'Spence') under a wide range of salt concentrations and using both an incremental (non-shock) and one-step (shock) salt increase protocol. The biomass and ion data for the 0 dS/m – 90 dS/m screen are presented in Fig. 2.1 and Suppl. Table 2.6. Biomass for leaf, stolon, and root tissue was correlated (Suppl. Table 2.7), and thus total biomass was used in all subsequent analyses. Trait data split by tissue type is presented in Suppl. Fig. 2.3. Two-tailed t-tests comparing traits in non-shock and shock treatments are presented in Suppl. Table 2.8.

T-tests indicate that there were no significant differences between shock and non-shock treatments at salt levels ≤30 dS/m in any accession (Suppl. Table 2.8). Significant differences were observed in Spence for potassium content at 60 dS/m in addition to sodium content and K^+/Na^+ at 90 dS/m. The only other significant differences observed were for potassium content at 60 dS/m for Durban and at 90 dS/m for 509018-3, and total biomass for KC9 at 30 dS/m.

While plants survived 60 dS/m and 90 dS/m salt levels for several weeks, growth essentially shut down under those extremely high salt levels (Fig. 2.1A, Suppl. Fig. 2.6). ANOVA analyses indicate there are significant differences in total biomass between accessions

at 10 dS/m and below, but not at 30 dS/m (Suppl. Table 2.9). We also tested the effects of genotype, treatment (non-shock *vs* shock), and genotype X treatment at each salt level (Table 2.1). The only treatment effects were observed in leaf potassium content at 90 dS/m. There were significant genotypic effects at all salt levels, though the vast majority of genotypic effects were seen at salt levels $\leq$ 10 dS/m (Table 2.1). A trend for optimal growth at 5 dS/m or 10 dS/m was seen for accessions 509018-3 and HI10 (Fig. 2.1A). As for salt screen 1, we observed a strong correlation (r^2=0.8686; p=0.021068) between growth under low salt, specifically 5 dS/m, and relative growth reduction under high salt (30 dS/m).

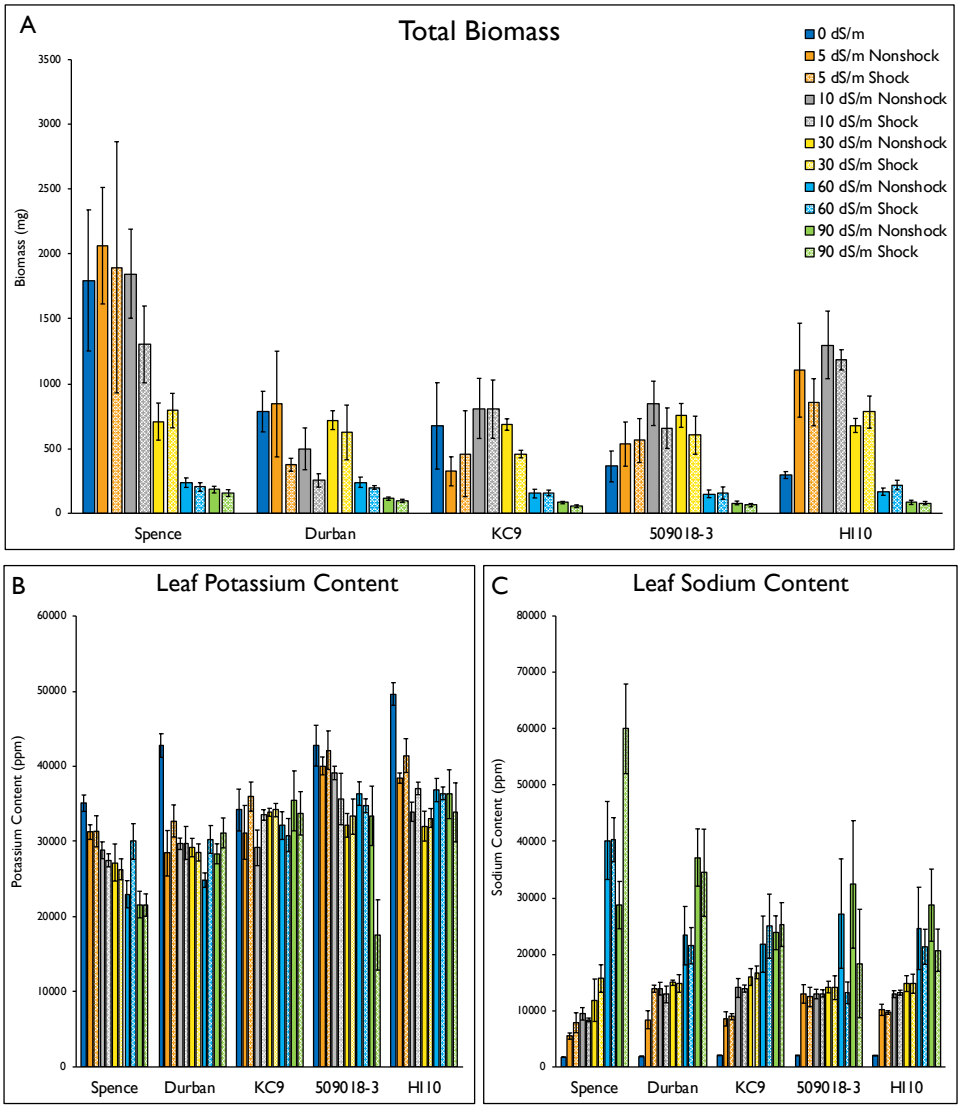

FIGURE 2.1. Total biomass & leaf ion measurements for plants grown at 0-90 dS/m salt concentrations. One-half of the plants experienced a gradual increase in salt concentration (nonshock, N ≥ 4 plants) and one-half experienced an immediate increase from 0 dS/m to the final concentration (shock, N ≥ 4 plants). For paired nonshock and shock colored bars in A-C, the untextured bar on the left represents the nonshock data while the textured right bar represents shock data. **(A)** Total biomass including stolon, leaf, and root tissue fractions. Green and red circles indicate tolerant and sensitive genotypes, respectively, based on turf quality measures after treating plants as trimmed turf. **(B)** Leaf potassium content shown in parts per million. **(C)** Leaf sodium content shown in parts per million.

Leaf potassium content significantly varied by genotype at all salt levels, by treatment only at 90 dS/m, and by genotype X treatment only at 60 dS/m (Table 2.1). Similar genotypic effects were observed for sodium content, though no genotypic differences exist at salt levels ≥ 30 dS/m and no significant treatment effects were observed at any salt level. Genotype X treatment effects for sodium were only observed at 90 dS/m. Under freshwater and low salt (5 dS/m and 10 dS/m), K^+ and Na^+ content were positively correlated, that is, accessions with more K^+ also had more Na^+, although this correlation was less significant at 10 dS/m and absent at 30 dS/m (Suppl. Table 2.10). K^+/Na^+ ratio correlated positively with K^+ under freshwater and negatively with Na^+ under salt levels ≥ 5 dS/m. Interestingly, at 10 dS/m and 30 dS/m, Na^+ content and K^+/Na^+ ratio correlated strongly negatively and positively, respectively, with total biomass (Suppl. Table 2.10). Accessions typically showed the highest reduction in leaf K^+ content and the highest increase in Na^+ when salt levels were increased from 0 dS/m to 5 dS/m.

Table 2.1. ANOVAs testing for interaction effects between genotype, treatment (nonshock/shock), and genotype X treatment in salt screen 2 split by salt level. Asterisks indicate significance at levels of 0.05 (*), 0.01 (**), and 0.001 (***).

Genotype	0 dS/m	5 dS/m	10 d S/m	30 dS/m	60 dS/m	90 dS/m
Total Biomass	0.01097*	0.03974*	0.0007827***	0.8822	0.1544	0.000195***
Leaf Sodium Content	2.14E-07***	1.64E-03**	1.40E-02*	0.6376	1.77E-01	7.21E-01
Leaf Potassium Content	3.66E-06***	2.19E-03**	2.66E-04***	4.46E-02*	1.05E-07***	2.17E-02*
Potassium:Sodium	5.90E-06***	2.06E-02*	1.96E-03**	0.2029	6.99E-02	7.52E-02
Treatment	**0 dS/m**	**5 dS/m**	**10 d S/m**	**30 dS/m**	**60 dS/m**	**90 dS/m**
Total Biomass	_	0.96264	0.5343567	0.3414	0.9181	0.456537
Leaf Sodium Content	_	0.749891	0.93089	0.9617	0.09679	0.156613
Leaf Potassium Content	_	0.513648	0.153543	0.59818	0.32517	0.001048**
Potassium:Sodium	_	0.63933	0.25152	0.6689	0.17188	0.55265
Genotype X Treatment	**0 dS/m**	**5 dS/m**	**10 d S/m**	**30 dS/m**	**60 dS/m**	**90 dS/m**
Total Biomass	_	0.95589	0.7790819	0.6537	0.7288	0.960882
Leaf Sodium Content	_	0.750944	0.93095	0.7947	0.63507	0.02938*
Leaf Potassium Content	_	0.877392	0.146851	0.94473	0.02337*	0.051972
Potassium:Sodium	_	0.77681	0.62538	0.2353	0.68167	0.72152

Salt Screen 3

Proline, biomass measurements and statistical comparisons for salt screen 3 are presented in Fig. 2.3, Suppl. Table 2.11, and Suppl. Table 2.12. Significant differences were observed in proline content between genotypes at all salt levels, with ‘HI10’ producing significantly more proline than ‘Spence’ under all treatments (Fig. 2.3A, Suppl. Table 2.11). All genotypes produced a significantly higher amount of proline at 30 dS/m compared to freshwater, though no significant increases were seen from 0 dS/m to 10 dS/m (Fig. 2.3A, Suppl. Table 2.12). We saw a significant correlation between growth under low salt (10 dS/m) and raw biomass reduction

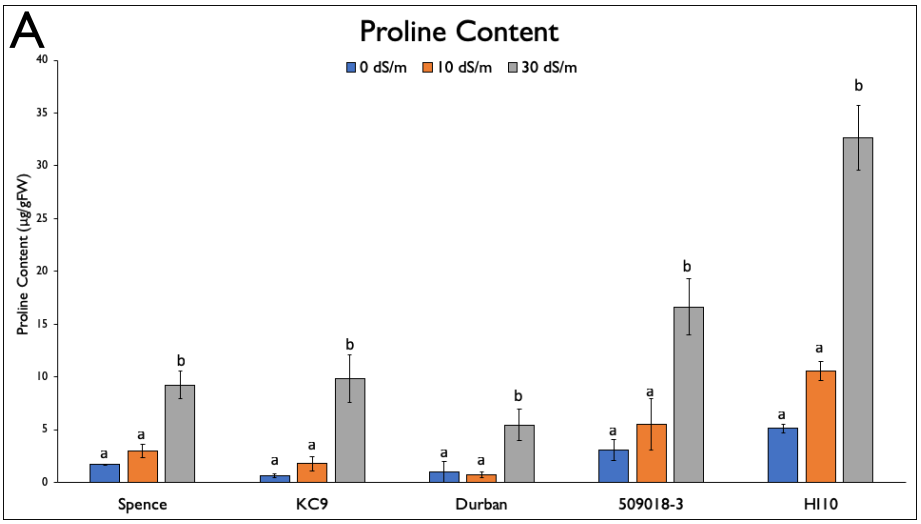
A
Proline Content
0 dS/m
10 dS/m
30 dS/m
Proline Content (µg/gFW)
Spence
KC9
Durban
509018-3
HI10

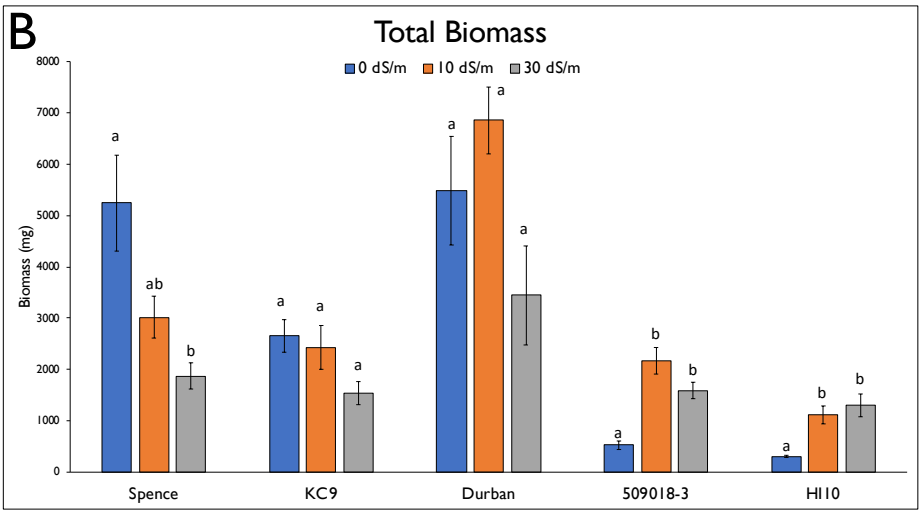
B
Total Biomass
0 dS/m
10 dS/m
30 dS/m
Biomass (mg)
Spence
KC9
Durban
509018-3
HI10

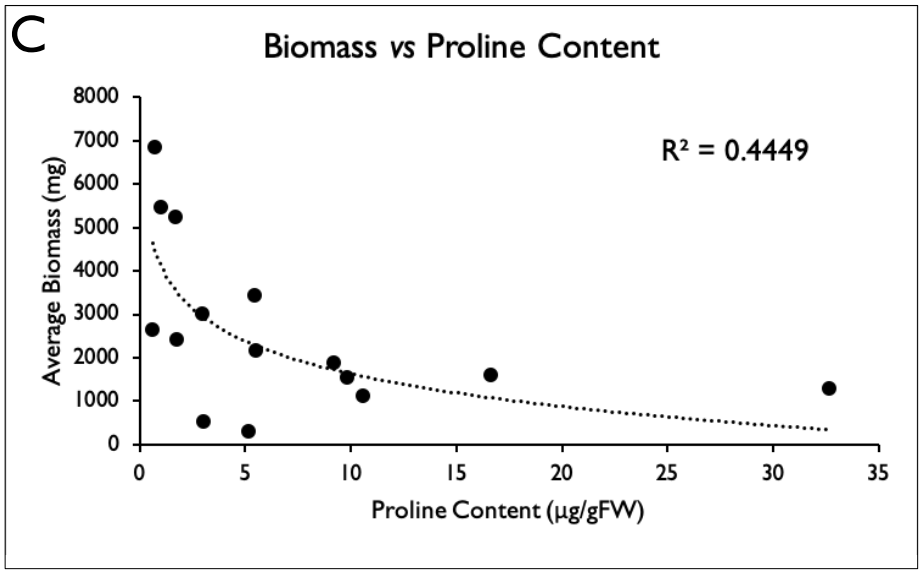
C
Biomass vs Proline Content
R² = 0.4449
Average Biomass (mg)
Proline Content (µg/gFW)

FIGURE 2.2. Leaf proline content **(A)** (N=4 for each genotype at each treatment level) and total biomass **(B)** data (N=3 for each genotype at each treatment level) of 'Spence', 'KC9', 'Durban', '509018-3', and 'HI10' genotypes grown at 0 dS/m, 10 dS/m, and 30 dS/m. The relationship between average biomass and proline content at each salt level is plotted in **(C)**. A one-way ANOVA with post-hoc Tukey's honest significant difference (HSD) tests was used to calculate adjusted P-values within each genotype in **(A)** and **(B)**. Letters indicate significant differences counted as $P<0.05$ for each genotype and were acquired through genotype-specific ANOVAs.

at 30 dS/m ($r^2 = 0.9109$, $p = 0.011609$). Though not statistically significant, we observed a correlation between growth under low salt (10 dS/m) and relative biomass loss under salt (30 dS/m) ($r^2 = 0.5347$, $p = 0.160377$) as seen under salt screens 1 and 2. A logarithmic relationship between proline content and total biomass accumulation was observed (Fig. 2.2C).

Discussion

To trim, or not to trim.

The classical way of assessing salt tolerance in turfgrass requires many months of hands-on time, as described in the materials and methods for the traditional screen. After a 30 day grow-in period, plants are clipped to a standard height and placed in ebb and flow bins for salt treatment. Every ~2 weeks, plants are clipped and visually scored for turf quality. Dry weight of the clippings provides a measure of growth. In these types of studies, there is a trend for clipping yield to positively correlate with turf quality measures under salt stress [18, 26]. We compared biomass measures from the 14 node-grown accessions in salt screen 1 with visual turf quality scores of the same accessions from a large-scale trimmed salt experiment that was conducted

under different environmental conditions (different location, different year, different time of year) (Suppl. Fig. 2.4). Biomass production at 10 dS/m in our experiment negatively correlated with turf quality measurements when those same genotypes were treated as turf in a traditional salt screen, indicating that genotypes that were slow-growing as ramets may have better turf quality. This initial observation needs to be confirmed by repeating this experiment (non-trimmed biomass *vs.* turf quality) on a larger scale and under the same environmental conditions. We also saw a negative correlation between growth under low salt (5 – 10 dS/m) and biomass reduction under high salt (30 dS/m) in our screens. It should be noted, however, that accessions were differentially affected by low salt levels, with some exhibiting glycophytic growth trends (higher growth under freshwater) while others exhibited halophytic growth trends (higher growth under low salt). Furthermore, we saw different growth behaviors under freshwater *vs.* low salt when screens were carried out in the greenhouse during the winter compared to the summer, which suggests a genotype X environmental (temperature and/or light) interaction. Experiments under controlled conditions are needed to confirm this.

It should also be noted that high coefficient of variance (CV) values were observed for total biomass measurements between individual ramets of the same accession. For example, the CV for total biomass in salt screen 1 varied widely in both control (5.2-76.8%) and salt (13.2-53.3%). In contrast, the CV for sodium ranged from 2.7-35.4% in control and 3.7-30.5% in salt, while the CV for potassium ranged from 6.2-16.1% in control and 6-10.5% in salt. These data indicate that there can be high variability in the growth of individual ramets, indicating that sufficient replication is needed to draw conclusions from individual ramets. Growth variation may be further mitigated by selecting more uniform nodes and ramets produced from those

nodes prior to salt stress. This could be accomplished through selecting nodes of more similar ages for propagation in addition to limiting the number of times ramets are transplanted.

In summary, while it has been argued that high growth rate under freshwater conditions should be a top trait considered by turfgrass breeders aimed at selecting salt tolerant accessions to allow turfgrasses to recover from wear [15], our results indicate that in the untrimmed state, slow-growing seashore paspalum varieties may exhibit higher turf quality measures under salt stress. Because untrimmed growth rate negatively correlates with turf quality, slow-growing accessions may be labeled more salt tolerant as compared to accessions that are fast-growing when grown as ramets. However, our experiments did not assess the threshold growth rate that is needed for an accession to recover from wear when used on a recreational surface.

Ion accumulation in leaf tissue is not linear

As high leaf sodium content results in tissue toxicity [2], leaf ion content is a key trait to measure under salt stress. In salt screen 1, leaf sodium and potassium content did not significantly differ between accessions under 10 dS/m control and salt conditions with the exception of the *P. distichum* 'Spence' (Suppl. Fig. 2.2B & C, Suppl. Table 2.2 & 2.3). We saw similar results in salt screen 2 where sodium concentrations at 10 dS/m and 30 dS/m appeared similar in seashore paspalum accessions (Fig. 2.1B & C). These results are similar to those found when seashore paspalum was treated as turf, whereby leaf sodium content did not linearly correlate with the salt concentration used for irrigation [13, 27]. Thus, although our screening methodology differs substantially from typical turfgrass salt screens, this pattern seen in leaf sodium accumulation was reiterated. Interestingly, seashore paspalum accessions tended to uptake more sodium under 10 dS/m salt compared with 'Spence'. Though at concentrations

above 30 dS/m, seashore paspalum accessions accumulated less sodium compared to 'Spence' (Fig. 2.1C). These data indicate that, compared with *P. distichum*, seashore paspalum may actively uptake sodium in low salt conditions and exclude sodium from leaf tissue in high salt conditions. We thus hypothesize that seashore paspalum actively utilizes sodium as an osmolyte, similar to other halophytes [28].

Leaf sodium levels in seashore paspalum accessions under control conditions were high compared to other warm season turf species [27]. Nevertheless, leaf tissue remained green with only low levels of chlorosis, even at high salt concentrations in our experiments (Suppl. Fig. 2.6). As seashore paspalum has little to no salt secretion capacity [27, 29], it likely uses sodium sequestering mechanisms yet to be determined to avoid tissue toxicity.

Paspalum is tolerant of salt shock

Salt shock occurs when plants experience a sudden change in salt level, resulting in cell plasmolysis and eventual cell death [30]. The osmotic shock experienced under sudden salt increase is considered distinct from salt stress, which involves a gradual increase in salt concentrations over time. A gradual increase is considered more reflective of the salt conditions plants come across in agricultural field settings, where soil salinity may increase over the course of a growing season [31]. What constitutes a shock or stress, however, will be species-dependent, and salt increases will almost certainly be perceived differently between glycophytes and halophytes. A glycophytic grass such as rice experiences salt shock resulting in plant death at 150 mM (15 dS/m) [32, 33]. In contrast, seashore paspalum enhances growth at similar concentrations in our experiments. Nevertheless, a slow increase in salt levels is the norm in seashore paspalum salt screens, which increases the duration of these screens considerably. To

our knowledge, our study is the first to compare plant growth in response to salt shock and non-shock conditions at a range of salt concentrations in a halophytic grass.

Though plant growth in response to salt shock is important, plasmolysis is another vital cellular trait to measure to accurately assess a plant's response to salt shock [31]. The level of cell plasmolysis in response to salt stress or shock was not investigated in this study. However, as we did not see any growth effects between shock and non-shock screens, at least at concentrations ≤30 dS/m, it is unlikely that plants experienced any significant negative consequences of salt shock at those salt levels. Most significant trait differences that occurred in response to salt shock occurred at 60 dS/m and 90 dS/m (Suppl. Table 2.8 & 2.9). Our results therefore show that both *P. vaginatum* and *P. distichum* are likely tolerant of salt shock up to concentrations of at least 30 dS/m under our experimental conditions and likely in their natural habitats. Indeed, there are several occasions in nature where seashore paspalum may experience sudden osmotic changes in its environment. Coastal, sandy dunes are one of seashore paspalum's natural habitats [6]. In these dunes, seashore paspalum grows in a soil mixture that is well-drained, and likely experiences seawater rising up from below the surface in addition to freshwater from above in the form of rainfall. Large fluctuations may also occur due to tidal fluctuations, flooding, and resulting intertidal pools that form. Consequently, it is probable that *Paspalum* has evolved mechanisms to cope with sudden changes in soil salinity. Though *P. distichum* grows mainly inland in freshwater habitats, it is also found in coastal regions with seashore paspalum [11]. Thus, *P. distichum* likely uses mechanisms to cope with rapidly changing salt conditions as well.

Elevated proline biosynthesis may be connected to biomass production

Proline is considered a highly beneficial amino acid in plants. Under stress conditions, it is produced and utilized for osmotic balance, reactive oxygen species (ROS) detoxification, and protein stabilization within the cytoplasm [35, 36]. It is known to accumulate at high concentrations under salt stress in leaf tissue, and is thought to act as the primary organic solute used for osmotic adjustment in seashore paspalum [9, 29]. Though more in-depth work needs to be conducted, it is intriguing to hypothesize that high proline production may be connected to the slow growth habit of accessions 'HI10' and '509018-3' under freshwater. The production of organic osmolytes is considered an energetically expensive process [37, 38] and proline concentrations have been linked with general growth phenotypes in many species [39]. For example, the overexpression of a barley proline transporter in *Arabidopsis* was shown to cause a reduction in biomass [40].

There are also known effects of proline biosynthesis on reproductive development, which may affect growth speed. The rate-limiting proline biosynthetic gene *Pyrroline-5-carboxylate synthetase* (*P5CS*) and the transporter *Proline transporter T* (*ProT*) are both vital for proper floral transition [41-43]. Additionally, the *FRIGIDA* (*FRI*) gene, a central regulator of flowering time that represses flowering through FLOWERING LOCUS C [44], was recently shown to activate *P5CS1* expression and enhance proline accumulation under drought stress [45]. Furthermore, different copies of the *P5CS* gene play distinct roles in development, with *p5cs2* mutants exhibiting slowed vegetative growth and reduced fertility compared with *p5cs1* mutants, which showed no mutant phenotype [46]. Finally, although high proline levels provide ATP (30 ATP result from one molecule of oxidized proline) [47], it may be energetically costly to constitutively produce. As we observed a logarithmic relationship between proline content and

total biomass (Fig. 2.2C), high proline concentrations may be connected to the slow growth rate observed in some seashore paspalum accessions, though analysis in more genotypes is needed to confirm.

The concentrations of other known organic osmolytes in seashore paspalum including glycine betaine, trigonelline, fructose, glucose, sucrose, and *myo*-inositol in addition to unknown osmolytes should be analyzed in slow-growing and fast-growing accessions to provide more insight into the connection between osmolyte production and growth speed under control and stress conditions [9].

Conclusion

Our results show that slowly and gradually increasing salt concentration is likely not necessary for seashore paspalum ramets. Our study thus helps lay the foundation for growing seashore paspalum as a model halophyte with more direct applications to glycophytic grass crops of interest. We also showed that sodium uptake is not linearly dependent upon the salt concentration of the irrigation mixture, and our data indicate that seashore paspalum is better able to exclude sodium at elevated salt concentrations compared to *P. distichum*. Furthermore, high proline production may be linked to growth in seashore paspalum varieties, though future work should focus on analyzing this trait in more accessions. Though more work is required to determine the application of our growth methods to paspalum breeders, conducting salt screens with untrimmed seashore paspalum ramets has the benefit that experimental results may better translate to related agronomically vital glycophytic grass crops.

Acknowledgements

We would like to thank Melanie Harrison at the USDA and Paul Raymer at UGA Griffin for their assistance in obtaining seashore paspalum and *P. distichum* accessions. We would also like to thank David Jespersen at UGA Griffin for assistance in measuring leaf ion content. Furthermore, we are grateful to the UGA greenhouse staff (Kevin Tarner, Mike Boyd, and Greg Cousins) for their assistance in setting up these experiments. Experiments in this chapter were funded through the grants shown below.

USDA-SCRI awarded to K.M. Devos (2015-51181-24291; PI: K.E. Kenworthy, University of Florida)

NIH T32 Training Grant (T32 GM 7103-41)

References

1. Qadir, M., et al., *Economics of salt-induced land degradation and restoration.* Natural Resources Forum, 2014. **38**(4): p. 282-295.
2. Munns, R. and M. Tester, *Mechanisms of salinity tolerance*, in *Annual Review of Plant Biology*. 2008, Annual Reviews: Palo Alto. p. 651-681.
3. Julkowska, M.M. and C. Testerink, *Tuning plant signaling and growth to survive salt.* Trends in Plant Science, 2015. **20**(9): p. 586-594.
4. Flowers, T.J., R. Munns, and T.D. Colmer, *Sodium chloride toxicity and the cellular basis of salt tolerance in halophytes.* Annals of Botany, 2015. **115**(3): p. 419-431.
5. Ali, A. and D.J. Yun, *Salt stress tolerance; what do we learn from halophytes?* Journal of Plant Biology, 2017. **60**(5): p. 431-439.
6. Lonard, R.I., F.W. Judd, and R. Stalter, *Biological Flora of Coastal Dunes and Wetlands: Paspalum vaginatum Sw.* Journal of Coastal Research, 2015. **31**(1): p. 213-223.
7. Uddin, M.K., et al., *Physiological and growth responses of six turfgrass species relative to salinity tolerance.* Scientific World Journal, 2012: p. 10.
8. Guo, H.L., et al., *Growth response and ion regulation of seashore paspalum accessions to increasing salinity.* Environmental and Experimental Botany, 2016. **131**: p. 137-145.
9. Lee, G., et al., *Synthesis of organic osmolytes and salt tolerance mechanisms in Paspalum vaginatum.* Environmental and Experimental Botany, 2008. **63**(1-3): p. 19-27.
10. Peacock, C.H. and A.E. Dudeck, *PHYSIOLOGICAL AND GROWTH-RESPONSES OF SEASHORE PASPALUM TO SALINITY.* Hortscience, 1985. **20**(1): p. 111-112.
11. HL Leithead, L.Y., TN Shiflet, *100 native forage grasses in 11 southern states.* Agricultural Handbook, Soil Conservation Service, USDA, 1971. **No. 389**: p. 216.

12. Eudy D, B.B., Harrison ML, Raymer P, Devos KM *Ploidy level and genetic diversity in the genus Paspalum, group Disticha.* Crop Science 2017. **57**: p. 3319-3332.

13. Lee, G.J., R.R. Duncan, and R.N. Carrow, *Nutrient uptake responses and inorganic ion contribution to solute potential under salinity stress in halophytic seashore paspalums.* Crop Science, 2007. **47**(6): p. 2504-2512.

14. Liu, Y.M., et al., *Identification of differentially expressed salt-responsive proteins in roots of two perennial grass species contrasting in salinity tolerance.* Journal of Plant Physiology, 2012. **169**(2): p. 117-126.

15. Lee, G., R.R. Duncan, and R.N. Carrow, *Salinity tolerance of seashore paspalum ecotypes: Shoot growth responses and criteria.* Hortscience, 2004. **39**(5): p. 1138-1142.

16. Pompeiano, A., et al., *Growth responses and physiological traits of seashore paspalum subjected to short-term salinity stress and recovery.* Agricultural Water Management, 2016. **163**: p. 57-65.

17. Shahba, M.A., M.S. Abbas, and S.F. Alshammary, *Drought Resistance Strategies of Seashore Paspalum Cultivars at Different Mowing Heights.* Hortscience, 2014. **49**(2): p. 221-229.

18. Shahba, M.A., S.F. Alshammary, and M.S. Abbas, *Effects of Salinity on Seashore Paspalum Cultivars at Different Mowing Heights.* Crop Science, 2012. **52**(3): p. 1358-1370.

19. Capiati, D.A., S.M. Pais, and M.T. Tellez-Inon, *Wounding increases salt tolerance in tomato plants: evidence on the participation of calmodulin-like activities in cross-tolerance signalling.* Journal of Experimental Botany, 2006. **57**(10): p. 2391-2400.

20. Dombrowski, J.E., *Salt stress activation of wound-related genes in tomato plants.* Plant Physiology, 2003. **132**(4): p. 2098-2107.

21. Wu, X.L., H.F. Shi, and Z.F. Guo, *Overexpression of a NF-YC Gene Results in Enhanced Drought and Salt Tolerance in Transgenic Seashore Paspalum.* Frontiers in Plant Science, 2018. **9**: p. 9.

22. FAO, *Saline waters as resources.* Food and Agriculture Organization of the United Nations, 1992.

23. Lee, G., R.N. Carrow, and R.R. Duncan, *Salinity tolerance of selected seashore paspalums and bermudagrasses: Root and verdure responses and criteria.* Hortscience, 2004. **39**(5): p. 1143-1147.

24. Abraham, E., et al., *Methods for Determination of Proline in Plants*, in *Plant Stress Tolerance: Methods and Protocols*, R. Sunkar, Editor. 2010, Humana Press Inc: Totowa. p. 317-331.

25. Bates, L.S., R.P. Waldren, and I.D. Teare, *RAPID DETERMINATION OF FREE PROLINE FOR WATER-STRESS STUDIES.* Plant and Soil, 1973. **39**(1): p. 205-207.

26. Shahba, M.A., *Comparative Responses of Bermudagrass and Seashore Paspalum Cultivars Commonly Used in Egypt to Combat Salinity Stress.* Horticulture Environment and Biotechnology, 2010. **51**(5): p. 383-390.

27. Chen, J.B., et al., *Growth responses and ion regulation of four warm season turfgrasses to long-term salinity stress.* Scientia Horticulturae, 2009. **122**(4): p. 620-625.

28. Flowers, T.J. and T.D. Colmer, *Salinity tolerance in halophytes.* New Phytologist, 2008. **179**(4): p. 945-963.

29. Marcum, K.B. and C.L. Murdoch, *SALINITY TOLERANCE MECHANISMS OF 6 C(4) TURFGRASSES.* Journal of the American Society for Horticultural Science, 1994. **119**(4): p. 779-784.

30. Munns, R., *Comparative physiology of salt and water stress.* Plant Cell and Environment, 2002. **25**(2): p. 239-250.

31. Shavrukov, Y., *Salt stress or salt shock: which genes are we studying?* J Exp Bot, 2012. **64**(1): p. 119-27.

32. Zou, J., et al., *Overexpression of OsHsp17.0 and OsHsp23.7 enhances drought and salt tolerance in rice.* Journal of Plant Physiology, 2012. **169**(6): p. 628-635.

33. Kawasaki, S., et al., *Gene expression profiles during the initial phase of salt stress in rice.* Plant Cell, 2001. **13**(4): p. 889-905.

34. Blits, K.C. and J.L. Gallagher, *MORPHOLOGICAL AND PHYSIOLOGICAL-RESPONSES TO INCREASED SALINITY IN MARSH AND DUNE ECOTYPES OF SPOROBOLUS-VIRGINICUS (L) KUNTH.* Oecologia, 1991. **87**(3): p. 330-335.

35. Hayat, S., et al., *Role of proline under changing environments A review.* Plant Signaling & Behavior, 2012. **7**(11): p. 1456-1466.

36. Munns, R., *Genes and salt tolerance: bringing them together.* New Phytologist, 2005. **167**(3): p. 645-663.

37. Shabala S, S.L., *Ion transport and osmotic adjustment in plants and bacteria.* Biomol Concepts. , 2011. **2**(5): p. 407-19.

38. Hare, P.D., W.A. Cress, and J. Van Staden, *Dissecting the roles of osmolyte accumulation during stress.* Plant Cell and Environment, 1998. **21**(6): p. 535-553.

39. Mattioli, R., P. Costantino, and M. Trovato, *Proline accumulation in plants Not only stress.* Plant Signaling & Behavior, 2009. **4**(11): p. 1016-1018.

40. Ueda, A., et al., *Altered expression of barley proline transporter causes different growth responses in Arabidopsis.* Planta, 2008. **227**(2): p. 277-286.

41. Mattioli, R., et al., *The proline biosynthetic genes P5CS1 and P5CS2 play overlapping roles in Arabidopsis flower transition but not in embryo development.* Physiologia Plantarum, 2009. **137**(1): p. 72-85.

42. Rentsch, D., et al., *Salt stress-induced proline transporters and salt stress-repressed broad specificity amino acid permeases identified by suppression of a yeast amino acid permease-targeting mutant.* Plant Cell, 1996. **8**(8): p. 1437-1446.

43. Guo, N., et al., *Overexpression of GmProT1 and GmProT2 increases tolerance to drought and salt stresses in transgenic Arabidopsis.* Journal of Integrative Agriculture, 2016. **15**(8): p. 1727-1743.

44. Michaels, S.D. and R.M. Amasino, *FLOWERING LOCUS C encodes a novel MADS domain protein that acts as a repressor of flowering.* Plant Cell, 1999. **11**(5): p. 949-956.

45. Chen, Q., et al., *Functional FRIGIDA allele enhances drought tolerance by regulating the P5CS1 pathway in Arabidopsis thaliana.* Biochemical and Biophysical Research Communications, 2018. **495**(1): p. 1102-1107.

46. Funck, D., et al., *Requirement of proline synthesis during Arabidopsis reproductive development.* Bmc Plant Biology, 2012. **12**: p. 12.

47. D.E., A., *Cellular Energy Metabolism and its Regulation* New York: Academic Press, 1977.

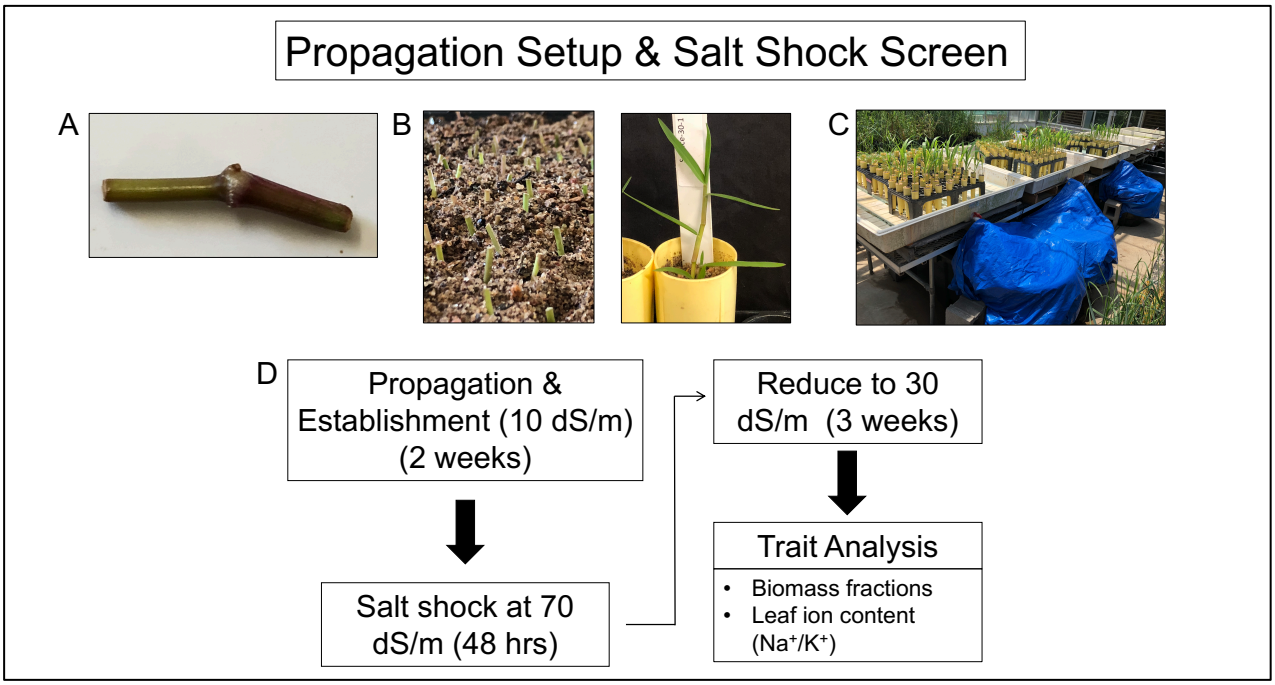

Supplemental Figure 2.1. Propagation setup and salt shock scheme. **(A)** Single nodes from growing stolon segments were cut. **(B)** Nodes were then placed into soil and tafter one week of growth, they were transferred into cone-tainers. **(C)** Plants were grown in ebb & flow irrigation bins placed on metal benches above resevoirs (covered in blue tarp to prevent evaporation), irrigated six times daily and once nightly with control or saltwater solutions. **(D)** Post-propagation and establishment, plants were salt shocked for 48 hours, and then grown at 30 dS/m for three weeks before trait analysis.

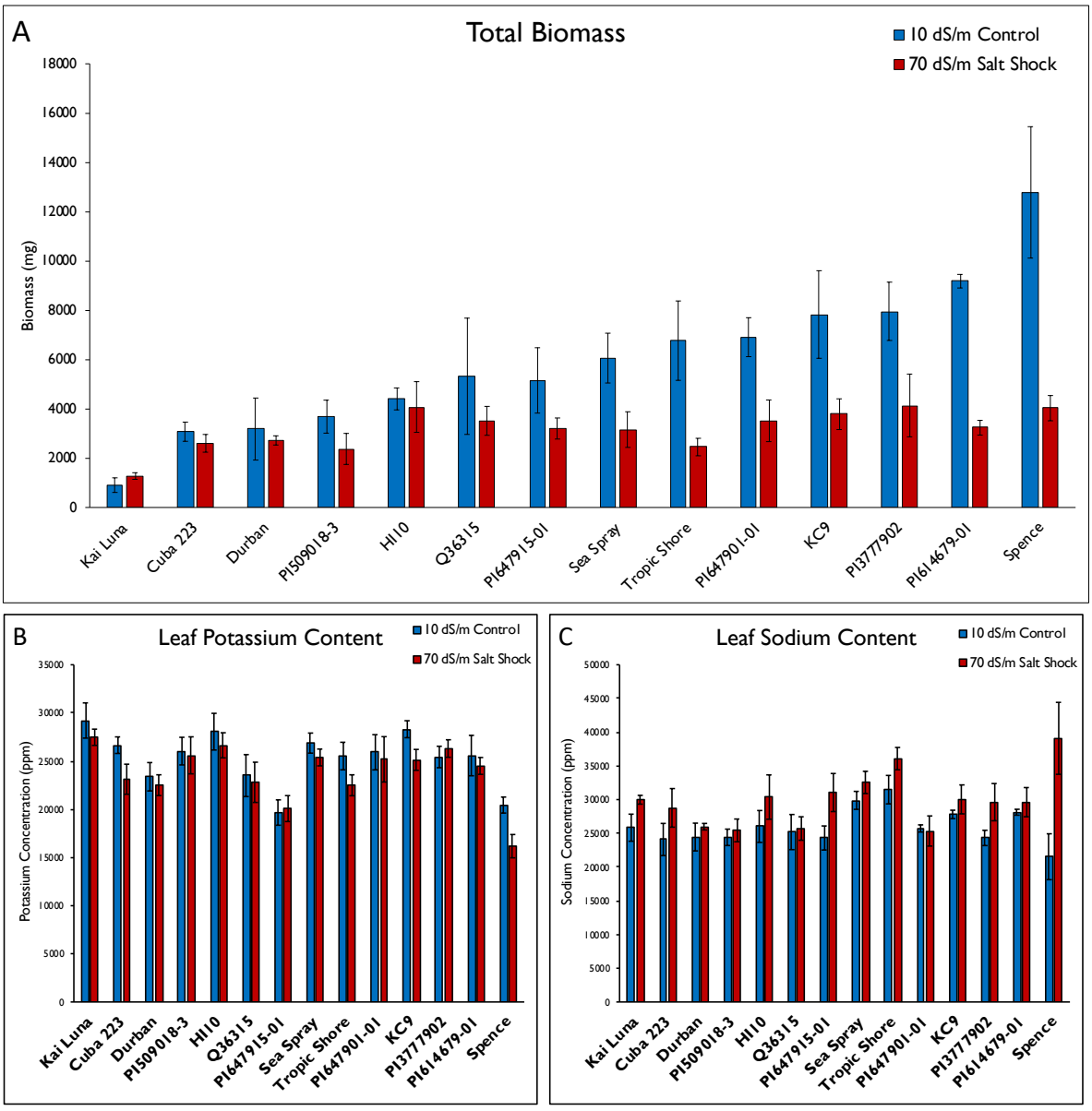

Supplemental Figure 2.2 Total biomass & leaf ion measurements post-salt shock (70 dS/m salt shock followed by 3 weeks at 30 dS/m) for 12 seashore paspalum genotypes and two *P. distichum* genotypes ('Tropic Shore' and 'Spence') in salt screen 1. **(A)** Total biomass including stolon, leaf, and root tissue fractions. **(B)** Leaf potassium content shown in parts per million. **(C)** Leaf sodium content shown in parts per million.

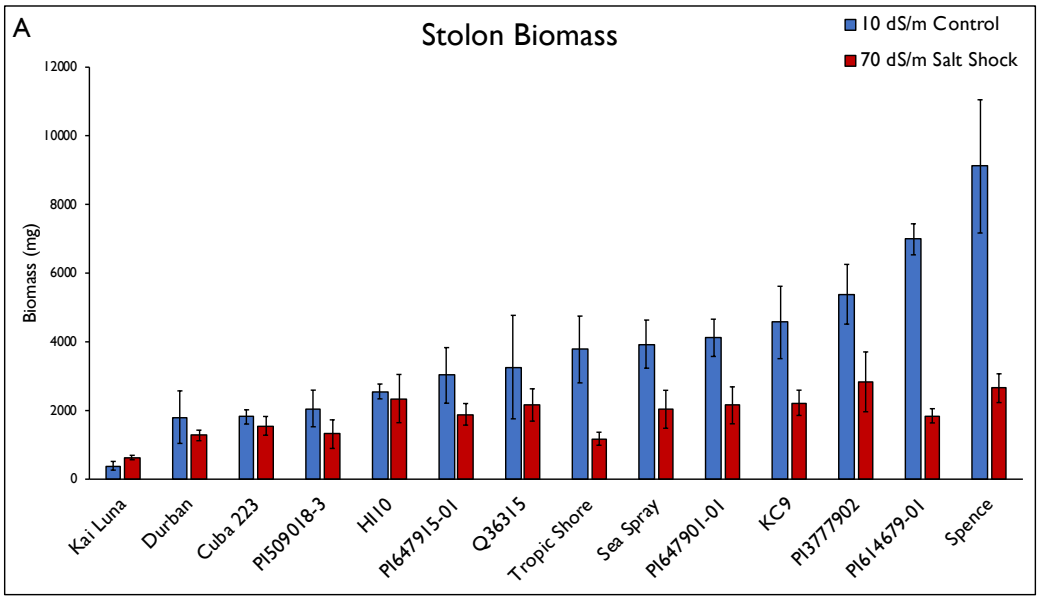
A
Stolon Biomass
10 dS/m Control
70 dS/m Salt Shock
Biomass (mg)
12000
10000
8000
6000
4000
2000
0
Kai Luna
Durban
Cuba 223
PI509018-3
HI10
PI647915-01
Q36315
Tropic Shore
Sea Spray
PI647901-01
KC9
PI3777902
PI614679-01
Spence

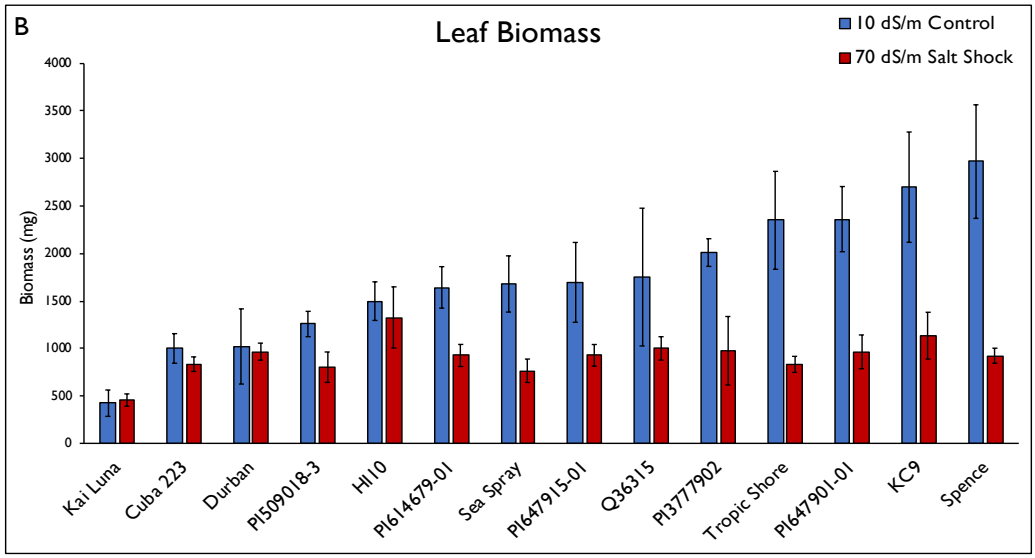
B
Leaf Biomass
10 dS/m Control
70 dS/m Salt Shock
Biomass (mg)
4000
3500
3000
2500
2000
1500
1000
500
0
Kai Luna
Cuba 223
Durban
PI509018-3
HI10
PI614679-01
Sea Spray
PI647915-01
Q36315
PI3777902
Tropic Shore
PI647901-01
KC9
Spence

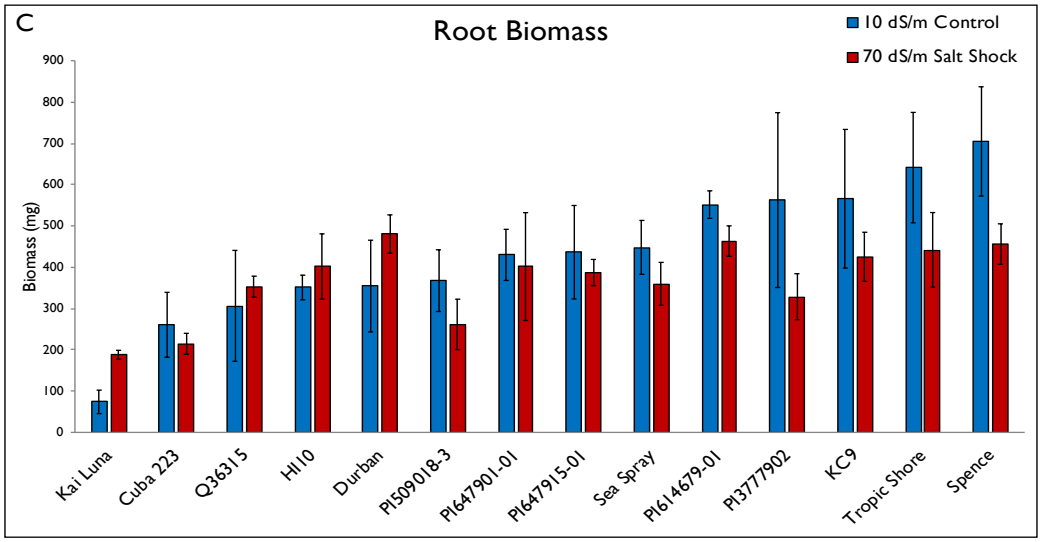
C
Root Biomass
10 dS/m Control
70 dS/m Salt Shock
Biomass (mg)
900
800
700
600
500
400
300
200
100
0
Kai Luna
Cuba 223
Q36315
HI10
Durban
PI509018-3
PI647901-01
PI647915-01
Sea Spray
PI614679-01
PI3777902
KC9
Tropic Shore
Spence

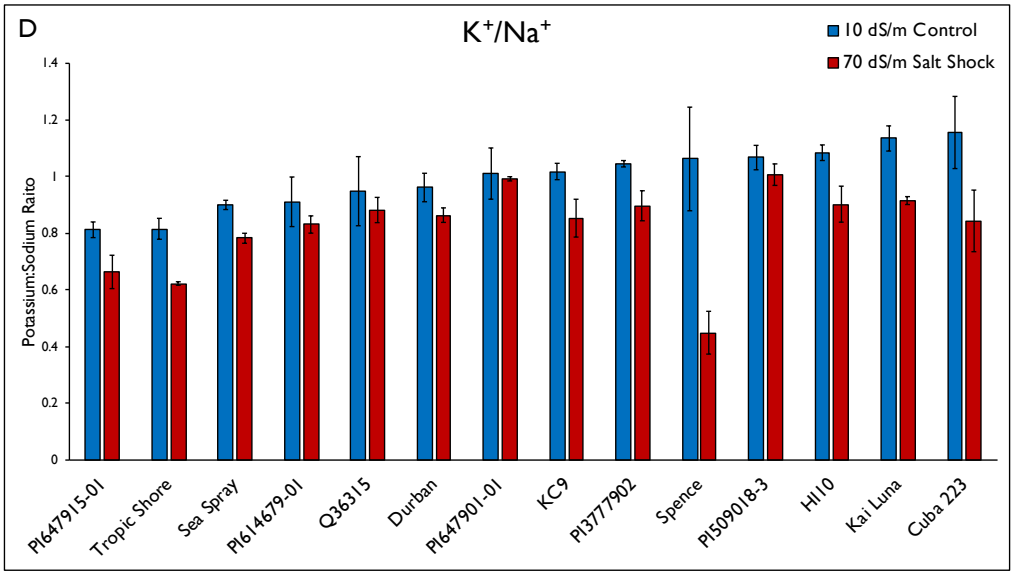

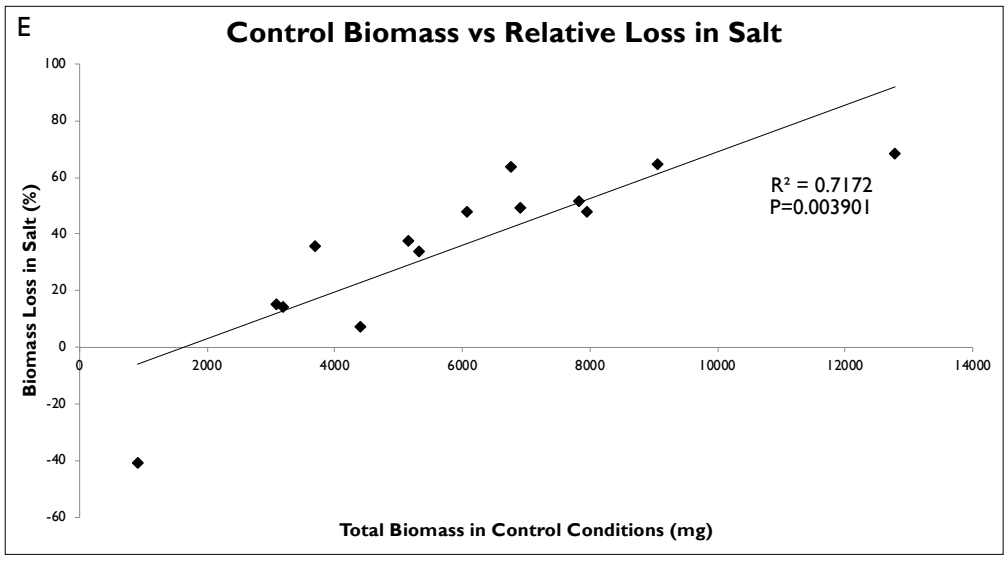

Supplemental Figure 2.3. Biomass fractions, potassium:sodium ratio, and the biomass production versus relative biomass loss in salt conditions post-salt shock (70 dS/m salt shock followed by 3 weeks at 30 dS/m) in salt screen 1. Biomass fractions are shown for **(A)** stolon, **(B)** leaf, and **(C)** root tissue. **(D)** Potassium:sodium ratios for leaf ion content. **(E)** The relationship between biomass production under control (10 dS/m) conditions and the relative biomass loss under salt (70 dS/m salt shock followed by 3 weeks at 30 dS/m. Red dots in **(E)**

indicate genotypes labeled as “sensitive” while green dots indicate genotypes labeled as “tolerant” based on turf quality measures when treating plants as trimmed turf in a large-scale salt screen.

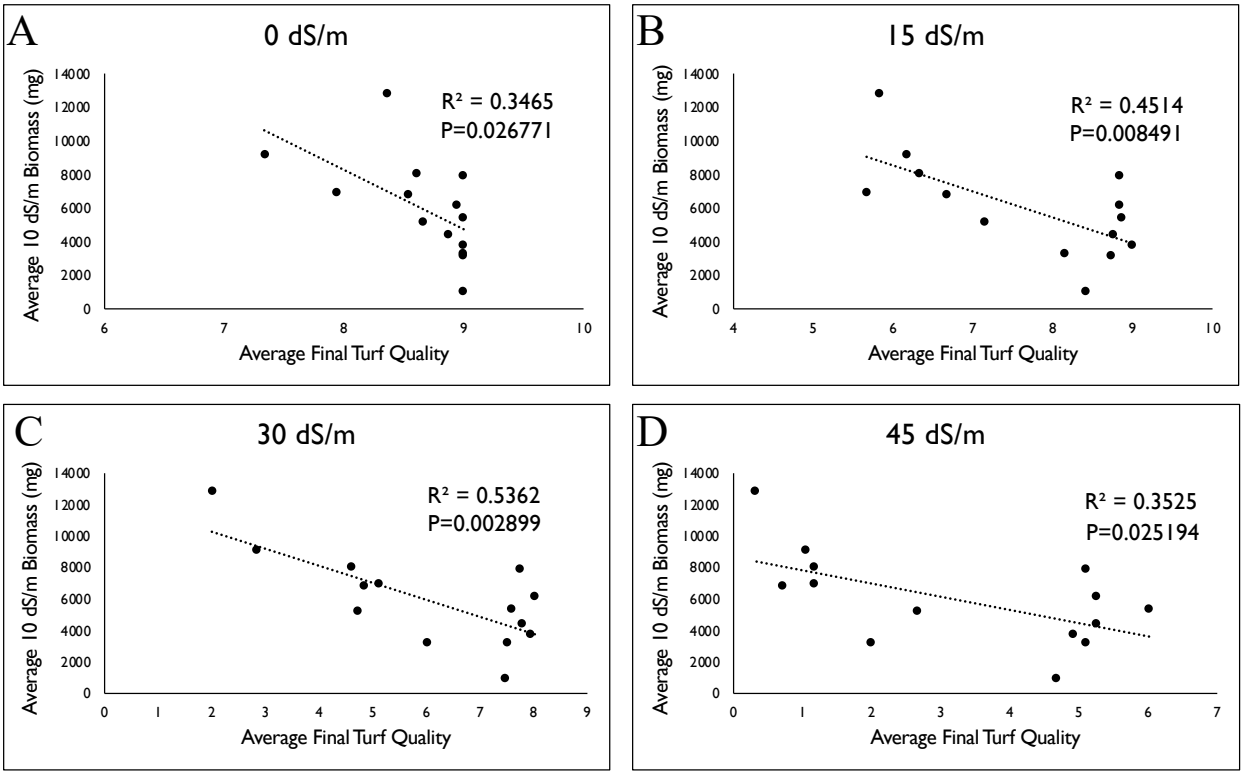

Supplemental Figure 2.4. Relationship between the amount of biomass produced under 10 dS/m control conditions in salt screen 1 and turf quality measurement when treated as trimmed turf in a traditional salt screen. Each dot represents the mean value for individual genotypes.

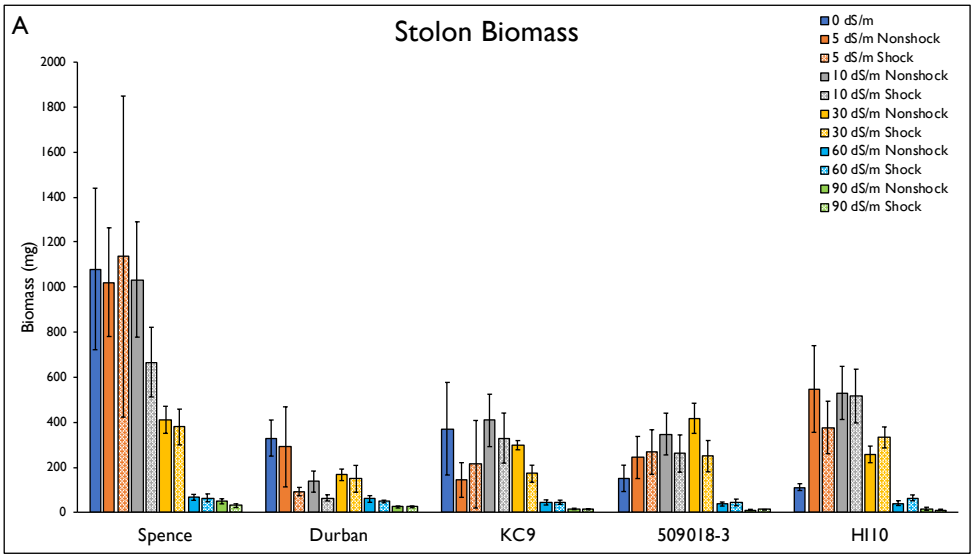
A
Stolon Biomass
Biomass (mg)
0
200
400
600
800
1000
1200
1400
1600
1800
2000
Spence
Durban
KC9
509018-3
HI10
0 dS/m
5 dS/m Nonshock
5 dS/m Shock
10 dS/m Nonshock
10 dS/m Shock
30 dS/m Nonshock
30 dS/m Shock
60 dS/m Nonshock
60 dS/m Shock
90 dS/m Nonshock
90 dS/m Shock

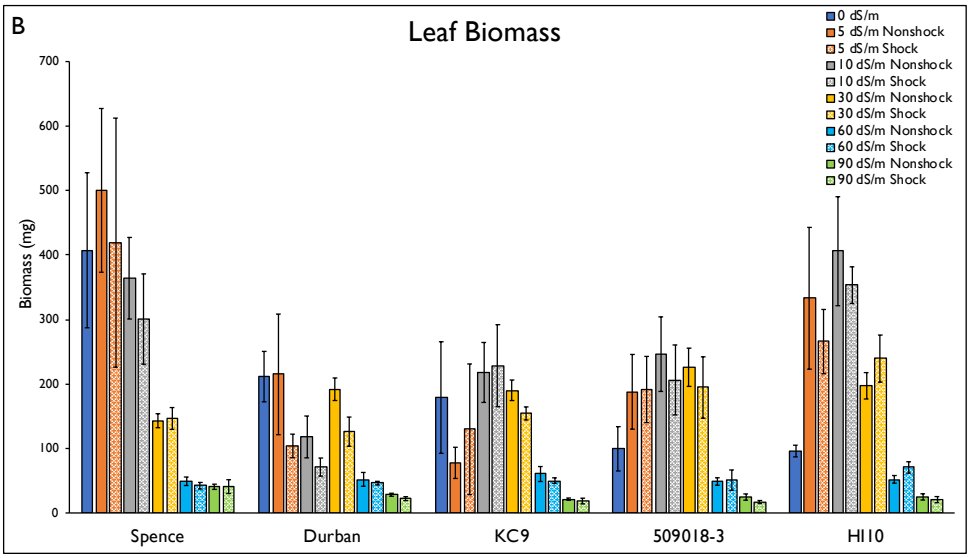
B
Leaf Biomass
Biomass (mg)
0
100
200
300
400
500
600
700
Spence
Durban
KC9
509018-3
HI10
0 dS/m
5 dS/m Nonshock
5 dS/m Shock
10 dS/m Nonshock
10 dS/m Shock
30 dS/m Nonshock
30 dS/m Shock
60 dS/m Nonshock
60 dS/m Shock
90 dS/m Nonshock
90 dS/m Shock

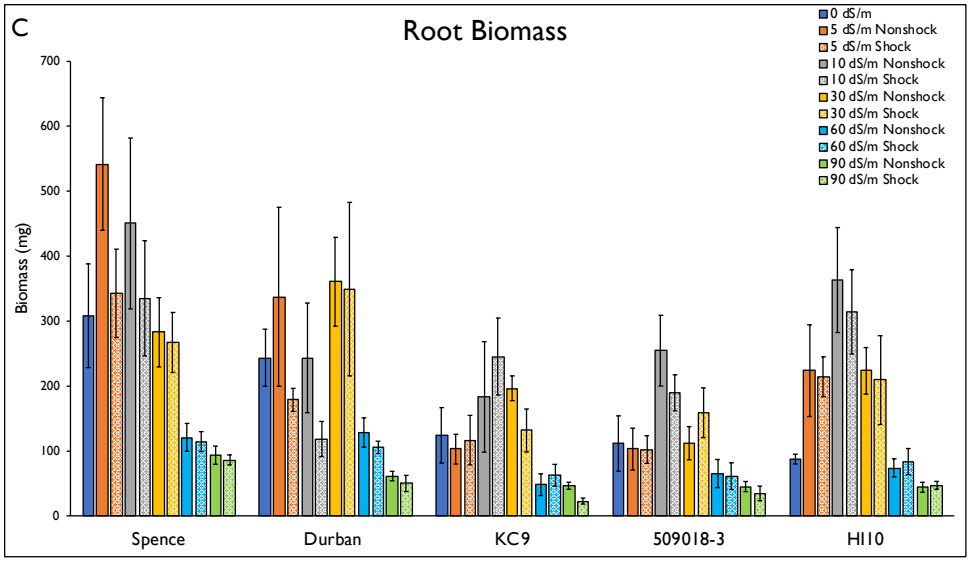
C
Root Biomass
Biomass (mg)
0
100
200
300
400
500
600
700
Spence
Durban
KC9
509018-3
HI10
0 dS/m
5 dS/m Nonshock
5 dS/m Shock
10 dS/m Nonshock
10 dS/m Shock
30 dS/m Nonshock
30 dS/m Shock
60 dS/m Nonshock
60 dS/m Shock
90 dS/m Nonshock
90 dS/m Shock

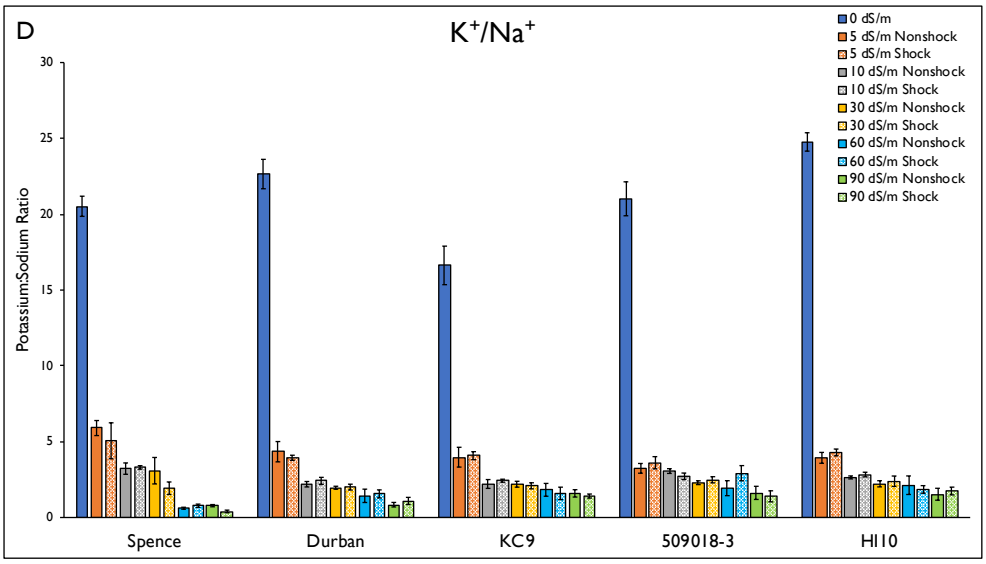

Supplemental Figure 2.5. Biomass fractions and potassium:sodium ratios for plants nonshock and salt shock plants grown at 0-90 dS/m salt concentrations in salt screen 2. One-half of the plants experienced a gradual increase in salt concentration (Nonshock, N ≥ 4 plants) and one-half experienced an immediate increase from 0 dS/m to the final concentration (Shock, N ≥ 4 plants). For paired Nonshock and Shock colored bars in A-D, the bar on the left represents the Nonshock data while the right bar represents Shock data. Biomass fractions are shown for **(A)** stolon, **(B)** leaf, and **(C)** root tissue. **(D)** Potassium:sodium ratios for leaf ion content.

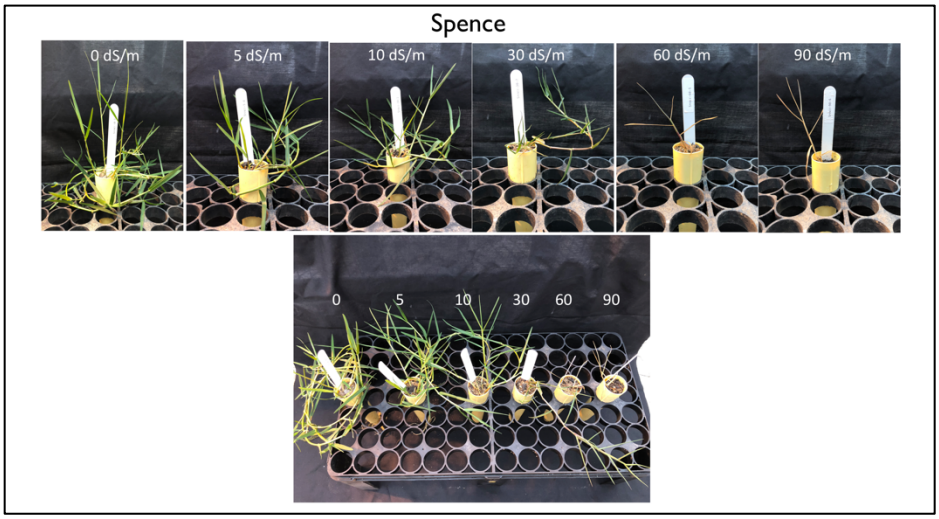
Spence
0 dS/m
5 dS/m
10 dS/m
30 dS/m
60 dS/m
90 dS/m
0
5
10
30
60
90

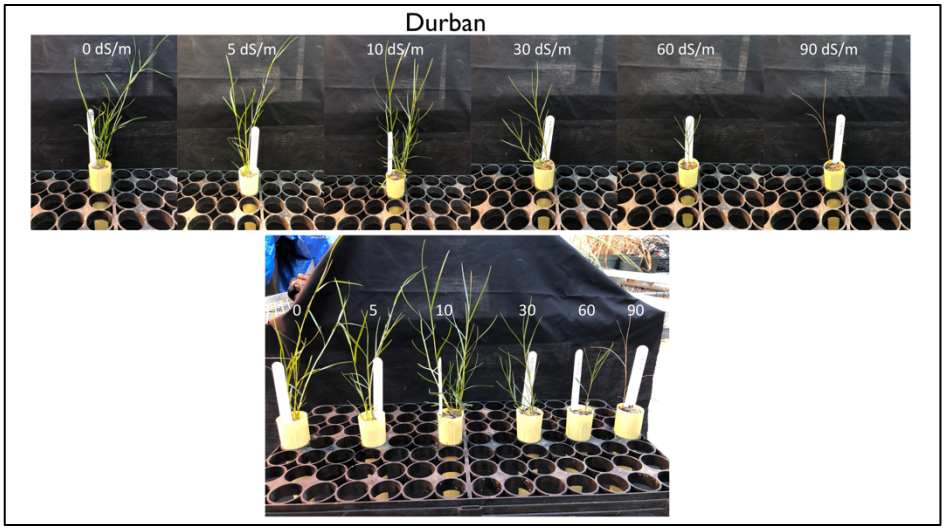
Durban
0 dS/m
5 dS/m
10 dS/m
30 dS/m
60 dS/m
90 dS/m
0
5
10
30
60
90

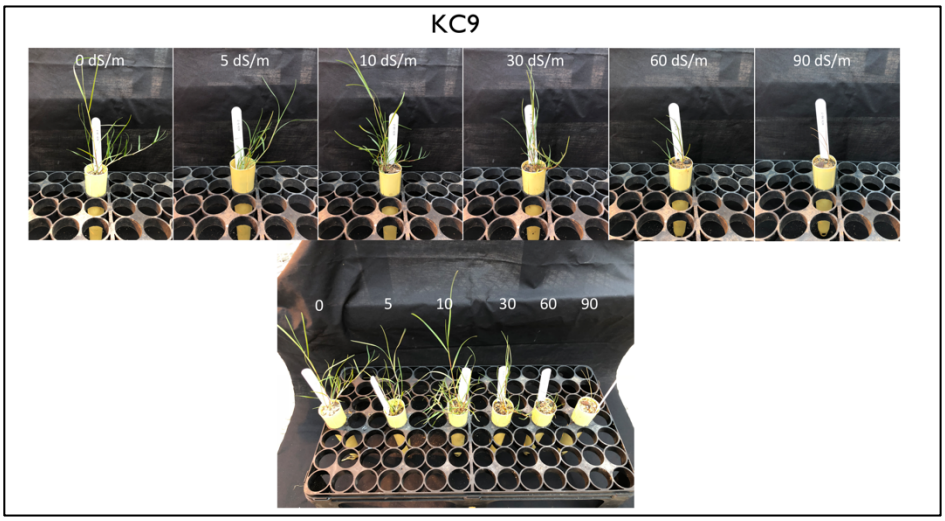
KC9
0 dS/m
5 dS/m
10 dS/m
30 dS/m
60 dS/m
90 dS/m
0
5
10
30
60
90

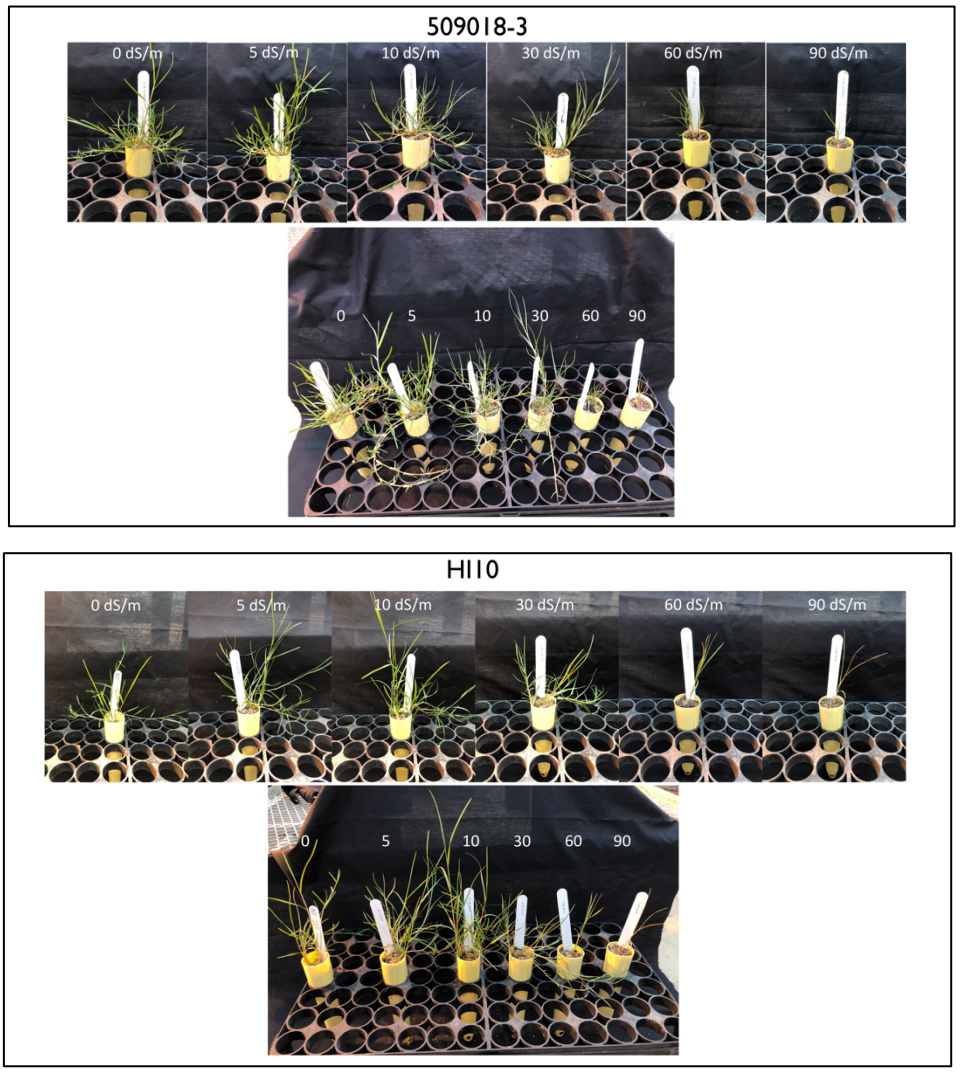

Supplemental Figure 2.6. Images of plants grown at 0-90 dS/m salt concentrations in salt screen 2. The *Paspalum distichum* 'Spence' genotype is shown in addition to the *Paspalum vaginatum* (seashore paspalum) genotypes 'Durban', 'KC9', '509018-3', and 'HI10'.

Supplemental Table 2.1. Raw values for all measured traits in salt screen 1.

Genotype	Stolon	Leaf	Root	Total Biomass	Na	K	K/Na
PI508018-3-control	3126.1	1480.1	372.8	4979	23968.26	27651.61	1.15367615
PI508018-3-control	1489.1	1018.2	235.4	2742.7	22564.305	23179.7	1.02727294
PI508018-3-control	1565	1272.6	494	3331.6	26709.315	27285.06	1.02155596
PI508018-3-salt	356.4	373.7	126.1	856.2	27043.59	26478.65	0.97911002
PI508018-3-salt	932	777.1	251.2	1960.3	28648.11	30657.32	1.07013412
PI508018-3-salt	2237.7	1132	423.4	3793.1	20826.075	22226.67	1.06725199
PI508018-3-salt	1720.4	926.2	245.1	2891.7	25238.505	23033.08	0.91261665
Q36315-control	4583.5	2229.2	342.4	7155.1	22230.03	19660.82	0.88442616
Q36315-control	258.5	325.5	57.9	641.9	22965.435	27211.75	1.18490026
Q36315-control	4953	2699	518.9	8170.9	30386.34	23619.56	0.77730849
Q36315-salt	1628	830.3	426.1	2884.4	29717.79	25159.07	0.84659963
Q36315-salt	2504	841	295.7	3640.7	24369.39	20393.92	0.83686625
Q36315-salt	3748.4	1463.3	400.3	5612	29116.095	26478.65	0.90941625
Q36315-salt	1983	1045	327.5	3355.5	25238.505	26258.72	1.04042296
Q36315-salt	943.4	823.1	314.6	2081.1	20157.525	15702.08	0.77896865
PI647915-control	3460.1	1558	560.2	5578.3	27645.285	21053.71	0.76156603
PI647915-control	1937	1459.1	335.3	3731.4	27845.85	23546.25	0.84559279
PI647915-control	849.3	682.4	131.2	1662.9	18085.02	16215.25	0.89661222
PI647915-control	3203.6	1531	356	5090.6	23232.855	17314.9	0.74527646
PI647915-control	5665	3248.1	798.5	9711.6	24770.52	20173.99	0.81443547
PI647915-salt	1366.2	995.1	331.4	2692.7	39545.475	17388.21	0.43970163
PI647915-salt	1503.1	752	401.2	2656.3	30252.63	20173.99	0.66685078
PI647915-salt	1809.8	633.6	302.2	2745.6	24168.825	18854.41	0.78011281
PI647915-salt	3112.5	1299.4	480.2	4892.1	35066.19	25159.07	0.71747373
PI647915-salt	1654.1	956	420.1	3030.2	26241.33	18781.1	0.71570686
HI10-control	2331.2	1221.5	318.4	3871.1	32057.715	32343.45	1.00891314
HI10-control	2076.9	1142.5	300.2	3519.6	23232.855	26478.65	1.13970711
HI10-control	3041.5	2030.2	435.4	5507.1	21427.77	23619.56	1.10228736
HI10-control	2772.5	1597.4	349.4	4719.3	27377.865	29777.6	1.08765238
HI10-salt	3278.1	1616	498.6	5392.7	39278.055	26991.82	0.68719849
HI10-salt	2075.1	816	240.1	3131.2	23366.565	23619.56	1.01082722
HI10-salt	427.5	331.6	185.3	944.4	23166	24059.42	1.038566
HI10-salt	1488.2	1902	498.5	3888.7	29784.645	27798.23	0.93330741
HI10-salt	4470.7	1967	585.1	7022.8	36336.435	30730.63	0.84572496
Durban-control	2945.4	1473.3	555.9	4974.6	26174.475	22739.84	0.86877922
Durban-control	352.3	231.5	172.6	756.4	20358.09	21200.33	1.04137127

Durban-control	2123.1	1356.8	334.3	3814.2	26843.025	26185.41	0.97550146
Durban-salt	1182.6	1100.6	556.8	2840	25773.345	22373.29	0.86807863
Durban-salt	927.2	1066.1	474	2467.3	26174.475	22446.6	0.85757594
Durban-salt	1323	706	351.7	2380.7	27177.3	25232.38	0.92843586
Durban-salt	1663.7	991.9	538.5	3194.1	24837.375	19954.06	0.80338844
Spence-control	5030.7	1599.2	353	6982.9	17683.89	21933.43	1.24030572
Spence-control	4820	1741.7	451	7012.7	29517.225	17681.45	0.59902142
Spence-control	13889	4593.3	1037.9	19520.2	30052.065	20027.37	0.66642242
Spence-control	8560.8	2874.4	756	12191.2	15811.95	20173.99	1.27586983
Spence-control	13252.3	4030.4	924.9	18207.6	14608.56	22373.29	1.53151919
Spence-salt	3752.4	1055.2	588.4	5396	30319.485	16141.94	0.53239493
Spence-salt	2261	1076.7	386.4	3724.1	57128.34	15115.6	0.26459022
Spence-salt	3240	1024	561.6	4825.6	30586.905	20833.78	0.68113397
Spence-salt	1308.5	731.5	380.7	2420.7	45562.425	14162.57	0.31083881
Spence-salt	2688.3	727.8	362.9	3779	31857.15	14602.43	0.45837214
Cuba223-control	1158.6	803.5	181.8	2143.9	26843.025	29704.29	1.10659249
Cuba223-control	1948.8	555	106.5	2610.3	14809.125	24425.97	1.64938644
Cuba223-control	1947	1244	219.7	3410.7	24235.68	26625.27	1.09859802
Cuba223-control	2407.1	1434.1	562.2	4403.4	27043.59	26551.96	0.98182083
Cuba223-control	1605.6	962.7	232.9	2801.2	27511.575	25965.48	0.94380202
Cuba223-salt	1479.8	752.1	162.1	2394	35667.885	17314.9	0.4854479
Cuba223-salt	941.2	635.6	147.2	1724	33929.655	26112.1	0.76959521
Cuba223-salt	2366	948	276	3590	19956.96	22886.46	1.14679089
Cuba223-salt	1018.7	767.5	233	2019.2	29049.24	25452.31	0.87617817
Cuba223-salt	1962.3	1067.3	254	3283.6	25305.36	23839.49	0.94207275
TropicShore-control	3645.2	2530.9	753.3	6929.4	33127.395	23399.63	0.70635285
TropicShore-control	562.4	531.6	138	1232	27377.865	22153.36	0.80917047
TropicShore-control	3174.3	2067	682.6	5923.9	30453.195	25818.86	0.84782106
TropicShore-control	5301.5	3124.4	695.7	9121.6	27645.285	25745.55	0.93128177
TropicShore-control	6205.1	3491.6	936.2	10632.9	38810.07	30510.7	0.78615421
TropicShore-salt	1551.2	1048.1	623.2	3222.5	39478.62	24572.59	0.62242778
TropicShore-salt	749.1	558.2	195.2	1502.5	38208.375	24352.66	0.63736445
TropicShore-salt	742.3	732.1	327	1801.4	35534.175	21346.95	0.60074421
TropicShore-salt	1633.3	915	674.2	3222.5	37205.55	23399.63	0.62892848
TropicShore-salt	1214	905.5	389.7	2509.2	29985.21	18781.1	0.62634545
KaiLuna-control	188.7	197.5	37.5	423.7	22029.465	25672.24	1.16535921
KaiLuna-control	358.2	396	95	849.2	26642.46	31756.97	1.19196838
KaiLuna-control	625	676.2	144.1	1445.3	28848.675	30217.46	1.04744707
KaiLuna-salt	490.1	295.5	175.5	961.1	31456.02	28604.64	0.90935344

KaiLuna-salt	561.2	382.1	155	1098.3	30854.325	28384.71	0.91995887
KaiLuna-salt	768.5	582.4	215.2	1566.1	29784.645	28677.95	0.96284344
KaiLuna-salt	531.5	383	204.6	1119.1	27645.285	24206.04	0.87559379
KaiLuna-salt	803.1	635.8	190.3	1629.2	30185.775	27504.99	0.91119045
PI614679-control	6112.2	1975.5	541.8	8629.5	28982.385	22446.6	0.77449113
PI614679-control	7622.7	1365	499.5	9487.2	27511.575	29557.67	1.07437215
PI614679-control	7223.6	1588	613.4	9425	27912.705	24719.21	0.88558991
PI614679-salt	1752	985	529.3	3266.3	28781.82	24059.42	0.8359242
PI614679-salt	1543	701	458.1	2702.1	26375.04	23253.01	0.88162937
PI614679-salt	2243	1091	402.5	3736.5	33729.09	26185.41	0.77634499
KC9-control	3359	2509.1	296.2	6164.3	26843.025	25672.24	0.95638401
KC9-control	2589.3	1252.9	342.8	4185	27778.995	29044.5	1.04555618
KC9-control	7363.8	4059.1	1029.3	12452.2	29584.08	29191.12	0.98671718
KC9-control	4946.5	2972.2	594.8	8513.5	27043.59	29337.74	1.08483156
KC9-salt	3176.5	1842.1	552	5570.6	38074.665	22519.91	0.59146706
KC9-salt	1584.1	438.1	562	2584.2	27845.85	25452.31	0.91404321
KC9-salt	1323.3	777.8	245	2346.1	26174.475	23033.08	0.8799825
KC9-salt	2068.1	1162.2	382.3	3612.6	30787.47	28458.02	0.92433773
KC9-salt	2970	1452	384.6	4806.6	27311.01	26185.41	0.95878585
PI647901-control	3627.3	1676.1	426.9	5730.3	25037.94	28458.02	1.1365959
PI647901-control	5201.5	2670	538.5	8410	25372.215	26918.51	1.06094442
PI647901-control	3523.5	2739.1	324.1	6586.7	26776.17	22373.29	0.83556722
PI647901-salt	3197.8	1293	658.8	5149.6	29450.37	29411.05	0.99866487
PI647901-salt	1410	681.2	233.6	2324.8	24837.375	24865.83	1.00114565
PI647901-salt	1846.1	917.1	312.1	3075.3	21762.045	21273.64	0.97755703
PI3777902-control	6450.3	2161	530.1	9141.4	26508.75	27651.61	1.04311256
PI3777902-control	3662	1718.1	213.1	5593.2	23767.695	24425.97	1.02769621
PI3777902-control	6046.4	2150	944.4	9140.8	22698.015	24206.04	1.06643863
PI3777902-salt	3391.5	970.1	331	4692.6	26508.75	24719.21	0.93249248
PI3777902-salt	3987.7	1603.1	423.8	6014.6	35133.045	27871.54	0.7933141
PI3777902-salt	1126.4	353.2	231	1710.6	27244.155	26332.03	0.96652034
SeaSpray-control	3211.6	1168.5	351.2	4731.3	26308.185	23839.49	0.90616247
SeaSpray-control	2975.5	1327.6	379.1	4682.2	30252.63	28458.02	0.94067921
SeaSpray-control	3218.4	1004	273.4	4495.8	26174.475	23399.63	0.8939866
SeaSpray-control	6389.1	2183.1	529.3	9101.5	29918.355	28384.71	0.94873899
SeaSpray-control	5742.4	2903.4	724.2	9370	34464.495	29191.12	0.84699108
SeaSpray-control	2066.7	1486	430.7	3983.4	32258.28	27944.85	0.86628456
SeaSpray-salt	2624.5	750.7	396.3	3771.5	26909.88	22373.29	0.83141545
SeaSpray-salt	3939	1244.7	548.5	5732.2	33862.8	25012.45	0.73864093

SeaSpray-salt	1426.4	632	285.2	2343.6	36737.565	27578.3	0.75068394
SeaSpray-salt	1066.8	619.1	291.9	1977.8	31322.31	25452.31	0.81259364
SeaSpray-salt	1122	576.4	276.3	1974.7	33929.655	26478.65	0.78039844

Supplemental Table 2.2. One-way ANOVA analyses conducted for freshwater control samples for total biomass, sodium content, potassium content, and K^+:Na^+ ratio in salt screen 1.

Genotype	Total Biomass Ave.	Significance Group (p<0.05)
Spence-control	12782.92	a
PI614679-control	9180.5667	ab
PI3777902-control	7958.4667	ab
KC9-control	7828.75	ab
PI647901-control	6909	ab
TropicShore-control	6767.96	ab
SeaSpray-control	6060.7	b
Q36315-control	5322.6333	b
PI647915-control	5154.96	b
HI10-control	4404.275	b
PI508018-3-control	3684.4333	b
Durban-control	3181.7333	b
Cuba223-control	3073.9	b
KaiLuna-control	906.0667	b

Genotype	Sodium Ave.	Significance Group (p<0.05)
TropicShore-control	31482.76	a
SeaSpray-control	29896.07	ab
PI614679-control	28135.56	ab
KC9-control	27812.42	ab
HI10-control	26024.05	ab
KaiLuna-control	25840.2	ab
PI647901-control	25728.77	ab
Q36315-control	25193.94	ab
Durban-control	24458.53	ab
PI508018-3-control	24413.96	ab
PI3777902-control	24324.82	ab
PI647915-control	24315.91	ab
Cuba223-control	24088.6	ab
Spence-control	21534.74	b

Genotype	Potassium Ave.	Significance Group (p<0.05)
KaiLuna-control	29215.56	a
KC9-control	28311.4	a
HI10-control	28054.82	a
SeaSpray-control	26869.64	a
Cuba223-control	26654.59	ab
PI508018-3-control	26038.79	abc
PI647901-control	25916.61	abc
PI614679-control	25574.49	abc

Genotype	Potassium:Sodium Ratio Ave.	Significance Group (p<0.05)
Cuba223-control	1.15604	a
KaiLuna-control	1.1349249	a
HI10-control	1.08464	a
PI508018-3-control	1.0675017	a
Spence-control	1.0626277	a
PI3777902-control	1.0457491	a
KC9-control	1.0183722	a
PI647901-control	1.0110358	a

TropicShore -control	25525.62	abc
PI3777902- control	25427.87	abc
Q36315- control	23497.38	abc
Durban -control	23375.19	abc
Spence- control	20437.91	bc
PI647915- control	19660.82	c

Durban- control	0.961884	a
Q36315- control	0.9488783	a
PI614679- control	0.9114844	a
SeaSpray- control	0.9004738	a
TropicShore -control	0.8161561	a
PI647915- control	0.8126966	a

Total Biomass	Df	Sum of Sq	RSS	AIC	Fvalue	Pr(>F)
<none>			361759393	891.45		
Genotype	13	465847355	827606747	910.97	4.0613	0.0002834

Sodium	Df	Sum of Sq	RSS	AIC	Fvalue	Pr(>F)
<none>			733732905	930.35		
Genotype	13	4.25E+08	1158736272	929.48	1.8268	0.07128

Potassium	Df	Sum of Sq	RSS	AIC	Fvalue	Pr(>F)
<none>			317305925	884.24		
Genotype	13	437236082	754542008	905.89	4.3459	0.0001483

Potassium/Sodium	Df	Sum of Sq	RSS	AIC	Fvalue	Pr(>F)
<none>			1.2863	-178.56		
Genotype	13	0.67684	1.9631	-181.3	1.6596	0.108

Supplemental Table 2.3. One-way ANOVA analyses conducted for salt-treated samples for total biomass, sodium content, potassium content, and potassium:sodium ratio in salt screen 1.

Genotype	Total Biomass Ave.	Significance Group (p<0.05)
PI3777902-salt	4139.267	a
HI10-salt	4075.96	a
Spence-salt	4029.08	a
KC9-salt	3784.02	a
PI647901-salt	3516.567	a
Q36315-salt	3514.74	a
PI614679-salt	3234.967	a
PI647915-salt	3203.38	a
SeaSpray-salt	3159.96	a
Durban-salt	2720.525	a
Cuba223-salt	2602.16	a
TropicShore-salt	2451.62	a
PI508018-3-salt	2375.325	a
KaiLuna-salt	1274.76	a

Genotype	Sodium Ave.	Significance Group (p<0.05)
Spence-salt	39090.86	a
TropicShore-salt	36082.39	ab
SeaSpray-salt	32552.44	ab
PI647915-salt	31054.89	ab
HI10-salt	30386.34	ab
KC9-salt	30038.69	ab
KaiLuna-salt	29985.21	ab
PI3777902-salt	29628.65	ab
PI614679-salt	29628.65	ab
Cuba223-salt	28781.82	ab
Durban-salt	25990.62	ab
Q36315-salt	25719.86	b
PI508018-3-salt	25439.07	b
PI647901-salt	25349.93	b

Genotype	Potassium Ave.	Significance Group (p<0.05)
KaiLuna-salt	27475.67	a
HI10-salt	26639.93	a
PI3777902-salt	26307.59	ab
PI508018-3-salt	25598.93	ab
SeaSpray-salt	25379	ab
PI647901-salt	25183.51	ab
KC9-salt	25129.75	ab
PI614679-salt	24499.28	ab

Genotype	Potassium:Sodium Ratio Ave.	Significance Group (p<0.05)
PI508018-3-salt	1.0072782	a
PI647901-salt	0.9924559	a
KaiLuna-salt	0.915788	ab
HI10-salt	0.9031248	ab
PI3777902-salt	0.8974423	abc
Q36315-salt	0.8824547	abc
Durban-salt	0.8643697	abc
KC9-salt	0.8537233	abc

Cuba223-salt	23121.05	ab
Q36315-salt	22798.49	ab
Durban-salt	22501.58	abc
TropicShore-salt	22490.59	abc
PI647915-salt	20071.36	bc
Spence-salt	16171.26	c

Cuba223-salt	0.844017	abc
PI614679-salt	0.8312995	abc
SeaSpray-salt	0.7827465	abc
PI647915-salt	0.6639692	bcd
TropicShore-salt	0.6231621	cd
Spence-salt	0.449466	d

Total Biomass	Df	Sum of Sq	RSS	AIC	Fvalue	Pr(>F)
<none>			80363270	900.65		
Genotype	13	38811392	119174662	899.08	1.7832	0.07374

Sodium	Df	Sum of Sq	RSS	AIC	Fvalue	Pr(>F)
<none>			1519791237	1082.9		
Genotype	13	944085306	2463876543	1086.9	2.2936	0.01876

Potassium	Df	Sum of Sq	RSS	AIC	Fvalue	Pr(>F)
<none>			413226089	1002.2		
Genotype	13	550081473	963307562	1028.6	4.9152	2.22E-05

Potassium:sodium	Df	Sum of Sq	RSS	AIC	Fvalue	Pr(>F)
<none>			0.68828	-251.04		
Genotype	13	1.3674	2.05566	-209.21	7.3353	1.27E-07

Supplementary Table 2.4. Final turf quality scores after 8 weeks under salt stress in a traditional salt screen. Scores are from a 0-9 scale with 0= no green tissue and 9=optimum quality.

Genotype	Final Ave. Turf Quality - 0 dS/m	Final Ave. Turf Quality - 15 dS/m	Final Ave. Turf Quality - 30 dS/m	Final Ave. Turf Quality - 45 dS/m
364981	9	3.166666667	0	0
647922	7.666666667	4.5	1.333333333	0.166666667
645598	7.9	6.166666667	6.166666667	0.333333333
Spence	8.366666667	5.833333333	2	0.333333333
576140	8.6	6.9	4.066666667	0.5
647917	8.333333333	7.2	4.766666667	0.666666667
Tropical Shore	8.533333333	6.666666667	4.833333333	0.733333333
Q 40522	7.5	5.6	3.266666667	0.833333333
647918	8.533333333	7	5.833333333	0.9
614679	7.333333333	6.166666667	2.833333333	1.066666667
377709	8.6	6.333333333	4.6	1.166666667
647901	7.933333333	5.666666667	5.1	1.166666667
Bahama	8.766666667	6.6	4.333333333	1.5
HI 36	8.666666667	7.166666667	5	1.566666667
299042	8.833333333	7.5	5.933333333	1.666666667
Q 37956	9	8.433333333	6	1.666666667
Aloha	8.333333333	7.166666667	6.233333333	1.833333333
Durban	9	8.166666667	6	2
647923	8.033333333	6.166666667	5	2.066666667
647900	8.266666667	6.766666667	4.166666667	2.166666667
Taylor 2	9	8.033333333	5.333333333	2.166666667
647913	8.8	6.5	6	2.266666667
HI 14	8.5	7.5	7.1	2.433333333
647921	8.6	5.666666667	5.166666667	2.5
Sea Isle Supreme	8.333333333	7.166666667	6.6	2.5
Talia Fera	8.933333333	8.1	6.766666667	2.5
647915	8.666666667	7.166666667	4.733333333	2.666666667
647919	8.8	6.766666667	5.9	3
FSP1	8.766666667	7.433333333	5.766666667	3
Temple 2	8.833333333	8	5.5	3
Sea Isle 1	8.433333333	7.333333333	6.833333333	3.166666667

TG Kona	8.833333333	8.333333333	6.266666667	3.166666667
509022	9	8.433333333	6.166666667	3.333333333
Sea Isle 2000	8.5	7	5.733333333	3.333333333
Salam	9	8.366666667	6.9	3.5
Taylor 1	8.933333333	8.1	6.833333333	3.5
Temple 1	9	7.666666667	6.333333333	3.5
FR-4	8.6	8.433333333	6.5	3.666666667
Seadwarf	8.933333333	8.766666667	7.833333333	3.666666667
TCR6	9	8.866666667	7.433333333	3.666666667
TOCGC	9	8.6	7.1	3.666666667
Hignight S ?	9	8.5	6.266666667	3.766666667
509020	9	7.7	5.666666667	3.833333333
576134	9	7.766666667	6.266666667	3.833333333
Polo	8.833333333	7.366666667	5.666666667	3.833333333
TF P7-4	9	8.166666667	8.1	3.833333333
647920	8.766666667	7.733333333	5.433333333	3.9
576138	9	8.233333333	6.266666667	4
276245	8.333333333	7.4	6.333333333	4.1
509021	9	8.5	7.5	4.166666667
Adalayd	9	8.733333333	7.533333333	4.166666667
Collier	9	8.666666667	7.833333333	4.166666667
Excalibur	8.833333333	8.5	7.1	4.166666667
HI 39	8.933333333	8.766666667	7.933333333	4.166666667
Q 36313	9	8.766666667	7.1	4.266666667
509023	8.833333333	7.866666667	6.333333333	4.333333333
Belize	8.933333333	7.933333333	6.433333333	4.333333333
HI 26	9	8.533333333	7.433333333	4.333333333
HI 32	9	8.733333333	7.6	4.333333333
HYB 7	9	8.166666667	7.5	4.333333333
HI 101	9	8.533333333	7.166666667	4.4
364368	8.9	8.833333333	7.6	4.433333333
Cal	9	8.1	7.366666667	4.5
K8	9	7.766666667	7.5	4.5
SIPV28-1	8.766666667	8	6.266666667	4.5
Vero Beach	8.933333333	8.6	7.033333333	4.5
561-79	8.766666667	7.833333333	7.066666667	4.566666667
TCR 3	9	8.5	7.933333333	4.6
647908	9	8.6	7.9	4.666666667

Cloister	9	8.7	7.733333333	4.666666667
Kai Luna	9	8.433333333	7.466666667	4.666666667
647914	9	8.766666667	7.566666667	4.766666667
HI 33	9	8.6	8.1	4.766666667
HYB 5	9	8.433333333	7.6	4.766666667
HH	9	8.533333333	7	4.833333333
Prince	9	8.666666667	7.666666667	4.833333333
TYB2	8.933333333	8.7	7.333333333	4.833333333
509018-3	9	9	7.933333333	4.933333333
509018-2	9	8.433333333	6.9	5
Wai Lua Kauai	9	8.933333333	6.933333333	5
Cuba 223	9	8.733333333	7.5	5.1
KC9	9	8.833333333	7.733333333	5.1
310-79	9	8.666666667	7.233333333	5.166666667
Kim1	8.866666667	8.933333333	6.433333333	5.166666667
Q 36315	9	8.866666667	7.6	5.2
HI 10	8.866666667	8.766666667	7.8	5.266666667
Sea Spray	8.933333333	8.833333333	8.033333333	5.266666667
Utah1	9	8.766666667	5.933333333	5.433333333

Supplemental Table 2.5. Two-tailed t-tests were conducted between trait values obtained for 10 dS/m control and 70 dS/m^{48hrs} plants in salt screen 1. Cells highlighted in yellow indicate $p<0.05$ and cells highlighted in orange indicate $p<0.01$.

Genotype	Total Biomass	Leaf Na	Leaf K	Leaf K/Na
509018-3	0.219069956	0.666671419	0.870851646	0.343809198
Q36315	0.376204841	0.866587336	0.834748725	0.557943151
PI647915	0.198844572	0.078369447	0.832872425	0.051546308
HI10	0.797222787	0.340784052	0.546294008	0.048297102
Durban	0.685896466	0.437314238	0.643395761	0.118842391
Spence	0.01214639	0.024118207	0.019766295	0.014682628
Cuba223	0.399868954	0.243678064	0.082489823	0.099457359
Tropic Shore	0.030760605	0.124642753	0.129677568	0.000866823
Kai Luna	0.238068882	0.0510519	0.357219133	0.001093178
PI614679	0.000127736	0.536123872	0.660701829	0.435772817
KC9	0.050292597	0.402224878	0.0646806	0.07807511
PI647901	0.042694433	0.876985618	0.817777175	0.847724345
PI3777902	0.092847625	0.150189437	0.573816504	0.052012829
Sea Spray	0.051675423	0.236734433	0.313284671	0.000871979

Supplemental Table 2.6. Raw values for all measured traits in salt screen 2.

Genotype	Salt	Treatment	Stolon	Leaf	Root	TotalBiomass	Na	K	K/Na
Spence	0dS/m	control	2161.5	642.5	308	3112	1846.017	37494.162	20.3108433
Spence	0dS/m	control	58.3	48.7	117.5	224.5	1602.342	36591.552	22.8362934
Spence	0dS/m	control	360.1	150.5	364.9	875.5	1724.1795	27204.408	15.7781762
Spence	0dS/m	control	3535.3	1287.3	979.4	5802	1724.1795	36411.03	21.1178882
Spence	0dS/m	control	1327.1	484	137.2	1948.3	1724.1795	34605.81	20.0708859
Spence	0dS/m	control	239.2	127.2	250.4	616.8	1724.1795	37674.684	21.8507899
Spence	0dS/m	control	185.7	160.3	157.9	503.9	1724.1795	33703.2	19.5473847
Spence	0dS/m	control	1242.5	482.4	373.1	2098	1602.342	34064.244	21.2590346
Spence	0dS/m	control	97	102.7	173.8	373.5	1724.1795	39840.948	23.1071927
Spence	0dS/m	control	1603.7	588.2	220.1	2412	1724.1795	33342.156	19.3379842
Spence	5dS/m	nonshock	288.7	137	233.5	659.2	4648.2795	28829.106	6.20210252
Spence	5dS/m	nonshock	1544.9	843.8	543	2931.7	7572.3795	29912.238	3.95017682
Spence	5dS/m	nonshock	1239.6	526.6	576.4	2342.6	5622.9795	34605.81	6.15435464
Spence	5dS/m	nonshock	626.7	307.4	485.1	1419.2	4770.117	31536.936	6.61135482
Spence	5dS/m	nonshock	1412	686.4	872	2970.4	4770.117	31356.414	6.57351046
Spence	5dS/m	shock	521.2	299.9	353	1174.1	5013.792	37133.118	7.40619435
Spence	5dS/m	shock	970.3	459.8	373.1	1803.2	12080.367	25399.188	2.10251791
Spence	5dS/m	shock	132	67.8	176.1	375.9	5622.9795	34244.766	6.09014598
Spence	5dS/m	shock	134.7	127.3	238.1	500.1	4282.767	31536.936	7.3636824
Spence	5dS/m	shock	3922.1	1141.2	573.1	5636.4	12202.2045	28468.062	2.33302613
Spence	10dS/m	nonshock	967.9	484.1	617.1	2069.1	9765.4545	30453.804	3.11852398
Spence	10dS/m	nonshock	401	151.8	65.3	618.1	13055.067	29370.672	2.24975268
Spence	10dS/m	nonshock	1947	499.4	291.6	2738	9765.4545	25579.71	2.61940804
Spence	10dS/m	nonshock	766.9	316.6	831.3	1914.8	6354.0045	27023.886	4.25304798
Spence	10dS/m	nonshock	1088.7	368.1	446.4	1903.2	8181.567	31717.458	3.87669721
Spence	10dS/m	shock	193.1	110	182.6	485.7	9278.1045	30814.848	3.3212439
Spence	10dS/m	shock	428	156.9	92.5	677.4	8547.0795	26843.364	3.14064752
Spence	10dS/m	shock	976.7	449.6	407.7	1834	8668.917	25760.232	2.97156288
Spence	10dS/m	shock	969	365.2	400.1	1734.3	7450.542	26662.842	3.57864461
Spence	10dS/m	shock	768.9	421.9	592.2	1783	7816.0545	27384.93	3.50367695
Spence	30dS/m	nonshock	525.1	135.3	414.1	1074.5	7450.542	34064.244	4.57204912
Spence	30dS/m	nonshock	308.9	175.3	242.1	726.3	22436.5545	22510.836	1.00331074
Spence	30dS/m	nonshock	504.1	128.4	162.6	795.1	11836.692	27023.886	2.28306067
Spence	30dS/m	nonshock	304.8	133.2	312	750	5622.9795	25218.666	4.48492939
Spence	30dS/m	shock	370.2	113.8	235.2	719.2	8303.4045	27384.93	3.29803637
Spence	30dS/m	shock	647.5	202.6	338.7	1188.8	13055.067	30814.848	2.36037456

Spence	30dS/m	shock	435.9	168.4	401.1	1005.4	15004.467	26482.32	1.76496239
Spence	30dS/m	shock	205.9	125.4	222.3	553.6	21340.017	23955.012	1.1225395
Spence	30dS/m	shock	234.3	122.6	138	494.9	20730.8295	22871.88	1.10327857
Spence	60dS/m	nonshock	83.6	47.1	180.6	311.3	38275.4295	28287.54	0.73905219
Spence	60dS/m	nonshock	108.6	75	150.9	334.5	66785.4045	24135.534	0.36138935
Spence	60dS/m	nonshock	53.8	41.4	112.2	207.4	34376.6295	21969.27	0.63907574
Spence	60dS/m	nonshock	35	38.8	107	180.8	34863.9795	23413.446	0.67156551
Spence	60dS/m	nonshock	49.7	43.5	54.1	147.3	26579.0295	17095.176	0.64318285
Spence	60dS/m	shock	31.3	30.4	86.3	148	37300.7295	32800.59	0.87935519
Spence	60dS/m	shock	52	38.1	95.5	185.6	41565.042	33703.2	0.81085447
Spence	60dS/m	shock	113.3	46.4	155.2	314.9	31939.8795	30273.282	0.9478208
Spence	60dS/m	shock	59.8	54	120.3	234.1	50459.1795	23232.924	0.46043008
Spence	90dS/m	nonshock	79.1	42.5	133.3	254.9	27797.4045	21608.226	0.77734689
Spence	90dS/m	nonshock	27.1	31	78.5	136.6	-	-	-
Spence	90dS/m	nonshock	73.4	41.9	120.4	235.7	27431.892	25038.144	0.9127385
Spence	90dS/m	nonshock	26.8	52.4	62.5	141.7	39981.1545	23052.402	0.5765817
Spence	90dS/m	nonshock	32.6	39	72.4	144	19634.292	16734.132	0.85229108
Spence	90dS/m	shock	60.1	83.3	115.5	258.9	79822.017	18178.308	0.22773551
Spence	90dS/m	shock	31.8	29.3	83.6	144.7	67638.267	21247.182	0.3141296
Spence	90dS/m	shock	16.4	25.2	76.2	117.8	46804.0545	18900.396	0.40381963
Spence	90dS/m	shock	18.5	31.5	71	121	69222.1545	22871.88	0.33041271
Spence	90dS/m	shock	19.4	35	84.7	139.1	36447.867	26482.32	0.72658079
Durban	0dS/m	control	466.1	324.5	417.1	1207.7	1846.017	50311.224	27.2539332
Durban	0dS/m	control	791	392	421.1	1604.1	1967.8545	42368.256	21.5301772
Durban	0dS/m	control	80.9	40.5	56.8	178.2	1967.8545	36952.596	18.7781139
Durban	0dS/m	control	185.1	132.9	213.4	531.4	1724.1795	38757.816	22.4789913
Durban	0dS/m	control	163.8	109.9	-	-	2089.692	40743.558	19.4973987
Durban	0dS/m	control	611.5	330.6	300.2	1242.3	1967.8545	42909.822	21.8053835
Durban	0dS/m	control	229.2	215.2	120.5	564.9	1846.017	52296.966	28.3296232
Durban	0dS/m	control	125.8	99.8	144.1	369.7	1846.017	39479.904	21.3865333
Durban	0dS/m	control	263.6	206.9	340.4	810.9	1846.017	39840.948	21.5821133
Durban	0dS/m	control	214	160.5	178.5	553	1846.017	43992.954	23.8312832
Durban	5dS/m	nonshock	987.5	564.6	870.8	2422.9	5744.817	28468.062	4.95543409
Durban	5dS/m	nonshock	189.8	198.8	226.1	614.7	4282.767	26843.364	6.26776194
Durban	5dS/m	nonshock	60.5	102.2	171.5	334.2	7085.0295	34064.244	4.80791844
Durban	5dS/m	nonshock	199.7	191.8	316.9	708.4	13420.5795	34786.332	2.59201415
Durban	5dS/m	nonshock	15	17	102.1	134.1	5866.6545	17997.786	3.06781079
Durban	5dS/m	shock	50.3	81.5	112.7	244.5	8547.0795	33342.156	3.90099987
Durban	5dS/m	shock	62.7	49.4	178.1	290.2	6232.167	28287.54	4.53895732

Durban	5dS/m	shock	114	144.4	196.6	455	7937.892	27745.974	3.49538316
Durban	5dS/m	shock	152.9	143.3	218	514.2	9887.292	39118.86	3.95647868
Durban	5dS/m	shock	79.1	101.1	187.8	368	9278.1045	35147.376	3.78820652
Durban	10dS/m	nonshock	71.2	113.4	196.8	381.4	12202.2045	28107.018	2.30343771
Durban	10dS/m	nonshock	298.2	209.7	550.2	1058.1	12324.042	32439.546	2.63221644
Durban	10dS/m	nonshock	112.4	88.3	146.1	346.8	14517.117	28648.584	1.97343481
Durban	10dS/m	nonshock	171.4	160	270.5	601.9	12324.042	30092.76	2.44179304
Durban	10dS/m	nonshock	27.5	18.1	53	98.6	18050.4045	29190.15	1.61714659
Durban	10dS/m	shock	102.5	117.1	215.2	434.8	12567.717	31897.98	2.53808866
Durban	10dS/m	shock	25	32.3	78.8	136.1	7328.7045	23232.924	3.170127
Durban	10dS/m	shock	79.8	58.3	66.7	204.8	15979.167	29009.628	1.8154656
Durban	10dS/m	shock	70	82.6	138.2	290.8	13786.092	28287.54	2.05188969
Durban	10dS/m	shock	42	65.6	93	200.6	14638.9545	36591.552	2.49960146
Durban	30dS/m	nonshock	112.2	129.2	266.3	507.7	16344.6795	29731.716	1.81904552
Durban	30dS/m	nonshock	230.1	237.4	138.3	605.8	15004.467	33342.156	2.22214864
Durban	30dS/m	nonshock	101.6	198.2	437	736.8	14029.767	28648.584	2.04198573
Durban	30dS/m	nonshock	179	201.2	463.1	843.3	15491.817	25760.232	1.66282832
Durban	30dS/m	nonshock	208.4	193.3	498	899.7	13786.092	28468.062	2.06498419
Durban	30dS/m	shock	38.9	68.1	116.5	223.5	16953.867	32981.112	1.9453445
Durban	30dS/m	shock	103.1	98.4	293.2	494.7	12689.5545	26843.364	2.11539058
Durban	30dS/m	shock	87.5	105.8	187.6	380.9	19634.292	26843.364	1.3671674
Durban	30dS/m	shock	379.4	185.4	868	1432.8	10861.992	27926.496	2.57102896
Durban	30dS/m	shock	133.5	172.8	280.6	586.9	13907.9295	28107.018	2.02093475
Durban	60dS/m	nonshock	43.3	34.8	65.3	143.4	32549.067	26482.32	0.81361226
Durban	60dS/m	nonshock	26.1	30.5	89.6	146.2	23533.092	22330.314	0.94888993
Durban	60dS/m	nonshock	58.2	42.5	167	267.7	36447.867	22691.358	0.62257026
Durban	60dS/m	nonshock	53	87.7	185.1	325.8	15248.142	26662.842	1.74859612
Durban	60dS/m	nonshock	114.2	65.1	134.7	314	8668.917	26121.276	3.01321099
Durban	60dS/m	shock	33.5	50.5	72.7	156.7	29015.7795	36952.596	1.27353449
Durban	60dS/m	shock	48.9	42.1	97	188	15613.6545	30995.37	1.98514512
Durban	60dS/m	shock	63.6	50.1	112.4	226.1	27066.3795	27384.93	1.01176923
Durban	60dS/m	shock	56.6	51.2	126.9	234.7	12445.8795	29551.194	2.37437571
Durban	60dS/m	shock	35.7	37.7	118	191.4	23411.2545	26482.32	1.13117902
Durban	90dS/m	nonshock	24.8	27.3	43.7	95.8	24751.467	28829.106	1.16474333
Durban	90dS/m	nonshock	20.5	23.8	68.4	112.7	48875.292	23593.968	0.48273815
Durban	90dS/m	nonshock	16.6	30.7	64.7	112	43636.2795	30634.326	0.70203799
Durban	90dS/m	nonshock	15	23.4	46.5	84.9	43392.6045	27745.974	0.63941712
Durban	90dS/m	nonshock	40	36	83.2	159.2	25116.9795	30995.37	1.2340405
Durban	90dS/m	shock	24.3	20.2	70.5	115	15248.142	29190.15	1.91434143

Durban	90dS/m	shock	29.3	24.7	73.3	127.3	23289.417	26843.364	1.15259923
Durban	90dS/m	shock	35.8	28.1	5.6	69.5	60571.692	32981.112	0.54449712
Durban	90dS/m	shock	13.9	11.3	39.5	64.7	39006.4545	28648.584	0.73445752
Durban	90dS/m	shock	16.4	26.7	60.1	103.2	34132.9545	38035.728	1.11434034
HI10	0dS/m	control	100.3	84.3	38.7	223.3	2211.5295	60781.5	27.4839201
HI10	0dS/m	control	86	86.5	90.6	263.1	1846.017	49047.57	26.5694032
HI10	0dS/m	control	92.4	89.1	94.4	275.9	1967.8545	53921.664	27.4012454
HI10	0dS/m	control	109.4	65	69.8	244.2	2089.692	49047.57	23.4711958
HI10	0dS/m	control	74.3	80.1	82.8	237.2	1967.8545	45437.13	23.0896796
HI10	0dS/m	control	101.5	149.6	123.1	374.2	1846.017	46339.74	25.1025532
HI10	0dS/m	control	232.6	136.4	101.1	470.1	2089.692	47783.916	22.8664875
HI10	0dS/m	control	62.9	60.4	67.7	191	1967.8545	50311.224	25.5665366
HI10	0dS/m	control	114	101.2	98.6	313.8	1967.8545	44173.476	22.4475316
HI10	0dS/m	control	143.2	107.4	107.3	357.9	2089.692	49408.614	23.6439695
HI10	5dS/m	nonshock	1096.2	685.3	457.4	2238.9	13907.9295	36049.986	2.59204549
HI10	5dS/m	nonshock	288.3	192.5	195.1	675.9	9765.4545	39118.86	4.0058412
HI10	5dS/m	nonshock	902.1	460.6	196.5	1559.2	9765.4545	40201.992	4.11675586
HI10	5dS/m	nonshock	370.1	272.2	252.3	894.6	8059.7295	38216.25	4.74162936
HI10	5dS/m	nonshock	81.6	53.9	16.7	152.2	9156.267	38577.294	4.213212
HI10	5dS/m	shock	38.4	89.6	99.6	227.6	9887.292	40924.08	4.1390585
HI10	5dS/m	shock	373.5	258.9	270.7	903.1	9034.4295	43812.432	4.84949625
HI10	5dS/m	shock	762.3	378.5	202.9	1343.7	9643.617	45798.174	4.74906604
HI10	5dS/m	shock	292.7	258.9	250.9	802.5	10740.1545	43631.91	4.06250301
HI10	5dS/m	shock	417.2	342.7	247	1006.9	9034.4295	32981.112	3.65060262
HI10	10dS/m	nonshock	137.3	182.6	162.9	482.8	13176.9045	32620.068	2.47554864
HI10	10dS/m	nonshock	479.5	394.8	571.6	1445.9	13786.092	38035.728	2.75899276
HI10	10dS/m	nonshock	486.1	262.5	183.3	931.9	14517.117	35508.42	2.44596913
HI10	10dS/m	nonshock	796.1	572.8	440.1	1809	11105.667	32981.112	2.96975517
HI10	10dS/m	nonshock	752	616.7	458.1	1826.8	11958.5295	30634.326	2.56171346
HI10	10dS/m	shock	966.2	336.2	90.8	1393.2	11836.692	39840.948	3.36588533
HI10	10dS/m	shock	463.6	359	310.9	1133.5	14151.6045	34786.332	2.45811929
HI10	10dS/m	shock	519.3	459	341	1319.3	12445.8795	36411.03	2.92554897
HI10	10dS/m	shock	325.4	295.3	331.2	951.9	13786.092	36591.552	2.65423675
HI10	10dS/m	shock	306.6	316.8	496.9	1120.3	13664.2545	37674.684	2.75717084
HI10	30dS/m	nonshock	296.1	256.1	144.5	696.7	17806.7295	32078.502	1.80148196
HI10	30dS/m	nonshock	171.2	133.1	171.2	475.5	14517.117	33522.678	2.30918288
HI10	30dS/m	nonshock	205	221.8	247	673.8	11958.5295	24496.578	2.04846072
HI10	30dS/m	nonshock	233	184.5	349.2	766.7	11471.1795	34064.244	2.96955025
HI10	30dS/m	nonshock	380	190.5	205	775.5	18172.242	36049.986	1.98379407

HI10	30dS/m	shock	413.7	341.9	229.1	984.7	10009.1295	35688.942	3.56563895
HI10	30dS/m	shock	198.5	129.4	130	457.9	13420.5795	36049.986	2.68617208
HI10	30dS/m	shock	350.3	282.4	467.1	1099.8	15248.142	29190.15	1.91434143
HI10	30dS/m	shock	445.2	249.8	127.4	822.4	14638.9545	32259.024	2.20364262
HI10	30dS/m	shock	254	193.3	91.8	539.1	20487.1545	32439.546	1.58340906
HI10	60dS/m	nonshock	23.2	35.2	43.4	101.8	11836.692	34425.288	2.90835379
HI10	60dS/m	nonshock	47.5	51.7	97.3	196.5	20243.4795	35147.376	1.73623196
HI10	60dS/m	nonshock	18.3	55.8	75.7	149.8	30112.317	36411.03	1.20917397
HI10	60dS/m	nonshock	35.8	46.6	42	124.4	50215.5045	35327.898	0.7035257
HI10	60dS/m	nonshock	78	71.4	111.2	260.6	10496.4795	42909.822	4.08802037
HI10	60dS/m	shock	102.6	100.7	82	285.3	14638.9545	36952.596	2.52426469
HI10	60dS/m	shock	42.5	61.5	90.1	194.1	18903.267	36591.552	1.93572635
HI10	60dS/m	shock	57.1	64.2	62.1	183.4	16710.192	35869.464	2.14656205
HI10	60dS/m	shock	84.8	77.7	153	315.5	24385.9545	38938.338	1.59675267
HI10	60dS/m	shock	33	48.7	30.3	112	31939.8795	33703.2	1.05520749
HI10	90dS/m	nonshock	1.5	11.3	25.4	38.2	31227.309	36717.66	1.1758189
HI10	90dS/m	nonshock	11.6	21.9	64.9	98.4	51799.392	37494.162	0.72383402
HI10	90dS/m	nonshock	5.9	19.8	27.2	52.9	22192.8795	23955.012	1.07940081
HI10	90dS/m	nonshock	18.2	38.6	50.4	107.2	24385.9545	42007.212	1.72259864
HI10	90dS/m	nonshock	40.2	32.8	52.2	125.2	13907.9295	41285.124	2.9684594
HI10	90dS/m	shock	17.2	21.8	52	91	16588.3545	39118.86	2.3582122
HI10	90dS/m	shock	15.2	24.6	51.5	91.3	23411.2545	36952.596	1.57841161
HI10	90dS/m	shock	12.6	35.1	64.9	112.6	34254.792	39840.948	1.16307663
HI10	90dS/m	shock	5.2	6.9	33.4	45.5	14395.2795	18539.352	1.28787718
HI10	90dS/m	shock	5.4	15	33.3	53.7	14882.6295	34912.44	2.34585158
509018	0dS/m	control	168.4	111.4	418.1	697.9	1967.8545	35327.898	17.952495
509018	0dS/m	control	83	62.3	21.7	167	1967.8545	41826.69	21.2549708
509018	0dS/m	control	4.4	13	39.1	56.5	1967.8545	30634.326	15.5673735
509018	0dS/m	control	116.4	83.5	68.6	268.5	1846.017	37133.118	20.1152633
509018	0dS/m	control	71.8	57.7	92	221.5	1967.8545	49228.092	25.0161239
509018	0dS/m	control	426.4	301.6	286	1014	2089.692	51394.356	24.5942254
509018	0dS/m	control	545.2	287.3	106.5	939	2211.5295	47603.394	21.5251002
509018	0dS/m	control	32	6.1	16	54.1	2211.5295	48867.048	22.0964939
509018	5dS/m	nonshock	125.4	163.7	107.7	396.8	19268.7795	41826.69	2.17069742
509018	5dS/m	nonshock	563.2	365.6	119.9	1048.7	12202.2045	39840.948	3.26506149
509018	5dS/m	nonshock	228.8	159.9	52.3	441	12445.8795	41646.168	3.3461812
509018	5dS/m	nonshock	5.8	10.5	23	39.3	10983.8295	35508.42	3.23279053
509018	5dS/m	nonshock	293.3	239.8	210.7	743.8	9887.292	41465.646	4.19383245
509018	5dS/m	shock	47.7	59.5	57.4	164.6	10374.642	38035.728	3.66622077

509018	5dS/m	shock	552.3	350.5	140.8	1043.6	18903.267	38577.294	2.0407739
509018	5dS/m	shock	157.5	164.5	93	415	11958.5295	48686.526	4.07128034
509018	5dS/m	shock	454.4	259.3	161.6	875.3	8790.7545	37313.64	4.24464589
509018	5dS/m	shock	124.9	123.5	58.2	306.6	11958.5295	48144.96	4.02599333
509018	10dS/m	nonshock	293.8	252.6	448	994.4	11105.667	38757.816	3.48991339
509018	10dS/m	nonshock	68.5	79.2	149.1	296.8	15613.6545	41104.602	2.63260609
509018	10dS/m	nonshock	444.1	257.9	154.4	856.4	11593.017	35869.464	3.09405774
509018	10dS/m	nonshock	300.3	203.1	241.6	745	14151.6045	39660.426	2.80253917
509018	10dS/m	nonshock	630.7	438.5	279.1	1348.3	12202.2045	40201.992	3.29464991
509018	10dS/m	shock	224.1	271	195.5	690.6	13664.2545	36952.596	2.7043258
509018	10dS/m	shock	246.7	208.8	235.5	691	14638.9545	41826.69	2.85721839
509018	10dS/m	shock	529.6	344.1	215.5	1089.2	13786.092	36049.986	2.61495324
509018	10dS/m	shock	11.2	17.9	81.4	110.5	11105.667	22691.358	2.04322334
509018	10dS/m	shock	292.6	189.5	219.7	701.8	12080.367	40743.558	3.37270863
509018	30dS/m	nonshock	422	284.9	103.5	810.4	14882.6295	35508.42	2.38589693
509018	30dS/m	nonshock	235	141.5	95.8	472.3	17563.0545	35869.464	2.04232493
509018	30dS/m	nonshock	530.4	236.2	31.3	797.9	12080.367	32078.502	2.65542446
509018	30dS/m	nonshock	594.4	291.8	145.1	1031.3	14395.2795	28468.062	1.97759703
509018	30dS/m	nonshock	305.5	175.2	183.7	664.4	11958.5295	28829.106	2.41075677
509018	30dS/m	shock	324	278.6	231	833.6	10252.8045	30995.37	3.02311138
509018	30dS/m	shock	193.6	194	225.7	613.3	9521.7795	27204.408	2.85707183
509018	30dS/m	shock	448.4	285.9	198	932.3	12567.717	30814.848	2.45190499
509018	30dS/m	shock	29.1	21.7	36	86.8	20365.317	39840.948	1.95631367
509018	30dS/m	shock	251	192.6	103	546.6	17563.0545	37674.684	2.14511001
509018	60dS/m	nonshock	58.5	64	56.5	179	17441.217	40924.08	2.34640048
509018	60dS/m	nonshock	20.7	37.8	8.5	67	65079.6795	33703.2	0.51787594
509018	60dS/m	nonshock	22.7	42.4	87.2	152.3	17319.3795	34786.332	2.00852069
509018	60dS/m	nonshock	43.9	51	108.4	203.3	11349.342	39299.382	3.46270136
509018	60dS/m	shock	77.3	74.1	137.7	289.1	7694.217	36049.986	4.68533523
509018	60dS/m	shock	35	51.4	35.6	122	17684.892	33883.722	1.91596997
509018	60dS/m	shock	11.8	11.7	29	52.5	15126.3045	34605.81	2.28779012
509018	60dS/m	shock	79.9	96	71.5	247.4	9521.7795	31897.98	3.35000196
509018	60dS/m	shock	13.8	21.3	31.7	66.8	15735.492	37313.64	2.37130431
509018	90dS/m	nonshock	7.5	20.6	36.1	64.2	51555.717	31356.414	0.6082044
509018	90dS/m	nonshock	4.1	13.1	19.8	37	66447.5738	36411.03	0.54796628
509018	90dS/m	nonshock	8.5	17.5	51.4	77.4	12445.8795	27926.496	2.24383468
509018	90dS/m	nonshock	20.5	33.7	64.6	118.8	9399.942	24316.056	2.58683043
509018	90dS/m	nonshock	10.6	38.4	53.6	102.6	22071.042	47061.828	2.13228845
509018	90dS/m	shock	13.5	18.8	79.3	111.6	8547.0795	23413.446	2.73935044

509018	90dS/m	shock	12.9	16.9	27.4	57.2	15979.167	21608.226	1.35227487
509018	90dS/m	shock	10.5	24.4	17.1	52	56073.6415	29551.194	0.52700686
509018	90dS/m	shock	8.1	10	25.9	44	6475.842	8069.076	1.24602731
509018	90dS/m	shock	11.2	14.5	22.9	48.6	4648.2795	5180.724	1.11454658
KC9	0dS/m	control	1592.9	662.9	342.4	2598.2	2211.5295	38938.338	17.606972
KC9	0dS/m	control	254.8	171.6	60.1	486.5	1967.8545	47422.872	24.0987695
KC9	0dS/m	control	87.2	106.1	142.6	335.9	2089.692	35869.464	17.1649525
KC9	0dS/m	control	17.7	6.5	28	52.2	1846.017	20705.616	11.2163734
KC9	0dS/m	control	24.6	27.4	58	110	1967.8545	26843.364	13.6409292
KC9	0dS/m	control	1294.1	587.6	342.1	2223.8	2089.692	39118.86	18.7199166
KC9	0dS/m	control	21.6	9.8	39	70.4	1967.8545	25218.666	12.8153103
KC9	0dS/m	control	3.6	8	37	48.6	2333.367	38035.728	16.3007911
KC9	0dS/m	control	44.5	31	66.5	142	1967.8545	35508.42	18.0442304
KC9	5dS/m	nonshock	441.9	164.2	143.8	749.9	10009.1295	42187.734	4.21492538
KC9	5dS/m	nonshock	121.2	85.5	42.8	249.5	12445.8795	26121.276	2.09878908
KC9	5dS/m	nonshock	99.4	61.2	166.7	327.3	5135.6295	27023.886	5.26203964
KC9	5dS/m	nonshock	19.9	18.1	88.5	126.5	8181.567	23593.968	2.88379573
KC9	5dS/m	nonshock	34	59.5	71.8	165.3	7694.217	37494.162	4.87303152
KC9	5dS/m	shock	8.2	16.5	42.7	67.4	10009.1295	37133.118	3.70992482
KC9	5dS/m	shock	796.8	433	222.1	1451.9	10130.967	34786.332	3.43366354
KC9	5dS/m	shock	37	48.5	87.2	172.7	9156.267	41104.602	4.48923147
KC9	5dS/m	shock	11	20.9	114.5	146.4	7572.3795	29370.672	3.87865822
KC9	10dS/m	nonshock	272.7	200.1	114.2	587	13664.2545	35869.464	2.62505825
KC9	10dS/m	nonshock	278.8	197.5	84.4	560.7	13055.067	32078.502	2.4571687
KC9	10dS/m	nonshock	747.9	299.5	205.8	1253.2	11227.5045	29370.672	2.61595727
KC9	10dS/m	nonshock	127.7	64.1	11.5	203.3	20487.1545	21969.27	1.07234365
KC9	10dS/m	nonshock	613	328.3	500.1	1441.4	11593.017	26482.32	2.28433375
KC9	10dS/m	shock	5.7	6.5	27.7	39.9	13664.2545	32800.59	2.40046685
KC9	10dS/m	shock	355.3	290.2	223.9	869.4	14517.117	35869.464	2.47083935
KC9	10dS/m	shock	280.1	226.6	340	846.7	12324.042	31717.458	2.57362463
KC9	10dS/m	shock	305	223.3	278.3	806.6	15979.167	32981.112	2.06400697
KC9	10dS/m	shock	702	395.3	357.1	1454.4	13055.067	34244.766	2.62310151
KC9	30dS/m	nonshock	342.2	216.1	215.7	774	12202.2045	34064.244	2.79164671
KC9	30dS/m	nonshock	331.4	165.7	216.3	713.4	15369.9795	33883.722	2.20453918
KC9	30dS/m	nonshock	249.4	175.9	232	657.3	14395.2795	32439.546	2.25348497
KC9	30dS/m	nonshock	319.2	238.7	194.7	752.6	21218.1795	33342.156	1.5713957
KC9	30dS/m	nonshock	247.7	154.9	123.9	526.5	16588.3545	35688.942	2.15144558
KC9	30dS/m	shock	176.1	150.7	143.4	470.2	15491.817	34425.288	2.22215948
KC9	30dS/m	shock	127.7	157.5	181.3	466.5	18172.242	33522.678	1.84471888

KC9	30dS/m	shock	127.5	138.5	88.7	354.7	19025.1045	35327.898	1.85690954
KC9	30dS/m	shock	316	191.2	28.9	536.1	18294.0795	31175.892	1.70415199
KC9	30dS/m	shock	108.4	133.6	215.1	457.1	12933.2295	36411.03	2.81530843
KC9	60dS/m	nonshock	61.1	71.2	76.4	208.7	10618.317	32259.024	3.03805434
KC9	60dS/m	nonshock	18.7	25.8	1.9	46.4	25360.6545	25760.232	1.0157558
KC9	60dS/m	nonshock	19.9	46.1	32.5	98.5	18781.4295	32439.546	1.72721389
KC9	60dS/m	nonshock	41	64.3	95.2	200.5	14882.6295	37313.64	2.50719404
KC9	60dS/m	nonshock	77.1	94.5	33.7	205.3	39250.1295	32800.59	0.83568106
KC9	60dS/m	shock	48.5	65.8	123.2	237.5	14273.442	34064.244	2.38654727
KC9	60dS/m	shock	29.4	41.2	49.2	119.8	20243.4795	31536.936	1.55788119
KC9	60dS/m	shock	39.9	45.6	70.2	155.7	41077.692	30634.326	0.74576551
KC9	60dS/m	shock	26.1	44.9	44.5	115.5	35838.6795	22691.358	0.63315274
KC9	60dS/m	shock	78.3	53.1	25.6	157	13420.5795	35327.898	2.63236755
KC9	90dS/m	nonshock	20.5	22.5	48.1	91.1	22558.392	36230.508	1.60607671
KC9	90dS/m	nonshock	7.8	21.2	42.6	71.6	33645.6045	26482.32	0.78709598
KC9	90dS/m	nonshock	8.4	16.7	27.8	52.9	24398.2575	33907.62	1.38975581
KC9	90dS/m	nonshock	23.5	19.6	60.1	103.2	14760.792	30453.804	2.06315515
KC9	90dS/m	nonshock	13.3	27.2	53.2	93.7	23654.9295	49950.18	2.11161821
KC9	90dS/m	shock	11.3	18.7	15.9	45.9	19268.7795	32620.068	1.69289747
KC9	90dS/m	shock	7.9	8.1	24.3	40.3	13719.618	23611.248	1.72098436
KC9	90dS/m	shock	11.4	23.9	17.9	53.2	26579.0295	36952.596	1.39029139
KC9	90dS/m	shock	12	9.7	15.6	37.3	32726.268	40941.36	1.25102441
KC9	90dS/m	shock	23.2	32	40.1	95.3	34011.117	34605.81	1.01748525

Supplemental Table 2.7. Pearson correlation coefficient (R) values and associated p-values for all traits measured in salt screen 2.

Trait Correlations	Leaf Potassium:Sodium Ratio	Leaf Potassium	Leaf Sodium	Leaf Biomass	Stolon Biomass	Root Biomass
Total Biomass	0.168708925	0.049369711	-0.318940815	0.968652853	0.973387178	0.792917181
Root Biomass	0.084588342	-0.035518661	-0.29051189	0.74527568	0.644773138	-
Stolon Biomass	0.177141273	0.046097957	-0.27326435	0.926764431	-	
Leaf Biomass	0.165787304	0.122147134	-0.31552848	-	-	
Leaf Sodium Content	-0.544220397	-0.328014992	-	-	-	
Leaf Potassium Content	0.551001037	-	-	-	-	
P-Values	**Leaf Potassium:Sodium Ratio**	**Leaf Potassium**	**Leaf Sodium**	**Leaf Biomass**	**Stolon Biomass**	**Root Biomass**
Total Biomass	0.003839	0.401281	<0.00001	<0.00001	<0.00001	<0.00001
Root Biomass	0.149777	0.545702	<0.00001	<0.00001	<0.00001	-
Stolon Biomass	0.002387	0.432673	<0.00001	<0.00001	-	-
Leaf Biomass	0.004526	0.037042	<0.00001	-	-	-
Leaf Sodium Content	<0.00001	<0.00001	-	-	-	-
Leaf Potassium Content	<0.00001	-	-	-	-	

Supplemental Table 2.8. Two-tailed t-tests were conducted between trait values obtained for non-shock and shock plants in salt screen 2. Cells highlighted in yellow indicate $p<0.05$ and cells highlighted in orange indicate $p<0.01$.

Genotype/Salt Level	Total Biomass	Leaf Na	Leaf K	Leaf K/Na
Spence-5dS/m	0.879868154	0.237869698	0.963382535	0.531720344
Spence-10dS/m	0.263507815	0.378725827	0.373945122	0.843779937
Spence-30dS/m	0.798797648	0.401795355	0.746341074	0.239303715
Spence-60dS/m	0.774332839	0.987409898	0.047212321	0.215682596
Spence-90dS/m	0.494882245	0.01486532	0.975812079	0.014209808
Durban-5dS/m	0.287280369	0.541027355	0.280099026	0.576956178
Durban-10dS/m	0.187742342	0.598979659	0.963987401	0.473170806
Durban-30dS/m	0.682100551	0.942289378	0.708251986	0.851833038
Durban-60dS/m	0.371081961	0.778134792	0.031744506	0.812739401
Durban-90dS/m	0.366559389	0.777555994	0.279433402	0.400810504
HI10-5dS/m	0.558729723	0.668998033	0.238304194	0.42402684
HI10-10dS/m	0.682341941	0.732546043	0.076738991	0.328187983
HI10-30dS/m	0.467975349	0.991445609	0.658082833	0.685810967
HI10-60dS/m	0.299664458	0.691734519	0.812336882	0.685559729
HI10-90dS/m	0.796460864	0.312642446	0.647966787	0.662197771
509018-5dS/m	0.913028414	0.820144429	0.480409605	0.495704322
509018-10dS/m	0.432809707	0.911387339	0.355611043	0.230031839
509018-30dS/m	0.403855049	0.959963289	0.693881768	0.443882496
509018-60dS/m	0.934149031	0.232359349	0.231770785	0.317571232
509018-90dS/m	0.388195878	0.372287862	0.032210824	0.697990476
KC9-5dS/m	0.681672142	0.733130525	0.382462875	0.987633106
KC9-10dS/m	0.986309462	0.95805468	0.115602294	0.503541897
KC9-30dS/m	0.002618832	0.671105854	0.787548625	0.714294306
KC9-60dS/m	0.89940762	0.68446294	0.672052529	0.701821729
KC9-90dS/m	0.077752908	0.774516245	0.745013085	0.541034274

Supplemental Table 2.9. ANOVA analyses for each trait in salt screen 2 (total biomass, leaf sodium content, leaf potassium content, and potassium:sodium ratio) split by salt treatment. If a trait was found to significantly differ between nonshock and shock treatments in two-tailed t-tests, that salt level was split into nonshock and shock values for the analysis.

Freshwater (0 dS/m)

Genotype	Total Biomass	groups
Spence	1796.65	a
Durban	784.6889	ab
KC9	674.1778	ab
509018-3	427.3125	b
HI10	295.07	b

Genotype	Na	groups
Spence	2049.079	a
Durban	2028.773	ab
KC9	2004.406	ab
509018-3	1894.752	b
HI10	1711.996	c

Genotype	K	groups
Spence	49625.24	a
Durban	42765.4	a
KC9	42751.87	ab
509018-3	35093.22	bc
HI10	34184.59	c

Genotype	K/Na	groups
Spence	24.76425	a
Durban	22.64736	ab
KC9	21.01526	ab
509018-3	20.52165	b
HI10	16.62314	c

Total Biomass	Df	Sum of Sq	RSS	AIC	F value	Pr(>F)
<none>			37593858	636.23		
Genotype	4	13728786	51322644	642.55	3.7432	0.01097
Sodium	**Df**	**Sum of Sq**	**RSS**	**AIC**	**F value**	**Pr(>F)**
<none>			555180	450.71		
Genotype	4	748599	1303778	482.84	14.158	2.14E-07
Potassium	**Df**	**Sum of Sq**	**RSS**	**AIC**	**F value**	**Pr(>F)**
<none>			1505319490	822.26		
Genotype	4	1566483749	3071803239	847.78	10.927	3.66E-06
Potassium:Sodium	**Df**	**Sum of Sq**	**RSS**	**AIC**	**F value**	**Pr(>F)**
<none>			343.85	103.53		
Genotype	4	341.38	685.23	127.94	10.425	5.90E-06

5 dS/m Salt Stress

Genotype	Total Biomass	groups
Spence	1981.28	a
HI10	980.46	ab
Durban	608.62	b
509018	547.47	b
KC9	384.1	b

Genotype	Na	groups
509018	12677.371	a
HI10	9899.476	ab
KC9	8926.129	b
Durban	7828.238	b
Spence	6658.598	b

Genotype	K	groups
509018	41104.6	a
HI10	39931.21	a
KC9	33201.75	b
Spence	31302.26	b
Durban	30580.17	b

Genotype	K/Na	groups
Spence	5.478707	a
Durban	4.137096	ab
HI10	4.112021	ab
KC9	3.871562	b
509018	3.425748	b

Total Biomass	Df	Sum of Sq	RSS	AIC	F value	Pr(>F)
<none>			33027544	667.63		
Genotype	4	16237729	49265273	679.22	5.4081	0.001247
Sodium	**Df**	**Sum of Sq**	**RSS**	**AIC**	**F value**	**Pr(>F)**
<none>			316038093	778.3		
Genotype	4	209892710	525930803	795.25	7.3055	0.0001331
Potassium	**Df**	**Sum of Sq**	**RSS**	**AIC**	**F value**	**Pr(>F)**
<none>			1104878406	839.63		
Genotype	4	973567248	2078445654	862.59	9.6927	1.04E-05
Potassium:Sodium	**Df**	**Sum of Sq**	**RSS**	**AIC**	**F value**	**Pr(>F)**
<none>			62.032	21.555		
Genotype	4	23.427	85.458	29.254	4.1542	0.006108

10 dS/m Salt Stress

Genotype	Total Biomass	groups
Spence	1575.76	a
HI10	1241.46	ab
KC9	806.26	bc
509018	752.4	bc
Durban	375.39	c

Genotype	Na	groups
KC9	13956.664	a
Durban	13371.844	a
HI10	13042.883	a
509018	12994.148	a
Spence	8888.225	b

Genotype	K	groups
509018	37385.85	a

Genotype	K/Na	groups
Spence	3.263321	a

HI10	35508.42	ab
KC9	31338.36	bc
Durban	29749.77	c
Spence	28161.17	c

509018	2.89062	ab
HI10	2.737294	abc
KC9	2.31869	bc
Durban	2.30432	c

Total Biomass	Df	Sum of Sq	RSS	AIC	F value	Pr(>F)
<none>			10358988	622.07		
Genotype	4	8664078	19023066	644.46	9.4093	1.29E-05
Sodium	**Df**	**Sum of Sq**	**RSS**	**AIC**	**F value**	**Pr(>F)**
<none>			200603934	770.24		
Genotype	4	164536849	365140783	792.19	9.2273	1.56E-05
Potassium	**Df**	**Sum of Sq**	**RSS**	**AIC**	**F value**	**Pr(>F)**
<none>			673998773	830.84		
Genotype	4	606352855	1280351629	854.92	10.121	6.26E-06
Potassium:Sodium	**Df**	**Sum of Sq**	**RSS**	**AIC**	**F value**	**Pr(>F)**
<none>			9.3959	-73.588		
Genotype	4	6.5698	15.9657	-55.079	7.8662	6.77E-05

30 dS/m Salt Stress

Genotype	Total Biomass	groups
Spence	811.9778	a
HI10	729.21	a
KC9_30_nonshock	684.76	a
509018	678.89	a
Durban	671.21	a
KC9_30_shock	456.92	a

Genotype	Na	groups
KC9	16369.05	a
Durban	14870.45	a
HI10	14772.98	a
509018	14115.05	a
Spence	13975.62	a

Genotype	K	groups
KC9	34028.14	a
509018	32728.38	ab
HI10	32583.96	ab
Durban	28865.21	bc
Spence	26702.96	c

Genotype	K/Na	groups
Spence	2.443616	a
509018	2.390551	a
HI10	2.306567	a
KC9	2.141576	a
Durban	1.983086	a

Total Biomass	Df	Sum of Sq	RSS	AIC	F value	Pr(>F)
<none>			2564173	544.4		
Genotype	5	425815	2989988	541.93	1.4281	0.2335
Sodium	**Df**	**Sum of Sq**	**RSS**	**AIC**	**F value**	**Pr(>F)**

<none>			655879804	814.07		
Genotype	4	35413717	691293521	808.65	0.5939	0.6689
Potassium	**Df**	**Sum of Sq**	**RSS**	**AIC**	**F value**	**Pr(>F)**
<none>			470272240	797.77		
Genotype	4	358179469	828451709	817.52	8.3781	4.09E-05
Potassium:Sodium	**Df**	**Sum of Sq**	**RSS**	**AIC**	**F value**	**Pr(>F)**
<none>			22.579	-27.965		
Genotype	4	1.3969	23.976	-33.024	0.6805	0.6092

60 dS/m Salt Stress

Genotype	Total Biomass	groups
Spence	229.3222	a
Durban	219.4	a
HI10	192.34	a
KC9	154.49	a
509018	153.2667	a

Genotype	Na	groups
Spence	40238.37	a
KC9	23374.7	b
HI10	22948.27	b
Durban	22400	b
509018	19661.37	b

Genotype	K	groups
HI10	36627.66	a
509018	35829.35	a
KC9	31482.78	ab
Durban_60_shock	30273.28	abc
Spence_60_shock	27421.03	bc
Durban_60_nonshock	24857.62	c
Spence_60_nonshock	24451.45	c

Genotype	K/Na	groups
509018	2.5495445	a
HI10	1.9903819	a
KC9	1.7079613	ab
Durban	1.4922883	ab
Spence	0.6836362	b

Total Biomass	**Df**	**Sum of Sq**	**RSS**	**AIC**	**F value**	**Pr(>F)**
<none>			221187	414.91		
Genotype	4	47364	268551	416.22	2.3019	0.07392
Sodium	**Df**	**Sum of Sq**	**RSS**	**AIC**	**F value**	**Pr(>F)**
<none>			6783675825	910.8		
Genotype	4	2468050844	9251726669	917.69	3.9111	0.008533
Potassium	**Df**	**Sum of Sq**	**RSS**	**AIC**	**F value**	**Pr(>F)**
<none>			608578158	799.06		
Genotype	6	941574266	1550152424	831.94	10.572	4.49E-07
Potassium:Sodium	**Df**	**Sum of Sq**	**RSS**	**AIC**	**F value**	**Pr(>F)**
<none>			32.588	-8.5882		
Genotype	4	17.06	49.648	3.6208	5.6278	0.0009827

90 dS/m Salt Stress

Genotype	Total Biomass	groups
Spence	169.44	a
Durban	104.43	b
HI10	81.6	b
509018	71.34	b
KC9	68.45	b

Genotype	Na	groups
Spence_90_shock	59986.87	a
Durban	35802.13	ab
Spence_90_nonshock	28711.19	b
509018	25364.42	b
HI10	24704.58	b
KC9	24532.28	b

Genotype	K	groups
HI10	35082.34	a
KC9	34575.55	a
509018_90_nonshock	33414.36	a
Durban	29749.77	ab
Spence	21568.11	bc
509018_90_shock	17564.53	c

Genotype	K/Na	groups
HI10	1.6403541	a
509018	1.509833	a
KC9	1.5030385	a
Durban	0.9683213	ab
Spence_90_nonshock	0.7797395	ab
Spence_90_shock	0.4005357	b

Total Biomass	Df	Sum of Sq	RSS	AIC	F value	Pr(>F)
<none>			58315	363.08		
Genotype	4	69924	128239	394.48	13.489	2.65E-07
Sodium	**Df**	**Sum of Sq**	**RSS**	**AIC**	**F value**	**Pr(>F)**
<none>			9.87E+09	948.9		
Genotype	5	5.59E+09	1.55E+10	960.88	4.8687	0.001289
Potassium	**Df**	**Sum of Sq**	**RSS**	**AIC**	**F value**	**Pr(>F)**
<none>			1993603358	870.55		
Genotype	5	1924863770	3918467128	893.66	8.3035	1.47E-05
Potassium:Sodium	**Df**	**Sum of Sq**	**RSS**	**AIC**	**F value**	**Pr(>F)**
<none>			14.6	-47.33		
Genotype	5	8.125	22.725	-35.65	4.7861	0.00145

Supplementary Table 2.10. Pearson correlations and associated P-values for measured traits in salt screen 2 (total biomass, leaf sodium content, leaf potassium content, and potassium:sodium ratio) split by salt treatment.

Freshwater (0 dS/m)				
Pearson Correlations	**Total Biomass**	**Na**	**K**	**K/Na**
Total Biomass	-	-0.2412	-0.1389	-0.0369
Na	-0.2412	-	0.3922	-0.0371
K	-0.1389	0.3922	-	0.9024
K/Na	-0.0369	-0.0371	0.9024	-
P-Values	**Total Biomass**	**Na**	**K**	**K/Na**
Total Biomass	-	0.1064	0.3572	0.8075
Na	0.1064	-	0.0071	0.7589
K	0.3572	0.0071	-	0
K/Na	0.8075	0.7589	0	-
5 dS/m Salt Stress				
Pearson Correlations	**Total Biomass**	**Na**	**K**	**K/Na**
Total Biomass	-	0.0081	-0.1616	-0.0062
Na	0.0081	-	0.4427	-0.8086
K	-0.1616	0.4427	-	-0.002
K/Na	-0.0062	-0.8086	-0.002	-
P-Values	**Total Biomass**	**Na**	**K**	**K/Na**
Total Biomass	-	0.9561	0.2674	0.9663
Na	0.9561	-	0.0014	0
K	0.2674	0.0014	-	0.9891
K/Na	0.9663	0	0.9891	-
10 dS/m Salt Stress				
Pearson Correlations	**Total Biomass**	**Na**	**K**	**K/Na**
Total Biomass	-	-0.5445	-0.0242	0.5471
Na	-0.5445	-	0.3047	-0.8014
K	-0.0242	0.3047	-	0.2417
K/Na	0.5471	-0.8014	0.2417	-
P-Values	**Total Biomass**	**Na**	**K**	**K/Na**
Total Biomass	-	0	0.8676	0
Na	0	-	0.0314	0
K	0.8676	0.0314	-	0.0909
K/Na	0	0	0.0909	-
30 dS/m Salt Stress				

Pearson Correlations	Total Biomass	Na	K	K/Na
Total Biomass	-	-0.4717	-0.265	0.3209
Na	-0.4717	-	0.0804	-0.877
K	-0.265	0.0804	-	0.229
K/Na	0.3209	-0.877	0.229	-
P-Values	**Total Biomass**	**Na**	**K**	**K/Na**
Total Biomass	-	0.0006	0.0658	0.0246
Na	0.0006	-	0.5829	0
K	0.0658	0.5829	-	0.1135
K/Na	0.0246	0	0.1135	-

60 dS/m Salt Stress				
Pearson Correlations	**Total Biomass**	**Na**	**K**	**K/Na**
Total Biomass	-	-0.0553	-0.0797	0.1801
Na	-0.0553	-	-0.3708	-0.8195
K	-0.0797	-0.3708	-	0.5881
K/Na	0.1801	-0.8195	0.5881	-
P-Values	**Total Biomass**	**Na**	**K**	**K/Na**
Total Biomass	-	0.7088	0.5903	0.2206
Na	0.7088	-	0.0095	0
K	0.5903	0.0095	-	0
K/Na	0.2206	0	0	-

90 dS/m Salt Stress				
Pearson Correlations	**Total Biomass**	**Na**	**K**	**K/Na**
Total Biomass	-	0.2394	-0.1727	-0.1893
Na	0.2394	-	0.0296	-0.7732
K	-0.1727	0.0296	-	0.3629
K/Na	-0.1893	-0.7732	0.3629	-
P-Values	**Total Biomass**	**Na**	**K**	**K/Na**
Total Biomass	-	0.0976	0.2354	0.1928
Na	0.0976	-	0.8398	0
K	0.2354	0.8398	-	0.0104
K/Na	0.1928	0	0.0104	-

Supplemental Table 2.11. ANOVA analyses conducted on proline measurements from plants grown in freshwater (0 dS/m), 10 dS/m, and 30 dS/m split by salt treatment in salt screen 3.

Freshwater (0 dS/m)		
Genotype/Treatment	**Proline Ave.**	**Significance Group (p<0.05)**
HI10-0	5.1362648	a
509018-0	3.0321571	ab
Spence-0	1.681372	bc
Durban-0	0.9825347	bc
KC9-0	0.626405	c

10 dS/m		
Genotype/Treatment	**Proline Ave.**	**Significance Group (p<0.05)**
HI10-10	10.5717921	a
509018-10	5.4962477	ab
Spence-10	2.9496037	b
KC9-10	1.7590683	b
Durban-10	0.7278291	b

30 dS/m		
Genotype/Treatment	**Proline**	**groups**
HI10-30	32.655855	a
509018-30	16.627516	b
KC9-30	9.833654	bc
Spence-30	9.205613	bc
Durban-30	5.449904	c

Freshwater	**Df**	**Sum of Sq**	**RSS**	**AIC**	**F value**	**Pr(>F)**
<none>			15.096	4.3738		
Genotype	4	53.998	69.094	26.7946	13.414	7.62E-05
10 dS/m	**Df**	**Sum of Sq**	**RSS**	**AIC**	**F value**	**Pr(>F)**
<none>			92.24	40.574		
Genotype	4	247.23	339.47	58.633	10.05	0.0003685
30 dS/m	**Df**	**Sum of Sq**	**RSS**	**AIC**	**F value**	**Pr(>F)**
<none>			308.02	64.689		
Genotype	4	1862.2	2170.21	95.737	22.671	3.25E-06

Supplemental Table 2.12. ANOVA analyses conducted on proline measurements from plants grown in freshwater (0 dS/m), 10 dS/m, and 30 dS/m split by genotype in salt screen 3.

HI10 Genotype/Treatment	Proline Ave.	Significance Group (p<0.05)
HI10-30	32.655855	a
HI10-10	10.571792	b
HI10-0	5.136265	b

509018-3 Genotype/Treatment	Proline Ave.	Significance Group (p<0.05)
509018-30	16.627516	a
509018-10	5.496248	b
509018-0	3.032157	b

Spence Genotype/Treatment	Proline Ave.	Significance Group (p<0.05)
Spence-30	9.205613	a
Spence-10	2.949604	b
Spence-0	1.681372	b

Durban Genotype/Treatment	Proline Ave.	Significance Group (p<0.05)
Durban-30	5.4499045	a
Durban-0	0.9825347	b
Durban-10	0.7278291	b

KC9 Genotype/Treatment	Proline Ave.	Significance Group (p<0.05)
KC9-30	9.833654	a
KC9-10	1.759068	b
KC9-0	0.626405	b

HI10	Df	Sum of Sq	RSS	AIC	F value	Pr(>F)
<none>			125.9	34.207		
Genotype	2	1699.4	1825.3	62.295	60.741	5.95E-06

509018-3	Df	Sum of Sq	RSS	AIC	F value	Pr(>F)
<none>			166.96	37.594		
Genotype	2	419.75	586.71	48.676	11.313	0.003499

Spence	Df	Sum of Sq	RSS	AIC	F value	Pr(>F)
<none>			25.409	15.002		
Genotype	2	129.81	155.223	32.719	22.99	0.0002905

Durban	Df	Sum of Sq	RSS	AIC	F value	Pr(>F)
<none>			29.235	16.685		
Genotype	2	56.427	85.662	25.586	8.6856	0.007925

KC9	Df	Sum of Sq	RSS	AIC	F value	Pr(>F)
<none>			67.853	26.789		
Genotype	2	201.67	269.526	39.341	13.375	0.002015

CHAPTER III

SEASHORE PASPALUM USES LEAF PAPILLAE FOR SODIUM SEQUESTRATION

[2] Spiekerman, J. J. and K.M. Devos. To be submitted to *New Phytologist*.

Abstract

Salinity is a growing issue worldwide, with nearly 30% of arable land predicted to be lost due to soil salinity in the next 30 years. Many grass crops, which provide two-thirds of the world's caloric intake, are salt sensitive. Therefore, studying mechanisms of salt tolerance in halophytic grasses, plants that thrive in salt conditions, may be an effective approach to ultimately improve salt sensitive grass crops. Seashore paspalum (*Paspalum vaginatum*) is a halophytic Panicoid grass able to grow in salt concentrations near that of seawater and is cultivated as a sustainable turfgrass species. Despite its widespread use, its ability to retain high sodium concentrations in photosynthetic tissue while maintaining growth remains unknown. We examined the leaf structure of seashore paspalum accession 'HI10' in comparison with *P. distichum* accession 'Spence', a salt sensitive relative that inhabits freshwater habitats, to better understand *Paspalum*'s sodium sequestration ability. Scanning electron microscopy (SEM) showed dense costal ridges of translucent papillae on the adaxial surface in both species. Light microscopy further indicated that papillae are unicellular extensions of the epidermis. Papillae are significantly larger in 'HI10' than in 'Spence', and papillae-enriched adaxial peels contain the majority of sodium found in leaf blades, indicating that papillae are major sinks for sodium. This is further confirmed using sodium-specific staining which illustrates that papillae sequester sodium when plants are grown under salt stress, though this sequestration may be more efficient in 'HI10' compared to 'Spence'. Papilla size also may affect surface hydrophobicity, as indicated by contact angle measurements of water droplets on the leaf surface, which offers a rapid means of approximating papilla size. Our results provide evidence for a novel mechanism of salt tolerance in the *Panicoideae*, an economically vital subfamily of grasses. Leaf papillae are the first known specialized structure for sodium sequestration in the Panicoid grasses, illustrating a

possible path for biotechnological improvement of salt-sensitive crops with analogous leaf structures.

Introduction

The amount of saline soils is increasing worldwide, with about 20% of irrigated land worldwide considered saline [1]. This is due to increased irrigation practices in agricultural fields necessitated by increased droughts due to climate change. This trend is alarming due the high salt sensitivity of most crop species that we rely on for vital resources. Yield reduction in crops in saline soils is in the order of US$12-27.3 billion dollars annually [2]. Thus, the improvement of salt tolerance in plants will become key in the coming decades. Though engineering-based solutions have been proposed, breeding salt tolerant crops is a more cost-effective means of improving growth in saline soils. Much work has focused on breeding salt tolerant species, but progress in this area has been slow due to the complex genetic and physiological nature of salt responses. Furthermore, most research has been conducted on glycophytic model systems that are salt-sensitive [3]. Consequently, the search for salt tolerance mechanisms in halophytes, species that can complete their life cycle in 200 mM salt concentrations, that may be transferred into glycophytes is of great interest [4, 5].

Both glycophytes and halophytes have evolved a multitude of salt tolerance mechanisms including sodium exclusion, sequestration and secretion, osmolyte production, ion homeostasis, and ROS detoxification [6]. Halophytes excel at sodium exclusion, sequestration, and excretion [7]. Furthermore, many mechanisms present in glycophytes, such as osmolyte production, are utilized in halophytes at higher efficiencies [8, 9]. However, halophytes also use mechanisms absent in glycophytes. Salt sequestration and secretion via salt glands is a halophyte-specific mechanism of coping with salt [7]. Salt glands are found in over 50 species in 14 angiosperm families with four subtypes: epidermal bladder cells (EBCs), complex multicellular glands, bicellular glands, and unicellular glands [10].The Poales order contains about 8% of all

halophytes [11], and has therefore been the focus of much salt gland-focused work [12]. As salt tolerance has independently evolved over 70 times in grass lineages [13], studying these salt sequestering/secreting structures in grasses is an excellent approach to better understand salt tolerance mechanisms in halophytes.

Most structural and physiological work on salt glands in grasses has been conducted in the *Chloridoideae* and *Oryzoideae* subfamilies. Grasses contain either unicellular or bicellular glands, often referred to as glandular trichomes or salt hairs, located on the leaf surface [10]. Salt glands in the *Chloridoideae* are bicellular and consist of a cap cell and a lower basal cell, both of which are cytoplasmically and mitochondria-dense [12]. The cuticle is thickened above the cap cell in some species, forming a cuticular chamber used for storing secreted salts [14]. Though microhairs are found on the leaf surface in all grass subfamilies except the *Pooideae* [12], salt-secreting unicellular hairs are only found in the *Oryzoideae* wild rice species *Porteresia coarctata* [10]. Due to the ubiquitous nature of leaf-borne microhairs in grasses, they have evolved diverse functions including the sequestration or secretion of substances ranging from callose to heavy metals [15, 16]. However, specialized salt sequestering structures in grasses have not been characterized outside of the *Chloridoideae* and *Oryzoideae* subfamilies.

The *Panicoideae* subfamily includes the agronomically important food crops maize and sorghum in addition to the biofuel grasses miscanthus, switchgrass, and sugarcane. One of the most salt-tolerant species in the *Panicoideae* is the halophyte *Paspalum vaginatum* (seashore paspalum). It is cultivated as a turfgrass species worldwide and derives its popularity from its ability to be irrigated with brackish water. Seashore paspalum can survive in salt concentrations near that of seawater [17] and uses osmolyte production, ion homeostasis, and sodium exclusion to cope with salt stress [18-20]. However, its ability to maintain growth while accumulating high

levels of sodium in leaf tissue remains perplexing. To date, no sequestration nor secretion structures have been identified in seashore paspalum nor in the *Panicoideae*.

Here, we study sodium sequestration in 'HI10', a seashore paspalum accession, and 'Spence', a *Paspalum distichum* accession. *Paspalum distichum* is more salt-sensitive and is typically found in freshwater habitats [21]. *Paspalum vaginatum* and *P. distichum* are the only two species that constitute group 'Disticha' in the tribe Paspaleae. Genetic diversity has been assessed in these two sister species [22]. The transferability of simple sequence repeat (SSR) markers from *P. vaginatum* to *P. distichum* but not other *Paspalum* species, supported that they are closely related [22]. They therefore represent a beneficial species-pair to study salt tolerance. We examined leaf structure and show that both *Paspalum* species contain dense rows of translucent papillae on the adaxial surface. The papillae are unicellular protrusions from epidermal cells with 'HI10' containing much larger papillae than 'Spence'. We further demonstrate that the papillae sequester sodium under salt stress. This study represents the first illustration of sodium sequestration in specialized leaf-borne organs within the *Panicoideae*.

Materials and Methods

Plant material and growth

P. vaginatum accession 'HI10' and *P. distichum* accession 'Spence' were used for comparative experiments. Additional *P. vaginatum* accessions ('509018-3', 'KC9', 'PI299042') and a *P. distichum* accession ('Tropic Shore') were also analyzed for some experiments. Individual ramets were grown via nodal propagation. Nodes were propagated and set up in irrigation bins as described in Chapter II. Sorghum accession BTX623, provided by Dr. Bill Rooney, Texas A&M University, was grown for comparison. Sorghum seeds were sowed at the

same time as nodes were started in the propagation process. To initiate salt stress, plants were subjected to 2.5 dS/m salt concentrations for two days, 5 dS/m for two days, 10 dS/m for five days, and then to the final concentration of 30 dS/m. Salt concentrations were acquired using Oceanic sea salt mix and plants remained untrimmed throughout all experiments. All experiments were conducted in the University of Georgia Plant Biology Greenhouses under a day/night temperature of 27°/18°C and 14-hr days.

Sodium and potassium ion measurements

After five weeks of growth under 0 dS/m, 10 dS/m, and 30 dS/m salt stress, tissue fractions (leaf blade, leaf sheath, stolon, and root) were separated and dried at 65°C for 3 days. After flash freezing in liquid nitrogen, samples were powdered in 2-mL tubes with BBs using a Qiagen TissueLyser II. Ten milligrams of powder were incubated in 2-mL tubes with 1.8 mL of 0.5 M nitric acid with continuous shaking for 48 hours at 25°C. Tubes were then centrifuged and the supernatant was diluted with deionized water (1:20 for sodium measurements and 1:25 for potassium measurements). Sodium and potassium ion content were measured on a Cole-Parmer single-channel digital flame photometer in parts per million (ppm). Exact values were calculated using standard curves ranging from 2-60 ppm for both sodium and potassium. For each organ fraction, ion levels were measured in three plants per accession per treatment.

Scanning electron microscopy (SEM) combined with energy-dispersive X-ray spectroscopy (EDS)

Leaf blades (second fully open, developed leaf on growing stolon segment) from *P. vaginatum* genotypes ‘HI10’, ‘509018-3’, and ‘KC9’ in addition to the *P. distichum* accession

'Spence' grown under freshwater (0 dS/m) and salt stress (30 dS/m) for five weeks were excised using a razor blade, placed in vials of fixative containing 2.5% glutaraldehyde in 0.1 M potassium phosphate buffer (pH 7.2) and stored overnight at 4°C. Two leaves per accession per treatment were analyzed. Samples were washed with buffer and post-fixed for 2-hr at 4°C in similarly buffered 1% osmium tetroxide. These samples were rinsed in distilled water, dehydrated in a graded ethanol series (25%, 50%, 75%, 95%, 100%) and critical point dried using a Samdri model 780-A Critical Point Dryer (Tousimis, Inc, Rockville, MD, USA). Samples were mounted on sticky carbon tabs placed on top of aluminum stubs, sputter-coated with gold-palladium (Leica EM Ace 600 Sputter Coater, USA) and viewed using a FEI FE-SEM Teneo Scanning Electron Microscope (Thermo Fisher Scientific, Hillsboro, OR, USA) operating at 10 kV. For EDS elemental analysis, full EDS spectra comprising all detectable elements were acquired. Subsequently, EDS maps were examined for elements of interest. Counts for abaxial glands and stomata were made by counting the number of glands and stomata within a 0.5 mm^2 area on four to five SEM images of the abaxial surface for each accession under 0 dS/m and 30 dS/m growth conditions.

Light microscopy

The *P. vaginatum* accession 'HI10', *P. distichum* accession 'Spence', and sorghum were analyzed in light microscopy experiments. The second fully open, developed leaf from a growing stolon segment was excised from three independent plants, and fixed in 2% formaldehyde for 48-hrs. For sorghum, the second fully open, developing leaf was used. Leaves or leaf segments were dehydrated in a graded ethanol series (10%, 20%, 30%, 40%, 50%, 60%, 70%, 80%, 90%, 95%, 100%) and embedded in medium grade LR White Resin (Electron Microscopy Sciences). One

μM-thick transversal sections were cut from embedded tissues using a Reichert Ultracut ES microtome and stained with a 0.1% toluidine blue solution. Samples were then examined under a bright-field light microscope. For dissecting microscope images, the same numbered leaf was excised from a growing stolon fragment from three independent plants per accession and visualized using Z-stack imaging on a Leica DVM 6 digital microscope. For counts of epidermal cell number, images of sections from three leaves per accession, each from an independent plant, were used. Epidermal cell size was determined on the same images by measuring the cell diameter at the widest point for each cell.

Sodium staining

CoroNa Green (Invitrogen) (15 μM in anhydrous dimethyl sulfoxide (DMSO)) was used to stain papillae for sodium content. CoroNa Green has absorbance and emission spectra of 492 and 516, respectively. Papillae were peeled from the adaxial surface of leaves (second fully open, developed leaf on growing stolon segment) from plants grown under freshwater (0 dS/m) and salt stress (30 dS/m) for six weeks. Strings of papillae were incubated with the dye for two hours in the dark prior to imaging. Samples were taken from three independent plants per genotype per treatment. Samples from the same leaves were also incubated in deionized water as a negative control. Imaging was conducted using a Zeiss LSM 880 upright confocal microscope using a 20X dry objective with the excitation wavelength set at 488 nm and emission detected at 516 nm using an argon laser. Z-stack imaging was conducted to obtain a three-dimensional view of the papillae.

Contact angle measurements

To determine leaf surface hydrophobicity, contact angles of static droplets of water were measured. The second fully open, developed leaf from a growing stolon segment of plants was used. Each leaf used for measurements was cut lengthwise, and one half was used for adaxial measurements while the other half was used for abaxial measurements. Three leaves, each from an independent plant, were excised from plants growing in freshwater (0 dS/m) and salt (30 dS/m) for approximately 2.5 months. To assess hydrophobicity, three to five drops of 1 μL H_2O were pipetted along the adaxial and abaxial leaf surfaces. Contact angles were measured using a Kruss DSA 100 Drop Shape Analyzer. Statistical significance was determined using a Student's two-tailed t-test for each comparison and statistical significance was counted as $P<0.05$.

Results

'HI10' and 'Spence' differ in salt response at 0 dS/m, 10 dS/m, and 30 dS/m

We previously showed that 'HI10' had enhanced growth under salt compared to freshwater while 'Spence' had reduced growth, similarly to what is typically observed in glycophytes (Chapter II Fig. 2.1A). We obtained similar results in the current experiment conducted with sorghum, 'HI10' and 'Spence' at 0 dS/m, 10 dS/m, and 30 dS/m (Fig. 3.1A-C). 'HI10' and 'Spence' also exhibit different leaf morphologies, with 'Spence' having larger, course-textured leaves (Fig. 3.1D) compared to 'HI10' (Fig. 3.1E). Comparison of Na^+ levels in above- and belowground organs of 'HI10', 'Spence' and sorghum revealed a different distribution of Na^+ in *Paspalum* than in sorghum (Figs 3.1F-H). At 30 dS/m, sorghum accumulates the highest amount of sodium in stem tissue, while the highest sodium levels in 'HI10' and 'Spence' are seen in roots (Figs. 3.1F-H). Within *Paspalum* leaf tissue, 'HI10'

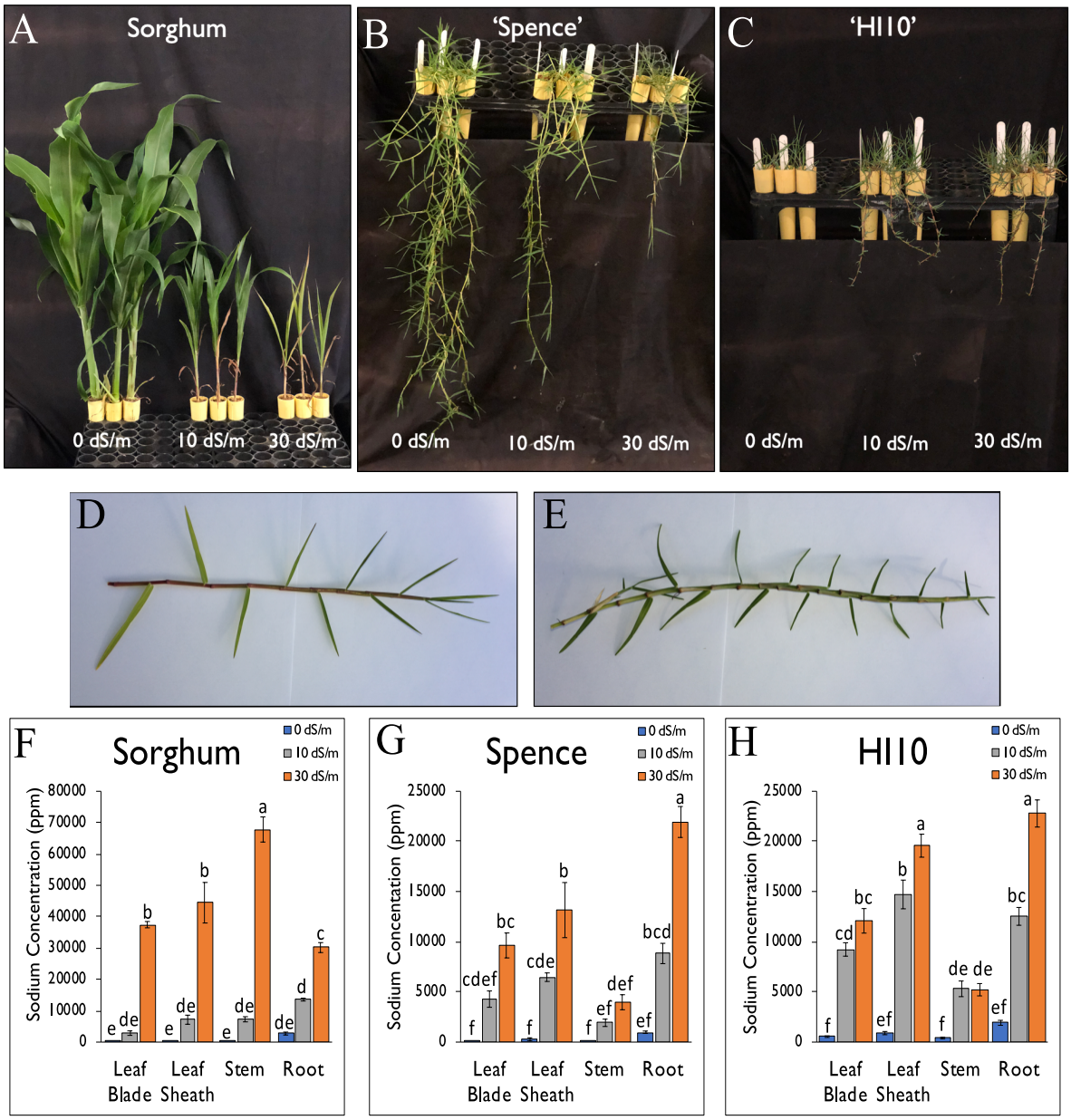

FIGURE 3.1. Growth response to salt stress, stolon/leaf morphology, and sodium distribution in sorghum, *P. distichum,* and *P. vaginatum*. Aboveground growth for three representative plants in freshwater (0 dS/m), 10 dS/m salt, and 30 dS/m salt after 6 weeks of growth under salt stress for **(A)** sorghum, **(B)** *P. distichum* accession 'Spence', and **(C)** *P. vaginatum* accession 'HI10'. Stolon and leaf morphology is shown for **(D)** 'Spence' and **(E)** 'HI10'. Sodium concentration in

leaf blade, leaf sheath, stem, and root tissue is shown for **(F)** sorghum, **(G)** 'Spence', and **(H)** 'HI10'. Letters in **F-H** indicate statistical significance at the level of $P<0.05$ as indicated by one-way ANOVA analyses conducted within each genotype.

sequesters a significantly higher amount of sodium in the leaf sheath relative to leaf blade tissue under both 10 dS/m and 30 dS/m. This same trend is seen in 'Spence', though the difference is not statistically significant.

'HI10' and 'Spence' exhibit distinct leaf surface morphologies

To further investigate the different salt accumulation patterns in 'HI10', 'Spence' and sorghum under salt stress, we compared their leaf anatomy. Scanning electron microscopy (SEM) indicates that papillae are found across the adaxial surface in both 'HI10' and 'Spence' (Fig. 3.2A). Costal ridges with papillae overarch grooves containing stomata (Suppl. Fig. 3.1A). Both the SEM images and the images acquired under a high-powered dissecting microscope without sample dehydration or other preparation show that the papillae are considerably larger in 'HI10' than in 'Spence' (Fig. 3.2A). Images obtained from the dissecting microscope also indicate that the papillae are translucent. SEM was used to also examine papilla size in *P. vaginatum* accessions '5090180-3', which grows similarly to 'HI10', and 'KC9', which grows more similarly to 'Spence' under salt stress (Chapter II, Fig. 2.1A). Papillae size did not appear to be different amongst *P. vaginatum* accessions, and all had large papillae compared to 'Spence' (Suppl. Fig. 3.1C).

Light microscopy indicates that papillae are unicellular, extended epidermal cells, and they form above each major longitudinal vein (Fig. 3.2 B-C). In contrast, sorghum epidermal

cells are not extended and remain uniform across the leaf surface (Fig. 3.2D). Though the number of epidermal cells above each vein is similar, their size, measured at their widest point, significantly differs between 'HI10' and 'Spence' (Figs. 3.2E-F).

Glandular trichome-like structures, morphologically similar to the bicellular trichomes found in the Panicoid grass Johnsongrass [15], are present on the abaxial surface of 'HI10' and 'Spence', though their density is significantly higher in the latter (Suppl. Fig. 3.2A-B) ($p=0.00130128$). Similar to stomatal density, gland density is not dependent upon salt treatment (Suppl. Fig. 3.2B-C). Energy dispersive spectroscopy (EDS) conducted on SEM samples shows that these structures secreted a silicon-containing substance (Suppl. Fig. 3.2D-E), though the composition and function of this exudate is unknown. This exudation was observed in only a few glands in both species under freshwater and salt stress conditions.

Contact angle measurements: a proxy for papillae size

Contact angle measurements of static water droplets have been used to assess the leaf surface hydrophobicity in species such as rice [23]. To determine if papilla size affects leaf surface hydrophobicity, we measured the contact angle of droplets placed on the adaxial and abaxial leaf surfaces of 'HI10', 'Spence', and sorghum. The adaxial leaf surface containing papillae was significantly more hydrophobic compared to the abaxial surface in both 'HI10' ($p=9.35E-16$) and 'Spence' ($p=4.78E-5$), while similar levels of hydrophobicity were observed on both surfaces in sorghum ($p=0.5971$) (Fig. 3.2G). There were no significant differences in abaxial leaf surface hydrophobicity between 'HI10' and 'Spence' ($p=0.9451$). However, adaxial surface hydrophobicity was significantly higher in 'HI10' compared to 'Spence' ($p=3.24E-09$). Compared to sorghum, the adaxial surface was significantly more hydrophobic in both 'HI10'

(p=7.268E-16) and ‘Spence’ (p=2.0265E-14). There were no or only marginal differences in the hydrophobicity of the abaxial surface between sorghum and seashore paspalum accessions ‘HI10’ (p=0.058678) and ‘Spence’ (p=0.032544).

To identify *P. vaginatum* accessions that may have smaller papillae compared to ‘HI10’, the *P. vaginatum* accession ‘PI299042’ was examined. ‘PI299042’ has a similar leaf size and texture as ‘Spence’, and has been reported to be more salt sensitive than ‘HI10’ based on visual turf quality scores (P. Raymer, Pers. Comm., Chapter II Suppl. Table 2.4). Papilla size in accession ‘PI299042’ appears to be slightly larger than in ‘Spence’ (Suppl. Fig. 3.1D-F), but more precise measurements are needed to confirm this. Adaxial surface hydrophobicity in accession ‘PI299042’ was intermediate between that of ‘HI10’ and ‘Spence (adaxial average=110.1±2.6, abaxial average=63.6±1.3). Another *P. distichum* accession, ‘Tropic Shore’, which performs more similarly to ‘Spence’ and ‘KC9’ under salt stress (Chapter II, Suppl. Fig. 2.2A), has papillae that appear to be slightly larger than those in ‘Spence’ when viewed under a dissecting microscope (Suppl. Fig. 3.1D). Contact angle measurements on ‘Tropic Shore’ confirm this (adaxial average = 114.4±0.86, abaxial average=64.1±1.23).

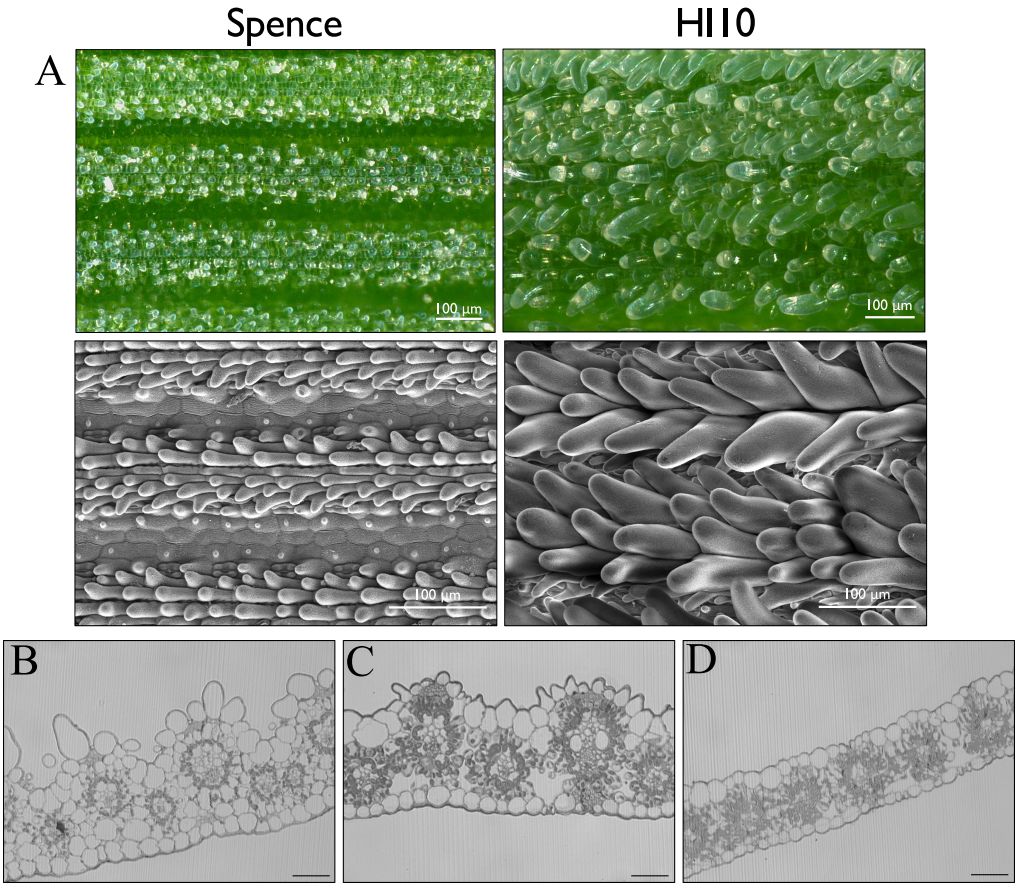
Spence
HI10
A
100 µm
100 µm
100 µm
100 µm
B
C
D

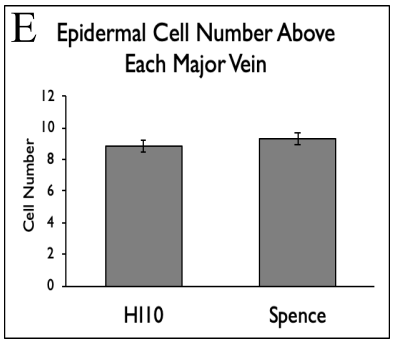
E
Epidermal Cell Number Above Each Major Vein
Cell Number
0
2
4
6
8
10
12
HI10
Spence

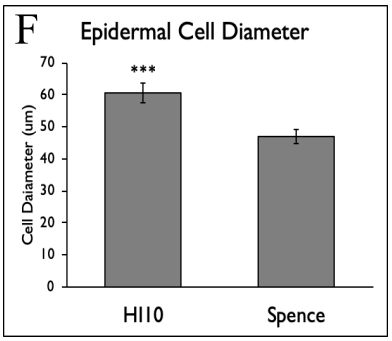
F
Epidermal Cell Diameter
***
Cell Daiameter (um)
0
10
20
30
40
50
60
70
HI10
Spence

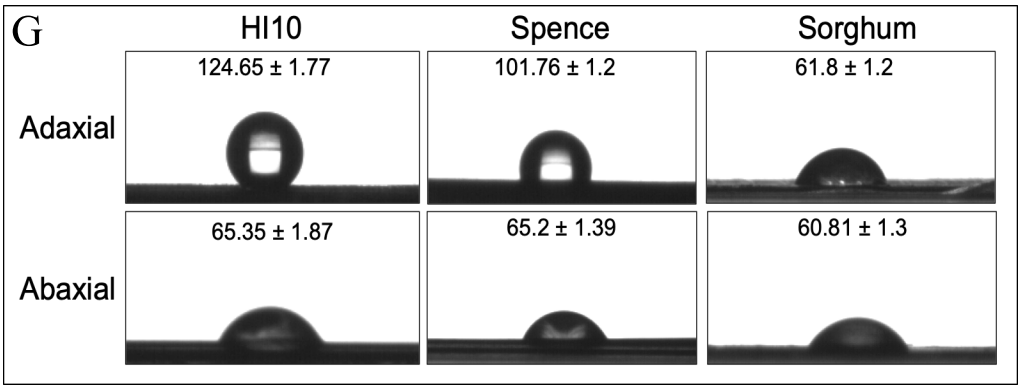
G
HI10
Spence
Sorghum
Adaxial
124.65 ± 1.77
101.76 ± 1.2
61.8 ± 1.2
Abaxial
65.35 ± 1.87
65.2 ± 1.39
60.81 ± 1.3

FIGURE 3.2. Morphological differences in leaf surface characteristics in *P. distichum* accession 'Spence' and *P. vaginatum* accession 'HI10'. **(A)** Scanning electron microscopy (SEM) and dissecting microscope images from plants grown in freshwater (0 dS/m). Representative light microscopy images are shown for freshwater leaf samples from **(B)** 'HI10', **(C)** 'Spence', and **(D)** sorghum. **(E)** The number of epidermal cells above each major vein and **(F)** the mean diameter of those epidermal cells (n=52 cells for 'Spence', 51 cells for 'HI10'), measured from images obtained by light microscopy. **(G)** Representative images of static water droplets on the adaxial and abaxial leaf surfaces, and corresponding mean contact angles for 'HI10', 'Spence' and sorghum (n=3-5 measurements made on three leaves from different plants for each accession for a total of 9-15 measurements). All values shown represent means ± standard error. Asterisks in **(F)** indicate statistical significance from a student's t-test (p=0.000576).

Leaf papillae sequester sodium under salt stress

Papillae can be peeled and isolated from the leaf surface relatively easily (Suppl. Fig. 3.1B). To determine if papillae sequester sodium under salt stress, ion content in adaxial papillae-enriched peels and underlying leaf tissue without papillae was compared. Under salt stress, sodium content is significantly higher in papillae-enriched peels compared with underling tissue in both 'Spence' and 'HI10' (Fig. 3.3A).

To confirm sodium sequestration, the CoroNa Green sodium stain was used to stain peeled papillae. Staining of papillae from plants grown under freshwater and 30 dS/m salt stress indicate that sodium is present in 'HI10' papillae under salt stress (Fig 3.3B). Sodium is also present in 'Spence' papillae, though it seems to be concentrated in papilla tips and not uniformly distributed as seen in 'HI10'. In 'Spence', strong fluorescence was observed both under

freshwater and salt conditions in the cell layer running underneath the costal ridges. EDS illustrates that this cell layer is silicon-reinforced (Suppl. Fig. 3.3A-B). Though more difficult to observe due to the large papillae size, siliconized cells were also observed in 'HI10' in the same location (Suppl. Fig. 3.3 C-D).

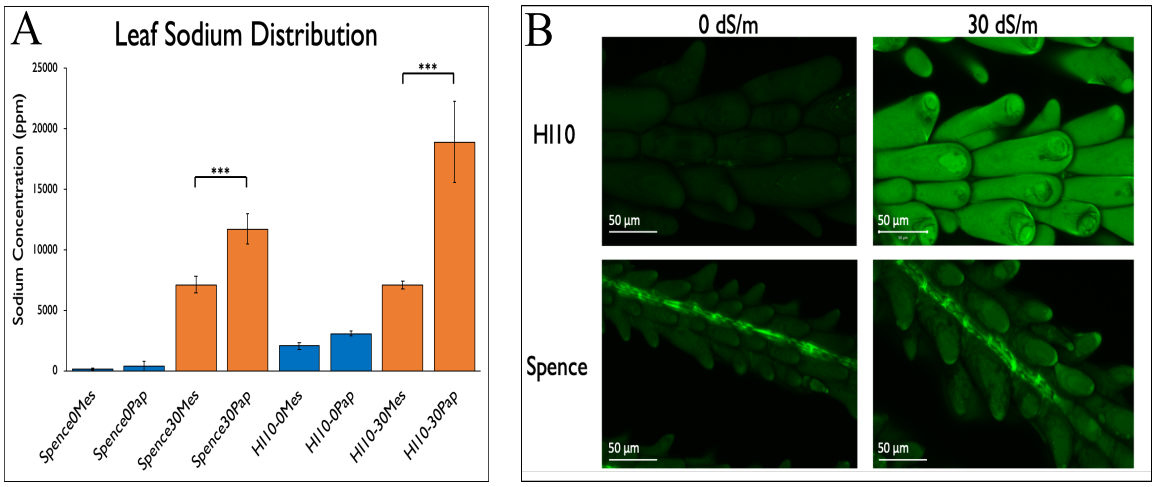

FIGURE 3.3. Sodium sequestration ability in papillae for the *P. distichum* accession 'Spence' and the *P. vaginatum* accession 'HI10'. **(A)** Leaf sodium distribution for papillae-enriched adaxial peels (suffix 'Pap') and underlying leaf tissue lacking papillae (suffix 'Mes') of plants grown in freshwater (0 dS/m) and salt stress (30 dS/m). **(B)** Representative images of peeled strings of papillae stained using the CoroNa Green sodium stain and visualized via confocal microscopy. Scale bars = 30 µm. Asterisks in **(A)** indicate statistical significance from a student's t-test comparing sodium in papillae-enriched adaxial peels and underlying leaf tissue lacking papillae from plants grown in 30 dS/m for 'Spence' ($p=0.031757$) and 'HI10' ($p=0.024231$).

Discussion

Papillae form and function

Leaf papillae are prevalent in several grass families, and their function varies by family and species. In the *Bambusoideae*, papillae are found in conical arrangements surrounding stomata on the leaf surface, and thus may affect transpiration [24]. These conical arrangements are also seen in *Spartina* species within the *Chloridoideae* [25]. The presence of stomata within intercostal grooves in *Paspalum* (Suppl. Fig. 3.1A) suggests that, similarly to encrypted stomata that are "covered" by cellular structures [26], the papillae may help prevent excessive water loss under stress. In the *Chloridoideae*, both saltwater and freshwater *Spartina* species have costal ridges covered with papillae that overarch grooves containing stomata [25]. While these papillae are smaller than in seashore paspalum, saltwater *Spartina* species have larger ridges than freshwater species and CO_2 exchange occurs primarily in adaxial stomata. Consequently, larger ridges in saltwater *Spartina* species increase the boundary layer over stomata, lowering leaf conductance to water vapor, and these species thus are more highly adapted to modulating water loss under stress conditions [25]. Similarly, 'HI10' appears to have larger costal ridges than 'Spence' and this may, at least in part, be caused by the larger papilla size of 'HI10' (Fig. 3.2B-C). Furthermore, the large ridges in *Spartina* fit together when leaf rolling occurs which covers stomata within grooves, further preventing excess water loss under times of stress [25]. Ridges on *Paspalum* leaves appear to fit together similarly when leaf rolling occurs [27], so it is likely that the larger ridges in 'HI10' help prevent water loss more efficiently compared to the small ridges in 'Spence'.

Sodium sequestration in Paspalum

A striking difference between the papillae present in seashore paspalum and other grass species is their size and high density. This begged the question as to whether they had evolved functions other than regulating transpiration. The structures that papillae most strongly resemble are adaxial salt-secreting unicellular hairs found in *P. coarctata*, a wild rice species [28, 29]. Though these unicellular structures are present in different subfamilies within the *Poaceae*, they appear to be structurally and functionally similar in that they are unicellular and have evolved sodium secretion/sequesteration. Similar to *Paspalum*, *P. coarctata* contains costal ridges and grooves, but in stark contrast to *Paspalum*, the papillae-like hairs in *P. coarctata* are found in the grooves instead of atop costal ridges [28]. However, *P. coarctata* still contains small papillae atop the costal ridges. In addition to the large papillae making up costal ridges in *Paspalum*, we observed sparse, undersized papillae in the intercostal grooves (Fig. 3.2A). We hypothesize that *Paspalum* papillae, and perhaps *P. coarctata* hairs, are distinct from bicellular macro/microhairs in grasses, and may have independently evolved from the same structures on the surface. Indeed, papillae are found on the leaf surface atop costal ridges and within intercostal grooves in many *Poaceae* subfamilies including the *Chloridoideae* [30, 31], *Oryzoideae* [28], *Bambusoideae* [32, 33], *Pooideae* [34, 35], and *Panicoideae* [36, 37]. Interestingly, although *Setaria italica,* a Panicoid grass, does not have leaf papillae, some wild relatives have sparsely populated costal and intercostal papillae on the adaxial surface [37]. It should be noted that though similar in unicellular structure, sodium sequestration and secreting mechanisms may differ between *P. coarctata, P. vaginatum,* and *P. distichum*. To date, the genetic mechanism behind sodium loading into unicellular salt hairs of *P. coarctata* is unknown, though it may be similar to the

mechanism recently identified in quinoa, involving the HKT1-type transporter responsible for one-way transport of sodium into unicellular bladder cells [38].

Furthermore, we observed differences in sodium distribution between 'HI10' and 'Spence' under both freshwater and salt stress conditions, indicating that sodium-concentrating mechanisms may differ between them (Fig. 3.3A-B). It seems clear that both 'Spence' and 'HI10' are efficient sodium excluders compared with the glycophyte sorghum, as they only take up about 25% of the sodium observed in sorghum in leaf blade tissue (Fig. 3.1F-H). Interestingly, most sodium in *Paspalum* leaf tissue appears to be concentrated in the leaf sheath (Fig. 3.1G-H), similar to results found in durum wheat [39]. Though 'HI10' and 'Spence' have similar levels of sodium in the underlying leaf tissue left after peeling papillae from the leaf surface, 'HI10' appears to have a higher concentration of sodium in the papillae-enriched adaxial peels (Fig. 3.3A). Results obtained for sodium staining with CoroNa Green (Fig. 3.3B) also indicate that perhaps 'Spence' is not as efficient as 'HI10' at shuttling sodium into the papillae due to sodium staining being concentrated in the underlying silicon-reinforced cell layer in 'Spence'. More detailed analyses of sodium distribution at a finer resolution in leaf tissue will be conducted in future studies to examine this further.

To date, no grass species except *Paspalum* and *P. coarctata* have been shown to sequester or secrete salt through the use of enlarged, unicellular, papillae-like structures. However, the prevalence of costal/intercostal leaf papillae and the evolution of parallel sodium sequestration mechanisms in the *Oryzoideae* and *Panicoideae* grass subfamilies suggests that other salt-tolerant grass species may have co-opted them for similar roles.

Potential genetics behind papillae development and function

There is little data available on the genetic control of papillae formation in plants. It is generally thought that epidermal outgrowths like papillae arose from modifications of unicellular trichomes over evolutionary time [10]. Trichomes in *Arabidopsis* are unicellular, have a high volume compared to epidermal cells, and contain a large vacuole, which are traits that can be taken advantage of to evolve sodium sequestration mechanisms. Thus, it has been proposed that genetic analyses of trichome formation in model species like *Arabidopsis* can be used to gain insight into the development of salt-sequestering structures found in dicots like quinoa [38, 40]. However, it is unclear whether unicellular papillae found on the leaf surface of seashore paspalum utilize a similar genetic framework during development as trichomes. Some genetic work has been conducted to understand the formation of epidermal papillae on other plant organs, such as the surface of stigma [41], trichome bases [42], and flower petals [43]. Some genes have been identified, such as the *GLASSY HAIR* (*GLH*) genes which contribute to papillae formation on trichome bases in *Arabidopsis* [44, 45]. It is possible that orthologous genes are associated with epidermal outgrowths such as leaf papillae in diverse plant species.

Papillae covering costal ridges and grooves in grass species are the most analogous to *Paspalum* papillae, and little is known about their development. In rice, some studies have focused on identification of genes that control the presence, density, and size of small papillae on the leaf surface. The *bright green leaf* (*bgl*) locus encodes the *OsRopGEF10* gene, which controls the presence of leaf surface papillae in coordination with the *OsRac1* gene [46]. Though not discussed, it appears that mutants of the rice *NARROW LEAF1* (*NAL1*) gene contain smaller papillae on the leaf surface compared with wildtype [47]. It is yet to be determined if similar genes are at play during the formation of leaf papillae in *Paspalum*.

Abaxial glands in P. vaginatum and P. distichum

The existence of salt gland-like structures on the abaxial leaf surface in *P. vaginatum* and *P. distichum* is intriguing because seashore paspalum does not exhibit secretion capacity under salt stress [48]. The function of the silicon-containing exudation we observed (Suppl. Fig. 3.2D-E) is unknown, but is unlikely to be related to salt stress as it was observed in both freshwater and salt conditions. Glands in the dicot *Plumbago capensis* also secrete small amounts of silicon, though the function of silicon in this secretion remains unknown [49]. Bicellular glands on the leaf surface contain silicon in cell walls in sugarcane [50], bamboo [51, 52] and sorghum [53], and silicon is also present in both the cell wall and lumen in papillae found on glumes in *Phalaris canariensis* [54]. Consequently, the silicon observed by EDS in our experiments may be cellular contents that were exuded during SEM prep. Cryo-SEM with EDS which involves analysis of frozen tissue without additional preparation would resolve whether this exudation occurred during plant growth or during SEM preparatory procedures.

Our data revealed that *Paspalum* sequesters sodium in the adaxial leaf papillae, but it is interesting that sequestration occurs in papillae rather than sodium being secreted through abaxial glands under salt stress as seen in the "Chloridoid-type" bicellular glands found in the *Chloridoideae* and *Danthanioideae* subfamilies [12, 55]. Abaxial glands in seashore paspalum are typically 30-40 μm in length (Suppl. Fig. 3.2A), which is similar to the size of salt glands in the *Chloridoideae*, *Danthanioideae* [12, 55]. The density of abaxial glands in *P. vaginatum* is about half of that seen in *P. distichum* (Suppl. Fig. 3.2B). Consequently, it is possible that *P. vaginatum* acquired the ability to sequester sodium in adaxial papillae due to the low density of salt-secreting structures on the abaxial surface. Salt gland density in Chloridoid species like *Limonium* and *Zoysia* range from 20-50 glands mm^2 [56, 57], while all three seashore paspalum

accessions examined contain less than half that (Suppl. Fig. 3.2B). Interestingly, gland density in *P. distichum* 'Spence' is closer to that seen in Chloridoid species (Suppl. Fig. 3.2B), though it is unclear why *P. distichum* appears to retain a high density of these glands.

It is intriguing to think of the possibility of increasing salt tolerance by inducing sodium secretion and/or sequestration in inactive glands found in glycophyic species. Species like maize can modulate the density of non-secreting hairs on the leaf surface under salt stress [58]. Their density nearly doubles in response to high salinity. Furthermore, it is interesting to note that abaxial glands in *P. vaginatum* and *P. distichum* closely resemble bicellular glands found on adaxial and abaxial leaf surfaces in another Panicoid grass, Johnsongrass, which can secrete salt when grown in lime-containing soil [15]. However, Johnsongrass glands did not secrete salts when grown under salt stress, implying that they are not sodium-responsive. *Sorghum bicolor* also contains bicellular glands on its leaf surface that can secrete salts, but similarly only when grown in lime-containing soil, and it is unknown whether this secretion contains sodium [15]. The mechanism behind lime-induced salt secretion is unknown, but these results imply that glands present in Panicoid grasses, including *Paspalum*, can potentially be induced to secrete, and perhaps even sequester salts under certain conditions. Alternatively, once we understand the genetics behind papilla formation in *Paspalum*, it may be possible to engineer glycophytic Panicoids to develop salt-sequestrating papillae to enhance their levels of salt tolerance.

Understanding sodium sequestration in Paspalum

We report that papilla size does not appear to differ amongst the *P. vaginatum* accessions tested (Suppl. Fig 1C). Nevertheless, these accessions differ in their salt response (Chapter II). While papillae in *P. distichum* accession 'Spence' are considerably smaller than the papillae in

P. vaginatum, another diploid *P. distichum* accession 'Tropic Shore', though salt sensitive (Chapter II), has papillae intermediate in size between 'HI10' and 'Spence' (Suppl. Fig. 3.1D). These results collectively suggest that once a certain size is reached, papillae size may not be the main factor contributing to salt tolerance, but sequestration ability in papillae or perhaps other tissue types like the leaf sheath may be more important. This is similar to the ability of only some salt glands found in the *Chloridoideae* to have salt secretion capacity [10]. For example, despite nearly identical structure, salt glands in some saltwater *Spartina* species secrete salt while those in freshwater *Spartina* species do not [25]. Thus, future studies will need to examine the sodium sequestering mechanism in papillae in diverse seashore paspalum accessions. It may be possible to use contact angle measurements to initially screen for large papillae size, but sequestration ability will also need to be assessed. We identified a *P. vaginatum* accession, 'PI299042', that differs from 'HI10' in both salt tolerance when treated as a trimmed turf and adaxial surface hydrophobicity. Consequently, crosses between accessions 'HI10' and 'PI299042' will be used for genetic mapping of papillae size and analysis of sequestration function in future studies. We are also attempting crosses between 'HI10' and 'Spence', but it is currently unknown whether *P. vaginatum* and *P. distichum* accessions with the same ploidy level are cross-compatible.

Conclusion

Our study provides the first evidence of unicellular sodium-sequestration structures in the *Panicoideae*, an economically crucial family of plants. We show that 'HI10' and 'Spence' differ in leaf morphology and contain sodium-sequestering papillae across the adaxial surface. The leaf papillae are a major sink for sodium sequestration under salt stress in *Paspalum*, and large

papillae may have an advantage over small papillae in the amount of salt they can store. Due to the prevalence of leaf papillae in the *Poaceae*, including on the leaf surface of economically vital crops like rice [46] and maize [59], it is important to further study the genetic mechanisms of papilla development and of sodium sequestration in these modified epidermal cells. We envision that, in the future, these mechanisms may be leveraged in salt-sensitive Panicoid crops currently unable to sequester sodium in the undersized papillae present on the leaf surface. It is logical to take advantage of pre-existing structures that may be modified rather than engineering the production of novel structures on the leaf surface to act as a collective sodium sink under salt stress. Future studies will focus on the underlying mechanisms behind sodium-loading into papillae cells and provide the groundwork for future introgression of this trait into salt-sensitive species.

Acknowledgements

We would like to thank Beth Richardson and John Shields in the Georgia Electron Microscopy lab at the University of Georgia for their help with SEM and Jason Locklin at the UGA New Materials Institute for help with contact angle measurements. Experiments in this chapter were funded through the grants shown below.

USDA-SCRI awarded to K.M. Devos (2015-51181-24291; PI: K.E. Kenworthy, University of Florida)

NIH T32 Training Grant (T32 GM 7103-41)

References

1. Mayak, S., T. Tirosh, and B.R. Glick, *Plant growth-promoting bacteria confer resistance in tomato plants to salt stress.* Plant Physiology and Biochemistry, 2004. **42**(6): p. 565-572.
2. Qadir, M., et al., *Economics of salt-induced land degradation and restoration.* Natural Resources Forum, 2014. **38**(4): p. 282-295.
3. Munns, R. and M. Gilliham, *Salinity tolerance of crops - what is the cost?* New Phytologist, 2015. **208**(3): p. 668-673.
4. Rajalakshmi, S. and A. Parida, *Halophytes as a source of genes for abiotic stress tolerance.* Journal of Plant Biochemistry and Biotechnology, 2012. **21**(1): p. S63-S67.
5. Roy, S. and U. Chakraborty, *Salt tolerance mechanisms in Salt Tolerant Grasses (STGs) and their prospects in cereal crop improvement.* Botanical Studies, 2014. **55**: p. 9.
6. Meng, X.Q., J. Zhou, and N. Sui, *Mechanisms of salt tolerance in halophytes: current understanding and recent advances.* Open Life Sciences, 2018. **13**(1): p. 149-154.
7. Flowers, T.J. and T.D. Colmer, *Salinity tolerance in halophytes.* New Phytologist, 2008. **179**(4): p. 945-963.
8. Grieve, C.M. and E.V. Maas, *BETAINE ACCUMULATION IN SALT-STRESSED SORGHUM.* Physiologia Plantarum, 1984. **61**(2): p. 167-171.
9. Wyn Jones RG, S.R., *Betaines.* In: Paleg LG, Aspinall D (eds) Physiology and Biochemistry of Drought Resistance in Plants, 1981. **Academic Press, Australia**: p. 171-204.
10. Dassanayake, M. and J.C. Larkin, *Making Plants Break a Sweat: the Structure, Function, and Evolution of Plant Salt Glands.* Front Plant Sci, 2017. **8**: p. 406.

11. Flowers, T.J., H.K. Galal, and L. Bromham, *Evolution of halophytes: multiple origins of salt tolerance in land plants.* Functional Plant Biology, 2010. **37**(7): p. 604-612.

12. Ceccoli, G., et al., *Salt Glands in the Poaceae Family and Their Relationship to Salinity Tolerance.* Botanical Review, 2015. **81**(2): p. 162-178.

13. Bennett, T.H., T.J. Flowers, and L. Bromham, *Repeated evolution of salt-tolerance in grasses.* Biol Lett, 2013. **9**(2).

14. Amarasinghe, V. and L. Watson, *COMPARATIVE ULTRASTRUCTURE OF MICROHAIRS IN GRASSES.* Botanical Journal of the Linnean Society, 1988. **98**(4): p. 303-319.

15. McWhorter, C.G., R.N. Paul, and J.C. Ouzts, *BICELLULAR TRICHOMES OF JOHNSONGRASS (SORGHUM-HALEPENSE) LEAVES - MORPHOLOGY, HISTOCHEMISTRY, AND FUNCTION.* Weed Science, 1995. **43**(2): p. 201-208.

16. Burke, D.J., J.S. Weis, and P. Weis, *Release of metals by the leaves of the salt marsh grasses Spartina alterniflora and Phragmites australis.* Estuarine Coastal and Shelf Science, 2000. **51**(2): p. 153-159.

17. Uddin, M.K., et al., *Physiological and growth responses of six turfgrass species relative to salinity tolerance.* Scientific World Journal, 2012: p. 10.

18. Guo, H.L., et al., *Growth response and ion regulation of seashore paspalum accessions to increasing salinity.* Environmental and Experimental Botany, 2016. **131**: p. 137-145.

19. Lee, G., et al., *Synthesis of organic osmolytes and salt tolerance mechanisms in Paspalum vaginatum.* Environmental and Experimental Botany, 2008. **63**(1-3): p. 19-27.

20. Peacock, C.H. and A.E. Dudeck, *PHYSIOLOGICAL AND GROWTH-RESPONSES OF SEASHORE PASPALUM TO SALINITY.* Hortscience, 1985. **20**(1): p. 111-112.

21. HL Leithead, L.Y., TN Shiflet, *100 native forage grasses in 11 southern states.* Agricultural Handbook, Soil Conservation Service, USDA, 1971. **No. 389**: p. 216.

22. Eudy D, B.B., Harrison ML, Raymer P, Devos KM *Ploidy level and genetic diversity in the genus Paspalum, group Disticha.* Crop Science 2017. **57**: p. 3319-3332.

23. Kurokawa, Y., et al., *Rice leaf hydrophobicity and gas films are conferred by a wax synthesis gene (LGF1) and contribute to flood tolerance.* New Phytologist, 2018. **218**(4): p. 1558-1569.

24. Zhang, Y.X., C.X. Zeng, and D.Z. Li, *Scanning electron microscopy of the leaf epidermis in Arundinarieae (Poaceae: Bambusoideae): evolutionary implications of selected micromorphological features.* Botanical Journal of the Linnean Society, 2014. **176**(1): p. 46-65.

25. Maricle, B.R., et al., *Diversity in leaf anatomy, and stomatal distribution and conductance, between salt marsh and freshwater species in the C-4 genus Spartina (Poaceae).* New Phytologist, 2009. **184**(1): p. 216-233.

26. Jordan, G.J., et al., *The evolutionary relations of sunken covered, and encrypted stomata to dry habitats in proteaceae.* American Journal of Botany, 2008. **95**(5): p. 521-530.

27. Ellis, R.P., *Comparative leaf anatomy of Paspalum paspalodes and P. vaginatum.* Bothalia, 1974. **11**(3): p. 235-241.

28. Flowers, T.J., et al., *SALT TOLERANCE IN THE HALOPHYTIC WILD RICE, PORTERESIA-COARCTATA TATEOKA.* New Phytologist, 1990. **114**(4): p. 675-684.

29. Sengupta, S. and A.L. Majumder, *Porteresia coarctata (Roxb.) Tateoka, a wild rice: a potential model for studying salt-stress biology in rice.* Plant Cell and Environment, 2010. **33**(4): p. 526-542.

30. Barhoumi, Z., et al., *Ultrastructure of Aeluropus littoralis leaf salt glands under NaCl stress.* Protoplasma, 2008. **233**(3-4): p. 195-202.

31. Milby, T.H., *LEAF ANATOMY OF BUFFALO GRASS, BUCHLOE-DACTYLOIDES (NUTT) ENGELM.* Botanical Gazette, 1971. **132**(4): p. 308-&.

32. Zhang, W.G., et al., *Gelidocalamus xunwuensis (Poaceae, Bambusoideae), a new species from southeastern Jiangxi, China.* Phytokeys, 2017(85): p. 59-67.

33. Leandro, T.D., V.L. Scatena, and L.G. Clark, *The contribution of foliar micromorphology and anatomy to the circumscription of species within the Chusquea ramosissima informal group (Poaceae, Bambusoideae, Bambuseae).* Plant Systematics and Evolution, 2017. **303**(6): p. 745-756.

34. Macfarlane, T.D. and L. Watson, *THE CLASSIFICATION OF POACEAE SUBFAMILY POOIDEAE.* Taxon, 1982. **31**(2): p. 178-203.

35. Ospina, J.C., S.S. Aliscioni, and S.S. Denham, *A revision of Festuca (Loliinae, Pooideae, Poaceae) in Chile.* Phytotaxa, 2015. **223**(1): p. 1-+.

36. Sanyal, D., P.C. Bhowmik, and K.N. Reddy, *Influence of leaf surface micromorphology, wax content, and surfactant on primisulfuron droplet spread on barnyardgrass (Echinochloa crus-galli) and green foxtail (Setaria viridis).* Weed Science, 2006. **54**(4): p. 627-633.

37. Aliscioni, S.S., J.C. Ospina, and N.E. Gomiz, *Morphology and leaf anatomy of Setaria s.l. (Poaceae: Panicoideae: Paniceae) and its taxonomic significance.* Plant Systematics and Evolution, 2016. **302**(2): p. 173-185.

38. Bohm, J., et al., *Understanding the Molecular Basis of Salt Sequestration in Epidermal Bladder Cells of Chenopodium quinoa.* Current Biology, 2018. **28**(19): p. 3075-+.

39. Davenport, R., et al., *Control of sodium transport in durum wheat.* Plant Physiology, 2005. **137**(3): p. 807-818.

40. Shabala, S., J. Bose, and R. Hedrich, *Salt bladders: do they matter?* Trends in Plant Science, 2014. **19**(11): p. 687-691.

41. Edlund, A.F., R. Swanson, and D. Preuss, *Pollen and stigma structure and function: The role of diversity in pollination.* Plant Cell, 2004. **16**: p. S84-S97.

42. Sambade, A., et al., *Actin-Dependent and -Independent Functions of Cortical Microtubules in the Differentiation of Arabidopsis Leaf Trichomes.* Plant Cell, 2014. **26**(4): p. 1629-1644.

43. Brehm, B.G. and D. Krell, *FLAVONOID LOCALIZATION IN EPIDERMAL PAPILLAE OF FLOWER PETALS - SPECIALIZED ADAPTATION FOR ULTRAVIOLET-ABSORPTION.* Science, 1975. **190**(4220): p. 1221-1223.

44. Fornero, C., et al., *Papillae formation on trichome cell walls requires the function of the mediator complex subunit Med25.* Plant Molecular Biology, 2017. **95**(4-5): p. 389-398.

45. Suo, B.X., S. Seifert, and V. Kirik, *Arabidopsis GLASSY HAIR genes promote trichome papillae development.* Journal of Experimental Botany, 2013. **64**(16): p. 4981-4991.

46. Yoo, J.H., et al., *The rice bright green leaf (bgl) locus encodes OsRopGEF10, which activates the development of small cuticular papillae on leaf surfaces.* Plant Molecular Biology, 2011. **77**(6): p. 631-641.

47. Cho, S.H., et al., *Rice NARROW LEAF1 Regulates Leaf and Adventitious Root Development.* Plant Molecular Biology Reporter, 2014. **32**(1): p. 270-281.

48. Chen, J.B., et al., *Growth responses and ion regulation of four warm season turfgrasses to long-term salinity stress.* Scientia Horticulturae, 2009. **122**(4): p. 620-625.

49. Sakai, W.S., *SCANNING ELECTRON-MICROSCOPY AND ENERGY DISPERSIVE-X-RAY ANALYSIS OF CHALK SECRETING LEAF GLANDS OF PLUMBAGO-CAPENSIS.* American Journal of Botany, 1974. **61**(1): p. 94-99.

50. Sakai, W.S. and W.G. Sanford, *A DEVELOPMENTAL-STUDY OF SILICIFICATION IN THE ABAXIAL EPIDERMAL-CELLS OF SUGARCANE LEAF BLADES USING SCANNING ELECTRON-MICROSCOPY AND ENERGY DISPERSIVE-X-RAY ANALYSIS.* American Journal of Botany, 1984. **71**(10): p. 1315-1322.

51. Motomura, H., T. Fujii, and M. Suzuki, *Distribution of silicified cells in the leaf blades of Pleioblastus chino (Franchet et Savatier) Makino (Bambusoideae).* Annals of Botany, 2000. **85**(6): p. 751-757.

52. Motomura, H., T. Fujii, and M. Suzuki, *Silica deposition in relation to ageing of leaf tissues in Sasa veitchii (Carriere) rehder (Poaceae : Bambusoideae).* Annals of Botany, 2004. **93**(3): p. 235-248.

53. Kumar, S., M. Soukup, and R. Elbaum, *Silicification in Grasses: Variation between Different Cell Types.* Frontiers in Plant Science, 2017. **8**: p. 8.

54. Hodson, M.J., A.G. Sangster, and D.W. Parry, *AN ULTRASTRUCTURAL-STUDY ON THE DEVELOPMENTAL PHASES AND SILICIFICATION OF THE GLUMES OF PHALARIS-CANARIENSIS L.* Annals of Botany, 1985. **55**(5): p. 649-665.

55. Reimer, E. and J.H. Cota-Sanchez, *An SEM survey of the leaf epidermis in danthonioid grasses (Poaceae : Danthonioideae).* Systematic Botany, 2007. **32**(1): p. 60-70.

56. Ding, F., et al., *Ca2+ significantly enhanced development and salt-secretion rate of salt glands of Limonium bicolor under NaCl treatment.* South African Journal of Botany, 2010. **76**(1): p. 95-101.

57. Yamamoto, A., et al., *The relationship between salt gland density and sodium accumulation/secretion in a wide selection from three Zoysia species.* Australian Journal of Botany, 2016. **64**(4): p. 277-284.

58. Ramadan, T. and T.J. Flowers, *Effects of salinity and benzyl adenine on development and function of microhairs of Zea mays L.* Planta, 2004. **219**(4): p. 639-648.

59. Juarez, M.T., R.W. Twigg, and M.C.P. Timmermans, *Specification of adaxial cell fate during maize leaf development.* Development, 2004. **131**(18): p. 4533-4544.

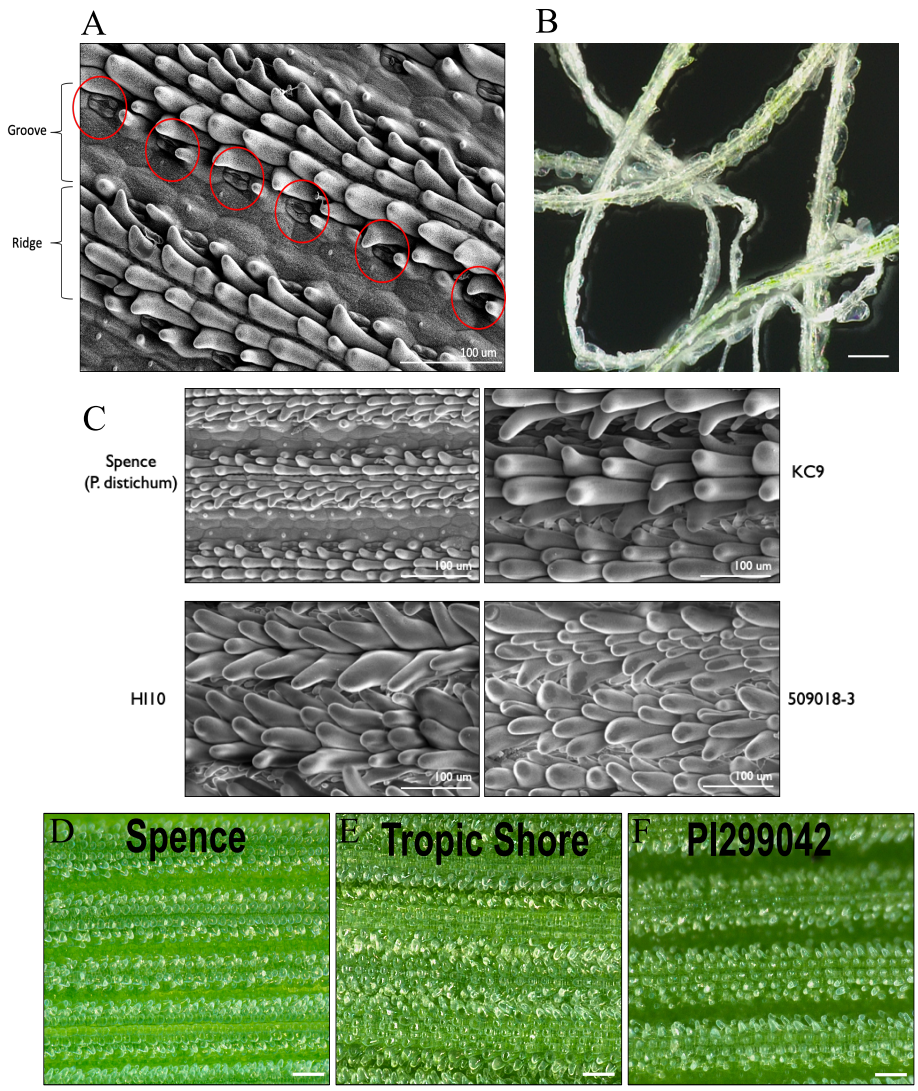

SUPPLEMENTAL FIGURE 3.1. Adaxial leaf surface morphologies and papilla characteristics in different *P. distichum* and *P. vaginatum* accessions. **(A)** SEM image illustrating papillae costal ridges overarching intercostal grooves containing stomata. Red circles in **(A)** indicate stomata. **(B)** Peeled strings of isolated papillae. **(C)** Representative scanning electron microscopy (SEM) images from *P. distichum* accession 'Spence' and *P. vaginatum* accessions 'HI10', 'KC9', and '509018-3' grown in freshwater (0 dS/m). **(D)** Images obtained from a dissecting microscope for *P. vaginatum* accession 'PI299042' and *P. distichum* accessions 'Spence' and 'Tropic Shore'. All scale bars = 100 µm.

A

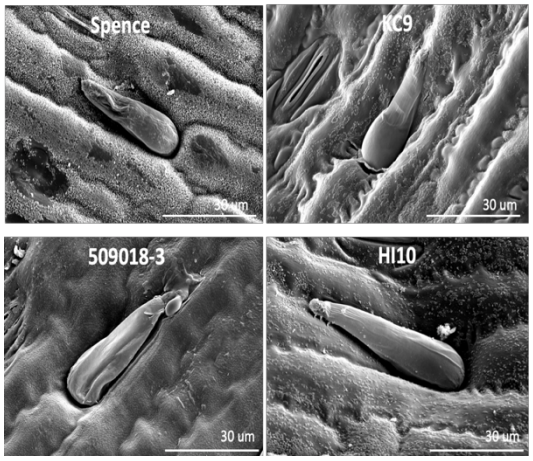
Spence
KC9
509018-3
HI10
30 um

B

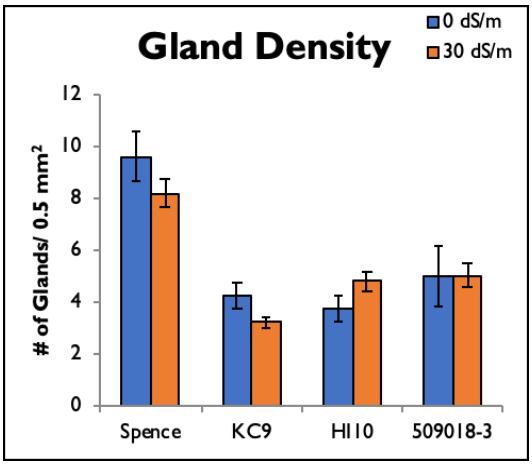
Gland Density
0 dS/m
30 dS/m
# of Glands/ 0.5 mm²
0
2
4
6
8
10
12
Spence
KC9
HI10
509018-3

C

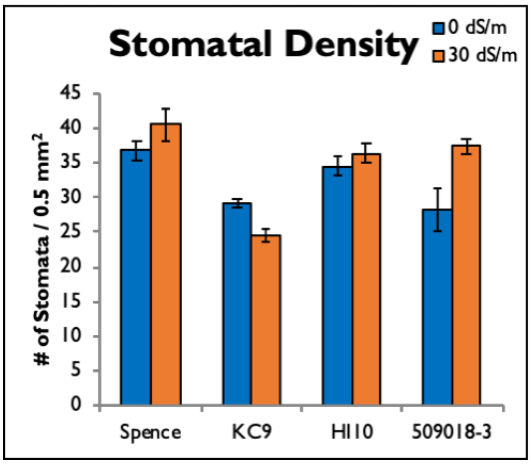
Stomatal Density
0 dS/m
30 dS/m
# of Stomata / 0.5 mm²
0
5
10
15
20
25
30
35
40
45
Spence
KC9
HI10
509018-3

D

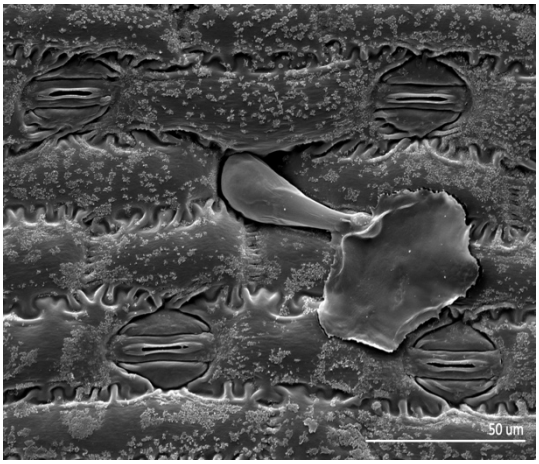
50 um

E

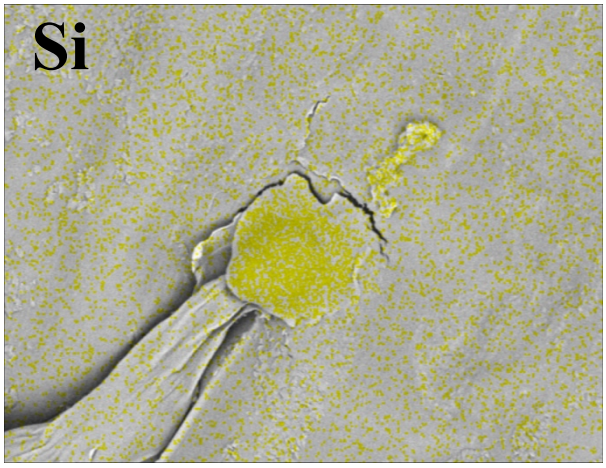
Si

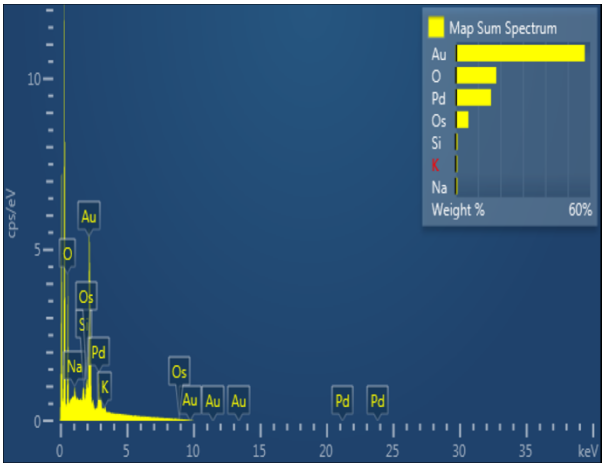
Map Sum Spectrum
Au
O
Pd
Os
Si
K
Na
Weight %
60%
cps/eV
keV
Au
O
Os
S
Pd
Na
K
Os
Au
Au
Au
Pd
Pd

SUPPLEMENTAL FIGURE 3.2. Abaxial leaf surface morphologies in *P. distichum* and *P. vaginatum* accessions. **(A)** Glands on the abaxial surface are shown for *P. distichum* accession 'Spence' and *P. vaginatum* accessions 'HI10', 'KC9', and '509018-3' (scale bars = 30 µm). **(B)** Density of glands and **(C)** stomata density on the abaxial surface for plants grown in freshwater (0 dS/m) and salt stress (30 dS/m). **(D)** Gland exudation in accession 'HI10'(scale bar = 50 µm) and **(E)** exudate element identification via EDS showing the presence of silicon (Si) (scale bar = 10 µm).

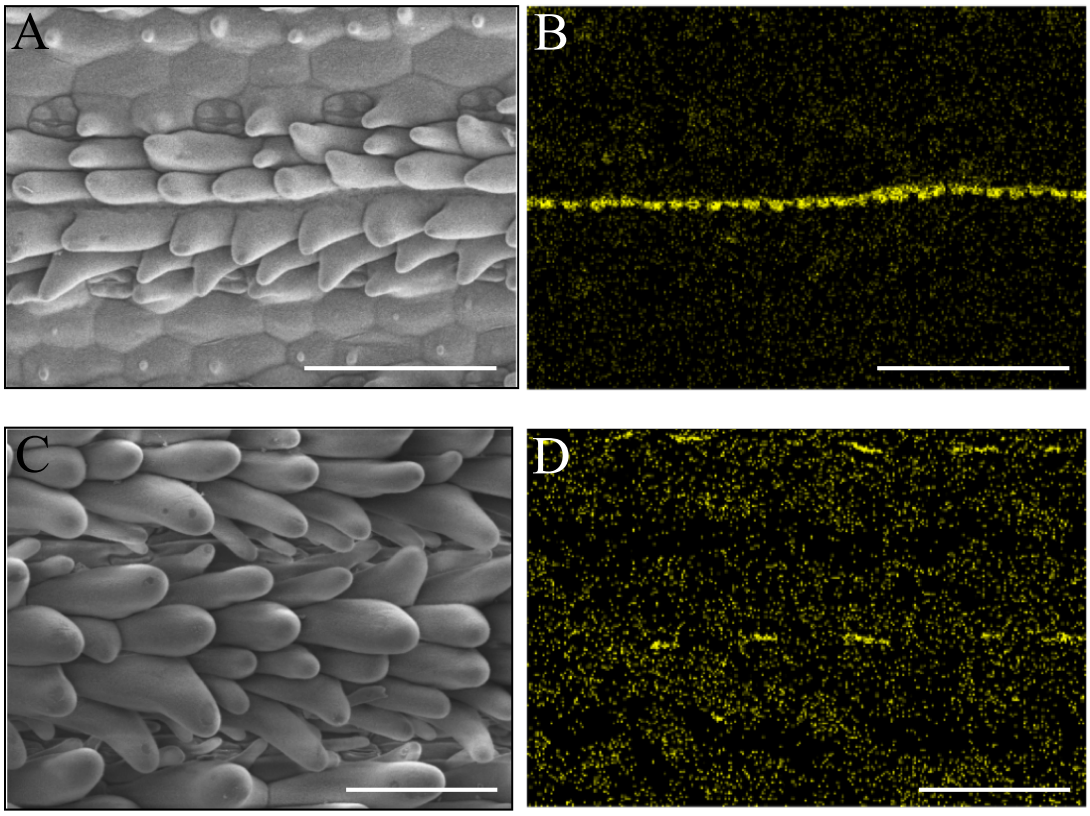

SUPPLEMENTAL FIGURE 3.3. Scanning electron microscopy (SEM) images and energy dispersive spectroscopy (EDS) maps of the adaxial leaf surface of *P. distichum* accession 'Spence' and *P. vaginatum* accession 'HI10'. **(A,C)** Representative SEM and **(B,D)** corresponding EDS map for silicon for **(A,B)** 'Spence' and **(C,D)** 'HI10'. Scale bars = 100 µm.

CHAPTER IV

COMPARATIVE TRANSCRIPTOME ANALYSIS IN SEASHORE PASPALUM AND A GLYCOPHYTIC RELATIVE UNDER SALT STRESS

[3] Spiekerman, J. J. and K.M. Devos. To be submitted to *BMC Plant Biology*.

Abstract

Nearly 20% of irrigated land is considered saline worldwide, and this amount will increase as climate change continues. Thus, it is imperative to examine the complex genetic responses of halophytic plants to salt stress with the aim of improving glycophytic crop relatives. Seashore paspalum (*Paspalum vaginatum*) is a halophytic grass closely related to agronomically crucial Panicoid grass species. Despite its popular use as a turfgrass, the genetics underlying its response to salt stress remain mostly uncharacterized. Here, we characterize the transcriptome of seashore paspalum accession 'HI10' and *P. distichum* accession 'Spence', a salt sensitive relative, in response to salt stress. We examined transcriptomic responses at three salt levels: freshwater (0 dSm), 10 dS/m where seashore paspalum enhances growth and *P. distichum* does not, and 30 dS/m where seashore paspalum continues to grow better than under freshwater conditions and *P. distichum* decreases growth. Our preliminary analyses show that 'HI10' and 'Spence' differ in vital regulators of a number of processes, including sodium/potassium transport, osmolyte biosynthesis/transport, gibberellin homeostasis, and senescence under salt stress, illustrating major differences in metabolism under salt stress. A transcription factor network analysis indicates that a large subset of genes may be distinctly regulated in 'HI10' and 'Spence' by three transcription factors: DIV2, MYB44, and AGL7. The HEAT SHOCK FACTOR1 (HSF1) pathway also appears to be differentially regulated between accessions. Collectively, our results illustrate that 'HI10' seems poised to cope with salt stress by regulating many stress-related genes under all conditions tested, including freshwater, as opposed to 'Spence', which activates these genes upon stress initiation. Our results provide the first salt-responsive transcriptomes for seashore paspalum and *P. distichum*, in addition to providing

insight into the genetic mechanisms used by halophytes to enhance and maintain growth under salt stress conditions.

Introduction

Salt stress is highly detrimental to crop production worldwide, with around 960 million hectares of land affected by salinity [1]. Most of the world's land surface consist of 'perennial dessert or drylands', which can only be used for crop production with the aid of irrigation [2]. Unfortunately, increased use of irrigation is highly correlated with increases in soil salinity, illustrating a need to breed crops with high levels of salt tolerance [2, 3]. Most crops are salt sensitive (glycophytes), and salt tolerance research has predominantly focused on glycophytic crop species of interest. Research on how halophytes, species that thrive under salt conditions, cope with salinity is currently limiting and thus needs to be a current focus of salt tolerance research.

Mechanisms used by halophytes to increase growth under low salt conditions remain mostly uncharacterized. Research suggests that halophytes outperform glycophytes in saline conditions by enhancing salt-response mechanisms also found in glycophytes, including ion exclusion, maintenance of K^+/Na^+ homeostasis, osmolyte production, and detoxification of reactive oxygen species (ROS) [4, 5]. The modification of genes in these pathways in glycophytes has met with some success [6-8], with some engineered plants having increased yield in the field, albeit only under high salt stress when yields were already greatly reduced [9]. Halophytes also use mechanisms absent in glycophytes such as salt exclusion and/or sequestration in glands and bladders [10], though the genetic mechanisms responsible for their function also remain mostly unknown. Due to the complexity of salt response, more in-depth analyses are required to better understand genetic mechanisms used by closely related glycophytes and halophytes under salt stress.

A popular halophytic turfgrass used worldwide due to its high salt tolerance is seashore paspalum (*Paspalum vaginatum*), a Panicoid grass closely related to crop species including maize and sorghum [11]. It is highly salt tolerant due to several physiological mechanisms including the production of osmolytes like proline and glycine betaine, enhanced K^+/Na^+ selectivity, and sodium exclusion in root tissue [12-14]. *P. distichum* is a sister species to seashore paspalum, inhabiting mostly freshwater habitats [15]. The genetic diversity within the *Paspalum* genus was recently explored with simple sequence repeat (SSR) markers [16] and confirmed the very close relationship between the two sister species. However, only a few studies have focused on the genetics underlying the high salt tolerance of seashore paspalum and none have been conducted in *P. distichum*. Though a proteomics study identified 18 salt-induced proteins [17], only two salt-responsive genes, a metallothionein (PvMET1) and a UDP-galactose (glucose)-4-epimerase (PvUGE1), have been characterized in seashore paspalum [18]. Currently no published genome exists, although a high-quality genome sequence is nearing completion (J. Schnable and J. Schmutz, pers. comm.). Only a single transcriptome-level experiment has been reported in seashore paspalum [19], though the focus was on general gene identification and annotation unrelated to salt stress. Consequently, seashore paspalum and *P. distichum* together represent an excellent pair of species that differ in salt response to investigate.

We have illustrated that 'HI10', a diploid *P. vaginatum* accession, and 'Spence', a diploid *P. distichum* accession, significantly differ in growth response under salt stress (Chapter II). Under freshwater (0 dS/m), 'HI10' is slow-growing while 'Spence' is quite vigorous, accumulating more than double the amount of biomass of 'HI10'. At 10 dS/m, 'HI10' exhibits typical halophytic behavior, enhancing growth relative to control conditions while this is not observed in 'Spence'. At 30 dS/m salt, 'HI10' continues to grow better than under freshwater

conditions while ‘Spence’ has significantly reduced growth. Here, we conduct RNA-sequencing in *P. vaginatum* accession ‘HI10’ and *P. distichum* accession ‘Spence’ under freshwater (0 dS/m), and 10 dS/m, and 30 dS/m salt with the aim of better understanding these growth differences. We show that several salt-response and growth-associated pathways including sodium/potassium transport, osmolyte biosynthesis/transport, gibberellin homeostasis, and senescence differ between ‘HI10’ and ‘Spence’. Furthermore, a transcription factor network analysis indicates that three transcription factors, DIV2, MYB44, and AGL7/AP1, may differentially regulate largely different subsets of genes in each accession under salt stress. Our results provide some insights into the factors that may be responsible for the growth habits observed in ‘HI10’ and ‘Spence’, thus illustrating mechanisms that may be used by other halophytes to grow under salt stress.

Materials and Methods

Plant materials, growth, and tissue collection

The *P. vaginatum* accession ‘HI10’ and the *P. distichum* accession ‘Spence’ were used for all experiments. All experiments were conducted in the University of Georgia Plant Biology Greenhouses in June-July 2018 under a day/night temperature of 27 °C/18 °C and 14-hr days. Nodes from growing stolon tissue were propagated to produce individual ramets of each species as described in Chapter II. Salt screens are also described in Chapter II. For the 10 dS/m salt treatment, the salt concentration in the bins was brought to and kept at 2.5 dS/m for two days, followed by 5 dS/m for two days and then 10 dS/m. The same stepwise increase was used for the 30 dS/m salt treatment, except that salt levels were kept at 10 dS/m for five days, and then increased to 30 dS/m. The control bin was left at 0 dS/m for the duration of the experiment. Once

the salt concentration in all bins had reached the desired level, plants were grown for a further three weeks before sampling the aboveground tissue (all stolon and leaf tissue). Harvested tissues were immediately frozen in liquid nitrogen and stored at -80 °C until analysis.

RNA-isolation, library preparation, and sequencing

Frozen tissue was powdered with a mortar and pestle. RNA was extracted from 100 mg of powdered tissue from each sample using Trizol and a Zymo RNA Clean & Concentrator Kit (Zymo Research). RNA integrity was assessed on an Agilent 2100 Bioanalyzer at the Georgia Genomics and Bioinformatics Core (GGBC) at the University of Georgia. For library preparation, 1.5 µg of total RNA was used as input in the Kapa Stranded mRNA-Seq Kit (KAPA). Libraries were prepared according to the manufacturer's recommendation, except that half quantities of reagents were used for all steps excluding library amplification. Library quality and quantity were assessed on a Fragment Analyzer™ Automated CE System at the GGBC prior to pooling. The 18 libraries discussed in this chapter were pooled and sequenced as part of a larger run on an Illumina NextSeq High Output flow cell for 150 cycles of 75-bp paired-end sequencing.

Differential expression analysis

Paired-end reads were screened for quality using the FastQC software (http://www.bioinformatics.babraham.ac.uk/projects/fastqc/). Using Trimmomatic [20], reads were trimmed for adapter sequence and low quality by removing reads with low mean phred scores (Q<15) in a sliding window of four bases. Trimmed reads were then aligned to a high quality *Paspalum vaginatum* genome sequence assembly (J. Schmutz and J. Jenkins, unpublished

data) using HISAT2, and transcript assembly and merging was conducted using StringTie [21]. Transcripts identified by StringTie were used for all subsequent differential expression analyses. Differential expression (DE) analysis was conducted using DESeq2 for the following comparisons: 0 dS/m *vs* 10 dS/m for 'HI10' and 'Spence', 0 dS/m *vs* 30 dS/m for 'HI10' and 'Spence', and 'HI10' *vs* 'Spence' under freshwater [22]. DESeq2 was also run on 'HI10' *vs* 'Spence' at 10 dS/m and 30 dS/m for some comparisons described throughout this chapter. Any transcript with a $\log_2$ fold change above/below 1 and false discovery rate (FDR)<0.05 was considered differentially expressed.

Gene ontology (GO) analysis

Paspalum transcript sequences were first annotated based on their homology, identified by BLASTN, with sorghum coding sequences downloaded from Phytozome [23]. Sorghum gene IDs were then converted to *Arabidopsis* IDs using the Sorghum Functional Genomics Database (SorghumFDB) (http://structuralbiology.cau.edu.cn/sorghum/index.html) [24]. If no *Arabidopsis* ID was acquired through SorghumFDB, sorghum peptide sequences were used as queries in a BLASTP analysis against *Arabidopsis* peptide sequences downloaded from Phytozome to acquire the closest *Arabidopsis* homolog. For GO analysis, *Arabidopsis* gene IDs were used as input in the PANTHER database (http://pantherdb.org) to acquire gene descriptions and enriched GO categories [25]. GO analyses were conducted separately on DE genes in the comparisons described above (0 dS/m *vs* 10 dS/m for 'HI10' and 'Spence', 0 dS/m *vs* 30 dS/m for 'HI10' and 'Spence',) for biological process, molecular function, cell component, and Reactome pathway GO subcategories. Enrichment in a category was considered statistically significant if FDR<0.05. All significantly enriched GO categories are illustrated in Fig. 4.3 and Fig. 4.4 unless more than

20 categories were significantly enriched, in which case only the top 20 are shown. GO analyses are summarized in Suppl. Table 4.1 for ‘HI10’ and Suppl. Table 4.2 for ‘Spence’.

Transcription factor network analysis

Transcription factor (TF) network analysis was conducted using the TF2Network software (http://bioinformatics.psb.ugent.be/webtools/TF2Network/) using *Arabidopsis* gene IDs as input[26]. Results were filtered for TF-gene interactions with experimentally-verified binding in *Arabidopsis* and TFs for which the corresponding binding site was present in a minimum of five genes in the input list of DE genes. Statistical significance was determined through TF2Network with the Benjamini-Hochberg method and counted as FDR<0.05. All figures associated with this network analysis were created using the TF2Network webtool.

Results

Sequencing and transcript assembly

The sequencing run yielded some 740 million total reads with 94% at or above the Q30 quality threshold. The number of trimmed paired-end reads per library ranged from 2.78 to 13.26 million (Table 4.1). The rates of alignment of the reads to the *Paspalum vaginatum* genome were relatively similar across libraries and ranged from 66.3% - 78.5%, with an average of 72.6% for ‘HI10’ and 71% for ‘Spence’ libraries (Table 4.1).

Table 4.1. The number of trimmed reads (in millions) used for mapping and the mapping rate (%) for each library.

Library ID	# of Trimmed Paired-End Reads (in millions)	Mapping Rate (%)
HI10-Freshwater-1	13.251035	71.53
HI10-Freshwater-2	5.049856	69.71
HI10-Freshwater-3	10.197423	72.53
HI10-10dS/m-1	7.591805	78.47
HI10-10dS/m-2	7.297521	72.41
HI10-10dS/m-3	8.710843	75.01
HI10-30dS/m-1	10.395749	69.88
HI10-30dS/m-2	6.218664	71.28
HI10-30dS/m-3	8.055579	72.92
Spence-Freshwater-1	6.523241	73.2
Spence-Freshwater-2	4.28862	66.33
Spence-Freshwater-3	6.004526	73.67
Spence-10dS/m-1	7.37499	72.22
Spence-10dS/m-2	6.805552	66.79
Spence-10dS/m-3	5.573506	70.52
Spence-30dS/m-1	7.527133	73.75
Spence-30dS/m-2	3.193484	72.39
Spence-30dS/m-3	2.780103	70.57

Principal components analysis (PCA) and sample-to-sample distance hierarchical clustering illustrate that samples cluster by genotype, then by salt treatment (Fig. 4.1A-B). After read alignment and transcript assembly, StringTie identified a total of 42,581 unique transcripts belonging to 29,506 genes. In the freshwater (0 dS/m) *vs.* 10 dS/m salt stress comparison, a total of 707 and 366 differentially expressed genes were identified for 'Spence' and 'HI10', respectively (Fig. 4.2A). Under 30 dS/m salt stress compared to freshwater (0 dS/m), a total of 995 and 743 differentially expressed genes were identified for 'Spence' and 'HI10', respectively (Fig. 4.2A). A large number of differentially expressed genes were also identified when

comparing the two accessions directly under freshwater (2,816 genes), 10 dS/m (2,500 genes), and 30 dS/m (2,594 genes) conditions (Fig. 4.2B).

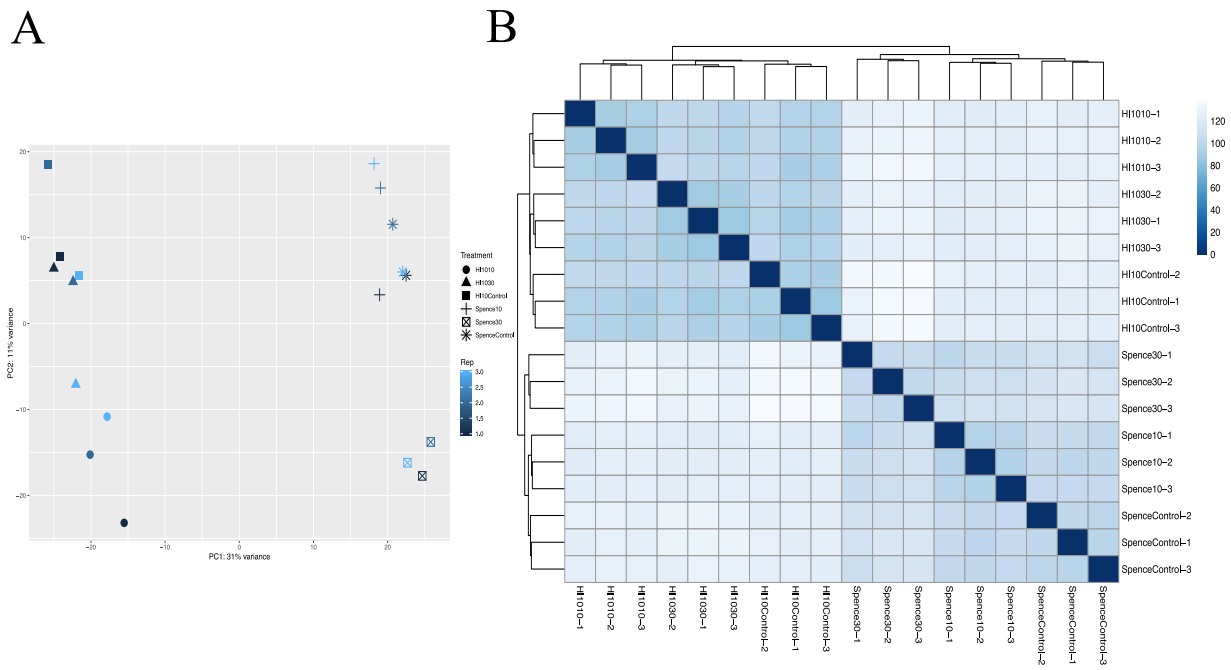

FIGURE 4.1. Quality control analysis on all analyzed RNA-seq libraries. **(A)** Principal components analysis (PCA) conducted on transformed read counts showing samples separated by their first two principal components. **(B)** Heatmap of the sample-to-sample distances between transformed read counts for all samples. Samples in **(B)** were hierarchically clustered based on sample-to-sample distances.

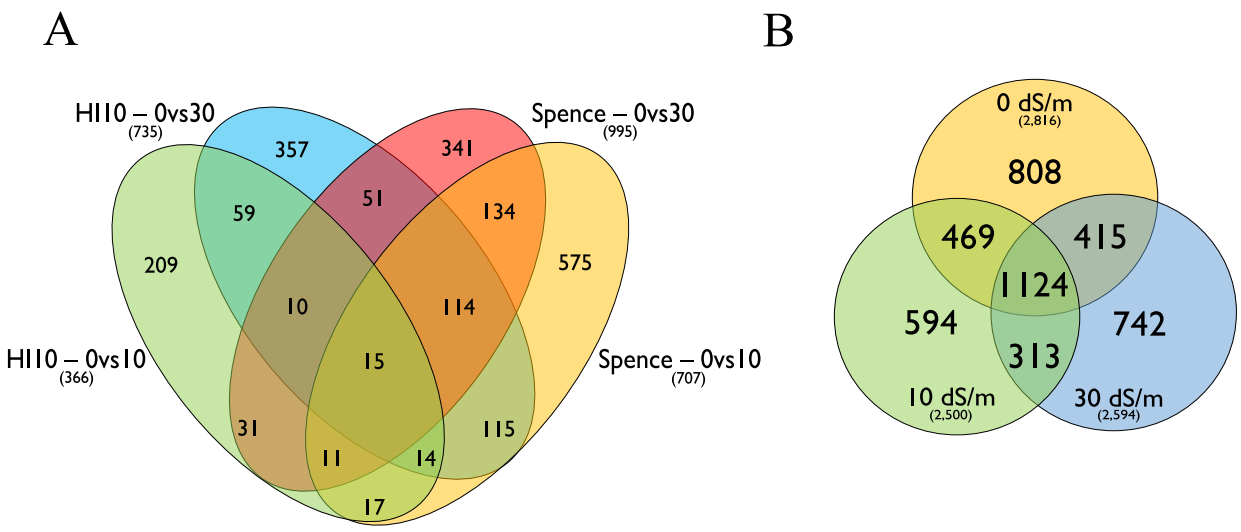

FIGURE 4.2. Overlap of differentially expressed genes in 'HI10' and 'Spence' in 0-10 dS/m and 0-30 dS/m comparisons. **(A)** and DE genes between 'HI10' and 'Spence' at 0 dS/m, 10 dS/m, and 30 dS/m **(B)**.

Transcriptome GO analysis – 0-10 dS/m salt stress comparison

GO analyses for biological process, molecular function, cell component, and Reactome pathways were conducted to examine enrichment of GO terms for DE genes (Fig. 4.3). Some GO terms were enriched in both the 'HI10' and 'Spence' 0 – 10 dS/m comparisons, while others were enriched in only one accession (Fig. 4.3).

For biological processes, 14 processes were enriched for 'HI10' and 47 were enriched for 'Spence', with an overlap of eight processes. As expected, overlapped biological processes were metabolic and stress-related, and include 'cellular metabolic process', 'response to light stimulus', and 'response to abiotic stimulus'. Though 'Spence' contains over double the number of DE genes (104) in the 'response to abiotic stimulus' category as 'HI10' (50), 36/50 genes are only DE in 'HI10'. Of these 36 genes only found in 'HI10', 17/36 fit into the 'response to light'

biological process. Of the processes only found in 'HI10', most seem to be associated with development including 'root development', 'multicellular organism development', and 'plant organ morphogenesis'. In 'Spence', most enriched biological processes include stress-associated processes such as 'response to stress', 'response to cold', and 'response to heat'.

For molecular function, differentially expressed genes in 'Spence' were enriched in functions related to binding cellular components including 'ion binding', 'small molecule binding', 'protein binding', and 'RNA binding'. Differentially expressed genes in 'HI10' were only enriched in two categories: 'transferase activity' and 'ligase activity, forming carbon-nitrogen bonds' categories. A few molecular functions were enriched in both accessions, and they were mostly related to binding different cellular components. These included 'catalytic activity', 'heterocyclic compound binding', 'organic cyclic compound binding', and 'mRNA binding'.

The only enriched cell component categories were found in 'HI10' and they were 'trans-golgi network' and 'golgi subcompartment'. No enriched cell component categories were seen for differentially expressed genes in 'Spence'.

Significantly enriched Reactome pathways were only found for 'Spence' and consisted of stress-related categories such as 'cellular response to stress' and 'cellular response to external stimuli'. Interestingly, many enriched categories in 'Spence' were associated with response to heat. Specifically, they appeared to be associated with the transcription factor HEAT SHOCK FACTOR1 (HSF1).

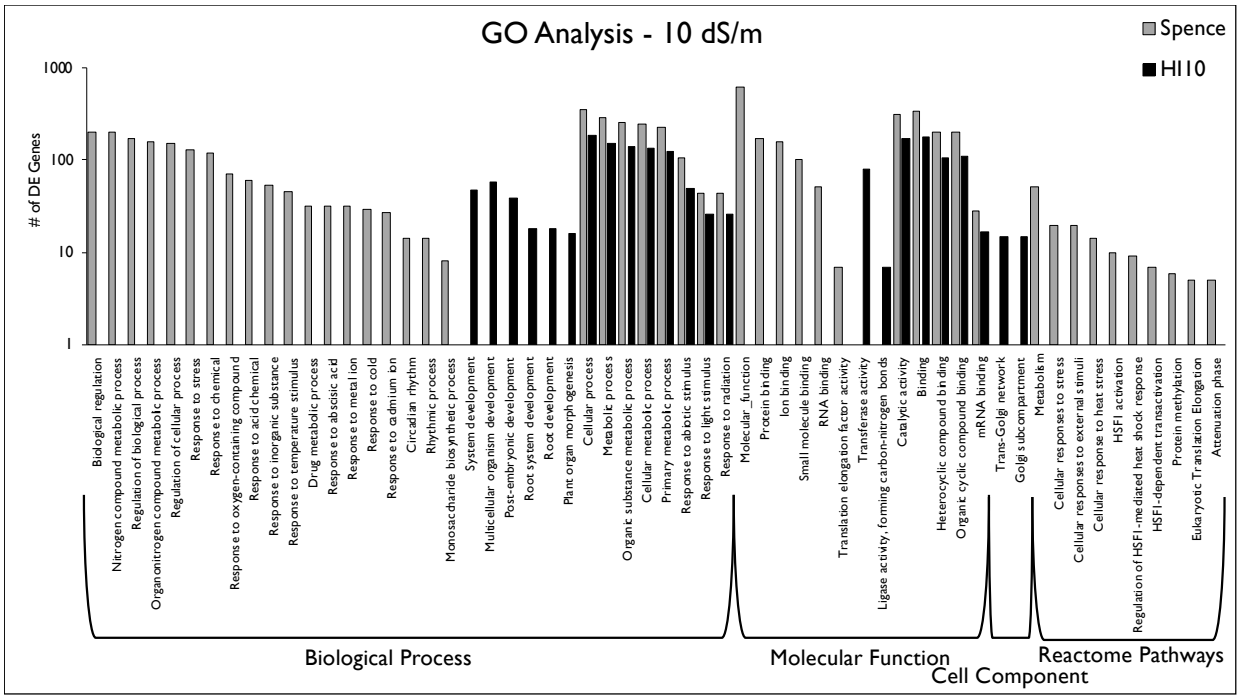

FIGURE 4.3. Gene ontology (GO) analysis results for DE genes at 10 dS/m relative to freshwater (0 dS/m) that are only found in 'HI10', only found in 'Spence', and overlapped. All significantly enriched GO categories are shown split by biological process, molecular function, cell component (only enriched in 'HI10'), and Reactome pathways (only enriched in 'Spence). If more than 20 GO categories were enriched, only the top 20 ranked by decreasing FDR values are shown. The top 20 were selected separately for categories only found in 'Spence', categories only found in 'HI10', and categories found in both 'Spence' and 'HI10'.

Transcriptome GO analysis – 0-30 dS/m salt stress comparison

The same GO parameters used for differentially expressed genes in the 0 – 10 dS/m comparison were applied to DE genes in the 0 – 30 dS/m comparison. Differentially expressed genes found in 'HI10' were enriched in 107 biological processes while those in 'Spence' were enriched in 115 with an overlap of 55 processes (Fig. 4.4A). Overlap was found for stress-related

categories including ‘response to oxidative stress’, ‘response to osmotic stress’, ‘response to abscisic acid’, and ‘response to reactive oxygen species’. Most enriched categories that were found only in ‘HI10’ and for which two or more related categories were identified were associated with nitrogen metabolism (‘organonitrogen compound metabolic process, ‘cellular nitrogen compound biosynthetic process’, ‘nitrogen compound metabolic process’), light (‘response to high light intensity’, ‘response to light intensity’), heat (‘cellular response to heat’, ‘heat acclimation’), protein folding (‘protein folding’, ‘protein complex oligomerization’), and reproductive development (‘reproductive structure development’, ‘reproductive system development’) in addition to positive regulation of many metabolic processes. Enriched categories found only in ‘Spence’ include many processes related to transport of ions or other substances such as ‘ion transmembrane transport’, ‘organic acid transmembrane transport, and ‘carboxylic acid transmembrane transport’. Four processes associated with cell wall biogenesis and processes related to polyphosphate biosynthesis (‘organic acid metabolic process’, ‘oxoacid metabolic process’), pyruvate (‘monocarboxylic acid metabolic process’, ‘carboxylic acid metabolic process’), malate transport (‘carboxylic acid transmembrane transport’, ‘organic acid transmembrane transport’), and glutamine family homeostasis (‘glutamine family amino acid metabolic process’) were also only observed in ‘Spence’.

For the molecular function GO category, ‘HI10’ DE genes were enriched in 26 categories while ‘Spence’ DE genes were enriched in 27, with nine overlapped categories (Fig. 4.4B). Overlapped categories included salt stress-associated functions including ‘ion binding’ and ‘anion transmembrane transporter activity’. Molecular functions found only in ‘HI10’ were mostly associated with Adenosine monophosphate (AMP) and Adenosine triphosphate (ATP) binding (‘drug binding’, ‘adenyl nucleotide binding’, ‘adenyl ribonucleotide binding’, ‘purine

ribonucleotide binding', 'purine nucleotide binding', 'ribonucleotide binding', 'ATP binding'). Similar to results found in the biological processes category, most categories found only in 'Spence' were associated with transport such as 'transmembrane transporter activity, 'organic acid transmembrane transporter activity', and 'amino acid transmembrane transporter activity'.

Many GO categories in the cell component category were enriched, with 62 found for 'Spence' and 32 found for 'HI10' (Fig. 4.4C). All categories enriched in 'HI10' overlapped with GO-enriched categories in 'Spence', with the exception of the 'intracellular organelle' category. Overlapped categories included many cell components related to chloroplasts including 'plastid', 'plastid stroma', and 'chloroplast envelope' in addition to four vacuole-associated categories. Most categories found only in 'Spence' appeared to also be associated with chloroplasts ('chloroplast thylakoid', 'chloroplast thylakoid membrane', 'photosynthetic membrane).

Reactome pathway analysis for genes differentially expressed in the 0-30 dS/m comparison showed no enriched categories for 'Spence' and six enriched categories for 'HI10' (Fig. 4.4D). Interestingly, several of the HSF1-related pathways enriched for DE genes in 'Spence' in the 0-10 dS/m comparison were enriched for 'HI10' in the 0-30 dS/m comparison (Fig. 4.4D). There was also an enrichment in the 'HSP90 chaperone cycle for steroid hormone receptors' pathway for 'HI10'.

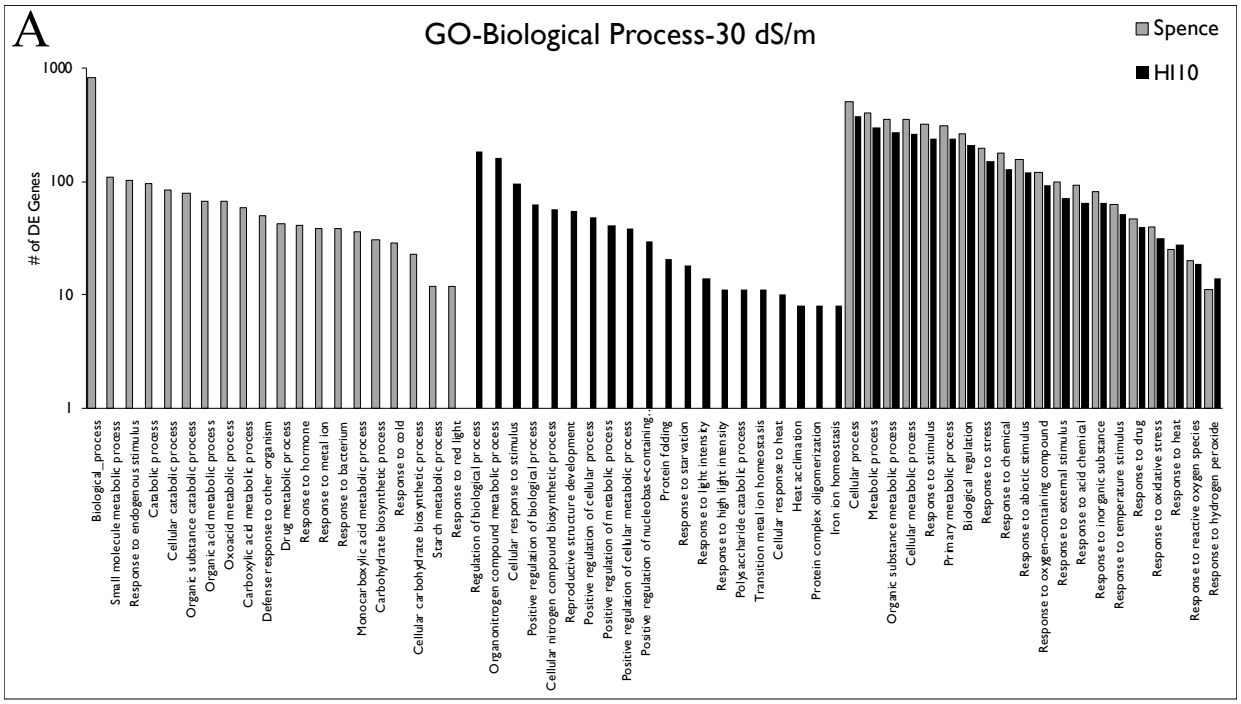
A
GO-Biological Process-30 dS/m
Spence
HI10
# of DE Genes
1000
100
10
1
Biological_process
Small molecule metabolic process
Response to endogenous stimulus
Catabolic process
Cellular catabolic process
Organic substance catabolic process
Organic acid metabolic process
Oxoacid metabolic process
Carboxylic acid metabolic process
Defense response to other organism
Drug metabolic process
Response to hormone
Response to metal ion
Response to bacterium
Monocarboxylic acid metabolic process
Carbohydrate biosynthetic process
Response to cold
Cellular carbohydrate biosynthetic process
Starch metabolic process
Response to red light
Regulation of biological process
Organonitrogen compound metabolic process
Cellular response to stimulus
Positive regulation of biological process
Cellular nitrogen compound biosynthetic process
Reproductive structure development
Positive regulation of cellular process
Positive regulation of metabolic process
Positive regulation of cellular metabolic process
Positive regulation of nucleobase-containing...
Protein folding
Response to starvation
Response to light intensity
Response to high light intensity
Polysaccharide catabolic process
Transition metal ion homeostasis
Cellular response to heat
Heat acclimation
Protein complex oligomerization
Iron ion homeostasis
Cellular process
Metabolic process
Organic substance metabolic process
Cellular metabolic process
Response to stimulus
Primary metabolic process
Biological regulation
Response to stress
Response to chemical
Response to abiotic stimulus
Response to oxygen-containing compound
Response to external stimulus
Response to acid chemical
Response to inorganic substance
Response to temperature stimulus
Response to drug
Response to oxidative stress
Response to heat
Response to reactive oxygen species
Response to hydrogen peroxide

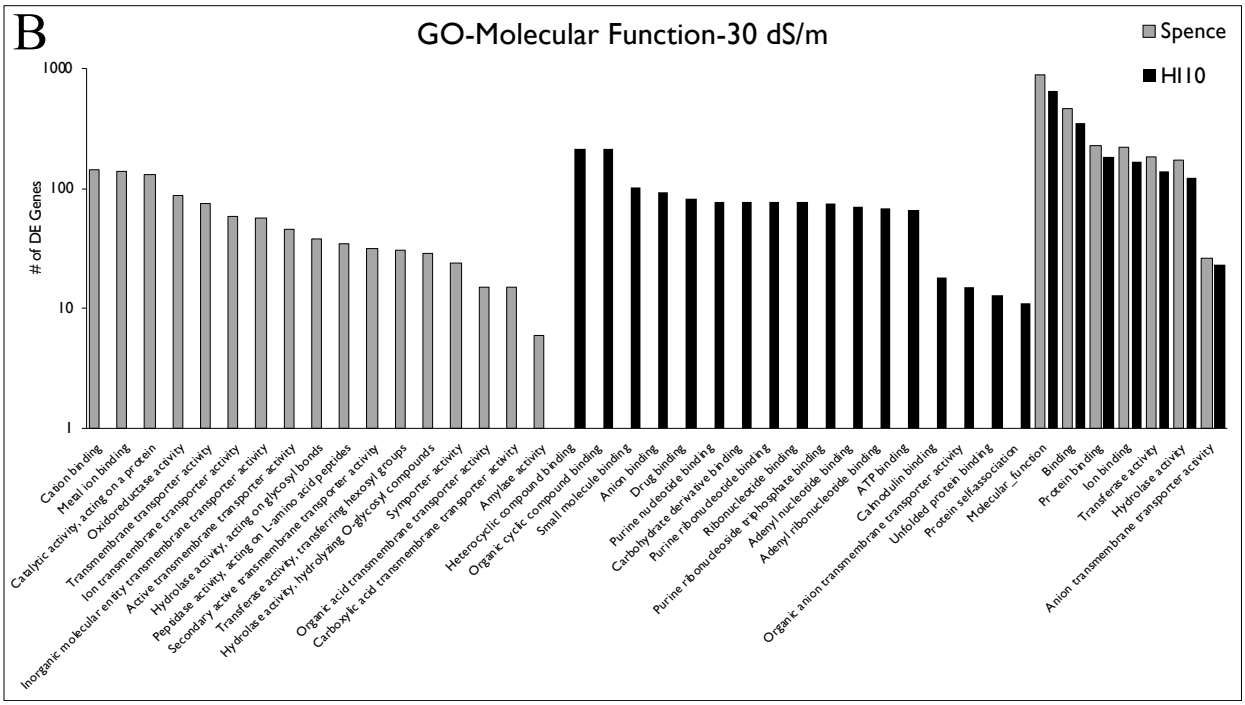
B
GO-Molecular Function-30 dS/m
Spence
HI10
# of DE Genes
1000
100
10
1
Cation binding
Metal ion binding
Catalytic activity, acting on a protein
Oxidoreductase activity
Transmembrane transporter activity
Ion transmembrane transporter activity
Inorganic molecular entity transmembrane transporter activity
Active transmembrane transporter activity
Hydrolase activity, acting on glycosyl bonds
Peptidase activity, acting on L-amino acid peptides
Secondary active transmembrane transporter activity
Transferase activity, transferring hexosyl groups
Hydrolase activity, hydrolyzing O-glycosyl compounds
Symporter activity
Organic acid transmembrane transporter activity
Carboxylic acid transmembrane transporter activity
Amylase activity
Heterocyclic compound binding
Organic cyclic compound binding
Small molecule binding
Anion binding
Drug binding
Purine nucleotide binding
Carbohydrate derivative binding
Purine ribonucleotide binding
Ribonucleotide binding
Purine ribonucleoside triphosphate binding
Adenyl nucleotide binding
Adenyl ribonucleotide binding
ATP binding
Calmodulin binding
Organic anion transmembrane transporter activity
Unfolded protein binding
Protein self-association
Molecular_function
Binding
Protein binding
Ion binding
Transferase activity
Hydrolase activity
Anion transmembrane transporter activity

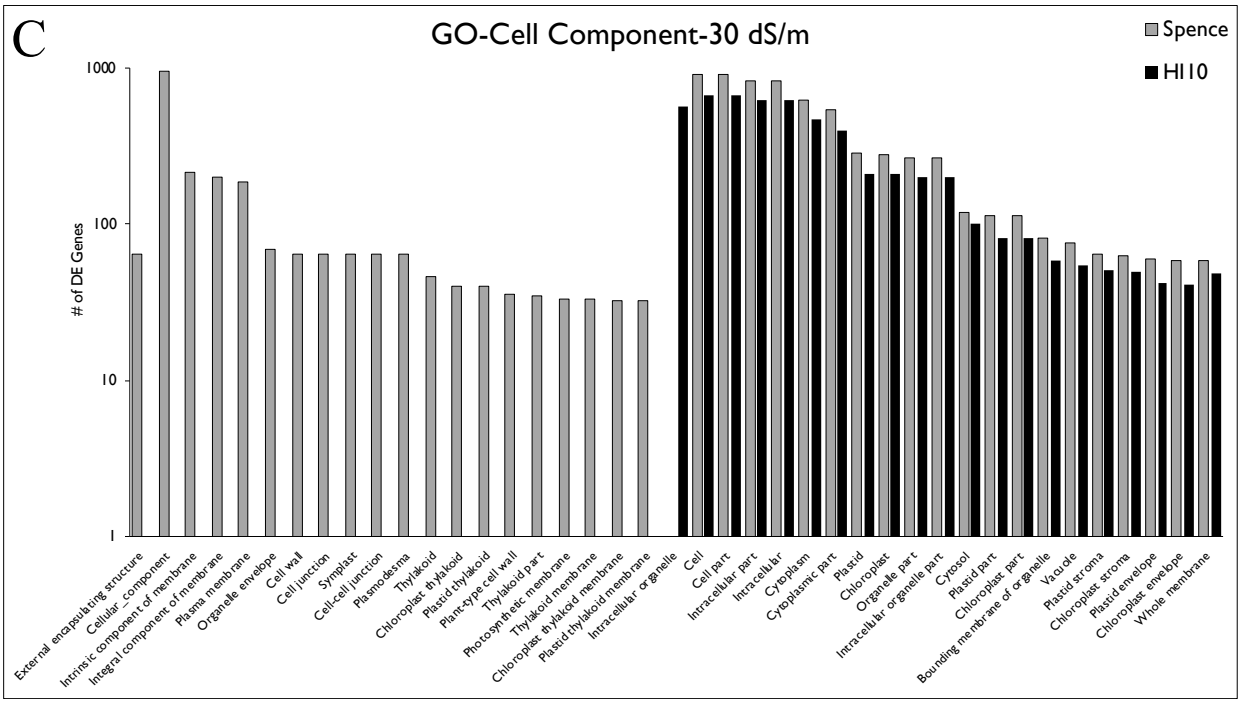

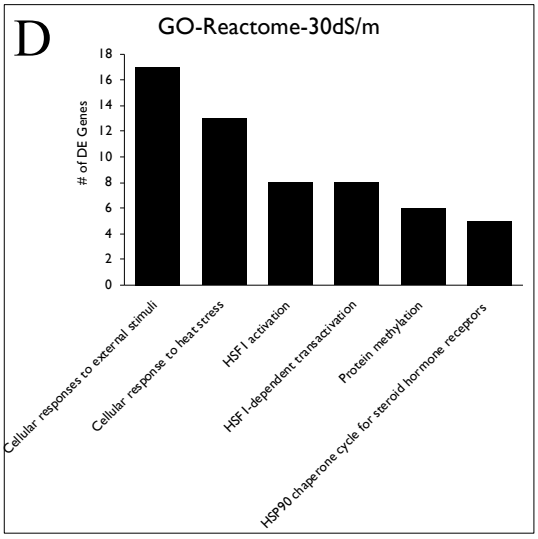

FIGURE 4.4. Gene ontology (GO) analysis results for DE genes at 30 dS/m relative to freshwater (0 dS/m) that are only found in 'HI10', only found in 'Spence', and overlapped. GO analyses are shown separately for biological process **(A)**, molecular function **(B)**, cell component **(C)**, and Reactome pathways (only enriched in 'HI10') **(D)**. All significantly enriched GO categories are shown. If more than 20 GO categories were enriched, only the top 20 ranked by decreasing FDR values are shown. The top 20 were selected separately for categories only found in 'Spence', categories only found in 'HI10', and categories found in both 'Spence' and 'HI10'.

Additional pathways of interest

While GO term and Reactome pathway enrichment provide an efficient way to identify processes that may be differentially regulated between species or treatments, individual genes that are differentially expressed but not part of an enriched pathway may still play important roles. We decided to focus on several pathways of interest associated with growth under salt stress conditions. Gibberellin (GA) is well characterized for controlling growth rate in response to stress [27]. This occurs through the coordinated action of DELLA proteins, which restrict growth upon salt stress initiation [28]. Thus, we investigated GA-associated pathways to determine if they contribute to the growth differences observed in 'HI10' and 'Spence' under salt stress. We also examined pathways behind osmolyte production, another crucial mechanism for coping with salt stress in *Paspalum*. In particular, proline and glycine betaine contribute to intraspecific differences in salt tolerance amongst seashore paspalum genotypes [13], and thus may also be responsible for growth differences between 'HI10' and 'Spence'. Furthermore, when examining the most highly differentially expressed genes in 'HI10' and 'Spence', many are associated with senescence, which could help determine the salt concentration (10 dS/m or 30 dS/m) at which 'HI10' and 'Spence' start senescing. While the reasoning behind examining sodium transport/homeostasis is apparent, we also decided to examine potassium transport/homeostasis. Seashore paspalum is known to maintain high potassium uptake under salt stress compared with other turfgrass species [29]. As we observed differences in leaf potassium content between 'HI10' and 'Spence' under salt stress in Chapter II, we decided to investigate genes involved with potassium transport and homeostasis. In summary, we focused on genes involved in gibberellin biosynthesis and transport, osmolyte production and transport, senescence, and sodium and potassium homeostasis and transport. The genes, the

treatments/accessions in which they were differentially expressed, and their function are listed in Suppl. Table 4.3 and Suppl. Table 4.4. An in-depth description of our findings is presented in the Discussion section.

Transcription factor network analysis

A gene regulatory network analysis using the TF2Network software [26] was conducted to investigate prominent transcriptional regulators in our dataset. TF2network is a repository of predicted and experimentally-verified protein-DNA interactions including interactions from over 900 transcription factors (TFs) in *Arabidopsis*. We probed this repository for overlap between our differentially expressed genes and experimentally-verified protein-DNA interactions. This analysis was conducted for genes that were DE within each accession between 0 and 10 dS/m salt (Fig. 4.5A) and between 0 and 30 dS/m salt (Fig. 4.5B). Results for this network analysis are also presented in Suppl. Table 4.5.

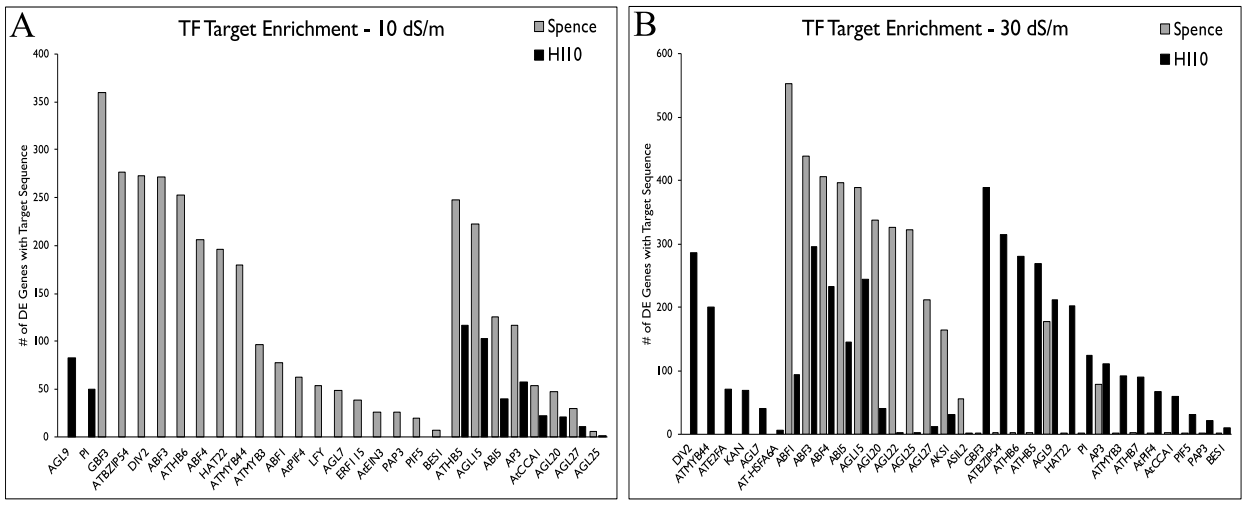

FIGURE 4.5. Transcription factor (TF) – gene regulatory network analysis using the TF2Network software showing the number of differentially expressed genes that contain

experimentally verified protein-DNA interactions with the given TF. **(A)** TF network analysis for DE genes at 10 dS/m relative to 0 dS/m in 'HI10' and 'Spence'. **(B)** TF network analysis for DE genes at 30 dS/m relative to 0 dS/m in 'HI10' and 'Spence'.

When analyzing TF binding sites in the genes that were differentially expressed in the 0-10 dS/m comparison for 'Spence' and 'HI10', enrichment was observed for 18 TFs in 'Spence' only, two in 'HI10' only and eight TFs that were common to 'Spence' and 'HI10' (Fig. 4.5A). For differentially expressed genes in the 0-30 dS/m comparison, binding-site enrichment was found for six TFs in 'HI10' only and 26 TFs in both 'HI10' and 'Spence' (Fig. 4.5B). In this comparison, a larger number of TFs (21) were either found in only 'HI10' or were present at a higher level in 'HI10'. The identity of these 21 TFs is presented in Table 4.2.

Table 4.2. Gene IDs and descriptions from the PANTHER database for the 21 transcription factors found in only 'HI10' or present at a higher level in 'HI10' in the 0-30 dS/m comparison.

Uniprot ID	TAIR ID	Gene Description	Panther Protein Class
Q9LN63	AT1G19350	Protein BRASSINAZOLE-RESISTANT 2;BZR2;ortholog	
P46668	AT2G22430	Homeobox-leucine zipper protein ATHB-6;ATHB-6;ortholog	Homeodomain transcription factor (PC00119)
P35632	AT3G54340	Floral homeotic protein APETALA 3;AP3;ortholog	MADS box transcription factor (PC00250)
Q9S9K9	AT1G22640	Transcription factor MYB3;MYB3;ortholog	DNA binding protein (PC00009);homeodomain transcription factor (PC00119)
Q9LZ21	AT5G04760	Duplicated homeodomain-like superfamily protein;T1E3_120;ortholog; (DIV2)	
O80536	AT1G09530	Transcription factor PIF3;PIF3;ortholog	
P46897	AT2G46680	Homeobox-leucine zipper protein ATHB-7;ATHB-7;ortholog	Homeodomain transcription factor (PC00119)

Q93WJ9	AT5G16560	Transcription repressor KAN1;KAN1;ortholog	
P46604	AT4G37790	Homeobox-leucine zipper protein HAT22;HAT22;ortholog	
Q9LZR0	AT5G03790	Putative homeobox-leucine zipper protein ATHB-51;ATHB-51;ortholog	Homeodomain transcription factor (PC00119)
P42775	AT4G01120	G-box-binding factor 2;GBF2;ortholog	
O22456	AT1G24260	Developmental protein SEPALLATA 3;SEP3;ortholog	MADS box transcription factor (PC00250)
P35631	AT1G69120	Floral homeotic protein APETALA 1;AP1;ortholog	MADS box transcription factor (PC00250)
Q84LH8	AT3G59060	Transcription factor PIF5;PIF5;ortholog	
Q9FDW1	AT5G67300	Transcription factor MYB44;MYB44;ortholog	
P48007	AT5G20240	Floral homeotic protein PISTILLATA;PI;ortholog	MADS box transcription factor (PC00250)
P42776	AT2G46270	G-box-binding factor 3;GBF3;ortholog	
P92973	AT2G46830	Protein CCA1;CCA1;ortholog	Chromatin/chromatin-binding protein (PC00077);metalloprotease (PC00153);transcription cofactor (PC00217)
Q8W2F3	AT2G43010	Transcription factor PIF4;PIF4;ortholog	
Q1PDN3	AT5G43840	Heat stress transcription factor A-6a;HSFA6A;ortholog	Winged helix/forkhead transcription factor (PC00246)
Q9FNY0	AT2G36010	Transcription factor E2FA	Nucleic acid binding (PC00171);transcription factor (PC00218)

As discussed above, TF binding site enrichment for genes that were DE between 0 and 10 dS/m salt was highest for Spence, while the reverse was true for DE genes in the 0-30 dS/m comparison. Furthermore, of the 19 TFs enriched for target genes in 'Spence' only in the 0-10 dS/m comparison, three TFs, DIV2, ATMYB44 and AGL7 (*i.e.* APETALA1, AP1), were enriched in 'HI10' only in the 0-30 dS/m comparison. These three TFs have binding sites in the Arabidopsis orthologs of a subset of 273 differentially expressed genes utilized by 'Spence' under low salt stress (10 dS/m) (Fig. 4.6A) and 283 genes used by 'HI10' under high salt stress

(30 dS/m) (Fig. 4.6B) with 68 of these genes overlapped. GO analysis on these 68 genes indicates that most, as expected, are associated with 'response to stimulus' processes. The identity of these 68 genes is listed in Suppl. Table 4.6. Only 10/68 of these genes are differentially expressed in both accessions in 'the 0-10 dS/m comparison, while 47/68 are DE in both accessions in the 0-30 dS/m comparison, indicating that expression of most of these genes is affected by both low and high salt stress in Spence, but only by high salt stress in 'HI10'.

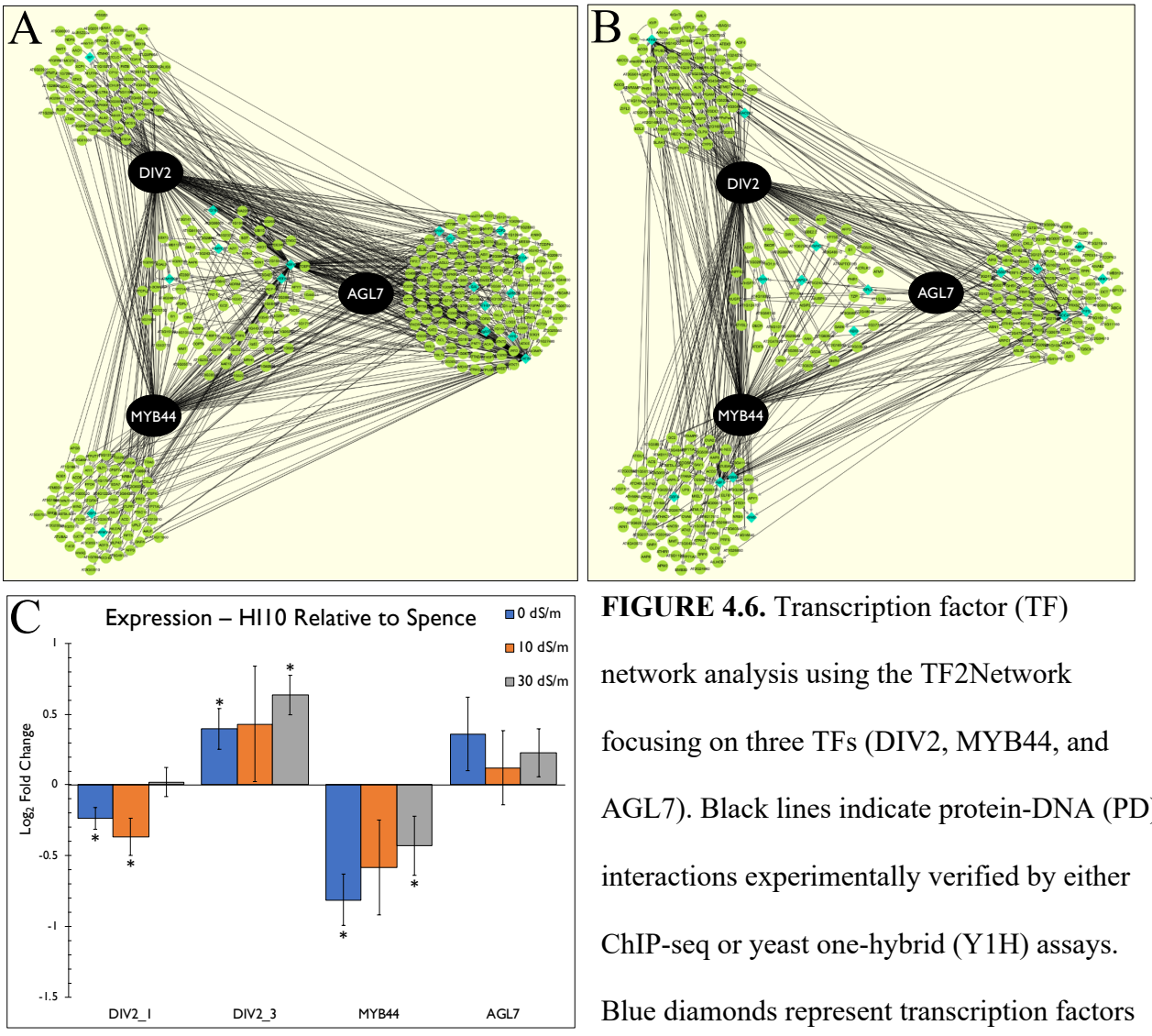

FIGURE 4.6. Transcription factor (TF) network analysis using the TF2Network focusing on three TFs (DIV2, MYB44, and AGL7). Black lines indicate protein-DNA (PD) interactions experimentally verified by either ChIP-seq or yeast one-hybrid (Y1H) assays. Blue diamonds represent transcription factors and green circles represent other genes. **(A)** Network of targeted genes for DIV2, MYB44, and

AGL7 for ‘Spence’ in the 0-10 dS/m comparison. **(B)** Network of targeted genes for DIV2, MYB44, and AGL7 for ‘HI10 in the 0-30 dS/m comparison. **(C)** Log_2 fold change values for DIV2, MYB44, and AGL7 comparing ‘HI10’ and ‘Spence’ under freshwater, 10 dS/m and 30 dS/m. Log_2 fold values represent changes in HI10 relative to Spence. Asterisks in **(B)** indicate statistical significance of $p<0.05$ provided by DEseq2.

Four DIV2 homologs were identified in the seashore paspalum transcriptome, numbered from 1-4 in order of decreasing similarity at the peptide level to sorghum DIV2. Though below our log_2fold change threshold of 1, the expression of DIV2_1, DIV2_3, and MYB44 significantly differed between accessions under freshwater. DIV2_1 and MYB44 were downregulated in ‘HI10’ *vs.* ‘Spence’ while DIV2_3 was upregulated (Fig. 4.6C). The expression of DIV2_1 and DIV2_3 also differed significantly at 10 dS/m and 30 dS/m, respectively.

Discussion

Differences in gibberellin homeostasis may be responsible for growth phenotypes in ‘HI10’ and ‘Spence’

Gibberellin is an essential hormone and its modulation significantly affects growth rates under stress [27]. Differences in GA homeostasis thus may be a significant contributor to the growth differences observed between ‘HI10’ and ‘Spence’. Though multiple regulators of gibberellin homeostasis differ between ‘HI10’ and ‘Spence’, a few stand out. The well-known GA biosynthetic enzyme GA20OX1, which results in semidwarfs when knocked out [30, 31], is differentially regulated between ‘Spence’ and ‘HI10’. Under 10 dS/m and 30 dS/m salt, ‘Spence’

downregulates GA20OX1 while GA20OX1 expression did not significantly differ in 'HI10' under either salt concentration relative to freshwater. However, another transcript mapping to GA20OX1 is expressed at a significantly lower level in 'HI10' compared to 'Spence' under freshwater. This may contribute to the slow-growth habit exhibited by 'HI10' (Chapter II, Fig. 2.2A) under freshwater conditions. No significant differences in GA20OX1 expression were observed when directly comparing 'HI10' and 'Spence' at either 10 dS/m or 30 dS/m, indicating that the expression level of GA20OX1 in 'HI10' may already be at an appropriate level to help 'HI10' grow under salt stress.

Similarly, the gibberellin-deficient mutant *ga2*, which is deficient in the GA-biosynthetic enzyme ent-kaurene synthase, exhibit severe dwarf phenotypes [32]. 'HI10' downregulates ent-kaurene synthase at 30 dS/m, and several transcripts are significantly downregulated in 'HI10' relative to 'Spence' in freshwater, 10 dS/m and 30 dS/m. These results further illustrate that gibberellin signaling may be responsible for growth differences seen between 'HI10' and 'Spence' through modulation of growth at high salt stress and in the absence of salt stress.

Gibberellin signaling is connected to light-induced pathways through the action of COP1, an E3 ubiquitin ligase, which is a vital repressor of photomorphogenesis [33, 34]. In darkness, COP1 degrades HY5, a transcription factor that positively regulates light-induced growth (ie. photomorphogenesis) in a gibberellin-dependent manner [34]. 'Spence' downregulates HY5 under both salt treatments. Another transcript mapping to HY5 is significantly lower in expression in 'HI10' compared to 'Spence' under freshwater while no differences were observed between accessions at 10 dS/m or 30 dS/m. Collectively, these data indicate that in 'HI10', the HY5 gene may be expressed under freshwater at a low level more appropriate for growth in salt.

HY5 thus may also contribute to the slow-growth phenotype of ‘HI10’ under freshwater compared with ‘Spence’.

Proline metabolism is distinctly regulated in ‘HI10’ and ‘Spence’

Many genes responsible for osmolyte production appear to be constitutively active in ‘HI10’ relative to ‘Spence’ under salt stress. ‘Spence’ upregulates the proline biosynthetic enzyme Delta-1-pyrroline-5-carboxylate synthase B (P5CSB) at both 10 dS/m and 30 dS/m, while in ‘HI10’ it is only upregulated at 30 dS/m. Interestingly, another transcript mapping to P5CSB is more highly expressed in ‘HI10’ compared to ‘Spence’ under freshwater, indicating production of proline in the absence of salt. These results confirm our observations in Chapter II, where ‘HI10’ produces significantly higher amounts of proline than ‘Spence’ in all salt conditions tested. The P5CS enzyme is the rate-limiting step in proline biosynthesis [35]. Thus, its significant upregulation in ‘HI10’ compared to ‘Spence’ under freshwater conditions paired with the induction in ‘Spence’ under both low (10 dS/m) and high (30 dS/m) salt stress, but only high salt in ‘HI10’ indicates that ‘HI10’ may constitutively produce proline at sufficient levels to tolerate low concentrations of salt. Proline production in ‘Spence’, on the other hand, is salt-induced. ‘Spence’ also upregulated the P5CSB paralog P5CSA, but only under 30 dS/m. In contrast to P5CSB, P5CSA was not DE between the two accessions under freshwater. P5CSA and P5CSB genes, characterized in the literature as P5CS1 and P5CS2, respectively, are thought to play distinct roles during development outside of their well-known roles producing osmolytes [36-38]. In *Arabidopsis*, salt stress-induced proline biosynthesis in *p5cs1* mutants is not fully compensated for by P5CS2, and *p5cs2* mutants are embryo lethal, indicating that P5CS1 may be more important for proline accumulation under salt stress [39]. Furthermore, P5CS enzymes are

subject to feedback inhibition by elevated proline levels [40], indicating that P5CSA and P5CSB in ‘HI10’ and ‘Spence’ may differ in their sensitivity to elevated proline. Collectively, our results indicate that ‘HI10’ and ‘Spence’ may be distinctly regulating P5CSA and P5CSB function under salt stress.

Despite the role of proline in protecting against abiotic stresses, elevated concentrations of the proline degradation product (s)-1-pyrroline-5-carboxylate (P5C) are damaging to cells [41]. At 30 dS/m, ‘Spence’ upregulates two transcripts mapping to Delta-1-pyrroline-5-carboxylate dehydrogenase 12A1 (ALDH12A1), which is involved in the second step of proline degradation and inhibits programmed cell death by converting the toxic proline catabolism intermediate P5C to glutamate [42]. Typically, proline dehydrogenase (ProDH), the enzyme that catalyzes the first step and is rate-limiting in the proline degradation pathway, is downregulated under abiotic stress [43-45]. ProDH was not DE in our study. Because proline is upregulated to a much larger extent in ‘Spence’ compared to ‘HI10’ (upregulation of both P5CSA and P5CSB at 30 dS/m salt), it is possible that the high levels of proline in ‘Spence’ at 30 dS/m induce expression of ALDH12A1. Application of external proline has been shown to upregulate ProDH within 2 hrs of treatment, while transcript levels of ALDH12A1 (synonym P5CDH) were not upregulated until 24 hrs after proline treatment [42]. After three weeks of salt treatment, however, elevated transcript levels were observed for ALDH12A1, but not ProDH. Our samples for RNA-Seq were taken after ~3 weeks at 30 dS/m. Our data suggest that ‘HI10’ and ‘Spence’ regulate proline synthesis and catabolism differently, with ‘HI10’ constitutively producing higher proline levels while proline production is salt-induced in ‘Spence’, which also experiences a higher sensitivity to elevated proline concentrations.

'HI10' and 'Spence' may differ in the type of osmolytes produced under salt stress

Interestingly a galactinol synthase gene, GOLS2, which is responsible for producing raffinose family oligosaccharide (RFOs)-based osmolytes from myo-inositol and UDP-glucose precursors [46, 47], was only upregulated in 'HI10' at 30 dS/m. Furthermore, the expression of all but one transcript mapping to GOLS2 are significantly higher in 'HI10' relative to 'Spence' under 0 dS/m, 10 dS/m, and 30 dS/m. The level of myo-inositol has been shown to increase in seashore paspalum under salt stress, though these changes were not thought to relate to intraspecific differences in salt tolerance between genotypes [13]. Osmolyte production under salt stress has never been assessed in *P. distichum,* so a more in-depth comparative analysis of omolyte content in these two accessions is needed. Similarly, betaine aldehyde dehydrogenase 1 (ALDH10A8), an enzyme in the biosynthetic pathway of the osmolyte glycine betaine, was upregulated in 'HI10' at 30 dS/m salt. Glycine betaine is another osmolyte thought to help prevent cellular water loss under abiotic stress [48], and is known to accumulate in seashore paspalum under salt stress [13]. Thus, RFO-type osmolytes and glycine betaine may have a larger role in conveying salt tolerance in 'HI10' compared to 'Spence'.

Transporters and sodium-dependent enzymes differ in 'HI10' and 'Spence' under salt stress

Many potassium transporters exhibited distinct patterns of expression in 'HI10' and 'Spence' and many appeared to be specific to only one accession or salt treatment, indicating that potassium transport is tightly regulated in both accessions. For example, the potassium transporter POT2 is downregulated in both accessions at 10 dS/m, while others like POT11 and POT1 are only found in 'Spence' and 'HI10', respectively. These results illustrate that 'HI10'

and ‘Spence’ differ in their utilization of potassium transporters, and that potassium transport in *Paspalum* is likely intricately regulated.

Only a few genes associated with sodium ion transport were found in either accession. One of the most interesting genes associated with sodium ion homeostasis was SHORT ROOT IN SALT MEDIUM 1 (RSA1). RSA1, a transcription factor that positively regulates Salt Overly Sensitive 1 (SOS1) and genes involved with ROS detoxification [49], was downregulated in ‘HI10’ at 10 dS/m. RSA1 expression was also lower in ‘HI10’ relative to ‘Spence’ under freshwater and 10 dS/m. SOS1 is a membrane-localized sodium/protein antiporter responsible for shuttling sodium outwards from cell interiors [50], indicating that its downregulation may be a mechanism utilized by ‘HI10’ to enhance sodium uptake into cells as opposed to excluding it at low salt concentrations. Indeed, ‘HI10’ absorbs more sodium under 10 dS/m salt stress compared with ‘Spence’ (Chapter II, Fig. 2.1C & Fig. 2.2C).

A few sodium-dependent enzymes differ between ‘HI10’ and ‘Spence’ as well. One transcript mapping to the tonoplast-localized dicarboxylate transporter TDT1 is downregulated in ‘Spence’ under both salt treatments, but not differentially expressed in ‘HI10’. This transcript is upregulated in ‘HI10’ at 10 dS/m relative to ‘Spence’. ‘Spence’ also downregulates a second transcript mapping to TDT1 that is upregulated in ‘HI10’ relative to ‘Spence’ at 10 dS/m and 30 dS/m. TDT1 is involved with malate and fumarate transport across the vacuolar membrane [51, 52]. These results indicate that ‘HI10’ and ‘Spence’ may differ in their regulation of sodium-coupled malate transport, which will need to be investigated further under salt stress. Two additional dicarboxylate transporters in the chloroplast, DIT1 and DIT2.1, differ in expression profile under salt between accessions, and both are involved with detoxifying the ammonia generated by the photorespiratory pathway. DIT1 transports 2-oxoglutarate into plastids during

primary ammonia assimilation [53, 54] while DIT2.1 transports the final product of ammonia assimilation, glutamate, outwards into the cytosol [53, 55]. DIT1 is downregulated only in 'Spence' under both salt treatments. DIT2.1 was downregulated in both accessions at 30 dS/m, and several transcripts significantly differ in expression between 'HI10' and 'Spence' under freshwater, 10 dS/m, and 30 dS/m indicating that 'HI10' and 'Spence' may differ in regulating the detoxification of photorespiration byproducts. Interestingly, the sodium/pyruvate cotransporter BASS2 (AT2G2690), which transports pyruvate across the chloroplast membrane in a sodium-dependent manner [56], was not found in our differentially expressed dataset. However, in DIT2.1, a sodium/sulphate symporter domain (InterPro:IPR001898) (Pfam domain: 00939.5 Na_Sulph_Symp) was identified [55] and when checked through InterPro, DIT1 also contains this domain. These data indicate that DIT1 and DIT2.1 transport may be sodium-coupled, and perhaps their function is modified in the presence of sodium. It is thus possible that DIT1 and DIT2.1 are connected to sodium-coupled transport across the chloroplast membrane, though more in-depth work on this subject is needed.

The most highly differentially expressed genes differ between 'HI10' and 'Spence'

Examination of genes that are most significantly differentially expressed in 'Spence' under 30 dS/m, shows that these genes are typically also differentially expressed in 'HI10' under 30 dS/m salt and in 'Spence', but not 'HI10', under 10 dS/m salt. This suggests that a salt level of 10 dS/m represents no stress or less stress in 'HI10' compared to 'Spence'. This may be due to a preparedness of 'HI10', even under freshwater conditions, to cope with salt stress that may benefit 'HI10' when salt stress is initiated compared with 'Spence'. More in-depth analyses of these highly differentially expressed genes are currently underway.

When examining the most highly differentially expressed genes, several well-characterized genes associated with senescence were found to exhibit interesting patterns. The bidirectional sugar transporter SWEET15 (ie. Senescence associated gene 29, SAG29) regulates cell growth under high salt stress, and generally promotes senescence [57]. SWEET15 is upregulated by both accessions at 30 dS/m, but only by 'Spence' at 10 dS/m. Similarly, SAG12, the most widely used senescence-associated reference gene involved with nitrogen mobilization [58, 59], follows this pattern, though downregulated. It is activated by developmentally coordinated senescence pathways, and not by stress or hormone-controlled pathways [60]. SAG12 is thought to breakdown proteins and provide materials necessary for increased nitrogen mobilization under low nitrogen conditions [58, 59], and thus its downregulation may be a mechanism to slow growth under stress. This is illustrated by its downregulation in both accessions at 30 dS/m and only in 'Spence' at 10 dS/m, indicating that growth inhibition may not have been initiated in 'HI10' at 10 dS/m. Interestingly, the same pattern of downregulation was observed for the nitrate reductase gene (NADH1) (ie. NIA1), involved with nitrate assimilation [61]. Our results illustrate that 'HI10' and 'Spence' are modifying senescence-related genes that may affect nitrogen allocation under salt stress, and that this regulation may differ between them.

The HSF1 pathway under salt stress

The GO analyses suggested that there was an enrichment of the HSF1 stress response pathway in 'Spence' at 10 dS/m and in 'HI10' at 30 dS/m, indicating that this pathway may be activated by each accession at different salt concentrations. At 10 dS/m, there were 11 genes identified in this pathway for 'Spence' but only three for 'HI10', two of which overlapped. At 30 dS/m, 10 genes in this pathway were identified for 'HI10', while eight were found for 'Spence'.

A closer look at the differentially expressed genes that shifted HSF1 pathways towards significant enrichment in 'HI10' identified four genes absent from 'Spence': regulatory-associated protein of TOR1 (RAPTOR1), heat stress transcription factor A-7A (HSFA7A), heat shock protein 90-4 (HSP90-4), and heat stress transcription factor B-2b (HSFB2B). The genes HSP90-4 and HSFB2B were only found in 'Spence' in the 0-10 dS/m comparison, indicating a possible role in initiating the use of this pathway in 'HI10' and 'Spence' at different salt concentrations.

The HSF1 pathway has been characterized in mammalian systems [62] and also in yeast [63, 64], where HSP90 negatively regulates HSF1 function. Connections between HSF1 and HSP90 have also been found in *Chlamydomonas* [65, 66]. The function of HSP90 in plants has been studied in *Arabidopsis*, where HSP90-1, -2, -3, and -4 is active in the cytosol [67]. When overexpressed, the cytoplasmic form of HSP90 reduces tolerance to oxidative stress [68], while other HSPs like HSP90-1 are strongly induced under stress [69]. Though the transcript upregulated in 'HI10' has homology to HSP90-4, it is possible that its function is beneficial under salt stress as observed for many other HSPs. 'Spence', on the other hand, downregulates another transcript mapping to HSP90-4 at 10 dS/m. Furthermore, the HSP90-1 gene is upregulated in both 'HI10' and 'Spence' at 30 dS/m. HSP proteins have diverse cellular roles and respond to stress in distinct manners [70], and thus elucidating the function of various HSPs in *Paspalum* will require more detailed work.

HSFB2B is responsible for suppressing heat shock response in the absence of heat stress, though it is also required for proper initiation of heat shock response [71]. Furthermore, HSFB2B is a major circadian regulator, where it helps sustain proper circadian rhythm following temperature and salt stress [72]. It has also been characterized in rice as a negative regulator of

drought and salt tolerance [73]. Collectively, the literature and our results suggest that regulation of heat shock proteins is likely vital under salt stress in *Paspalum*, though more detailed work needs to be conducted to determine the function of HSP90-4 and HSFB2B.

DIV2, MYB44, and AGL7 may cooperatively regulate salt response in Paspalum

Our transcription factor network analysis indicates that three TFs, DIV2, MYB44, and AGL7, regulate a large subset of genes that are used differently by 'Spence' and 'HI10'. DIV2 negatively affects salt tolerance by acting on the ABA pathway; *div2* mutants exhibit high ABA sensitivity, increased ABA content and higher salt tolerance [74], indicating that downstream ABA responses may differ in 'HI10' and 'Spence'. Similarly, MYB44 interacts with the ABA receptor PYL8 [75] and is a negative regulator of ABA signaling [76]. Modulating MYB44 expression has significant effects on traits like stomatal closure when overexpressed [77] and antioxidative capacity when dominantly repressed [78]. Collectively, these results show that 'HI10' and 'Spence' may be modulating traits such as stomatal aperture under salt stress, though more in-depth physiological studies are needed. AGL7 (*i.e.* APETALA1, AP1) coordinates floral meristem identity along with LEAFY (LHY), and *ap1* mutants are unable to transition from an inflorescence meristem to a floral meristem [79]. AGL7/AP1 is also downregulated when a highly salt-induced R2R3-MYB transcription factor from chrysanthemum is overexpressed in *Arabidopsis*, resulting in later flowering [80]. Opposingly, in mutants of the Cyclin-dependent kinase G2 (CDKG2), which have increased salt tolerance, AP1/AGL7 is significantly upregulated and flowering time was accelerated [81]. Results from the literature indicate that AGL7/AP1 may represent a central regulator of flowering time under salt stress, and combined with our network analysis, indicate that AGL7/AP1 may be coordinating flowering distinctly in

'HI10' and 'Spence'. Consequently, the processes of ABA homeostasis, the control of stomatal closure, and control over flowering time under salt stress may be vital differentiators to focus on in future work distinguishing *P. vaginatum* and *P. distichum*.

GO categories differ between 'HI10' and 'Spence' under salt stress

Though not as informative as examining major regulators in pathways of interest, our GO analysis yielded several insights into mechanisms used by 'HI10' and 'Spence' under salt stress. The 'root development' biological process found in 'HI10' under 10 dS/m provided several regulators of root development absent from 'Spence' including a stabilizer of iron transporters termed Argonaute 1 (AGO1), the auxin transporter BIG, the root meristem gene OBERON 4 (OBE4), and the phosphoinositide phosphatase ROOT HAIR DEFECTIVE 4 (RHD4), none of which have any clear connection to salt stress. Furthermore at 10 dS/m, most of the processes found for 'HI10' appear to be related to growth, while those found in 'Spence' are related to stress response, indicating that 10 dS/m may represent a more stressful salt treatment for 'Spence' compared to 'HI10'. Indeed, over double the number of differentially expressed genes for 'Spence' (104) were part of the 'response to abiotic stimulus' category compared with 'HI10' (50). Together with the large number of differentially expressed genes found in 'Spence' (707) compared to 'HI10' (366), our results suggest that 'Spence' likely experienced more drastic changes in terms of total transcriptome adjustment under 10 dS/m salt stress.

At 30 dS/m, similar results were found for the number of differentially expressed genes with 995 found in 'Spence' and 735 found in 'HI10', though this difference is smaller than that found at 10 dS/m. Both accessions had many differentially expressed genes associated with stress response, where this was true at 10 dS/m only for 'Spence'. In contrast to 'Spence', 'HI10'

may be better at modifying nitrogen metabolism in addition to protein folding as indicated by enriched processes. Interestingly, four categories related to cell wall biogenesis were found only in ‘Spence’, indicating that cell wall integrity in ‘Spence’ may need to be modified under high salt stress. Molecular functions related to AMP/ATP-binding were only found in ‘HI10’, indicating possible alterations to ATP homeostasis not seen in ‘Spence. Enriched cellular components at 30 dS/m illustrate that most differentially expressed genes appear to be related to chloroplast function. Thus, both accessions are likely modifying photosynthetic processes under high salt stress.

Conclusion

Collectively, our results indicate that regulators of salt tolerance pathways, including sodium/potassium transport, osmolyte biosynthesis/transport, gibberellin homeostasis, and senescence differ between ‘HI10’ and ‘Spence’ under salt stress. Though there are many important growth regulators in play, a significant contributor to the high salt tolerance observed in ‘HI10’ likely arises from some major regulators being constitutively active. Furthermore, the TFs DIV2, MYB44, and AGL7 appear to regulate a large subset of differentially expressed genes in ‘HI10’ and ‘Spence’, and this regulation differs between them. We thus provide several lines of evidence that will help future studies differentiate halophytic and glycophytic species pairs and also help identify markers of salt tolerance that can be leveraged in salt sensitive glycophytic species.

Acknowledgements

Experiments in this chapter were funded through the grants shown below.

USDA-SCRI awarded to K.M. Devos (2015-51181-24291; PI: K.E. Kenworthy, University of Florida)

NIH T32 Training Grant (T32 GM 7103-41)

References

1. Wicke, B., et al., *The global technical and economic potential of bioenergy from salt-affected soils.* Energy & Environmental Science, 2011. **4**(8): p. 2669-2681.
2. Flowers, T.J., *Improving crop salt tolerance.* Journal of Experimental Botany, 2004. **55**(396): p. 307-319.
3. Ghassemi F , J.A., Nix HA., *Salinization of land and water resources. human causes, extent, management, and case studies.* 1995, Sydney: University of New South Wales: CAB Internationals.
4. Himabindu, Y., et al., *Salt-tolerant genes from halophytes are potential key players of salt tolerance in glycophytes.* Environmental and Experimental Botany, 2016. **124**: p. 39-63.
5. Flowers, T.J., R. Munns, and T.D. Colmer, *Sodium chloride toxicity and the cellular basis of salt tolerance in halophytes.* Annals of Botany, 2015. **115**(3): p. 419-431.
6. Shen, Y.G., et al., *Overexpression of proline transporter gene isolated from halophyte confers salt tolerance in Arabidopsis.* Acta Botanica Sinica, 2002. **44**(8): p. 956-962.
7. Wang, Y.C., et al., *Enhanced salt tolerance of transgenic poplar plants expressing a manganese superoxide dismutase from Tamarix androssowii.* Molecular Biology Reports, 2010. **37**(2): p. 1119-1124.
8. Yang, Y., et al., *Overexpression of the PtSOS2 gene improves tolerance to salt stress in transgenic poplar plants.* Plant Biotechnology Journal, 2015. **13**(7): p. 962-973.
9. Roy, S.J., S. Negrao, and M. Tester, *Salt resistant crop plants.* Current Opinion in Biotechnology, 2014. **26**: p. 115-124.

10. Ceccoli, G., et al., *Salt Glands in the Poaceae Family and Their Relationship to Salinity Tolerance.* Botanical Review, 2015. **81**(2): p. 162-178.

11. Lonard, R.I., F.W. Judd, and R. Stalter, *Biological Flora of Coastal Dunes and Wetlands: Paspalum vaginatum Sw.* Journal of Coastal Research, 2015. **31**(1): p. 213-223.

12. Guo, H.L., et al., *Growth response and ion regulation of seashore paspalum accessions to increasing salinity.* Environmental and Experimental Botany, 2016. **131**: p. 137-145.

13. Lee, G., et al., *Synthesis of organic osmolytes and salt tolerance mechanisms in Paspalum vaginatum.* Environmental and Experimental Botany, 2008. **63**(1-3): p. 19-27.

14. Peacock, C.H. and A.E. Dudeck, *PHYSIOLOGICAL AND GROWTH-RESPONSES OF SEASHORE PASPALUM TO SALINITY.* Hortscience, 1985. **20**(1): p. 111-112.

15. HL Leithead, L.Y., TN Shiflet, *100 native forage grasses in 11 southern states.* Agricultural Handbook, Soil Conservation Service, USDA, 1971. **No. 389**: p. 216.

16. Eudy D, B.B., Harrison ML, Raymer P, Devos KM *Ploidy level and genetic diversity in the genus Paspalum, group Disticha.* Crop Science 2017. **57**: p. 3319-3332.

17. Liu, Y.M., et al., *Identification of differentially expressed salt-responsive proteins in roots of two perennial grass species contrasting in salinity tolerance.* Journal of Plant Physiology, 2012. **169**(2): p. 117-126.

18. Endo, N., et al., *Putative UDP-galactose epimerase and metallothioneine of Paspalum vaginalum enhanced the salt tolerance of rice, Oryza sativa L. from transplanting to harvest stages.* Breeding Science, 2005. **55**(2): p. 163-173.

19. Jia, X.P., et al., *Characterization of the global transcriptome using Illumina sequencing and novel microsatellite marker information in seashore paspalum.* Genes & Genomics, 2015. **37**(1): p. 77-86.

20. Bolger, A.M., M. Lohse, and B. Usadel, *Trimmomatic: a flexible trimmer for Illumina sequence data.* Bioinformatics, 2014. **30**(15): p. 2114-2120.

21. Pertea, M., et al., *Transcript-level expression analysis of RNA-seq experiments with HISAT, StringTie and Ballgown.* Nature Protocols, 2016. **11**(9): p. 1650-1667.

22. Love, M.I., W. Huber, and S. Anders, *Moderated estimation of fold change and dispersion for RNA-seq data with DESeq2.* Genome Biology, 2014. **15**(12): p. 38.

23. Goodstein, D.M., et al., *Phytozome: a comparative platform for green plant genomics.* Nucleic Acids Research, 2012. **40**(D1): p. D1178-D1186.

24. Tian, T., et al., *SorghumFDB: sorghum functional genomics database with multidimensional network analysis.* Database-the Journal of Biological Databases and Curation, 2016: p. 16.

25. Mi, H.Y., et al., *Large-scale gene function analysis with the PANTHER classification system.* Nature Protocols, 2013. **8**(8): p. 1551-1566.

26. Kulkarni, S.R., et al., *TF2Network: predicting transcription factor regulators and gene regulatory networks in Arabidopsis using publicly available binding site information.* Nucleic Acids Research, 2018. **46**(6): p. 15.

27. Colebrook, E.H., et al., *The role of gibberellin signalling in plant responses to abiotic stress.* Journal of Experimental Biology, 2014. **217**(1): p. 67-75.

28. Achard, P., et al., *Integration of plant responses to environmentally activated phytohormonal signals.* Science, 2006. **311**(5757): p. 91-94.

29. Uddin, M.K., et al., *The effect of salinity on growth and ion accumulation in six turfgrass species.* Plant Omics, 2012. **5**(3): p. 244-252.

30. Spielmeyer, W., M.H. Ellis, and P.M. Chandler, *Semidwarf (sd-1), "green revolution" rice, contains a defective gibberellin 20-oxidase gene.* Proceedings of the National Academy of Sciences of the United States of America, 2002. **99**(13): p. 9043-9048.

31. Jia, Q.J., et al., *GA-20 oxidase as a candidate for the semidwarf gene sdw1/denso in barley.* Functional & Integrative Genomics, 2009. **9**(2): p. 255-262.

32. Yamaguchi, S., et al., *The GA2 locus of Arabidopsis thaliana encodes ent-kaurene synthase of gibberellin biosynthesis.* Plant Physiology, 1998. **116**(4): p. 1271-1278.

33. Deng, X.W., T. Caspar, and P.H. Quail, *COP1 - A REGULATORY LOCUS INVOLVED IN LIGHT-CONTROLLED DEVELOPMENT AND GENE-EXPRESSION IN ARABIDOPSIS.* Genes & Development, 1991. **5**(7): p. 1172-1182.

34. Alabadi, D., et al., *Gibberellins modulate light signaling pathways to prevent Arabidopsis seedling de-etiolation in darkness.* Plant Journal, 2008. **53**(2): p. 324-335.

35. Yoshiba, Y., et al., *Stress-responsive and developmental regulation of Delta(1)-pyrroline-5-carboxylate synthetase 1 (P5CS1) gene expression in arabidopsis thaliana.* Biochemical and Biophysical Research Communications, 1999. **261**(3): p. 766-772.

36. Mattioli, R., et al., *The proline biosynthetic genes P5CS1 and P5CS2 play overlapping roles in Arabidopsis flower transition but not in embryo development.* Physiologia Plantarum, 2009. **137**(1): p. 72-85.

37. Strizhov, N., et al., *Differential expression of two P5CS genes controlling proline accumulation during salt-stress requires ABA and is regulated by ABA1, ABI1 and AXR2 in Arabidopsis.* Plant Journal, 1997. **12**(3): p. 557-569.

38. Funck, D., et al., *Requirement of proline synthesis during Arabidopsis reproductive development.* Bmc Plant Biology, 2012. **12**: p. 12.

39. Szekely, G., et al., *Duplicated P5CS genes of Arabidopsis play distinct roles in stress regulation and developmental control of proline biosynthesis.* Plant Journal, 2008. **53**(1): p. 11-28.

40. Hong, Z.L., et al., *Removal of feedback inhibition of Delta(1)-pyrroline-5-carboxylate synthetase results in increased proline accumulation and protection of plants from osmotic stress.* Plant Physiology, 2000. **122**(4): p. 1129-1136.

41. Deuschle, K., et al., *The role of Delta(1)-Pyrroline-5-carboxylate dehydrogenase in proline degradation.* Plant Cell, 2004. **16**(12): p. 3413-3425.

42. Deuschle, K., et al., *A nuclear gene encoding mitochondrial triangle(1)-pyrroline-5-carboxylate dehydrogenase and its potential role in protection from proline toxicity.* Plant Journal, 2001. **27**(4): p. 345-355.

43. Sharma, S. and P.E. Verslues, *Mechanisms independent of abscisic acid (ABA) or proline feedback have a predominant role in transcriptional regulation of proline metabolism during low water potential and stress recovery.* Plant Cell and Environment, 2010. **33**(11): p. 1838-1851.

44. Kiyosue, T., et al., *A nuclear gene encoding mitochondrial proline dehydrogenase, an enzyme involved in proline metabolism, is upregulated by proline but downregulated by dehydration in Arabidopsis.* Plant Cell, 1996. **8**(8): p. 1323-1335.

45. Funck, D., S. Eckard, and G. Muller, *Non-redundant functions of two proline dehydrogenase isoforms in Arabidopsis.* Bmc Plant Biology, 2010. **10**: p. 13.

46. Nishizawa, A., Y. Yabuta, and S. Shigeoka, *Galactinol and raffinose constitute a novel function to protect plants from oxidative damage.* Plant Physiology, 2008. **147**(3): p. 1251-1263.

47. Karner, U., et al., *myo-Inositol and sucrose concentrations affect the accumulation of raffinose family oligosaccharides in seeds.* Journal of Experimental Botany, 2004. **55**(405): p. 1981-1987.

48. Takabe, T., *Engineering of betaine biosynthesis and transport for abiotic stress tolerance in plants.* Journal of Plant Biochemistry and Biotechnology, 2012. **21**(1): p. S58-S62.

49. Guan, Q.M., et al., *A Nuclear Calcium-Sensing Pathway Is Critical for Gene Regulation and Salt Stress Tolerance in Arabidopsis.* Plos Genetics, 2013. **9**(8): p. 16.

50. Shi, H.Z., et al., *The Arabidopsis thaliana salt tolerance gene SOS1 encodes a putative Na+/H+ antiporter.* Proceedings of the National Academy of Sciences of the United States of America, 2000. **97**(12): p. 6896-6901.

51. Emmerlich, V., et al., *The plant homolog to the human sodium/dicarboxylic cotransporter is the vacuolar malate carrier.* Proceedings of the National Academy of Sciences of the United States of America, 2003. **100**(19): p. 11122-11126.

52. Hurth, M.A., et al., *Impaired pH homeostasis in arabidopsis lacking the vacuolar dicarboxylate transporter and analysis of carboxylic acid transport across the tonoplast.* Plant Physiology, 2005. **137**(3): p. 901-910.

53. Taniguchi, M., et al., *Identifying and characterizing plastidic 2-oxoglutarate/malate and dicarboxylate transporters in Arabidopsis thaliana.* Plant and Cell Physiology, 2002. **43**(7): p. 706-717.

54. Kinoshita, H., et al., *The chloroplastic 2-oxoglutarate/malate transporter has dual function as the malate valve and in carbon/nitrogen metabolism.* Plant Journal, 2011. **65**(1): p. 15-26.

55. Renne, P., et al., *The Arabidopsis mutant dct is deficient in the plastidic glutamate/malate translocator DiT2.* Plant Journal, 2003. **35**(3): p. 316-331.

56. Furumoto, T., et al., *A plastidial sodium-dependent pyruvate transporter.* Nature, 2011. **476**(7361): p. 472-U131.

57. Seo, P.J., et al., *An Arabidopsis senescence-associated protein SAG29 regulates cell viability under high salinity.* Planta, 2011. **233**(1): p. 189-200.

58. James, M., et al., *SAG12, a Major Cysteine Protease Involved in Nitrogen Allocation during Senescence for Seed Production in Arabidopsis thaliana.* Plant and Cell Physiology, 2018. **59**(10): p. 2052-2063.

59. James, M., et al., *A New Role for SAG12 Cysteine Protease in Roots of Arabidopsis thaliana.* Frontiers in Plant Science, 2019. **9**: p. 11.

60. Noh, Y.S. and R.M. Amasino, *Identification of a promoter region responsible for the senescence-specific expression of SAG12.* Plant Molecular Biology, 1999. **41**(2): p. 181-194.

61. Wilkinson, J.Q. and N.M. Crawford, *IDENTIFICATION AND CHARACTERIZATION OF A CHLORATE-RESISTANT MUTANT OF ARABIDOPSIS-THALIANA WITH MUTATIONS IN BOTH NITRATE REDUCTASE STRUCTURAL GENES NIA1 AND NIA2.* Molecular & General Genetics, 1993. **239**(1-2): p. 289-297.

62. Knauf, U., et al., *Repression of human heat shock factor 1 activity at control temperature by phosphorylation.* Genes & Development, 1996. **10**(21): p. 2782-2793.

63. Truman, A.W., et al., *In the yeast heat shock response, Hsf1-directed induction of Hsp90 facilitates the activation of the Slt2 (Mpk1) mitogen-activated protein kinase required for cell integrity.* Eukaryotic Cell, 2007. **6**(4): p. 744-752.

64. Leach, M.D., et al., *Hsp90 Orchestrates Transcriptional Regulation by Hsf1 and Cell Wall Remodelling by MAPK Signalling during Thermal Adaptation in a Pathogenic Yeast.* Plos Pathogens, 2012. **8**(12): p. 20.

65. Schulz-Raffelt, M., M. Lodha, and M. Schroda, *Heat shock factor 1 is a key regulator of the stress response in Chlamydomonas.* Plant Journal, 2007. **52**(2): p. 286-295.

66. Schmollinger, S., et al., *Dissecting the Heat Stress Response in Chlamydomonas by Pharmaceutical and RNAi Approaches Reveals Conserved and Novel Aspects.* Molecular Plant, 2013. **6**(6): p. 1795-1813.

67. Cha, J.Y., et al., *Structural and functional differences of cytosolic 90-kDa heat-shock proteins (Hsp90s) in Arabidopsis thaliana.* Plant Physiology and Biochemistry, 2013. **70**: p. 368-373.

68. Song, H.M., P.X. Fan, and Y.X. Li, *Overexpression of Organellar and Cytosolic AtHSP90 in Arabidopsis thaliana Impairs Plant Tolerance to Oxidative Stress.* Plant Molecular Biology Reporter, 2009. **27**(3): p. 342-349.

69. Krishna, P. and G. Gloor, *The Hsp90 family of proteins in Arabidopsis thaliana.* Cell Stress & Chaperones, 2001. **6**(3): p. 238-246.

70. Sarkar, N.K., Y.K. Kim, and A. Grover, *Rice sHsp genes: genomic organization and expression profiling under stress and development.* Bmc Genomics, 2009. **10**: p. 18.

71. Ikeda, M., N. Mitsuda, and M. Ohme-Takagi, *Arabidopsis HsfB1 and HsfB2b Act as Repressors of the Expression of Heat-Inducible Hsfs But Positively Regulate the Acquired Thermotolerance.* Plant Physiology, 2011. **157**(3): p. 1243-1254.

72. Kolmos, E., et al., *HsfB2b-mediated repression of PRR7 directs abiotic stress responses of the circadian clock.* Proceedings of the National Academy of Sciences of the United States of America, 2014. **111**(45): p. 16172-16177.

73. Xiang, J.H., et al., *Heat shock factor OsHsfB2b negatively regulates drought and salt tolerance in rice.* Plant Cell Reports, 2013. **32**(11): p. 1795-1806.

74. Fang, Q., et al., *AtDIV2, an R-R-type MYB transcription factor of Arabidopsis, negatively regulates salt stress by modulating ABA signaling.* Plant Cell Reports, 2018. **37**(11): p. 1499-1511.

75. Zhao, Y., et al., *The ABA Receptor PYL8 Promotes Lateral Root Growth by Enhancing MYB77-Dependent Transcription of Auxin-Responsive Genes.* Science Signaling, 2014. **7**(328): p. 11.

76. Jaradat, M.R., et al., *Multiple roles of the transcription factor AtMYBR1/AtMYB44 in ABA signaling, stress responses, and leaf senescence.* Bmc Plant Biology, 2013. **13**: p. 19.

77. Jung, C., et al., *Overexpression of AtMYB44 enhances stomatal closure to confer abiotic stress tolerance in transgenic Arabidopsis.* Plant Physiology, 2008. **146**(2): p. 623-635.

78. Persak, H. and A. Pitzschke, *Dominant Repression by Arabidopsis Transcription Factor MYB44 Causes Oxidative Damage and Hypersensitivity to Abiotic Stress.* International Journal of Molecular Sciences, 2014. **15**(2): p. 2517-2537.

79. Irish, V.F. and I.M. Sussex, *FUNCTION OF THE APETALA-1 GENE DURING ARABIDOPSIS FLORAL DEVELOPMENT.* Plant Cell, 1990. **2**(8): p. 741-753.

80. Shan, H., et al., *Heterologous Expression of the Chrysanthemum R2R3-MYB Transcription Factor CmMYB2 Enhances Drought and Salinity Tolerance, Increases*

Hypersensitivity to ABA and Delays Flowering in Arabidopsis thaliana. Molecular Biotechnology, 2012. **51**(2): p. 160-173.

81. Ma, X.Y., et al., *CYCLIN-DEPENDENT KINASE G2 regulates salinity stress response and salt mediated flowering in Arabidopsis thaliana.* Plant Molecular Biology, 2015. **88**(3): p. 287-299.

Supplemental Table 4.1. GO analyses split by biological process, molecular function, cell component, and Reactome pathways for 'HI10' under 10 dS/m (0 dS/m vs 10 dS/m) and 30 dS/m (0 dS/m vs 30 dS/m). Only significantly enriched categories with a false discovery rate (FDR) value < 0.05 shown. Samples are ordered by FDR statistical significance.

HI10 - 0-10 GO biological process complete	Arabidopsis thaliana - REFLIST (27581)	Input	Expected	Fold Enrichment	P-value	FDR
cellular process (GO:0009987)	10295	187	137.73	1.36	2.35E-07	1.39E-03
cellular metabolic process (GO:0044237)	7157	137	95.75	1.43	2.88E-06	5.69E-03
metabolic process (GO:0008152)	8211	153	109.85	1.39	2.39E-06	7.08E-03
response to light stimulus (GO:0009416)	739	26	9.89	2.63	1.24E-05	1.47E-02
organic substance metabolic process (GO:0071704)	7417	138	99.23	1.39	1.18E-05	1.74E-02
system development (GO:0048731)	1829	47	24.47	1.92	2.26E-05	1.91E-02
response to radiation (GO:0009314)	760	26	10.17	2.56	1.98E-05	1.95E-02
response to abiotic stimulus (GO:0009628)	2098	50	28.07	1.78	1.03E-04	4.37E-02
plant organ morphogenesis (GO:1905392)	385	16	5.15	3.11	9.83E-05	4.48E-02
primary metabolic process (GO:0044238)	6707	124	89.73	1.38	6.91E-05	4.55E-02
root system development (GO:0022622)	468	18	6.26	2.87	9.45E-05	4.66E-02
multicellular organism development (GO:0007275)	2612	59	34.95	1.69	7.89E-05	4.67E-02
root development (GO:0048364)	466	18	6.23	2.89	8.98E-05	4.83E-02
post-embryonic development (GO:0009791)	1476	39	19.75	1.97	6.76E-05	5.00E-02
GO molecular function complete	**Arabidopsis thaliana - REFLIST (27581)**	**Input**	**Expected**	**Fold Enrichment**	**P-value**	**FDR**
catalytic activity (GO:0003824)	8874	169	118.72	1.42	6.32E-08	1.95E-04
binding (GO:0005488)	10042	178	134.35	1.32	4.42E-06	6.81E-03
transferase activity (GO:0016740)	3728	81	49.88	1.62	1.14E-05	1.17E-02
ligase activity, forming carbon-nitrogen bonds (GO:0016879)	59	7	0.79	8.87	2.63E-05	2.03E-02
mRNA binding (GO:0003729)	420	17	5.62	3.03	8.17E-05	4.20E-02

heterocyclic compound binding (GO:1901363)	5683	108	76.03	1.42	9.72E-05	4.28E-02
organic cyclic compound binding (GO:0097159)	5705	109	76.33	1.43	7.57E-05	4.66E-02

GO cell component complete	Arabidopsis thaliana - REFLIST (27581)	Input	Expected	Fold Enrichment	P-value	FDR
cell part (GO:0044464)	22695	351	303.63	1.16	2.91E-13	1.57E-10
cell (GO:0005623)	22697	351	303.66	1.16	2.91E-13	3.15E-10
intracellular part (GO:0044424)	21258	332	284.41	1.17	2.56E-10	6.94E-08
intracellular (GO:0005622)	21258	332	284.41	1.17	2.56E-10	9.25E-08
intracellular organelle (GO:0043229)	19520	308	261.15	1.18	2.40E-08	5.20E-06
organelle (GO:0043226)	19561	308	261.7	1.18	3.24E-08	5.85E-06
cytoplasm (GO:0005737)	14521	241	194.27	1.24	1.22E-06	1.89E-04
intracellular membrane-bounded organelle (GO:0043231)	19207	298	256.97	1.16	1.92E-06	2.60E-04
membrane-bounded organelle (GO:0043227)	19316	299	258.42	1.16	2.34E-06	2.81E-04
chloroplast (GO:0009507)	5248	108	70.21	1.54	2.67E-06	2.90E-04
plastid (GO:0009536)	5292	108	70.8	1.53	4.00E-06	3.93E-04
organelle part (GO:0044422)	5381	106	71.99	1.47	2.23E-05	1.86E-03
intracellular organelle part (GO:0044446)	5375	106	71.91	1.47	2.19E-05	1.98E-03
trans-Golgi network (GO:0005802)	317	15	4.24	3.54	4.05E-05	3.13E-03
membrane (GO:0016020)	7769	138	103.94	1.33	1.48E-04	1.07E-02
Golgi subcompartment (GO:0098791)	368	15	4.92	3.05	1.97E-04	1.34E-02
cytoplasmic part (GO:0044444)	12257	198	163.98	1.21	4.87E-04	3.10E-02
plasma membrane (GO:0005886)	3572	71	47.79	1.49	7.66E-04	4.61E-02

HI10 - 0-30

GO biological process complete	Arabidopsis thaliana - REFLIST (27581)	Input	Expected	Fold Enrichment	P-value	FDR
response to abiotic stimulus (GO:0009628)	2098	119	56.52	2.11	7.28E-14	4.31E-10
cellular process (GO:0009987)	10295	376	277.34	1.36	4.13E-13	1.22E-09

response to stimulus (GO:0050896)	5731	238	154.39	1.54	1.58E-12	3.11E-09
response to stress (GO:0006950)	3158	153	85.07	1.8	2.12E-12	3.14E-09
response to temperature stimulus (GO:0009266)	622	52	16.76	3.1	5.09E-12	6.03E-09
response to inorganic substance (GO:0010035)	945	65	25.46	2.55	3.36E-11	2.85E-08
response to oxygen-containing compound (GO:1901700)	1596	92	42.99	2.14	2.97E-11	2.93E-08
response to heat (GO:0009408)	220	28	5.93	4.72	1.05E-10	7.79E-08
response to chemical (GO:0042221)	2777	128	74.81	1.71	4.26E-09	2.80E-06
metabolic process (GO:0008152)	8211	297	221.19	1.34	5.81E-09	3.44E-06
organic substance metabolic process (GO:0071704)	7417	271	199.81	1.36	1.88E-08	1.01E-05
cellular metabolic process (GO:0044237)	7157	262	192.8	1.36	3.44E-08	1.70E-05
response to hydrogen peroxide (GO:0042542)	78	14	2.1	6.66	1.23E-07	5.61E-05
response to acid chemical (GO:0001101)	1178	65	31.73	2.05	1.46E-07	6.17E-05
response to drug (GO:0042493)	593	40	15.97	2.5	3.94E-07	1.56E-04
response to oxidative stress (GO:0006979)	424	32	11.42	2.8	5.64E-07	1.96E-04
response to external stimulus (GO:0009605)	1388	71	37.39	1.9	5.40E-07	2.00E-04
response to reactive oxygen species (GO:0000302)	176	19	4.74	4.01	1.04E-06	3.43E-04
biological regulation (GO:0065007)	5681	209	153.04	1.37	1.41E-06	4.40E-04
primary metabolic process (GO:0044238)	6707	239	180.68	1.32	1.88E-06	5.56E-04
response to extracellular stimulus (GO:0009991)	264	23	7.11	3.23	2.46E-06	6.61E-04
response to antibiotic (GO:0046677)	304	25	8.19	3.05	2.38E-06	6.70E-04
response to radiation (GO:0009314)	760	45	20.47	2.2	2.72E-06	7.00E-04
response to light stimulus (GO:0009416)	739	44	19.91	2.21	3.52E-06	8.68E-04
response to starvation (GO:0042594)	180	18	4.85	3.71	5.33E-06	1.26E-03
response to nutrient levels (GO:0031667)	224	20	6.03	3.31	7.85E-06	1.79E-03

cellular response to extracellular stimulus (GO:0031668)	208	19	5.6	3.39	9.77E-06	2.14E-03
carbohydrate metabolic process (GO:0005975)	810	45	21.82	2.06	1.06E-05	2.24E-03
cellular response to external stimulus (GO:0071496)	214	19	5.76	3.3	1.41E-05	2.79E-03
positive regulation of biological process (GO:0048518)	1271	62	34.24	1.81	1.39E-05	2.85E-03
polysaccharide metabolic process (GO:0005976)	302	23	8.14	2.83	1.88E-05	3.60E-03
regulation of biological process (GO:0050789)	5001	182	134.72	1.35	2.20E-05	3.83E-03
organonitrogen compound metabolic process (GO:1901564)	4315	161	116.24	1.39	2.19E-05	3.93E-03
carbohydrate catabolic process (GO:0016052)	182	17	4.9	3.47	2.18E-05	4.03E-03
protein folding (GO:0006457)	266	21	7.17	2.93	2.63E-05	4.45E-03
cellular response to starvation (GO:0009267)	148	15	3.99	3.76	2.76E-05	4.54E-03
response to high light intensity (GO:0009644)	81	11	2.18	5.04	2.94E-05	4.70E-03
response to toxic substance (GO:0009636)	207	18	5.58	3.23	3.05E-05	4.75E-03
cellular response to heat (GO:0034605)	67	10	1.8	5.54	3.27E-05	4.83E-03
response to osmotic stress (GO:0006970)	665	38	17.91	2.12	3.40E-05	4.90E-03
cellular response to nutrient levels (GO:0031669)	169	16	4.55	3.51	3.24E-05	4.93E-03
polysaccharide catabolic process (GO:0000272)	85	11	2.29	4.8	4.38E-05	6.17E-03
cellular carbohydrate metabolic process (GO:0044262)	344	24	9.27	2.59	4.68E-05	6.44E-03
response to water deprivation (GO:0009414)	346	24	9.32	2.57	5.10E-05	6.86E-03
biosynthetic process (GO:0009058)	2823	112	76.05	1.47	5.27E-05	6.93E-03
response to salt stress (GO:0009651)	590	34	15.89	2.14	6.59E-05	8.47E-03
cellular response to stimulus (GO:0051716)	2335	95	62.9	1.51	8.44E-05	1.06E-02

heat acclimation (GO:0010286)	48	8	1.29	6.19	1.01E-04	1.22E-02
glucan metabolic process (GO:0044042)	168	15	4.53	3.31	1.04E-04	1.23E-02
transition metal ion homeostasis (GO:0055076)	94	11	2.53	4.34	1.00E-04	1.23E-02
regulation of cellular process (GO:0050794)	4398	159	118.48	1.34	1.16E-04	1.27E-02
response to abscisic acid (GO:0009737)	554	32	14.92	2.14	1.11E-04	1.27E-02
response to water (GO:0009415)	353	24	9.51	2.52	1.10E-04	1.27E-02
protein complex oligomerization (GO:0051259)	49	8	1.32	6.06	1.15E-04	1.28E-02
response to alcohol (GO:0097305)	558	32	15.03	2.13	1.21E-04	1.31E-02
organic substance biosynthetic process (GO:1901576)	2706	106	72.9	1.45	1.41E-04	1.49E-02
response to light intensity (GO:0009642)	156	14	4.2	3.33	1.67E-04	1.70E-02
positive regulation of cellular process (GO:0048522)	1010	49	27.21	1.8	1.66E-04	1.73E-02
positive regulation of metabolic process (GO:0009893)	804	41	21.66	1.89	1.73E-04	1.73E-02
cellular glucan metabolic process (GO:0006073)	160	14	4.31	3.25	2.13E-04	2.10E-02
positive regulation of cellular metabolic process (GO:0031325)	755	39	20.34	1.92	2.57E-04	2.49E-02
response to organic substance (GO:0010033)	1916	79	51.61	1.53	2.62E-04	2.50E-02
cellular nitrogen compound biosynthetic process (GO:0044271)	1272	57	34.27	1.66	2.86E-04	2.69E-02
glucan catabolic process (GO:0009251)	30	6	0.81	7.42	3.18E-04	2.69E-02
iron ion homeostasis (GO:0055072)	58	8	1.56	5.12	3.24E-04	2.70E-02
response to biotic stimulus (GO:0009607)	989	47	26.64	1.76	3.17E-04	2.72E-02
positive regulation of nucleobase-containing compound metabolic process (GO:0045935)	538	30	14.49	2.07	2.94E-04	2.72E-02
response to other organism (GO:0051707)	988	47	26.62	1.77	3.14E-04	2.73E-02

reproductive structure development (GO:0048608)	1218	55	32.81	1.68	3.03E-04	2.76E-02
response to external biotic stimulus (GO:0043207)	988	47	26.62	1.77	3.14E-04	2.77E-02
nitrogen compound metabolic process (GO:0006807)	5875	200	158.27	1.26	3.39E-04	2.78E-02
reproductive system development (GO:0061458)	1220	55	32.87	1.67	3.09E-04	2.78E-02
response to lipid (GO:0033993)	751	38	20.23	1.88	3.87E-04	3.14E-02
cellular response to stress (GO:0033554)	924	44	24.89	1.77	4.47E-04	3.53E-02
cellular biosynthetic process (GO:0044249)	2576	99	69.39	1.43	4.55E-04	3.54E-02
cellular polysaccharide metabolic process (GO:0044264)	238	17	6.41	2.65	4.47E-04	3.57E-02
heme biosynthetic process (GO:0006783)	21	5	0.57	8.84	5.10E-04	3.92E-02
cell communication (GO:0007154)	1626	68	43.8	1.55	5.24E-04	3.97E-02
positive regulation of RNA metabolic process (GO:0051254)	506	28	13.63	2.05	5.37E-04	3.97E-02
monosaccharide metabolic process (GO:0005996)	116	11	3.12	3.52	5.32E-04	3.99E-02
regulation of metabolic process (GO:0019222)	3118	115	84	1.37	6.78E-04	4.96E-02
GO molecular function complete	**Arabidopsis thaliana - REFLIST (27581)**	**Input**	**Expected**	**Fold Enrichment**	**P-value**	**FDR**
catalytic activity (GO:0003824)	8874	341	239.06	1.43	1.74E-14	5.37E-11
binding (GO:0005488)	10042	355	270.52	1.31	4.52E-10	6.97E-07
protein binding (GO:0005515)	4534	185	122.14	1.51	7.85E-09	8.07E-06
molecular_function (GO:0003674)	21881	644	589.45	1.09	3.64E-07	2.25E-04
heterocyclic compound binding (GO:1901363)	5683	211	153.09	1.38	6.91E-07	3.55E-04
organic cyclic compound binding (GO:0097159)	5705	211	153.69	1.37	9.07E-07	4.00E-04
ion binding (GO:0043167)	4476	167	120.58	1.38	1.47E-05	5.66E-03
anion transmembrane transporter activity (GO:0008509)	302	23	8.14	2.83	1.88E-05	6.45E-03
hydrolase activity (GO:0016787)	3164	124	85.23	1.45	3.50E-05	1.08E-02

unfolded protein binding (GO:0051082)	119	13	3.21	4.06	4.61E-05	1.29E-02
transferase activity (GO:0016740)	3728	140	100.43	1.39	5.95E-05	1.41E-02
drug binding (GO:0008144)	1914	82	51.56	1.59	5.82E-05	1.49E-02
adenyl nucleotide binding (GO:0030554)	1582	70	42.62	1.64	9.00E-05	1.85E-02
protein self-association (GO:0043621)	92	11	2.48	4.44	8.40E-05	1.85E-02
adenyl ribonucleotide binding (GO:0032559)	1575	69	42.43	1.63	1.23E-04	2.10E-02
anion binding (GO:0043168)	2263	92	60.96	1.51	1.17E-04	2.11E-02
purine nucleotide binding (GO:0017076)	1813	77	48.84	1.58	1.32E-04	2.15E-02
calmodulin binding (GO:0005516)	231	18	6.22	2.89	1.13E-04	2.18E-02
purine ribonucleotide binding (GO:0032555)	1804	76	48.6	1.56	1.76E-04	2.71E-02
small molecule binding (GO:0036094)	2611	102	70.34	1.45	2.34E-04	3.44E-02
ribonucleotide binding (GO:0032553)	1828	76	49.24	1.54	2.59E-04	3.63E-02
carbohydrate derivative binding (GO:0097367)	1866	77	50.27	1.53	2.96E-04	3.80E-02
ATP binding (GO:0005524)	1553	67	41.84	1.6	2.87E-04	3.85E-02
organic anion transmembrane transporter activity (GO:0008514)	189	15	5.09	2.95	3.42E-04	4.22E-02
purine ribonucleoside triphosphate binding (GO:0035639)	1783	74	48.03	1.54	3.85E-04	4.56E-02
GO cellular component complete	**Arabidopsis thaliana - REFLIST (27581)**	**Input**	**Expected**	**Fold Enrichment**	**P-value**	**FDR**
plastid part (GO:0044435)	1469	82	39.57	2.07	2.11E-09	7.61E-07
chloroplast part (GO:0044434)	1452	81	39.12	2.07	2.90E-09	7.85E-07
plastid (GO:0009536)	5292	212	142.56	1.49	1.46E-09	7.93E-07
chloroplast (GO:0009507)	5248	211	141.38	1.49	1.29E-09	1.40E-06
plastid stroma (GO:0009532)	779	51	20.99	2.43	2.56E-08	5.55E-06
chloroplast stroma (GO:0009570)	769	49	20.72	2.37	9.38E-08	1.69E-05
cytoplasm (GO:0005737)	14521	464	391.18	1.19	1.15E-07	1.78E-05
cell (GO:0005623)	22697	663	611.43	1.08	2.54E-07	3.06E-05
cell part (GO:0044464)	22695	663	611.38	1.08	2.54E-07	3.44E-05

organelle part (GO:0044422)	5381	201	144.96	1.39	8.61E-07	8.48E-05
intracellular organelle part (GO:0044446)	5375	201	144.8	1.39	8.41E-07	9.11E-05
cytosol (GO:0005829)	2290	101	61.69	1.64	1.77E-06	1.60E-04
plastid envelope (GO:0009526)	700	42	18.86	2.23	3.60E-06	3.00E-04
cytoplasmic part (GO:0044444)	12257	394	330.19	1.19	4.05E-06	3.13E-04
chloroplast envelope (GO:0009941)	681	41	18.35	2.23	4.57E-06	3.30E-04
intracellular part (GO:0044424)	21258	620	572.67	1.08	2.94E-05	1.88E-03
intracellular (GO:0005622)	21258	620	572.67	1.08	2.94E-05	1.99E-03
vacuole (GO:0005773)	1091	54	29.39	1.84	4.01E-05	2.41E-03
whole membrane (GO:0098805)	964	48	25.97	1.85	8.13E-05	4.63E-03
bounding membrane of organelle (GO:0098588)	1266	58	34.1	1.7	1.38E-04	7.50E-03
plant-type vacuole (GO:0000325)	160	14	4.31	3.25	2.13E-04	1.10E-02
organelle membrane (GO:0031090)	1811	75	48.79	1.54	3.25E-04	1.60E-02
chloroplast membrane (GO:0031969)	255	18	6.87	2.62	3.51E-04	1.65E-02
plastid membrane (GO:0042170)	262	18	7.06	2.55	4.74E-04	1.90E-02
membrane (GO:0016020)	7769	254	209.29	1.21	4.45E-04	1.93E-02
vacuolar part (GO:0044437)	627	33	16.89	1.95	4.64E-04	1.93E-02
vacuolar membrane (GO:0005774)	624	33	16.81	1.96	4.44E-04	2.00E-02
cell periphery (GO:0071944)	4199	149	113.12	1.32	5.33E-04	2.06E-02
intracellular membrane-bounded organelle (GO:0043231)	19207	560	517.41	1.08	6.68E-04	2.49E-02
apoplast (GO:0048046)	488	27	13.15	2.05	6.97E-04	2.52E-02
membrane-bounded organelle (GO:0043227)	19316	562	520.35	1.08	8.55E-04	2.99E-02
intracellular organelle (GO:0043229)	19520	566	525.85	1.08	1.21E-03	4.10E-02
GO Reactome pathways complete	**Arabidopsis thaliana - REFLIST (27581)**	**Input**	**Expected**	**Fold Enrichment**	**P-value**	**FDR**
Cellular response to heat stress (R-ATH-3371556)	78	13	2.1	6.19	7.33E-07	5.79E-04

HSF1 activation (R-ATH-3371511)	37	8	1	8.03	1.97E-05	5.19E-03
HSF1-dependent transactivation (R-ATH-3371571)	37	8	1	8.03	1.97E-05	7.79E-03
Protein methylation (R-ATH-8876725)	24	6	0.65	9.28	1.11E-04	2.19E-02
HSP90 chaperone cycle for steroid hormone receptors (SHR) (R-ATH-3371497)	16	5	0.43	11.6	1.76E-04	2.78E-02
Cellular responses to external stimuli (R-ATH-8953897)	233	17	6.28	2.71	3.56E-04	4.68E-02

Supplemental Table 4.2. GO analyses split by biological process, molecular function, cell component, and Reactome pathways for 'Spence' under 10 dS/m (0 dS/m vs 10 dS/m) and 30 dS/m (0 dS/m vs 30 dS/m). Only significantly enriched categories with a false discovery rate (FDR) value < 0.05 shown. Samples are ordered by FDR statistical significance.

Spence - 0-10 GO biological process complete	Arabidopsis thaliana - REFLIST (27581)	Input	Expected	Fold Enrichment	P-value	FDR
cellular process (GO:0009987)	10295	355	267.26	1.33	5.51E-11	1.63E-07
response to stimulus (GO:0050896)	5731	226	148.78	1.52	3.16E-11	1.87E-07
response to abiotic stimulus (GO:0009628)	2098	104	54.46	1.91	7.21E-10	1.42E-06
response to temperature stimulus (GO:0009266)	622	45	16.15	2.79	3.18E-09	4.70E-06
metabolic process (GO:0008152)	8211	285	213.16	1.34	1.73E-08	2.05E-05
response to stress (GO:0006950)	3158	132	81.98	1.61	6.49E-08	6.40E-05
response to chemical (GO:0042221)	2777	119	72.09	1.65	1.24E-07	1.05E-04
organic substance metabolic process (GO:0071704)	7417	258	192.54	1.34	1.47E-07	1.09E-04
response to inorganic substance (GO:0010035)	945	54	24.53	2.2	1.82E-07	1.20E-04
cellular metabolic process (GO:0044237)	7157	246	185.8	1.32	8.56E-07	5.07E-04
response to cadmium ion (GO:0046686)	345	27	8.96	3.01	1.15E-06	6.21E-04
response to acid chemical (GO:0001101)	1178	60	30.58	1.96	1.71E-06	8.42E-04
response to metal ion (GO:0010038)	478	32	12.41	2.58	2.87E-06	1.06E-03
response to light stimulus (GO:0009416)	739	43	19.18	2.24	2.34E-06	1.07E-03
biological regulation (GO:0065007)	5681	201	147.48	1.36	2.86E-06	1.13E-03
circadian rhythm (GO:0007623)	108	14	2.8	4.99	2.68E-06	1.13E-03
primary metabolic process (GO:0044238)	6707	230	174.11	1.32	3.59E-06	1.25E-03
response to radiation (GO:0009314)	760	43	19.73	2.18	5.50E-06	1.81E-03
response to cold (GO:0009409)	428	29	11.11	2.61	6.71E-06	2.09E-03
rhythmic process (GO:0048511)	119	14	3.09	4.53	7.43E-06	2.20E-03

response to oxygen-containing compound (GO:1901700)	1596	72	41.43	1.74	1.18E-05	3.33E-03
nitrogen compound metabolic process (GO:0006807)	5875	202	152.51	1.32	1.72E-05	4.63E-03
organonitrogen compound metabolic process (GO:1901564)	4315	156	112.02	1.39	1.97E-05	5.06E-03
drug metabolic process (GO:0017144)	543	32	14.1	2.27	3.75E-05	9.26E-03
monosaccharide biosynthetic process (GO:0046364)	43	8	1.12	7.17	3.94E-05	9.32E-03
regulation of biological process (GO:0050789)	5001	174	129.83	1.34	4.62E-05	1.05E-02
response to abscisic acid (GO:0009737)	554	32	14.38	2.23	5.02E-05	1.10E-02
regulation of cellular process (GO:0050794)	4398	155	114.17	1.36	8.61E-05	1.76E-02
response to alcohol (GO:0097305)	558	32	14.49	2.21	8.42E-05	1.78E-02
small molecule metabolic process (GO:0044281)	1587	68	41.2	1.65	9.56E-05	1.83E-02
organic substance catabolic process (GO:1901575)	1317	59	34.19	1.73	9.30E-05	1.83E-02
cellular response to stimulus (GO:0051716)	2335	92	60.62	1.52	1.07E-04	1.99E-02
catabolic process (GO:0009056)	1486	64	38.58	1.66	1.19E-04	2.07E-02
organonitrogen compound catabolic process (GO:1901565)	845	42	21.94	1.91	1.17E-04	2.10E-02
hexose biosynthetic process (GO:0019319)	26	6	0.67	8.89	1.33E-04	2.25E-02
hexose metabolic process (GO:0019318)	86	10	2.23	4.48	1.61E-04	2.65E-02
regulation of transcription from RNA polymerase II promoter in response to stress (GO:0043618)	28	6	0.73	8.25	1.89E-04	3.02E-02
response to external stimulus (GO:0009605)	1388	60	36.03	1.67	1.98E-04	3.08E-02
response to organic substance (GO:0010033)	1916	77	49.74	1.55	2.04E-04	3.10E-02
regulation of DNA-templated transcription in response to stress (GO:0043620)	29	6	0.75	7.97	2.23E-04	3.30E-02
cellular response to acid chemical (GO:0071229)	399	24	10.36	2.32	2.45E-04	3.54E-02
cellular catabolic process (GO:0044248)	1308	57	33.96	1.68	2.60E-04	3.66E-02
response to lipid (GO:0033993)	751	37	19.5	1.9	3.22E-04	4.43E-02
response to extracellular stimulus (GO:0009991)	264	18	6.85	2.63	3.38E-04	4.54E-02
response to heat (GO:0009408)	220	16	5.71	2.8	3.67E-04	4.82E-02

monosaccharide metabolic process (GO:0005996)	116	11	3.01	3.65	3.94E-04	4.86E-02
cellular response to alcohol (GO:0097306)	199	15	5.17	2.9	3.90E-04	4.91E-02
GO molecular function complete	**Arabidopsis thaliana - REFLIST (27581)**	**Input**	**Expected**	**Fold Enrichment**	**P-value**	**FDR**
catalytic activity (GO:0003824)	8874	317	230.37	1.38	2.71E-11	8.36E-08
binding (GO:0005488)	10042	338	260.69	1.3	5.50E-09	4.24E-06
molecular_function (GO:0003674)	21881	629	568.03	1.11	4.90E-09	7.55E-06
organic cyclic compound binding (GO:0097159)	5705	202	148.1	1.36	2.37E-06	1.04E-03
protein binding (GO:0005515)	4534	168	117.7	1.43	2.04E-06	1.05E-03
heterocyclic compound binding (GO:1901363)	5683	202	147.53	1.37	1.82E-06	1.12E-03
mRNA binding (GO:0003729)	420	28	10.9	2.57	1.27E-05	4.91E-03
small molecule binding (GO:0036094)	2611	101	67.78	1.49	8.16E-05	2.79E-02
translation elongation factor activity (GO:0003746)	36	7	0.93	7.49	9.41E-05	2.90E-02
ion binding (GO:0043167)	4476	156	116.2	1.34	1.21E-04	3.40E-02
RNA binding (GO:0003723)	1140	52	29.59	1.76	1.45E-04	3.72E-02
GO cellular component complete	**Arabidopsis thaliana - REFLIST (27581)**	**Input**	**Expected**	**Fold Enrichment**	**P-value**	**FDR**
cytoplasm (GO:0005737)	14521	475	376.96	1.26	2.49E-13	2.69E-10
cytosol (GO:0005829)	2290	119	59.45	2	1.28E-12	6.91E-10
plastid (GO:0009536)	5292	210	137.38	1.53	1.15E-10	4.15E-08
chloroplast (GO:0009507)	5248	208	136.24	1.53	1.84E-10	4.97E-08
cell part (GO:0044464)	22695	648	589.16	1.1	1.31E-09	2.37E-07
intracellular part (GO:0044424)	21258	617	551.86	1.12	2.02E-09	2.73E-07
cell (GO:0005623)	22697	648	589.21	1.1	1.31E-09	2.83E-07
chloroplast part (GO:0044434)	1452	79	37.69	2.1	2.40E-09	2.89E-07
intracellular (GO:0005622)	21258	617	551.86	1.12	2.02E-09	3.12E-07
plastid part (GO:0044435)	1469	79	38.14	2.07	3.14E-09	3.40E-07

cytoplasmic part (GO:0044444)	12257	396	318.19	1.24	1.00E-08	9.88E-07
chloroplast envelope (GO:0009941)	681	45	17.68	2.55	4.67E-08	4.21E-06
plastid envelope (GO:0009526)	700	45	18.17	2.48	8.87E-08	7.39E-06
chloroplast stroma (GO:0009570)	769	47	19.96	2.35	1.90E-07	1.47E-05
plastid stroma (GO:0009532)	779	47	20.22	2.32	3.75E-07	2.71E-05
chloroplast membrane (GO:0031969)	255	23	6.62	3.47	7.75E-07	5.24E-05
plastid membrane (GO:0042170)	262	23	6.8	3.38	1.19E-06	7.59E-05
vacuole (GO:0005773)	1091	56	28.32	1.98	3.01E-06	1.63E-04
organelle part (GO:0044422)	5381	192	139.69	1.37	2.89E-06	1.65E-04
intracellular organelle part (GO:0044446)	5375	192	139.53	1.38	2.84E-06	1.71E-04
organelle membrane (GO:0031090)	1811	80	47.01	1.7	6.54E-06	3.37E-04
membrane (GO:0016020)	7769	257	201.68	1.27	9.90E-06	4.88E-04
vacuolar part (GO:0044437)	627	35	16.28	2.15	4.58E-05	2.16E-03
vacuolar membrane (GO:0005774)	624	34	16.2	2.1	1.21E-04	5.45E-03
organelle envelope (GO:0031967)	1189	54	30.87	1.75	1.31E-04	5.48E-03
envelope (GO:0031975)	1189	54	30.87	1.75	1.31E-04	5.70E-03
bounding membrane of organelle (GO:0098588)	1266	56	32.87	1.7	2.07E-04	8.29E-03
intracellular membrane-bounded organelle (GO:0043231)	19207	544	498.61	1.09	2.38E-04	8.59E-03
cellular_component (GO:0005575)	25217	681	654.63	1.04	2.32E-04	8.65E-03
membrane-bounded organelle (GO:0043227)	19316	546	501.44	1.09	2.67E-04	9.33E-03
whole membrane (GO:0098805)	964	45	25.03	1.8	3.02E-04	1.02E-02
plant-type vacuole (GO:0000325)	160	13	4.15	3.13	4.86E-04	1.59E-02
intracellular organelle (GO:0043229)	19520	549	506.74	1.08	5.32E-04	1.69E-02
organelle (GO:0043226)	19561	549	507.8	1.08	7.12E-04	2.20E-02
spliceosomal complex (GO:0005681)	155	12	4.02	2.98	1.17E-03	3.51E-02
plasma membrane (GO:0005886)	3572	123	92.73	1.33	1.34E-03	3.92E-02
GO Reactome pathways complete	**Arabidopsis thaliana -**	**Input**	**Expected**	**Fold Enrichment**	**P-value**	**FDR**

	REFLIST (27581)					
Cellular response to heat stress (R-ATH-3371556)	78	14	2.02	6.91	7.93E-08	6.26E-05
HSF1 activation (R-ATH-3371511)	37	10	0.96	10.41	2.25E-07	8.87E-05
Cellular responses to stress (R-ATH-2262752)	205	20	5.32	3.76	1.33E-06	3.51E-04
Unclassified (UNCLASSIFIED)	23669	567	614.44	0.92	1.87E-06	3.69E-04
Cellular responses to external stimuli (R-ATH-8953897)	233	20	6.05	3.31	7.94E-06	1.26E-03
Eukaryotic Translation Elongation (R-ATH-156842)	11	5	0.29	17.51	3.54E-05	4.67E-03
Regulation of HSF1-mediated heat shock response (R-ATH-3371453)	64	9	1.66	5.42	9.26E-05	9.14E-03
HSF1-dependent transactivation (R-ATH-3371571)	37	7	0.96	7.29	1.09E-04	9.60E-03
Protein methylation (R-ATH-8876725)	24	6	0.62	9.63	9.08E-05	1.03E-02
Metabolism (R-ATH-1430728)	1116	51	28.97	1.76	1.77E-04	1.40E-02
Attenuation phase (R-ATH-3371568)	22	5	0.57	8.75	5.20E-04	3.73E-02

Spence - 0-30

GO biological process complete	Arabidopsis thaliana - REFLIST (27581)	Input	Expected	Fold Enrichment	P-value	FDR
response to stimulus (GO:0050896)	5731	323	209.45	1.54	2.77E-16	1.64 E-12
response to abiotic stimulus (GO:0009628)	2098	154	76.68	2.01	1.40E-15	2.76 E-12
cellular process (GO:0009987)	10295	504	376.25	1.34	1.13E-15	3.35 E-12
response to oxygen-containing compound (GO:1901700)	1596	122	58.33	2.09	1.26E-13	1.86 E-10
response to chemical (GO:0042221)	2777	176	101.49	1.73	2.28E-12	2.25 E-09
response to stress (GO:0006950)	3158	194	115.42	1.68	1.98E-12	2.35 E-09
response to temperature stimulus (GO:0009266)	622	62	22.73	2.73	1.36E-11	1.15 E-08
response to inorganic substance (GO:0010035)	945	81	34.54	2.35	1.77E-11	1.31 E-08
response to acid chemical (GO:0001101)	1178	93	43.05	2.16	2.81E-11	1.85 E-08
metabolic process (GO:0008152)	8211	399	300.09	1.33	8.59E-11	5.08 E-08

cellular metabolic process (GO:0044237)	7157	353	261.57	1.35	4.11E-10	2.21 E-07
small molecule metabolic process (GO:0044281)	1587	109	58	1.88	1.48E-09	7.31 E-07
response to external stimulus (GO:0009605)	1388	98	50.73	1.93	3.04E-09	1.38 E-06
cellular carbohydrate metabolic process (GO:0044262)	344	39	12.57	3.1	3.65E-09	1.54 E-06
organic substance metabolic process (GO:0071704)	7417	356	271.07	1.31	9.09E-09	3.59 E-06
carbohydrate metabolic process (GO:0005975)	810	65	29.6	2.2	2.05E-08	7.59 E-06
response to organic substance (GO:0010033)	1916	120	70.02	1.71	3.14E-08	1.09 E-05
response to cold (GO:0009409)	428	41	15.64	2.62	1.52E-07	5.01 E-05
response to hormone (GO:0009725)	1599	101	58.44	1.73	2.91E-07	8.21 E-05
cellular polysaccharide metabolic process (GO:0044264)	238	28	8.7	3.22	2.90E-07	8.58 E-05
response to oxidative stress (GO:0006979)	424	40	15.5	2.58	2.77E-07	8.64 E-05
catabolic process (GO:0009056)	1486	95	54.31	1.75	3.62E-07	9.74 E-05
response to endogenous stimulus (GO:0009719)	1615	101	59.02	1.71	4.72E-07	1.16 E-04
response to light stimulus (GO:0009416)	739	57	27.01	2.11	4.58E-07	1.18 E-04
organic substance biosynthetic process (GO:1901576)	2706	149	98.9	1.51	1.02E-06	2.40 E-04
response to radiation (GO:0009314)	760	57	27.78	2.05	1.08E-06	2.46 E-04
biosynthetic process (GO:0009058)	2823	154	103.17	1.49	1.22E-06	2.67 E-04
cellular biosynthetic process (GO:0044249)	2576	143	94.14	1.52	1.34E-06	2.83 E-04
cellular catabolic process (GO:0044248)	1308	84	47.8	1.76	1.56E-06	3.18 E-04
response to biotic stimulus (GO:0009607)	989	68	36.14	1.88	2.23E-06	4.01 E-04
response to other organism (GO:0051707)	988	68	36.11	1.88	2.20E-06	4.08 E-04
response to external biotic stimulus (GO:0043207)	988	68	36.11	1.88	2.20E-06	4.21 E-04
response to heat (GO:0009408)	220	25	8.04	3.11	2.18E-06	4.31 E-04
primary metabolic process (GO:0044238)	6707	312	245.12	1.27	2.59E-06	4.37 E-04
carbohydrate biosynthetic process (GO:0016051)	317	31	11.59	2.68	2.58E-06	4.50 E-04
polysaccharide metabolic process (GO:0005976)	302	30	11.04	2.72	2.80E-06	4.60 E-04

starch metabolic process (GO:0005982)	54	12	1.97	6.08	2.94E-06	4.71 E-04
glucan metabolic process (GO:0044042)	168	21	6.14	3.42	3.67E-06	5.72 E-04
response to osmotic stress (GO:0006970)	665	50	24.3	2.06	4.69E-06	7.12 E-04
response to drug (GO:0042493)	593	46	21.67	2.12	5.89E-06	8.71 E-04
cellular glucan metabolic process (GO:0006073)	160	20	5.85	3.42	6.21E-06	8.96 E-04
cellular carbohydrate biosynthetic process (GO:0034637)	205	23	7.49	3.07	6.65E-06	9.16 E-04
drug metabolic process (GO:0017144)	543	43	19.84	2.17	6.93E-06	9.33 E-04
response to lipid (GO:0033993)	751	54	27.45	1.97	6.63E-06	9.35 E-04
response to antibiotic (GO:0046677)	304	29	11.11	2.61	8.33E-06	1.10 E-03
defense response to other organism (GO:0098542)	682	50	24.92	2.01	9.58E-06	1.23 E-03
response to metal ion (GO:0010038)	478	39	17.47	2.23	9.73E-06	1.23 E-03
carbohydrate catabolic process (GO:0016052)	182	21	6.65	3.16	1.12E-05	1.39 E-03
monocarboxylic acid metabolic process (GO:0032787)	430	36	15.72	2.29	1.17E-05	1.41 E-03
response to water deprivation (GO:0009414)	346	31	12.65	2.45	1.42E-05	1.69 E-03
organic acid metabolic process (GO:0006082)	1032	67	37.72	1.78	1.74E-05	1.98 E-03
oxoacid metabolic process (GO:0043436)	1030	67	37.64	1.78	1.71E-05	1.99 E-03
response to water (GO:0009415)	353	31	12.9	2.4	1.96E-05	2.19 E-03
response to reactive oxygen species (GO:0000302)	176	20	6.43	3.11	2.20E-05	2.41 E-03
biological regulation (GO:0065007)	5681	265	207.62	1.28	2.28E-05	2.45 E-03
response to red light (GO:0010114)	69	12	2.52	4.76	2.60E-05	2.70 E-03
response to salt stress (GO:0009651)	590	44	21.56	2.04	2.57E-05	2.71 E-03
organic substance catabolic process (GO:1901575)	1317	79	48.13	1.64	3.79E-05	3.87 E-03
response to bacterium (GO:0009617)	493	38	18.02	2.11	4.08E-05	4.09 E-03
carboxylic acid metabolic process (GO:0019752)	882	58	32.23	1.8	4.35E-05	4.29 E-03
biological_process (GO:0008150)	21267	831	777.24	1.07	4.88E-05	4.74 E-03
multi-organism process (GO:0051704)	1482	86	54.16	1.59	5.38E-05	5.05 E-03

response to abscisic acid (GO:0009737)	554	41	20.25	2.02	6.40E-05	5.92 E-03
response to alcohol (GO:0097305)	558	41	20.39	2.01	6.80E-05	6.19 E-03
response to cadmium ion (GO:0046686)	345	29	12.61	2.3	9.07E-05	8.14 E-03
organic cyclic compound biosynthetic process (GO:1901362)	930	59	33.99	1.74	9.80E-05	8.66 E-03
small molecule biosynthetic process (GO:0044283)	670	46	24.49	1.88	1.20E-04	1.05 E-02
pyrimidine-containing compound biosynthetic process (GO:0072528)	49	9	1.79	5.03	1.83E-04	1.57 E-02
cellular polysaccharide biosynthetic process (GO:0033692)	161	17	5.88	2.89	1.99E-04	1.68 E-02
glutamine family amino acid metabolic process (GO:0009064)	62	10	2.27	4.41	2.10E-04	1.75 E-02
pyrimidine-containing compound metabolic process (GO:0072527)	63	10	2.3	4.34	2.35E-04	1.94 E-02
ion transmembrane transport (GO:0034220)	313	26	11.44	2.27	2.60E-04	2.08 E-02
cellular response to external stimulus (GO:0071496)	214	20	7.82	2.56	2.57E-04	2.09 E-02
ion transport (GO:0006811)	663	44	24.23	1.82	2.74E-04	2.13 E-02
glucan catabolic process (GO:0009251)	30	7	1.1	6.38	2.71E-04	2.14 E-02
response to hydrogen peroxide (GO:0042542)	78	11	2.85	3.86	2.94E-04	2.26 E-02
cellular response to organic substance (GO:0071310)	765	49	27.96	1.75	3.17E-04	2.41 E-02
cell wall organization or biogenesis (GO:0071554)	433	32	15.82	2.02	3.29E-04	2.46 E-02
cellular response to nutrient levels (GO:0031669)	169	17	6.18	2.75	3.35E-04	2.48 E-02
organic acid transmembrane transport (GO:1903825)	80	11	2.92	3.76	3.57E-04	2.52 E-02
amino acid transmembrane transport (GO:0003333)	54	9	1.97	4.56	3.48E-04	2.54 E-02
plant-type cell wall organization or biogenesis (GO:0071669)	229	21	8.37	2.51	3.53E-04	2.55 E-02
carboxylic acid transmembrane transport (GO:1905039)	80	11	2.92	3.76	3.57E-04	2.55 E-02
cellular response to chemical stimulus (GO:0070887)	963	58	35.19	1.65	3.70E-04	2.57 E-02
organic cyclic compound catabolic process (GO:1901361)	256	22	9.36	2.35	4.27E-04	2.90 E-02

organophosphate metabolic process (GO:0019637)	555	38	20.28	1.87	4.24E-04	2.92 E-02
cellular lipid metabolic process (GO:0044255)	675	44	24.67	1.78	4.39E-04	2.95 E-02
response to toxic substance (GO:0009636)	207	19	7.57	2.51	4.45E-04	2.96 E-02
antibiotic catabolic process (GO:0017001)	69	10	2.52	3.97	4.52E-04	2.97 E-02
plant-type cell wall biogenesis (GO:0009832)	142	15	5.19	2.89	4.60E-04	2.99 E-02
response to extracellular stimulus (GO:0009991)	264	22	9.65	2.28	5.95E-04	3.75 E-02
cell wall biogenesis (GO:0042546)	195	18	7.13	2.53	5.85E-04	3.77 E-02
response to nutrient levels (GO:0031667)	224	20	8.19	2.44	5.94E-04	3.78 E-02
aromatic compound catabolic process (GO:0019439)	246	21	8.99	2.34	6.23E-04	3.80 E-02
hexose metabolic process (GO:0019318)	86	11	3.14	3.5	6.21E-04	3.83 E-02
phosphorus metabolic process (GO:0006793)	1735	92	63.41	1.45	6.21E-04	3.87 E-02
monosaccharide metabolic process (GO:0005996)	116	13	4.24	3.07	6.52E-04	3.94 E-02
nucleobase-containing small molecule metabolic process (GO:0055086)	450	32	16.45	1.95	6.60E-04	3.95 E-02
polysaccharide biosynthetic process (GO:0000271)	181	17	6.61	2.57	6.87E-04	4.03 E-02
cellular response to starvation (GO:0009267)	148	15	5.41	2.77	6.83E-04	4.04 E-02
mRNA cis splicing, via spliceosome (GO:0045292)	36	7	1.32	5.32	7.05E-04	4.09 E-02
defense response to bacterium (GO:0042742)	393	29	14.36	2.02	7.21E-04	4.14 E-02
phospholipid metabolic process (GO:0006644)	182	17	6.65	2.56	7.27E-04	4.14 E-02
cellular response to extracellular stimulus (GO:0031668)	208	19	7.6	2.5	7.50E-04	4.23 E-02
regulation of cellular process (GO:0050794)	4398	202	160.73	1.26	7.64E-04	4.27 E-02
anion transmembrane transport (GO:0098656)	134	14	4.9	2.86	7.76E-04	4.29 E-02
organophosphate biosynthetic process (GO:0090407)	339	26	12.39	2.1	8.01E-04	4.39 E-02
regulation of mRNA splicing, via spliceosome (GO:0048024)	37	7	1.35	5.18	8.13E-04	4.41 E-02
starch catabolic process (GO:0005983)	17	5	0.62	8.05	8.61E-04	4.63 E-02
cell communication (GO:0007154)	1626	86	59.43	1.45	9.06E-04	4.83 E-02

fatty acid derivative metabolic process (GO:1901568)	38	7	1.39	5.04	9.34E-04	4.85 E-02
cellular transition metal ion homeostasis (GO:0046916)	63	9	2.3	3.91	9.44E-04	4.86 E-02
carboxylic acid transport (GO:0046942)	121	13	4.42	2.94	9.33E-04	4.89 E-02
organic acid transport (GO:0015849)	121	13	4.42	2.94	9.33E-04	4.93 E-02
GO molecular function complete	**Arabidopsis thaliana - REFLIST (27581)**	**Input**	**Expected**	**Fold Enrichment**	**P-value**	**FDR**
catalytic activity (GO:0003824)	8874	462	324.32	1.42	9.15E-19	2.82 E-15
molecular_function (GO:0003674)	21881	881	799.68	1.1	5.50E-11	5.65 E-08
binding (GO:0005488)	10042	457	367	1.25	1.19E-08	9.20 E-06
protein binding (GO:0005515)	4534	230	165.7	1.39	2.82E-07	1.45 E-04
hydrolase activity (GO:0016787)	3164	172	115.63	1.49	2.43E-07	1.50 E-04
inorganic molecular entity transmembrane transporter activity (GO:0015318)	755	57	27.59	2.07	9.45E-07	4.16 E-04
ion transmembrane transporter activity (GO:0015075)	800	58	29.24	1.98	2.95E-06	9.08 E-04
symporter activity (GO:0015293)	209	24	7.64	3.14	2.94E-06	1.01 E-03
ion binding (GO:0043167)	4476	222	163.58	1.36	2.78E-06	1.07 E-03
hydrolase activity, acting on glycosyl bonds (GO:0016798)	442	38	16.15	2.35	4.07E-06	1.14 E-03
cation binding (GO:0043169)	2621	141	95.79	1.47	7.83E-06	2.01 E-03
metal ion binding (GO:0046872)	2598	139	94.95	1.46	1.20E-05	2.84 E-03
transmembrane transporter activity (GO:0022857)	1214	75	44.37	1.69	2.59E-05	5.70 E-03
amylase activity (GO:0016160)	15	6	0.55	10.94	6.52E-05	1.34 E-02
oxidoreductase activity (GO:0016491)	1494	86	54.6	1.58	7.72E-05	1.49 E-02
transferase activity (GO:0016740)	3728	181	136.25	1.33	1.03E-04	1.87 E-02
anion transmembrane transporter activity (GO:0008509)	302	26	11.04	2.36	1.22E-04	2.09 E-02
active transmembrane transporter activity (GO:0022804)	683	46	24.96	1.84	1.47E-04	2.27 E-02

organic acid transmembrane transporter activity (GO:0005342)	128	15	4.68	3.21	1.67E-04	2.33 E-02
transferase activity, transferring hexosyl groups (GO:0016758)	392	31	14.33	2.16	1.46E-04	2.37 E-02
carboxylic acid transmembrane transporter activity (GO:0046943)	128	15	4.68	3.21	1.67E-04	2.45 E-02
secondary active transmembrane transporter activity (GO:0015291)	419	32	15.31	2.09	2.38E-04	3.19 E-02
hydrolase activity, hydrolyzing O-glycosyl compounds (GO:0004553)	368	29	13.45	2.16	2.70E-04	3.47 E-02
catalytic activity, acting on a protein (GO:0140096)	2578	129	94.22	1.37	4.40E-04	4.68 E-02
peptidase activity, acting on L-amino acid peptides (GO:0070011)	490	35	17.91	1.95	4.37E-04	4.81 E-02
amino acid transmembrane transporter activity (GO:0015171)	82	11	3	3.67	4.32E-04	4.93 E-02

GO cellular component complete	**Arabidopsis thaliana - REFLIST (27581)**	**Input**	**Expected**	**Fold Enrichment**	**P-value**	**FDR**
cell periphery (GO:0071944)	4199	243	153.46	1.58	5.31E-13	1.92 E-10
chloroplast part (GO:0044434)	1452	113	53.07	2.13	4.08E-13	2.21 E-10
plastid part (GO:0044435)	1469	114	53.69	2.12	3.46E-13	3.74 E-10
cell (GO:0005623)	22697	907	829.5	1.09	1.95E-11	3.51 E-09
membrane (GO:0016020)	7769	384	283.93	1.35	2.61E-11	3.54 E-09
plastid (GO:0009536)	5292	283	193.41	1.46	2.53E-11	3.92 E-09
cell part (GO:0044464)	22695	907	829.43	1.09	1.94E-11	4.20 E-09
chloroplast (GO:0009507)	5248	282	191.8	1.47	1.65E-11	4.48 E-09
cytoplasm (GO:0005737)	14521	630	530.7	1.19	6.24E-10	7.51 E-08
external encapsulating structure (GO:0030312)	758	65	27.7	2.35	1.92E-09	1.89 E-07
cell wall (GO:0005618)	756	65	27.63	2.35	1.83E-09	1.98 E-07
chloroplast envelope (GO:0009941)	681	59	24.89	2.37	6.65E-09	5.54 E-07
plastid envelope (GO:0009526)	700	60	25.58	2.35	6.62E-09	5.98 E-07
plastid stroma (GO:0009532)	779	64	28.47	2.25	1.09E-08	8.41 E-07

chloroplast stroma (GO:0009570)	769	63	28.1	2.24	1.57E-08	1.13 E-06
cytoplasmic part (GO:0044444)	12257	535	447.96	1.19	6.87E-08	4.65 E-06
apoplast (GO:0048046)	488	45	17.83	2.52	7.79E-08	4.69 E-06
intracellular organelle part (GO:0044446)	5375	268	196.44	1.36	7.75E-08	4.94 E-06
organelle part (GO:0044422)	5381	268	196.66	1.36	9.67E-08	5.51 E-06
vacuole (GO:0005773)	1091	75	39.87	1.88	5.73E-07	2.96 E-05
plant-type cell wall (GO:0009505)	373	36	13.63	2.64	5.50E-07	2.98 E-05
organelle membrane (GO:0031090)	1811	109	66.19	1.65	9.40E-07	4.63 E-05
plasma membrane (GO:0005886)	3572	186	130.55	1.42	1.20E-06	5.65 E-05
bounding membrane of organelle (GO:0098588)	1266	82	46.27	1.77	1.55E-06	7.01 E-05
vacuolar part (GO:0044437)	627	48	22.91	2.09	6.27E-06	2.61 E-04
thylakoid (GO:0009579)	595	46	21.75	2.12	6.20E-06	2.68 E-04
cell junction (GO:0030054)	953	64	34.83	1.84	8.26E-06	2.98 E-04
symplast (GO:0055044)	953	64	34.83	1.84	8.26E-06	3.09 E-04
cell-cell junction (GO:0005911)	953	64	34.83	1.84	8.26E-06	3.20 E-04
plasmodesma (GO:0009506)	953	64	34.83	1.84	8.26E-06	3.31 E-04
vacuolar membrane (GO:0005774)	624	47	22.81	2.06	1.00E-05	3.50 E-04
cellular_component (GO:0005575)	25217	959	921.6	1.04	1.07E-05	3.52 E-04
Unclassified (UNCLASSIFIED)	2364	49	86.4	0.57	1.07E-05	3.63 E-04
plastid membrane (GO:0042170)	262	26	9.58	2.72	1.28E-05	4.09 E-04
chloroplast membrane (GO:0031969)	255	25	9.32	2.68	2.25E-05	6.97 E-04
chloroplast thylakoid (GO:0009534)	519	40	18.97	2.11	2.43E-05	7.30 E-04
intracellular part (GO:0044424)	21258	832	776.91	1.07	3.49E-05	9.94 E-04
intracellular (GO:0005622)	21258	832	776.91	1.07	3.49E-05	1.02 E-03
plastid thylakoid (GO:0031976)	520	40	19	2.1	3.69E-05	1.03 E-03
intrinsic component of membrane (GO:0031224)	4577	216	167.28	1.29	9.12E-05	2.47 E-03
chloroplast thylakoid membrane (GO:0009535)	408	32	14.91	2.15	1.21E-04	3.20 E-03

plastid thylakoid membrane (GO:0055035)	409	32	14.95	2.14	1.25E-04	3.23 E-03
photosynthetic membrane (GO:0034357)	429	33	15.68	2.1	1.68E-04	4.14 E-03
thylakoid membrane (GO:0042651)	428	33	15.64	2.11	1.65E-04	4.17 E-03
thylakoid part (GO:0044436)	471	35	17.21	2.03	2.05E-04	4.93 E-03
integral component of membrane (GO:0016021)	4315	202	157.7	1.28	2.58E-04	6.08 E-03
cytosol (GO:0005829)	2290	118	83.69	1.41	2.64E-04	6.08 E-03
organelle envelope (GO:0031967)	1189	69	43.45	1.59	3.00E-04	6.62 E-03
envelope (GO:0031975)	1189	69	43.45	1.59	3.00E-04	6.76 E-03
plastoglobule (GO:0010287)	79	11	2.89	3.81	3.24E-04	7.03 E-03
membrane part (GO:0044425)	5102	233	186.46	1.25	3.36E-04	7.13 E-03
whole membrane (GO:0098805)	964	58	35.23	1.65	3.74E-04	7.79 E-03
plant-type vacuole (GO:0000325)	160	16	5.85	2.74	5.25E-04	1.07 E-02
organelle subcompartment (GO:0031984)	896	53	32.75	1.62	1.17E-03	2.35 E-02
transporter complex (GO:1990351)	19	5	0.69	7.2	1.31E-03	2.58 E-02
intracellular membrane-bounded organelle (GO:0043231)	19207	749	701.96	1.07	1.47E-03	2.84 E-02
Golgi membrane (GO:0000139)	376	27	13.74	1.96	1.52E-03	2.88 E-02
extracellular region (GO:0005576)	3169	149	115.82	1.29	1.88E-03	3.51 E-02
nuclear speck (GO:0016607)	86	10	3.14	3.18	2.07E-03	3.80 E-02
membrane-bounded organelle (GO:0043227)	19316	751	705.94	1.06	2.27E-03	4.10 E-02
intrinsic component of plasma membrane (GO:0031226)	348	25	12.72	1.97	2.54E-03	4.50 E-02
nucleosome (GO:0000786)	47	7	1.72	4.08	2.77E-03	4.84 E-02

Supplemental Table 4.3. Gene description and ID information for gibberellin biosynthesis and transport, sodium and potassium homeostasis and transport, osmolyte production and transport, and senescence genes of interest.

Gene Description Gibberellin biosynthesis and transport	Uniprot ID	TAIR ID	Transcript ID	Sorghum ID
Telomere repeat-binding factor 1;TRB1;ortholog	Q8VWK4	AT1G49950	MSTRG.547.1	Sobic.001G156900
			MSTRG.509.6	Sobic.001G151100
			MSTRG.547.4	Sobic.001G156900
			MSTRG.547.2	Sobic.001G156900
Phosphatidylinositol N-acetyglucosaminlytransferase subunit P-like protein;TRM13;ortholog	O80829	AT2G45900	MSTRG.5861.2	Sobic.006G176500
			MSTRG.7469.1	Sobic.005G154500
			MSTRG.5861.1	Sobic.006G176500
Protein REVEILLE 6;RVE6;ortholog	Q8H0W3	AT5G52660	MSTRG.13904.1	Sobic.010G004300
			MSTRG.13904.2	Sobic.010G004300
			MSTRG.9282.1	Sobic.004G281800
			MSTRG.9282.6	Sobic.004G281800
			MSTRG.23652.1	Sobic.004G154000
			MSTRG.29112.1	Sobic.004G154000
BTB/POZ and TAZ domain-containing protein 4;BT4;ortholog	Q9FJX5	AT5G67480	MSTRG.25364.4	Sobic.003G385100
Transcription factor MYB59;MYB59;ortholog	Q4JL84	AT5G59780	MSTRG.6457.2	Sobic.005G224800
			MSTRG.21906.5	Sobic.008G133700
			MSTRG.21906.6	Sobic.008G133700
			MSTRG.27858.2	Sobic.005G224700
			MSTRG.8810.1	Sobic.004G352200
			MSTRG.6457.1	Sobic.005G224800
			MSTRG.20151.1	Sobic.009G016600
			MSTRG.20151.2	Sobic.009G016600
MADS-box protein SOC1;SOC1;ortholog	O64645	AT2G45660	MSTRG.25445.1	Sobic.003G406800
			MSTRG.3962.1	Sobic.001G497600
			MSTRG.11314.1	Sobic.004G003401
Gibberellin 20 oxidase 1;GA20OX1;ortholog	Q39110	AT4G25420	MSTRG.25223.1	Sobic.003G379500
			MSTRG.24143.1	Sobic.003G263300

DELLA protein GAI;GAI;ortholog	Q9LQT8	AT1G14920	MSTRG.23964.1	Sobic.003G237201
Ent-kaur-16-ene synthase, chloroplastic;GA2;ortholog	Q9SAK2	AT1G79460	MSTRG.26708.2	Sobic.005G195800
			MSTRG.6164.1	Sobic.006G211400
			MSTRG.6165.2	Sobic.006G211500
Gibberellin 2-beta-dioxygenase 8;GA2OX8;ortholog	O49561	AT4G21200	MSTRG.5639.1	Sobic.006G150800
Acid beta-fructofuranosidase 4, vacuolar;BFRUCT4;ortholog	Q39041	AT1G12240	MSTRG.11302.1	Sobic.004G004800
			MSTRG.28633.1	Sobic.004G004800
Acid beta-fructofuranosidase 3, vacuolar;BFRUCT3;ortholog	Q43348	AT1G62660	MSTRG.5726.1	Sobic.006G160700
			MSTRG.7734.1	Sobic.005G122600
Transcription factor bHLH93;BHLH93;ortholog	Q9LSL1	AT5G65640	MSTRG.4098.1	Sobic.001G513700
			MSTRG.14037.1	Sobic.009G059700
Gibberellin-regulated protein 8;At2g39540;ortholog	O80641	AT2G39540	MSTRG.649.1	Sobic.001G170301
Protein phosphatase 2C 3;AIP1;ortholog	Q9LNW3	AT1G07430	MSTRG.3347.1	Sobic.001G424400
			MSTRG.3216.1	Sobic.001G406300
			MSTRG.14824.1	Sobic.009G161800
Transcription factor PIF1;PIF1;ortholog	Q8GZM7	AT2G20180	MSTRG.15953.2	Sobic.002G031000
			MSTRG.15953.1	Sobic.002G031000
Transcription factor HY5;HY5;ortholog	O24646	AT5G11260	MSTRG.10667.2	Sobic.004G085600
			MSTRG.25421.1	Sobic.003G403800
Casein kinase-like protein;MRG7.15;ortholog	Q9FK52	AT5G18190	MSTRG.16093.3	Sobic.002G047700
Zinc finger protein 8;ZFP8;ortholog	P93751	AT2G41940	MSTRG.17116.1	Sobic.002G219300
Potassium ion transport				
K(+) efflux antiporter 4;KEA4;ortholog	Q9ZUN3	AT2G19600	MSTRG.12167.2	Sobic.010G168900
Potassium channel KAT2;KAT2;ortholog	Q38849	AT4G18290	MSTRG.10478.1	Sobic.004G107500
			MSTRG.10479.1	Sobic.004G107500
			MSTRG.25550.1	Sobic.003G421900
Potassium transporter 2;POT2;ortholog	O22881	AT2G40540	MSTRG.2953.4	Sobic.001G379900
Potassium transporter 11;POT11;ortholog	O64769	AT2G35060	MSTRG.16499.2	Sobic.002G130800
			MSTRG.20074.2	Sobic.007G075100
			MSTRG.19117.1	Sobic.005G197100
			MSTRG.6180.1	Sobic.006G213500
Potassium channel SKOR;SKOR;ortholog	Q9M8S6	AT3G02850	MSTRG.13068.1	Sobic.010G102800

Plasma membrane-associated cation-binding protein 1;PCAP1;ortholog	Q96262	AT4G20260	MSTRG.10297.1	Sobic.004G128600
			MSTRG.18138.1	Sobic.002G339900
			MSTRG.22440.1	Sobic.003G005800
Ethylene-responsive transcription factor RAP2-11;RAP2-11;ortholog	Q6J9S1	AT5G19790	MSTRG.17521.1	Sobic.002G269600
			MSTRG.17101.1	Sobic.002G217100
Auxin response factor 2;ARF2;ortholog	Q94JM3	AT5G62000	MSTRG.7586.1	Sobic.005G132000
Sulfhydryl oxidase 1;QSOX1;ortholog	Q8W4J3	AT1G15020	MSTRG.15438.2	Sobic.009G224000
			MSTRG.15438.4	Sobic.009G224000
Probable peptide/nitrate transporter At3g43790;ZIFL2;ortholog	Q3EAQ5	AT3G43790	MSTRG.23230.1	Sobic.003G131800
			MSTRG.23202.1	Sobic.003G125701
			MSTRG.22680.1	Sobic.003G033200
			MSTRG.8536.1	Sobic.008G016000
Potassium transporter 5;POT5;ortholog	Q9M7K4	AT4G13420	MSTRG.741.1	Sobic.001G184300
			MSTRG.4894.1	Sobic.006G061300
			MSTRG.14998.1	Sobic.002G001800
			MSTRG.685.1	Sobic.001G175500
			MSTRG.739.1	Sobic.001G184000
			MSTRG.15754.1	Sobic.002G001800
Potassium transporter 1;POT1;ortholog	O22397	AT2G30070	MSTRG.17126.1	Sobic.002G220600
K(+) efflux antiporter 3, chloroplastic;KEA3;ortholog	Q9M0Z3	AT4G04850	MSTRG.22253.1	Sobic.008G173800
			MSTRG.22253.2	Sobic.008G173800
Probable cyclic nucleotide-gated ion channel 14;CNGC14;ortholog	Q9SJA4	AT2G24610	MSTRG.17735.2	Sobic.002G294800
Potassium channel AKT2/3;AKT2;ortholog	Q38898	AT4G22200	MSTRG.14714.3	Sobic.009G147500
			MSTRG.27670.1	Sobic.007G153500
			MSTRG.26944.1	Sobic.003G128600
			MSTRG.29351.1	Sobic.009G147200
			MSTRG.14714.2	Sobic.009G147200
			MSTRG.29350.1	Sobic.009G146800
Sodium ion transport				
ATP/GTP-binding protein family;emb1579;ortholog; Protein SHORT ROOT IN SALT MEDIUM 1 (RSA1)	F4IS91	AT2G03150	MSTRG.12153.1	Sobic.010G169600
			MSTRG.22271.1	Sobic.008G176300

Sodium-dependent phosphate transport protein 1, chloroplastic;ANTR1;ortholog	O82390	AT2G29650	MSTRG.28554.1	Sobic.003G133700
			MSTRG.23215.3	Sobic.003G133700
Dicarboxylate transporter 1, chloroplastic;DIT1;ortholog	Q9LXV3	AT5G12860	MSTRG.16328.1	Sobic.008G112300
			MSTRG.21687.1	Sobic.008G112300
Dicarboxylate transporter 2.1, chloroplastic;DIT2-1;ortholog	Q9FMF7	AT5G64290	MSTRG.17235.1	Sobic.002G233700
			MSTRG.17235.2	Sobic.002G233700
			MSTRG.17235.4	Sobic.002G233700
			MSTRG.16809.1	Sobic.002G179900
Tonoplast dicarboxylate transporter;TDT;ortholog	Q8LG88	AT5G47560	MSTRG.17306.1	Sobic.002G245400
			MSTRG.17305.4	Sobic.002G245400
Proline biosynthesis and transport				
Delta-1-pyrroline-5-carboxylate synthase B;P5CSB;ortholog	P54888	AT3G55610	MSTRG.25027.1	Sobic.003G356000
			MSTRG.28828.2	Sobic.003G246100
			MSTRG.14813.2	Sobic.009G160100
Pyrroline-5-carboxylate reductase;PROC1;ortholog	P54904	AT5G14800	MSTRG.25572.1	Sobic.003G424300
Delta-1-pyrroline-5-carboxylate synthase A;P5CSA;ortholog	P54887	AT2G39800	MSTRG.14813.1	Sobic.009G160100
Proline transporter 1;PROT1;ortholog	P92961	AT2G39890	MSTRG.13365.1	Sobic.002G001000
			MSTRG.13365.2	Sobic.002G001000
			MSTRG.13365.3	Sobic.002G001000
			MSTRG.13365.5	Sobic.002G001000
			MSTRG.25284.1	Sobic.003G395900
			MSTRG.4078.3	Sobic.001G511000
Delta-1-pyrroline-5-carboxylate dehydrogenase 12A1, mitochondrial;ALDH12A1;ortholog	Q8VZC3	AT5G62530	MSTRG.15342.1	Sobic.009G212600
			MSTRG.15342.4	Sobic.009G212600
Phosphatidylinositol 3-kinase VPS34;VPS34;ortholog	P42339	AT1G60490	MSTRG.19982.1	Sobic.007G088100
			MSTRG.19982.2	Sobic.007G088100
Glycine betaine biosynthesis and transport				
Betaine aldehyde dehydrogenase 1, chloroplastic;ALDH10A8;ortholog	Q9S795	AT1G74920	MSTRG.19677.1	Sobic.007G130800
Myo-inositol biosynthesis and transport				
Galactinol synthase 2;GOLS2;ortholog	Q9FXB2	AT1G56600	MSTRG.18847.1	Sobic.002G423600

			MSTRG.18061.1	Sobic.002G329000
			MSTRG.18041.1	Sobic.002G329000
Inositol 1,3,4-trisphosphate 5/6-kinase 4;ITPK4;ortholog	O80568	AT2G43980	MSTRG.17493.3	Sobic.002G266300
			MSTRG.17493.1	Sobic.002G266300
			MSTRG.17493.2	Sobic.002G266300
			MSTRG.17079.1	Sobic.002G214300
Monosaccharide-sensing protein 2;MSSP2;ortholog	Q8LPQ8	AT4G35300	MSTRG.8101.1	Sobic.001G312900
			MSTRG.2104.1	Sobic.001G293800
			MSTRG.2264.2	Sobic.001G312900
			MSTRG.10536.5	Sobic.004G099300
			MSTRG.10536.2	Sobic.004G099300
			MSTRG.10536.4	Sobic.004G099300
Polyol transporter 5;PLT5;ortholog	Q8VZ80	AT3G18830	MSTRG.3751.1	Sobic.001G469500
			MSTRG.3751.3	Sobic.001G469600
			MSTRG.18244.1	Sobic.002G353900
			MSTRG.19078.1	Sobic.001G434900
			MSTRG.7154.1	Sobic.005G196300
			MSTRG.7155.1	Sobic.005G196300
			MSTRG.28209.1	Sobic.008G111100
Senescence				
Bidirectional sugar transporter SWEET15 (AtSWEET15) (Protein SUGARS WILL EVENTUALLY BE EXPORTED TRANSPORTERS 15) (Senescence-associated protein 29)	Q9FY94	AT5G13170	MSTRG.10056.1	Sobic.004G157100
Senescence-specific cysteine protease SAG12 (EC 3.4.22.-) (Cysteine proteinase SAG12) (Protein SENESCENCE-ASSOCIATED GENE 12)	Q9FJ47	AT5G45890	MSTRG.12419.1	Sobic.001G086800
			MSTRG.16932.1	Sobic.002G195800
			MSTRG.25980.1	Sobic.002G195800
			MSTRG.12490.1	Sobic.004G038400
			MSTRG.29360.1	Sobic.006G022800
			MSTRG.18322.1	Sobic.002G252700
Nitrate reductase [NADH] 1 (NR1) (EC 1.7.1.1)	P11832	AT1G77760	MSTRG.19479.1	Sobic.007G153900
			MSTRG.19476.1	Sobic.007G153900
			MSTRG.19478.1	Sobic.007G153900
			MSTRG.9869.1	Sobic.004G179700

Supplementary Table 4.4. The gene IDs, treatments/accessions of differentially expression, and function of genes involved with gibberellin biosynthesis and transport, sodium and potassium homeostasis and transport, osmolyte production and transport, and senescence.

Gibberellin biosynthesis and transport																				
Gene Description	**Uniprot ID**	**TAIR ID**	**Transcript ID**	**Sorghum ID**	**HI10 - 10 dS/m - log2FoldChange**	**HI10 - 10 dS/m - padj**	**HI10 - 30 dS/m - log2FoldChange**	**HI10 - 30 dS/m - padj**	**Spence - 10 dS/m - log2FoldChange**	**Spence - 10 dS/m - padj**	**Spence - 30 dS/m - log2FoldChange**	**Spence - 30 dS/m - padj**	**0 dS/m**	**0 dS/m - padj**	**10 dS/m**	**10 dS/m - padj**	**30 dS/m**	**30 dS/m - padj**
Telomere repeat-binding factor 1;TRB1;ortholog	Q8VWK4	AT1G49950	MSTRG.547.1	Sobic.001G156900	1.1012333305	0.001453855	N/A	N/A	N/A	N/A	N/A	N/A	N/A	N/A	N/A	N/A	N/A	N/A
			MSTRG.509.6	Sobic.001G151100	N/A	N/A	N/A	N/A	N/A	N/A	N/A	N/A	10.04049	1.21956E-07	N/A	N/A	N/A	N/A
			MSTRG.547.4	Sobic.001G156900	N/A	N/A	N/A	N/A	N/A	N/A	N/A	N/A	N/A	N/A	N/A	N/A	6.943186	0.001511146
			MSTRG.547.2	Sobic.001G156900	N/A	N/A	N/A	N/A	N/A	N/A	N/A	N/A	N/A	N/A	N/A	N/A	5.6689579	0.000802662
Phosphatidylinositol N-acetylglucosaminyltransferase subunit P-like protein;TRM13;ortholc	Q80829	AT2G45900	MSTRG.5861.2	Sobic.006G176500	-5.940434475	0.002638101	N/A	N/A	N/A	N/A	N/A	N/A	N/A	N/A	N/A	N/A	N/A	N/A
			MSTRG.7469.1	Sobic.005G154500	N/A	N/A	N/A	N/A	N/A	N/A	N/A	N/A	-3.92985	0.026005188	N/A	N/A	N/A	N/A
			MSTRG.5861.1	Sobic.006G176500	N/A	N/A	N/A	N/A	N/A	N/A	N/A	N/A	N/A	N/A	-1.9424778	0.00260977	N/A	N/A
Protein REVEILLE 6;RVE6;ortholog	Q8H0W3	AT5G52660	MSTRG.13904.1	Sobic.010G004300	N/A	N/A	1.358504683	1.07071E-09	N/A	N/A	N/A	N/A	N/A	N/A	N/A	N/A	N/A	N/A
			MSTRG.13904.2	Sobic.010G004300	N/A	N/A	N/A	N/A	N/A	N/A	N/A	N/A	N/A	N/A	-1.1200746	0.040078526	N/A	N/A
			MSTRG.9282.1	Sobic.004G281800	N/A	N/A	2.451866929	0.048431803	N/A	N/A	N/A	N/A	N/A	N/A	N/A	N/A	N/A	N/A
			MSTRG.9282.6	Sobic.004G281800	N/A	N/A	N/A	N/A	-6.249430006	0.007403323	N/A	N/A	N/A	N/A	N/A	N/A	N/A	N/A
			MSTRG.23652.1	Sobic.004G154000	N/A	N/A	N/A	N/A	N/A	N/A	N/A	N/A	2.30936	4.87322E-06	N/A	N/A	N/A	N/A
			MSTRG.29112.1	Sobic.004G154000	N/A	N/A	N/A	N/A	N/A	N/A	N/A	N/A	2.770152	5.44728E-22	N/A	N/A	N/A	N/A
BTB/POZ and TAZ domain-containing protein 4;BT4;ortholog	Q9FJX5	AT5G67480	MSTRG.25364.4	Sobic.003G385100	N/A	N/A	-2.353866116	9.43023E-06	N/A	N/A	N/A	N/A	N/A	N/A	N/A	N/A	N/A	N/A
Transcription factor MYB59/MYB59;ortholog	Q4JLB4	AT5G59780	MSTRG.6457.2	Sobic.005G224800	N/A	N/A	N/A	N/A	-5.343512072	5.64496E-05	N/A	N/A	N/A	N/A	6.36037644	5.34426E-05	N/A	N/A
			MSTRG.21906.5	Sobic.008G133700	N/A	N/A	N/A	N/A	-21.93007593	1.25697E-06	N/A	N/A	N/A	N/A	N/A	N/A	N/A	N/A
			MSTRG.21906.6	Sobic.008G133700	N/A	N/A	N/A	N/A	N/A	N/A	N/A	N/A	N/A	N/A	5.6983763	2.98223E-05	N/A	N/A
			MSTRG.27858.2	Sobic.005G224700	N/A	N/A	N/A	N/A	N/A	N/A	7.049754822	0.000675639	N/A	N/A	N/A	N/A	N/A	N/A
			MSTRG.8810.1	Sobic.004G352200	N/A	N/A	N/A	N/A	N/A	N/A	N/A	N/A	1.734079	7.54525E-07	N/A	N/A	N/A	N/A
			MSTRG.6457.1	Sobic.005G224800	N/A	N/A	N/A	N/A	N/A	N/A	N/A	N/A	N/A	N/A	1.29737382	0.003758415	1.1458527	0.00034702
			MSTRG.20151.1	Sobic.009G016600	N/A	N/A	N/A	N/A	N/A	N/A	N/A	N/A	N/A	N/A	2.03702691	0.042615592	N/A	N/A
			MSTRG.20151.2	Sobic.009G016600	N/A	N/A	N/A	N/A	N/A	N/A	N/A	N/A	N/A	N/A	1.81396631	3.627888E-13	N/A	N/A
MADS-box protein SOC1;SOC1;ortholog	O64645	AT2G45660	MSTRG.25445.1	Sobic.003G406800	N/A	N/A	N/A	N/A	N/A	N/A	1.086013799	0.001189782	N/A	N/A	N/A	N/A	N/A	N/A
			MSTRG.3962.1	Sobic.001G497600	N/A	N/A	N/A	N/A	N/A	N/A	N/A	N/A	1.1854466	6.25157E-05	N/A	N/A	N/A	N/A
			MSTRG.11314.1	Sobic.004G002401	N/A	N/A	N/A	N/A	N/A	N/A	N/A	N/A	N/A	N/A	3.24737422	0.006905752	3.1901504	8.80269E-06
Gibberellin 20 oxidase 1;GA20OX1;ortholog	Q39110	AT4G25420	MSTRG.25223.1	Sobic.003G379500	N/A	N/A	N/A	N/A	-1.743605645	2.45389E-09	-1.864076784	0.004473124	N/A	N/A	N/A	N/A	N/A	N/A
			MSTRG.24143.1	Sobic.003G263300	N/A	N/A	N/A	N/A	N/A	N/A	N/A	N/A	-1.824494	1.65381E-10	N/A	N/A	N/A	N/A
DELLA protein GAI;GAI;ortholog	Q9LQT8	AT1G14920	MSTRG.23964.1	Sobic.003G237201	N/A	N/A	N/A	N/A	-1.098133994	0.005670576	N/A	N/A	N/A	N/A	N/A	N/A	N/A	N/A
Ent-kaur-16-ene synthase, chloroplastic;GA2;ortholog	Q9SAK2	AT1G79460	MSTRG.26708.2	Sobic.005G195800	N/A	N/A	N/A	N/A	N/A	N/A	N/A	N/A	-9.08201	0.010369193	N/A	N/A	N/A	N/A
			MSTRG.6164.1	Sobic.006G211400	N/A	N/A	-1.099656291	0.00031737	N/A	N/A	N/A	N/A	N/A	N/A	-1.79428886	5.35231E-13	-1.8619024	8.2631BE-05
			MSTRG.6165.2	Sobic.006G211500	N/A	N/A	N/A	N/A	N/A	N/A	N/A	N/A	N/A	N/A	-5.8040511	0.030832274	N/A	N/A
Gibberellin 2-beta-dioxygenase 8;GA2OX8;ortholog	O49561	AT4G21200	MSTRG.5639.1	Sobic.006G150800	N/A	N/A	-1.040367665	0.000450393	N/A	N/A	-2.012571971	0.000137926	N/A	N/A	N/A	N/A	N/A	N/A
Acid beta-fructofuranosidase 4, vacuolar;BFRUCT4;ortholog	Q39041	AT1G12240	MSTRG.11302.1	Sobic.004G004800	N/A	N/A	N/A	N/A	-1.416329453	0.009812604	-1.573031952	0.000642969	N/A	N/A	N/A	N/A	N/A	N/A
			MSTRG.28633.1	Sobic.004G004800	N/A	N/A	N/A	N/A	-1.565919753	0.026486685	N/A	N/A	N/A	N/A	N/A	N/A	N/A	N/A
Acid beta-fructofuranosidase 3, vacuolar;BFRUCT3;ortholog	Q43348	AT1G62660	MSTRG.5726.1	Sobic.006G160700	N/A	N/A	N/A	N/A	-1.363545352	0.000111042	-1.420626847	0.002747415	N/A	N/A	2.76874711	1.23243E-10	2.3645667	6.73492E-15
			MSTRG.7734.1	Sobic.005G122600	N/A	N/A	N/A	N/A	N/A	N/A	N/A	N/A	-1.475119	0.001876792	N/A	N/A	N/A	N/A
Transcription factor bHLH93;BHLH93;ortholog	Q9LSL1	AT5G65640	MSTRG.4098.1	Sobic.001G013700	N/A	N/A	N/A	N/A	-1.062026433	0.000609426	N/A	N/A	N/A	N/A	N/A	N/A	N/A	N/A
			MSTRG.14037.1	Sobic.009G059700	N/A	N/A	N/A	N/A	N/A	N/A	N/A	N/A	-1.66068	4.50369E-12	N/A	N/A	N/A	N/A
Gibberellin-regulated protein 8;At2g39540;ortholog	O80641	AT2G39540	MSTRG.649.1	Sobic.001G170301	N/A	N/A	1.78167165	1.66158E-46	N/A	N/A	2.144432037	1.01833E-17	N/A	N/A	N/A	N/A	N/A	N/A
Protein phosphatase 2C 3;AP13;ortholog	Q9LNW3	AT1G07430	MSTRG.3347.1	Sobic.001G424400	N/A	N/A	2.379097648	2.31509E-23	N/A	N/A	N/A	N/A	N/A	N/A	-1.1290116	0.012301317	N/A	N/A
			MSTRG.321.6	Sobic.001G406300	N/A	N/A	N/A	N/A	N/A	N/A	N/A	N/A	-1.91115	0.000133923	N/A	N/A	N/A	N/A
			MSTRG.14824.1	Sobic.009G161800	N/A	N/A	N/A	N/A	N/A	N/A	N/A	N/A	N/A	N/A	-1.3569411	0.000468404	N/A	N/A
Transcription factor PIF1;PIF1;ortholog	Q8GZM7	AT2G20180	MSTRG.15953.2	Sobic.002G031000	N/A	N/A	-3.863406391	0.012907877	N/A	N/A	N/A	N/A	N/A	N/A	N/A	N/A	N/A	N/A
			MSTRG.15953.1	Sobic.002G031000	N/A	N/A	N/A	N/A	N/A	N/A	-1.536609233	0.035573966	N/A	N/A	N/A	N/A	N/A	N/A
Transcription factor HY5;HY5;ortholog	O24646	AT5G11260	MSTRG.10667.2	Sobic.004G085600	N/A	N/A	N/A	N/A	-1.2679941B6	9.45815E-12	-1.317982905	2.60105E-08	N/A	N/A	N/A	N/A	N/A	N/A
			MSTRG.25421.1	Sobic.003G403800	N/A	N/A	N/A	N/A	N/A	N/A	N/A	N/A	-2.39572	0.029000511	N/A	N/A	N/A	N/A
Casein kinase-like protein;PRR7.15;ortholog	Q9FK52	AT5G18190	MSTRG.16093.3	Sobic.002G047700	N/A	N/A	N/A	N/A	N/A	N/A	7.883590076	0.035949544	N/A	N/A	N/A	N/A	N/A	N/A
Zinc finger protein 8;ZFP8;ortholog	P93751	AT2G41940	MSTRG.17116.1	Sobic.002G219300	N/A	N/A	N/A	N/A	-1.503853839	0.000150457	N/A	N/A	N/A	N/A	N/A	N/A	N/A	N/A
Potassium ion transport																		
Gene Description	**Uniprot ID**	**TAIR ID**	**Transcript ID**	**Sorghum ID**	**HI10 - 10 dS/m - log2FoldChange**	**HI10 - 10 dS/m - padj**	**HI10 - 30 dS/m - log2FoldChange**	**HI10 - 30 dS/m - padj**	**Spence - 10 dS/m - log2FoldChange**	**Spence - 10 dS/m - padj**	**Spence - 30 dS/m - log2FoldChange**	**Spence - 30 dS/m - padj**	**0 dS/m**	**0 dS/m - padj**	**10 dS/m**	**10 dS/m - padj**	**30 dS/m**	**30 dS/m - padj**
K(+) efflux antiporter 4;KEA4;ortholog	Q9ZUN3	AT2G19600	MSTRG.12167.2	Sobic.010G168900	-9.057143017	7.61675E-07	N/A	N/A	N/A	N/A	N/A	N/A	N/A	N/A	-7.3815765	0.000709072	N/A	N/A
Potassium channel KAT3;KAT2;ortholog	Q38849	AT4G18290	MSTRG.10478.1	Sobic.004G107500	-1.567751055	0.029171265	N/A	N/A	-1.224203276	0.001610835	N/A	N/A	N/A	N/A	N/A	N/A	N/A	N/A
			MSTRG.10479.1	Sobic.004G107500	N/A	N/A	N/A	N/A	-1.977201434	2.87198E-07	N/A	N/A	N/A	N/A	N/A	N/A	N/A	N/A
			MSTRG.25550.1	Sobic.003G421900	N/A	N/A	N/A	N/A	N/A	N/A	N/A	N/A	-1.18295	0.045853029	N/A	N/A	N/A	N/A
Potassium transporter 2;POT2;ortholog	O22881	AT3G40540	MSTRG.2953.4	Sobic.001G379900	-4.457692412	0.03073428	N/A	N/A	-4.197383024	0.038146762	N/A	N/A	N/A	N/A	N/A	N/A	N/A	N/A
Potassium transporter 11;POT11;ortholog	O64769	AT2G35060	MSTRG.16499.2	Sobic.002G130800	-7.124589596	0.042407895	N/A	N/A	N/A	N/A	N/A	N/A	N/A	N/A	-9.9679844	0.001107439	N/A	N/A
			MSTRG.20074.2	Sobic.007G075100	-4.784362215	0.00989227	N/A	N/A	N/A	N/A	N/A	N/A	N/A	N/A	N/A	N/A	N/A	N/A
			MSTRG.19117.1	Sobic.005G197100	N/A	N/A	N/A	N/A	N/A	N/A	N/A	N/A	2.222353	1.27741E-05	N/A	N/A	N/A	N/A
			MSTRG.6180.1	Sobic.006G213500	N/A	N/A	N/A	N/A	N/A	N/A	N/A	N/A	N/A	N/A	N/A	N/A	-3.1358589	5.94295E-07
Potassium channel SKOR;SKOR;ortholog	Q9M856	AT3G02850	MSTRG.13068.1	Sobic.010G102800	N/A	N/A	1.931817424	4.2231 6E-50	N/A	N/A	N/A	N/A	N/A	N/A	N/A	N/A	N/A	N/A
Plasma membrane-associated cation-binding protein 1;PCAP1;ortholog	Q96262	AT4G20260	MSTRG.10297.1	Sobic.004G128600	N/A	N/A	-1.152673524	0.000510013	-1.28211276	0.002425768	-1.764854187	3.41E-05	N/A	N/A	1.05347881	0.008166061	N/A	N/A
			MSTRG.18138.1	Sobic.002G339900	1.198048035	4.32598E-08	N/A	N/A	N/A	N/A	N/A	N/A	N/A	N/A	N/A	N/A	N/A	N/A
			MSTRG.22440.1	Sobic.003G005800	N/A	N/A	N/A	N/A	N/A	N/A	N/A	N/A	N/A	N/A	2.55773296	0.007251022	N/A	N/A
Ethylene-responsive transcription factor RAP2-11;RAP2-11;ortholog	Q6J9S1	AT5G19790	MSTRG.17521.1	Sobic.002G269600	N/A	N/A	-1.36066316	0.009784646	N/A	N/A	N/A	N/A	N/A	N/A	N/A	N/A	N/A	N/A
			MSTRG.17101.1	Sobic.002G217100	N/A	N/A	N/A	N/A	N/A	N/A	N/A	N/A	-3.45062	8.31576E-17	N/A	N/A	N/A	N/A
Auxin response factor 2;ARF2;ortholog	Q94JM3	AT5G62000	MSTRG.7586.1	Sobic.005G132000	N/A	N/A	2.178939826	0.021040192	N/A	N/A	N/A	N/A	N/A	N/A	N/A	N/A	N/A	N/A
Sulfhydryl oxidase 1;QSOX1;ortholog	Q8VY4J3	AT1G15020	MSTRG.15438.2	Sobic.009G224000	N/A	N/A	-4.414673755	0.038513736	N/A	N/A	N/A	N/A	N/A	N/A	N/A	N/A	N/A	N/A
			MSTRG.15438.4	Sobic.009G224000	N/A	N/A	N/A	N/A	-7.6596698	0.01988435	N/A	N/A	N/A	N/A	N/A	N/A	5.66561B2	0.019816143
Probable peptide/nitrate transporter At3g43790;ZIFL2;ortholog	Q3EAQ5	AT3G43790	MSTRG.23230.1	Sobic.003G231800	N/A	N/A	N/A	N/A	-1.189624284	1.05469E-06	N/A	N/A	N/A	N/A	N/A	N/A	N/A	N/A
			MSTRG.23202.1	Sobic.003G125701	N/A	N/A	N/A	N/A	N/A	N/A	-1.583060802	3.28467E-05	N/A	N/A	N/A	N/A	N/A	N/A
			MSTRG.22680.1	Sobic.003G033200	N/A	N/A	N/A	N/A	N/A	N/A	N/A	N/A	1.348504	0.017786383	N/A	N/A	N/A	N/A
			MSTRG.8536.1	Sobic.008G016000	N/A	N/A	N/A	N/A	N/A	N/A	N/A	N/A	N/A	N/A	1.5673948	0.046043352	N/A	N/A
Potassium transporter 5;POT5;ortholog	Q9M7K4	AT4G13420	MSTRG.741.1	Sobic.001G184300	N/A	N/A	N/A	N/A	N/A	N/A	-1.357175322	0.016577823	N/A	N/A	-1.3868934	0.001287191	N/A	N/A
			MSTRG.4894.1	Sobic.006G061300	N/A	N/A	N/A	N/A	N/A	N/A	-1.743203272	0.023735379	N/A	N/A	N/A	N/A	N/A	N/A
			MSTRG.14998.1	Sobic.002G001800	N/A	N/A	N/A	N/A	N/A	N/A	-1.031488268	0.034996674	N/A	N/A	-5.102717	1.07193E-08	-5.4349796	1.11281E-13
			MSTRG.685.1	Sobic.001G175500	N/A	N/A	N/A	N/A	N/A	N/A	N/A	N/A	1.694004	0.00063321	N/A	N/A	N/A	N/A
			MSTRG.739.1	Sobic.001G184000	N/A	N/A	N/A	N/A	N/A	N/A	N/A	N/A	N/A	N/A	-1.4039451	0.00289902	-1.3585689	0.000316579
			MSTRG.15754.1	Sobic.002G001800	N/A	N/A	N/A	N/A	N/A	N/A	N/A	N/A	N/A	N/A	N/A	N/A	-1.0236471	0.000107961
Potassium transporter 1;POT1;ortholog	O22397	AT2G30070	MSTRG.17126.1	Sobic.002G220600	N/A	N/A	N/A	N/A	-1.070467536	0.019174528	N/A	N/A	N/A	N/A	N/A	N/A	1.100073	0.034487097
K(+) efflux antiporter 3, chloroplastic;KEA3;ortholog	Q9M0Z3	AT4G04850	MSTRG.22253.1	Sobic.008G173800	N/A	N/A	N/A	N/A	N/A	N/A	4.5429261 47	0.039259515	N/A	N/A	N/A	N/A	N/A	N/A
			MSTRG.22253.2	Sobic.008G173800	N/A	N/A	N/A	N/A	N/A	N/A	N/A	N/A	N/A	N/A	-9.5738398	1.74221E-09	N/A	N/A
Probable cyclic nucleotide-gated ion channel 14;CNGC14;ortholog	Q9SJA4	AT2G24610	MSTRG.17735.2	Sobic.002G294800	N/A	N/A	N/A	N/A	9.253119944	4.55556E-12	N/A	N/A	N/A	N/A	-9.7109847	3.86628E-13	N/A	N/A
Potassium channel AKT3/3;AKT2;ortholog	Q38898	AT4G22200	MSTRG.14714.3	Sobic.009G147500	N/A	N/A	N/A	N/A	8.3838294	0.043131938	N/A	N/A	N/A	N/A	N/A	N/A	N/A	N/A
			MSTRG.27670.1	Sobic.007G153500	N/A	N/A	N/A	N/A	N/A	N/A	N/A	N/A	1.435886	0.037033934	N/A	N/A	N/A	N/A
			MSTRG.26944.1	Sobic.003G128600	N/A	N/A	N/A	N/A	N/A	N/A	N/A	N/A	1.48068	0.010109039	N/A	N/A	N/A	N/A
			MSTRG.29351.1	Sobic.009G147200	N/A	N/A	N/A	N/A	N/A	N/A	N/A	N/A	N/A	N/A	-2.187924	0.0032911 5	-2.3060621	0.000824556
			MSTRG.14714.2	Sobic.009G147200	N/A	N/A	N/A	N/A	N/A	N/A	N/A	N/A	N/A	N/A	N/A	N/A	6.6229054	0.014277004
			MSTRG.29350.1	Sobic.009G146800	N/A	N/A	N/A	N/A	N/A	N/A	N/A	N/A	N/A	N/A	N/A	N/A	-4.7709073	0.005742213

Sodium ion transport																			
Gene Description	**Uniprot ID**	**TAIR ID**	**Transcript ID**	**Sorghum ID**	**HI10 - 10 dS/m - log2FoldChange**	**HI10 - 10 dS/m - padj**	**HI10 - 30 dS/m - log2FoldChange**	**HI10 - 30 dS/m - padj**	**Spence - 10 dS/m - log2FoldChange**	**Spence - 10 dS/m - padj**	**Spence - 30 dS/m - log2FoldChange**	**Spence - 30 dS/m - padj**	**0 dS/m**	**0 dS/m - padj**	**10 dS/m**	**10 dS/m - padj**	**30 dS/m**	**30 dS/m - padj**
ATP/GTP-binding protein family;amb1579;ortholog; Protein SHORT ROOT IN SALT MEDIUM 1 (RSA1)	F4I591	AT2G03150	MSTRG.13153.1	Sobic.010G169600	-1.220289246	0.001481794	N/A	N/A	N/A	N/A	N/A	N/A	N/A	N/A	-1.610282	0.000275609	N/A	N/A
			MSTRG.22271.1	Sobic.008G176300	N/A	N/A	N/A	N/A	N/A	N/A	N/A	N/A	-1.22586	0.011075928	N/A	N/A	N/A	N/A
Sodium-dependent phosphate transport protein 1, chloroplastic;ANTR1;ortholog	Q82390	AT2G29650	MSTRG.28554.1	Sobic.003G133700	N/A	N/A	-7.590452526	6.60949E-05	N/A	N/A	N/A	N/A	N/A	N/A	N/A	N/A	-8.8298685	1.82138E-11
			MSTRG.23215.3	Sobic.003G133700	N/A	N/A	N/A	N/A	N/A	N/A	N/A	N/A	N/A	N/A	N/A	N/A	5.9525735	0.008601437
Dicarboxylate transporter 1, chloroplastic;DIT1;ortholog	Q9LXV3	AT5G12860	MSTRG.16328.1	Sobic.008G112300	N/A	N/A	N/A	N/A	-1.561714936	0.000133732	-1.244259724	2.29233E-06	N/A	N/A	1.19080302	0.020269222	-1.2442972	2.29233E-06
			MSTRG.21687.1	Sobic.008G112300	N/A	N/A	N/A	N/A	N/A	N/A	-1.3565331 38	7.09621E-18	N/A	N/A	N/A	N/A	N/A	N/A
Dicarboxylate transporter 2.1, chloroplastic;DIT2-1;ortholog	Q9FMF7	AT5G64290	MSTRG.17235.1	Sobic.002G233700	N/A	N/A	-1.081907254	0.033203646	N/A	N/A	N/A	0.008661806	N/A	N/A	N/A	N/A	N/A	N/A
			MSTRG.17235.2	Sobic.002G233700	N/A	N/A	N/A	N/A	N/A	N/A	N/A	N/A	N/A	N/A	-9.895311	7.11572E-12	-10.689265	1.34683E-11
			MSTRG.17235.4	Sobic.002G233700	N/A	N/A	N/A	N/A	N/A	N/A	N/A	N/A	N/A	N/A	-4.7829013	1.80237E-08	N/A	N/A
			MSTRG.16809.1	Sobic.002G179900	N/A	N/A	N/A	N/A	N/A	N/A	N/A	N/A	1.302008	0.031466061	N/A	N/A	N/A	N/A
Tonoplast dicarboxylate transporter;TDT;ortholog	Q8LGB8	AT5G47560	MSTRG.17306.1	Sobic.002G245400	N/A	N/A	N/A	N/A	-1.449312066	0.015681487	-1.244259724	2.29233E-06	N/A	N/A	1.19080302	0.020269222	N/A	N/A
			MSTRG.17305.4	Sobic.002G245400	N/A	N/A	N/A	N/A	N/A	N/A	-1.187054808	6.7913E-07	N/A	N/A	1.6731747	1.640825-53	2.4867724	6.73307E-59
Proline biosynthesis and transport																		
Gene Description	**Uniprot ID**	**TAIR ID**	**Transcript ID**	**Sorghum ID**	**HI10 - 10 dS/m - log2FoldChange**	**HI10 - 10 dS/m - padj**	**HI10 - 30 dS/m - log2FoldChange**	**HI10 - 30 dS/m - padj**	**Spence - 10 dS/m - log2FoldChange**	**Spence - 10 dS/m - padj**	**Spence - 30 dS/m - log2FoldChange**	**Spence - 30 dS/m - padj**	**0 dS/m**	**0 dS/m - padj**	**10 dS/m**	**10 dS/m - padj**	**30 dS/m**	**30 dS/m - padj**
Delta-1-pyrroline-5-carboxylate synthase B;P5CSB;ortholog	P54888	AT3G55610	MSTRG.25027.1	Sobic.003G356000	N/A	N/A	1.084392398	5.83235E-54	1.864505105	5.53896E-10	2.332573793	3.69214E-22	N/A	N/A	N/A	N/A	N/A	N/A
			MSTRG.28828.2	Sobic.003G246100	N/A	N/A	N/A	N/A	N/A	N/A	N/A	N/A	6.509518	0.00755602	N/A	N/A	N/A	N/A
			MSTRG.14813.2	Sobic.009G160100	N/A	N/A	N/A	N/A	N/A	N/A	N/A	N/A	N/A	N/A	N/A	N/A	11.296177	6.36838E-19
Pyrroline-5-carboxylate reductase;PROC1;ortholog	P54904	AT5G14800	MSTRG.25572.1	Sobic.003G424300	N/A	N/A	1.13747759	1.256628-10	1.226955241	9.50239E-05	1.175175348	0.001433841	N/A	N/A	N/A	N/A	N/A	N/A
Delta-1-pyrroline-5-carboxylate synthase A;P5CSA;ortholog	P54887	AT2G39800	MSTRG.14813.1	Sobic.009G160100	N/A	N/A	N/A	N/A	N/A	N/A	1.327035633	4.95154E-20	N/A	N/A	N/A	N/A	N/A	N/A
Proline transporter 1;PROT1;ortholog	P92961	AT2G39890	MSTRG.13365.1	Sobic.002G001000	2.192985512	0.033412053	2.59209812	0.0351127469	N/A	N/A	N/A	N/A	N/A	N/A	N/A	N/A	N/A	N/A
			MSTRG.13365.2	Sobic.002G001000	N/A	N/A	-2.392717513	0.009757233	-3.204167681	0.016223423	N/A	N/A	N/A	N/A	3.29733749	0.000145896	N/A	N/A
			MSTRG.13365.3	Sobic.002G001000	N/A	N/A	N/A	N/A	N/A	N/A	N/A	N/A	N/A	N/A	10.1267295	0.007370594	N/A	N/A
			MSTRG.13365.5	Sobic.002G001000	-9.371197795	0.032816347	-9.66788368	0.021399683	N/A	N/A	N/A	N/A	N/A	N/A	N/A	N/A	N/A	N/A
			MSTRG.25284.1	Sobic.003G395900	N/A	N/A	N/A	N/A	N/A	N/A	-1.185811063	0.000669276	N/A	N/A	N/A	N/A	N/A	N/A
			MSTRG.4078.3	Sobic.001G511000	N/A	N/A	N/A	N/A	N/A	N/A	N/A	N/A	4.946819	0.014804675	N/A	N/A	N/A	N/A
Delta-1-pyrroline-5-carboxylate dehydrogenase 12A1, mitochondrial;ALDH12A1;ortholog	Q8VZC3	AT5G62530	MSTRG.15342.1	Sobic.009G212600	N/A	N/A	N/A	N/A	N/A	N/A	1.293639613	4.66109E-11	N/A	N/A	N/A	N/A	N/A	N/A
			MSTRG.15342.4	Sobic.009G212600	N/A	N/A	N/A	N/A	N/A	N/A	6.966227047	0.008517015	N/A	N/A	N/A	N/A	N/A	N/A
Phosphatidylinositol 3-kinase VPS34;VPS34;ortholog	P42339	AT1G60490	MSTRG.19982.1	Sobic.007G088100	N/A	N/A	-2.189243771	0.006316501	N/A	N/A	N/A	N/A	N/A	N/A	N/A	N/A	N/A	N/A
			MSTRG.19982.2	Sobic.007G088100	N/A	N/A	7.600214782	2.36174E-11	N/A	N/A	N/A	N/A	N/A	N/A	N/A	N/A	9.4285667	5.26012E-13
Glycine betaine biosynthesis and transport																		
Gene Description	**Uniprot ID**	**TAIR ID**	**Transcript ID**	**Sorghum ID**	**HI10 - 10 dS/m - log2FoldChange**	**HI10 - 10 dS/m - padj**	**HI10 - 30 dS/m - log2FoldChange**	**HI10 - 30 dS/m - padj**	**Spence - 10 dS/m - log2FoldChange**	**Spence - 10 dS/m - padj**	**Spence - 30 dS/m - log2FoldChange**	**Spence - 30 dS/m - padj**	**0 dS/m**	**0 dS/m - padj**	**10 dS/m**	**10 dS/m - padj**	**30 dS/m**	**30 dS/m - padj**
Betaine aldehyde dehydrogenase 1, chloroplastic;ALDH10A8;ortholog	Q9S795	AT1G74920	MSTRG.19677.1	Sobic.007G130800	N/A	N/A	1.023582044	4.04831E-59	N/A	N/A	N/A	N/A	N/A	N/A	N/A	N/A	N/A	N/A
Myo-inositol biosynthesis and transport																		
Gene Description	**Uniprot ID**	**TAIR ID**	**Transcript ID**	**Sorghum ID**	**HI10 - 10 dS/m - log2FoldChange**	**HI10 - 10 dS/m - padj**	**HI10 - 30 dS/m - log2FoldChange**	**HI10 - 30 dS/m - padj**	**Spence - 10 dS/m - log2FoldChange**	**Spence - 10 dS/m - padj**	**Spence - 30 dS/m - log2FoldChange**	**Spence - 30 dS/m - padj**	**0 dS/m**	**0 dS/m - padj**	**10 dS/m**	**10 dS/m - padj**	**30 dS/m**	**30 dS/m - padj**
Galactinol synthase 2;GOLS2;ortholog	Q9FXB2	AT1G56600	MSTRG.18847.1	Sobic.002G423600	N/A	N/A	1.483314867	2.92356E-06	N/A	N/A	N/A	N/A	N/A	N/A	1.60042514	0.000199025	2.4745269	4.44992E-11
			MSTRG.18061.1	Sobic.002G329000	N/A	N/A	N/A	N/A	N/A	N/A	N/A	N/A	6.933341	2.79263E-07	N/A	N/A	N/A	N/A
			MSTRG.18041.1	Sobic.003G329000	N/A	N/A	N/A	N/A	N/A	N/A	N/A	N/A	-1.59827	0.008534069	N/A	N/A	N/A	N/A
Inositol 1,3,4-trisphosphate 5/6-kinase 4;ITPK4;ortholog	Q80568	AT2G43980	MSTRG.17493.3	Sobic.002G266300	-3.142300366	0.001813129	N/A	N/A	N/A	N/A	N/A	N/A	N/A	N/A	N/A	N/A	2.7857036	0.033178448
			MSTRG.17493.1	Sobic.002G266300	N/A	N/A	N/A	N/A	N/A	N/A	1.002051276	0.000529553	N/A	N/A	N/A	N/A	N/A	N/A
			MSTRG.17493.2	Sobic.002G266300	N/A	N/A	N/A	N/A	N/A	N/A	N/A	N/A	N/A	N/A	N/A	N/A	7.9798258	8.5297E-06
			MSTRG.17079.1	Sobic.002G214300	N/A	N/A	N/A	N/A	N/A	N/A	N/A	N/A	1.167013	2.07297E-05	N/A	N/A	N/A	N/A
Monosaccharide-sensing protein 2;MSSP2;ortholog	Q8LPQ8	AT4G35300	MSTRG.8101.1	Sobic.001G312900	N/A	N/A	N/A	N/A	1.877779949	0.000535827	3.224516446	9.47179E-13	N/A	N/A	N/A	N/A	N/A	N/A
			MSTRG.2104.1	Sobic.001G293800	N/A	N/A	N/A	N/A	N/A	N/A	N/A	N/A	-1.71334	4.80135E-74	N/A	N/A	N/A	N/A
			MSTRG.2264.2	Sobic.001G312900	N/A	N/A	N/A	N/A	N/A	N/A	N/A	N/A	N/A	N/A	7.12383964	0.004127146	N/A	N/A
			MSTRG.10536.5	Sobic.004G099300	N/A	N/A	N/A	N/A	N/A	N/A	N/A	N/A	N/A	N/A	11.7647966	0.014527614	N/A	N/A
			MSTRG.10536.2	Sobic.004G099300	N/A	N/A	N/A	N/A	N/A	N/A	N/A	N/A	N/A	N/A	-12.970914	1.06408E-22	N/A	N/A
			MSTRG.10536.4	Sobic.004G099300	N/A	N/A	N/A	N/A	N/A	N/A	N/A	N/A	N/A	N/A	N/A	N/A	11.190329	0.017620684
Polyol transporter 5;PLT5;ortholog	Q8VZB0	AT3G18830	MSTRG.3751.1	Sobic.001G469500	N/A	N/A	N/A	N/A	-1.778607835	9.76553E-05	N/A	N/A	N/A	N/A	N/A	N/A	N/A	N/A
			MSTRG.3751.3	Sobic.001G469600	N/A	N/A	N/A	N/A	N/A	N/A	N/A	N/A	N/A	N/A	-1.0911235	3.54272E-08	N/A	N/A
			MSTRG.18244.1	Sobic.002G353900	N/A	N/A	N/A	N/A	-4.546096391	0.033213824	N/A	N/A	N/A	N/A	N/A	N/A	N/A	N/A
			MSTRG.19078.1	Sobic.001G434900	N/A	N/A	N/A	N/A	N/A	N/A	N/A	N/A	-1.14684	0.017891763	N/A	N/A	N/A	N/A
			MSTRG.7154.1	Sobic.005G196300	N/A	N/A	N/A	N/A	N/A	N/A	N/A	N/A	N/A	N/A	6.07306018	0.002010773	N/A	N/A
			MSTRG.7155.1	Sobic.005G196300	N/A	N/A	N/A	N/A	N/A	N/A	N/A	N/A	N/A	N/A	5.713551 18	0.007243121	3.958557	0.021745336
			MSTRG.28209.1	Sobic.008G111100	N/A	N/A	N/A	N/A	N/A	N/A	N/A	N/A	N/A	N/A	2.02743987	0.002611908	2.3557404	0.015954789
Senescence																		
Gene Description	**Uniprot ID**	**TAIR ID**	**Transcript ID**	**Sorghum ID**	**HI10 - 10 dS/m - log2FoldChange**	**HI10 - 10 dS/m - padj**	**HI10 - 30 dS/m - log2FoldChange**	**HI10 - 30 dS/m - padj**	**Spence - 10 dS/m - log2FoldChange**	**Spence - 10 dS/m - padj**	**Spence - 30 dS/m - log2FoldChange**	**Spence - 30 dS/m - padj**	**0 dS/m**	**0 dS/m - padj**	**10 dS/m**	**10 dS/m - padj**	**30 dS/m**	**30 dS/m - padj**
Bidirectional sugar transporter SWEET15 (AtSWEET15) (Protein SUGARS WILL EVENTUALLY BE EXPORTED TRANSPORT	Q9FY94	AT5G13170	MSTRG.10056.1	Sobic.004G157100	N/A	N/A	2.365290623	9.2796E-101	1.42003391	1.47554E-12	2.436622908	6.07304E-50	N/A	N/A	N/A	N/A	N/A	N/A
Senescence-specific cysteine protease SAG12 (EC 3.4.22.-) (Cysteine proteinase SAG12) (Protein SENESCENCE-ASSOCIATE	Q9FJ47	AT5G45890	MSTRG.12419.1	Sobic.001G086800	N/A	-4.17803068	3.533566-71	-2.580504332	1.42284E-45	-3.199785297	4.58590-36	N/A	N/A	2.04304238	0.008617801	-1.0453355	2.19231E-07
			MSTRG.16932.1	Sobic.003G195800	N/A	N/A	N/A	N/A	N/A	N/A	N/A	-8.72192	4.66854E-09	N/A	N/A	N/A	N/A	N/A
			MSTRG.23980.1	Sobic.002G195800	N/A	N/A	N/A	N/A	N/A	N/A	N/A	N/A	-2.10357	0.000380972	N/A	N/A	N/A	N/A
			MSTRG.12490.1	Sobic.004G038400	N/A	N/A	N/A	N/A	N/A	N/A	N/A	N/A	N/A	N/A	1.64436105	0.010461141	N/A	N/A
			MSTRG.29360.1	Sobic.006G022800	N/A	N/A	N/A	N/A	N/A	N/A	N/A	N/A	N/A	N/A	-8.6811444	1.28087E-11	-9.0474538	6.19047E-11
			MSTRG.18322.1	Sobic.002G252700	N/A	N/A	N/A	N/A	N/A	N/A	N/A	N/A	N/A	N/A	N/A	N/A	3.2986782	1.988E-10
Nitrate reductase [NADH] 1 (NR1) (EC 1.7.1.1)	P11832	AT1G77760	MSTRG.19479.1	Sobic.007G153900	N/A	-1.124600335	1.04978E-19	-1.866301241	2.75849E-05	-1.919744654	1.46403E-32	N/A	N/A	1.68636061	0.018998823	1.2074209	2.00064E-38
			MSTRG.19476.1	Sobic.007G153900	N/A	N/A	N/A	-1.995165627	0.011566647	N/A	N/A	N/A	N/A	N/A	N/A	N/A	N/A	N/A
			MSTRG.19478.1	Sobic.007G153900	N/A	N/A	N/A	-1.643726494	0.000823311	N/A	N/A	N/A	N/A	N/A	-5.918457	0.003189241	-6.5975857	0.000192824
			MSTRG.9869.1	Sobic.004G179700	N/A	N/A	N/A	N/A	N/A	N/A	N/A	N/A	1.318555	3.29413E-13	N/A	N/A	N/A	N/A

Supplementary Table 4.5. Raw data for transcription factor network analysis for DE genes in 'HI10' and 'Spence' at 10 dS/m and 30 dS/m All statistically significant (FDR<0.05) results for transcription factors targeting 5 or more genes in each comparison are shown. Raw list of protein-DNA hits is excluded. Samples are ordered by number of genes with experimentally binding.

HI10 0-10 dS/m

Regulator	Symbol	# of Coexpressed Input Genes	# of Input Genes with Experimentally Verified Binding Site (Protein-DNA, PD)	PWM_num	PWM_source	PWM_name	rank	p-value	q-value	#hits
AT5G65310	ATHB5	2	117	PWM1430	CisBP	M2532_1.01	133	0.00181394782	0.02445418282	67
AT5G13790	AGL15	2	103	PWM1467	CisBP	M2211_1.01	70	0.00025656783	0.00657178383	71
AT5G13790	AGL15	2	103	PWM2148	JASPAR	MA0548.1	72	0.00025656783	0.00638923434	71
AT5G13790	AGL15	2	103	PWM3200	DAP-seq	AGL15_col	145	0.00181394782	0.02243038888	67
AT1G24260	AGL9	0	83	PWM2163	JASPAR	MA0563.1	114	0.00114071176	0.01794117676	68
AT1G24260	AGL9	0	83	PWM983	CisBP	M2226_1.01	124	0.00114071176	0.01649430707	68
AT3G54340	AP3	4	58	PWM833	CisBP	M2219_1.01	65	0.00015094545	0.00416375757	72
AT3G54340	AP3	4	58	PWM2156	JASPAR	MA0556.1	80	0.00042896262	0.00961411	70
AT5G20240	PI	8	50	PWM1000	CisBP	M2222_1.01	10	3.10E-07	5.55842E-05	82
AT5G20240	PI	8	50	PWM2159	JASPAR	MA0559.1	21	2.34161E-06	0.00019992979	79
AT2G36270	ABI5	2	40	PWM719	AthaMAP	T04543	189	0.00435964	0.04135891212	65
AT2G46830	AtCCA1	21	22	PWM44	AGRIS		32	1.5367E-05	0.00086103	76

AT2G46830	AtCCA1	21	22	PWM171	AGRIS		135	0.0018139 47	0.0240918 98	67
AT2G45660	AGL20	9	21	PWM2154	JASPAR	MA0554.1	59	0.0001509 45	0.0045871 9	72
AT2G45660	AGL20	9	21	PWM98	AthaMAP		194	0.0043596 4	0.0402929 61	65
AT1G77080	AGL27	2	11	PWM1181	CisBP	M2221_1.01	128	0.0018139 47	0.0254094 24	67

HI10 0-10 dS/m

Regulator	Symbol	# of Coexpressed Input Genes	# of Input Genes with Experimentally Verified Binding Site (Protein-DNA, PD)	PWM_num	PWM_source	PWM_name	rank	p-value	q-value	#hits
AT5G65310	ATHB5	2	117	PWM1430	CisBP	M2532_1.01	133	0.0018139 47	0.0244541 82	67
AT5G13790	AGL15	2	103	PWM1467	CisBP	M2211_1.01	70	0.0002565 67	0.0065717 83	71
AT5G13790	AGL15	2	103	PWM2148	JASPAR	MA0548.1	72	0.0002565 67	0.0063892 34	71
AT5G13790	AGL15	2	103	PWM3200	DAP-seq	AGL15_col	145	0.0018139 47	0.0224303 88	67
AT1G24260	AGL9	0	83	PWM2163	JASPAR	MA0563.1	114	0.0011407 11	0.0179411 76	68
AT1G24260	AGL9	0	83	PWM983	CisBP	M2226_1.01	124	0.0011407 11	0.0164943 07	68
AT3G54340	AP3	4	58	PWM833	CisBP	M2219_1.01	65	0.0001509 45	0.0041637 57	72
AT3G54340	AP3	4	58	PWM2156	JASPAR	MA0556.1	80	0.0004289 62	0.0096141 1	70
AT5G20240	PI	8	50	PWM1000	CisBP	M2222_1.01	10	3.10E-07	5.55842E-05	82
AT5G20240	PI	8	50	PWM2159	JASPAR	MA0559.1	21	2.34161E-06	0.0001999 29	79
AT2G36270	ABI5	2	40	PWM719	AthaMAP	T04543	189	0.0043596 4	0.0413589 12	65
AT2G46830	AtCCA1	21	22	PWM44	AGRIS		32	1.5367E-05	0.0008610 3	76

AT2G46830	AtCCA1	21	22	PWM171	AGRIS		135	0.001813947	0.02409181898	67
AT2G45660	AGL20	9	21	PWM2154	JASPAR	MA0554.1	59	0.000150945	0.0045871 9	72
AT2G45660	AGL20	9	21	PWM98	AthaMAP		194	0.004359 64	0.040 2929 61	65
AT1G77080	AGL27	2	11	PWM1181	CisBP	M2221_1.01	128	0.001813947	0.025 4094 24	67

Spence 0-10 dS/m

Regulator	Symbol	# of Coexpressed Input Genes	# of Input Genes with Experimentally Verified Binding Site (Protein-DNA, PD)	PWM_num	PWM_source	PWM_name	rank	p-value	q-value	#hits
AT2G46270	GBF3	9	360	PWM951	CisBP	M0260_1.01	13	2.51E-07	3.46128E-05	139
AT2G46270	GBF3	9	360	PWM2930	DAP-seq	GBF3_col	47	1.2642E-05	0.000482277	131
AT4G01120	ATBZIP54	15	277	PWM1232	CisBP	M0262_1.01	40	7.9933E-06	0.000358 3	132
AT5G04760	AT5G047600	10	273	PWM820	CisBP	M1238_1.01	266	0.002930 46	0.019753063	117
AT4G34000	ABF3	24	272	PWM954	CisBP	M0263_1.01	85	4.7345E-05	0.000998 7	128
AT4G34000	ABF3	24	272	PWM2529	JASPAR	MA0930.1	122	0.000163197	0.002398463	125
AT2G22430	ATHB6	10	253	PWM3154	DAP-seq	ATHB6_col	300	0.004028969	0.024079805	116
AT5G65310	ATHB5	2	248	PWM3138	DAP-seq	ATHB5_col	384	0.007400441	0.034554663	114
AT5G13790	AGL15	0	223	PWM3200	DAP-seq	AGL15_col	133	0.000241984	0.003262235	124

AT5G13790	AGL15	0	223	PWM2148	JASPAR	MA0548.1	284	0.004028969	0.025436414	116
AT5G13790	AGL15	0	223	PWM1467	CisBP	M2211_1.01	320	0.005486604	0.030742128	115
AT3G19290	ABF4	21	206	PWM746	AGRIS		31	1.91369E-06	0.000110685	135
AT3G19290	ABF4	21	206	PWM966	CisBP	M0253_1.01	137	0.000241984	0.003166987	124
AT4G37790	HAT22	10	196	PWM3160	DAP-seq	HAT22_col	145	0.000355469	0.004395554	123
AT5G67300	ATMYB44	13	179	PWM73	AthaMAP	T02559	205	0.001065023	0.009315059	120
AT2G36270	ABI5	21	126	PWM2530	JASPAR	MA0931.1	2	4.58328E-06	5.11E-09	146
AT2G36270	ABI5	21	126	PWM957	CisBP	M0257_1.01	4	1.28089E-05	2.86E-08	143
AT2G36270	ABI5	21	126	PWM621	AthaMAP	T04543	36	0.000154888	3.10985E-06	134
AT2G36270	ABI5	21	126	PWM2904	DAP-seq	ABI5_col	143	0.000355469	0.004457031	123
AT2G36270	ABI5	21	126	PWM589	AthaMAP	T04543	202	0.001065023	0.009453401	120
AT2G36270	ABI5	21	126	PWM719	AthaMAP	T04543	234	0.002111024	0.016177015	118
AT3G54340	AP3	5	116	PWM833	CisBP	M2219_1.01	346	0.005486604	0.028432026	115
AT3G54340	AP3	5	116	PWM2156	JASPAR	MA0556.1	368	0.007400441	0.036057004	114
AT1G22640	ATMYB3	12	96	PWM2634	JASPAR	MA1038.1	290	0.004028969	0.024910143	116
AT1G49720	ABF1	25	78	PWM974	CisBP	M0254_1.01	7	1.27665E-05	4.98E-08	142
AT1G49720	ABF1	25	78	PWM326	AGRIS		43	0.000333302	7.9933E-06	132

AT1G49720	ABF1	25	78	PWM1495	CisBP	M2233_1.01	87	7.21842E-05	0.001487658	127
AT1G49720	ABF1	25	78	PWM2170	JASPAR	MA0570.1	173	0.000745762	0.007729198	121
AT2G43010	AtPIF4	8	63	PWM818	CisBP	M2224_1.01	72	3.07683E-05	0.000766216	129
AT2G43010	AtPIF4	8	63	PWM2161	JASPAR	MA0561.1	106	0.000109042	0.001844452	126
AT2G46830	AtCCA1	54	54	PWM1555	PBM		120	0.000163197	0.002438437	125
AT2G46830	AtCCA1	54	54	PWM2571	JASPAR	MA0972.1	123	0.000163197	0.002378963	125
AT5G61850	LFY	1	54	PWM806	AthaMAP		391	0.007400441	0.033936038	114
AT1G69120	AGL7	3	48	PWM671	AGRIS		150	0.000355469	0.004249036	123
AT1G69120	AGL7	3	48	PWM2539	JASPAR	MA0940.1	369	0.007400441	0.035959325	114
AT2G45660	AGL20	27	47	PWM2154	JASPAR	MA0554.1	367	0.007400441	0.036155288	114
AT5G07310	ERF115	28	38	PWM1285	CisBP	M0036_1.01	273	0.004028969	0.026461324	116
AT1G77080	AGL27	2	30	PWM2609	JASPAR	MA1012.1	370	0.007400441	0.035862137	114
AT1G09530	PAP3	16	26	PWM1019	CisBP	M2223_1.01	44	1.2642E-05	0.000515116	131
AT1G09530	PAP3	16	26	PWM2160	JASPAR	MA0560.1	105	0.000109042	0.001862018	126
AT1G09530	PAP3	16	26	PWM829	AthaMAP	T04492	135	0.000241984	0.003213906	124
AT1G09530	PAP3	16	26	PWM1305	CisBP	M2733_1.01	209	0.001506637	0.012925036	119
AT1G09530	PAP3	16	26	PWM962	AthaMAP	T04492	269	0.002930046	0.019532769	117
AT1G09530	PAP3	16	26	PWM1609	PBM		283	0.004028969	0.025526295	116

AT1G09530	PAP3	16	26	PWM841	CisBP	M2732_1.01	347	0.005486604	0.028350089	115
AT3G20770	AtEIN3	1	26	PWM264	AthaMAP		373	0.007400441	0.035573702	114
AT3G20770	AtEIN3	1	26	PWM824	CisBP	M0606_1.01	392	0.007400441	0.033849466	114
AT3G59060	PIF5	38	19	PWM2162	JASPAR	MA0562.1	172	0.000745762	0.007774135	121
AT3G59060	PIF5	38	19	PWM904	CisBP	M2225_1.01	206	0.001065023	0.009269084	120
AT1G19350	BES1	20	7	PWM2149	JASPAR	MA0549.1	69	3.07683E-05	0.000799529	129
AT1G19350	BES1	20	7	PWM1485	CisBP	M2212_1.01	77	4.7345E-05	0.001102461	128
AT5G10140	AGL25	21	6	PWM510	AthaMAP		148	0.000355469	0.004306455	123
AT5G10140	AGL25	21	6	PWM3204	DAP-seq	AGL25_col	183	0.000745762	0.007306837	121
AT5G10140	AGL25	21	6	PWM2158	JASPAR	MA0558.1	285	0.004028969	0.025347163	116
AT5G10140	AGL25	21	6	PWM50	AthaMAP		390	0.007400441	0.034023053	114

Spence 0-30 dS/m

Regulator	Symbol	# of Coexpressed Input Genes	# of Input Genes with Experimentally Verified Binding Site (Protein-DNA, PD)	PWM_num	PWM_source	PWM_name	rank	p-value	q-value	#hits
AT2G46270	GBF3	8	552	PWM2930	DAP-seq	GBF3_col	51	2.21E-08	7.76E-07	189
AT2G46270	GBF3	8	552	PWM951	CisBP	M0260_1.01	284	0.000139775	0.000882454	168
AT4G01120	ATBZI	23	439	PWM1232	CisBP	M0262_1.01	416	0.001320686	0.005692286	161

	P54									
AT4G01120	ATBZIP54	23	439	PWM1233	CisBP	M0262_1.01	480	0.002355255	0.008797 86	159
AT4G34000	ABF3	32	406	PWM954	CisBP	M0263_1.01	154	4.72826E-06	5.50504E-05	177
AT4G34000	ABF3	32	406	PWM2529	JASPAR	MA0930.1	158	7.07951E-06	8.0339E-05	176
AT5G65310	ATHB5	6	397	PWM3138	DAP-seq	ATHB5_col	215	3.32352E-05	0.000277166	172
AT5G65310	ATHB5	6	397	PWM1430	CisBP	M2532_1.01	491	0.002355255	0.008600 76	159
AT5G65310	ATHB5	6	397	PWM395	AGRIS		546	0.003112 14	0.010219902	158
AT5G65310	ATHB5	6	397	PWM1719	JASPAR	MA0110.2	601	0.005319701	0.015870589	156
AT2G22430	ATHB6	20	388	PWM3154	DAP-seq	ATHB6_col	320	0.000274969	0.001540685	166
AT5G13790	AGL15	4	355	PWM3200	DAP-seq	AGL15_col	109	8.79E-07	1.44638E-05	181
AT5G13790	AGL15	4	355	PWM1467	CisBP	M2211_1.01	106	8.79E-07	1.48732E-05	181
AT5G13790	AGL15	4	355	PWM2148	JASPAR	MA0548.1	138	3.13656E-06	4.07526E-05	178
AT5G13790	AGL15	4	355	PWM659	AGRIS		786	0.014276721	0.032567634	152
AT1G24260	AGL9	3	338	PWM983	CisBP	M2226_1.01	474	0.001769906	0.006695024	160
AT1G24260	AGL9	3	338	PWM2163	JASPAR	MA0563.1	530	0.003112 14	0.010528427	158

AT3G19290	ABF4	20	326	PWM746	AGRIS		90	3.64E-07	7.25574E-06	183
AT3G19290	ABF4	20	326	PWM966	CisBP	M0253_1.01	127	1.35257E-06	1.90957E-05	180
AT4G37790	HAT22	8	323	PWM3160	DAP-seq	HAT22_col	276	0.00013977	0.00090833	168
AT5G20240	PI	16	212	PWM2159	JASPAR	MA0559.1	63	9.24E-08	2.62861E-06	186
AT5G20240	PI	16	212	PWM1000	CisBP	M2222_1.01	137	3.13656E-06	4.10501E-05	178
AT2G36270	ABI5	27	196	PWM2530	JASPAR	MA0931.1	3	2.21E-12	1.32E-09	206
AT2G36270	ABI5	27	196	PWM957	CisBP	M0257_1.01	11	7.04E-11	1.15E-08	200
AT2G36270	ABI5	27	196	PWM2904	DAP-seq	ABI5_col	56	3.58E-08	1.14627E-06	188
AT2G36270	ABI5	27	196	PWM621	AthaMAP	T04543	86	2.32E-07	4.83825E-06	184
AT2G36270	ABI5	27	196	PWM607	AthaMAP	T04543	520	0.00023552	0.00081210	159
AT2G36270	ABI5	27	196	PWM589	AthaMAP	T04543	619	0.00053197	0.01054090	156
AT2G36270	ABI5	27	196	PWM719	AthaMAP	T04543	788	0.01042767	0.03024849	152
AT3G54340	AP3	13	178	PWM833	CisBP	M2219_1.01	125	1.35257E-06	1.94013E-05	180
AT3G54340	AP3	13	178	PWM2156	JASPAR	MA0556.1	130	2.06667E-06	2.85041E-05	179
AT1G22640	ATMYB3	17	172	PWM2634	JASPAR	MA1038.1	314	0.00027496	0.00157012	166
AT1G22640	ATMYB3	17	172	PWM1105	CisBP	M1221_1.01	412	0.00013206	0.00057475	161

AT1G22640	ATMYB3	17	172	PWM678	AGRIS		861	0.02241484	0.04667807	150
AT2G46680	ATHB7	37	165	PWM3156	DAP-seq	ATHB7_col	438	0.00132068	0.00540637	161
AT1G49720	ABF1	30	138	PWM974	CisBP	M0254_1.01	73	1.47E-07	3.6078E-06	185
AT1G49720	ABF1	30	138	PWM326	AGRIS		123	1.35257E-06	1.97167E-05	180
AT1G49720	ABF1	30	138	PWM1495	CisBP	M2233_1.01	424	0.00132068	0.00558488	161
AT1G49720	ABF1	30	138	PWM2170	JASPAR	MA0570.1	565	0.00408328	0.01295810	157
AT2G43010	APIF4	10	116	PWM2161	JASPAR	MA0561.1	8	2.28E-11	5.10E-09	202
AT2G43010	APIF4	10	116	PWM818	CisBP	M2224_1.01	13	1.23E-10	1.69E-08	199
AT5G61850	LFY	9	90	PWM806	AthaMAP		472	0.00176990	0.00672339	160
AT5G61850	LFY	9	90	PWM2189	JASPAR	MA0590.1	495	0.00235525	0.00853125	159
AT2G46830	ATCCA1	70	79	PWM1555	PBM		374	0.00071999	0.00345174	163
AT2G46830	ATCCA1	70	79	PWM2571	JASPAR	MA0972.1	497	0.00235525	0.00849627	159
AT5G07310	ERF115	37	75	PWM1285	CisBP	M0036_1.01	481	0.00235525	0.00877957	159
AT1G51140	AKS1	4	62	PWM1529	CisBP	M0226_1.01	801	0.01795285	0.04018532	151
AT2G45660	AGL20	36	56	PWM2154	JASPAR	MA0554.1	54	3.58E-08	1.18872E-06	188
AT1G09530	PAP3	16	40	PWM2160	JASPAR	MA0560.1	9	4.02E-11	8.00E-09	201
AT1G09530	PAP3	16	40	PWM1019	CisBP	M2223_1.01	5	2.28E-11	8.17E-09	202

AT1G09530	PAP3	16	40	PWM829	AthaMAP	T04492	25	6.23E-10	4.47E-08	196
AT1G09530	PAP3	16	40	PWM962	AthaMAP	T04492	92	3.64E-07	7.09801E-06	183
AT1G09530	PAP3	16	40	PWM841	CisBP	M2732_1.01	91	3.64E-07	7.17601E-06	183
AT1G09530	PAP3	16	40	PWM1305	CisBP	M2733_1.01	100	8.79E-07	1.57656E-05	181
AT1G09530	PAP3	16	40	PWM1609	PBM		118	1.35257E-06	2.05522E-05	180
AT1G77080	AGL27	1	39	PWM1181	CisBP	M2221_1.01	16	3.64E-10	4.08E-08	197
AT1G77080	AGL27	1	39	PWM2609	JASPAR	MA1012.1	64	9.24E-08	2.58753E-06	186
AT3G59060	PIF5	48	34	PWM904	CisBP	M2225_1.01	96	5.68E-07	1.06047E-05	182
AT3G59060	PIF5	48	34	PWM2162	JASPAR	MA0562.1	139	3.13656E-06	4.04594E-05	178
AT1G19350	BES1	23	14	PWM2149	JASPAR	MA0549.1	41	8.23E-09	3.60E-07	191
AT1G19350	BES1	23	14	PWM1485	CisBP	M2212_1.01	44	1.35E-08	5.51E-07	190
AT5G10140	AGL25	30	7	PWM2158	JASPAR	MA0558.1	10	7.04E-11	1.26E-08	200
AT5G10140	AGL25	30	7	PWM3204	DAP-seq	AGL25_col	47	1.35E-08	5.16E-07	190
AT5G10140	AGL25	30	7	PWM50	AthaMAP		743	0.011273534	0.027205176	153
AT5G54680	bHLH105	13	5	PWM1375	CisBP	M0166_1.01	269	0.000139775	0.000931662	168

Supplementary Table 4.6. The names, gene description, and Panther protein class for 68 genes co-bound by transcription factors DIV2, MYB44, and AGL7 in 'Spence' in the 0-10 dS/m comparison and 'HI10' in the 0-30 dS/m comparison.

Uniprot ID	TAIR ID	Gene Description	Panther Protein Class
Q8LD26	AT1G56220	Dormancy-associated protein homolog 3;At1g56220;ortholog	
Q9SQG2	AT3G04080	Apyrase 1;APY1;ortholog	
Q8RWR1	AT3G20810	Lysine-specific demethylase JMJ30;JMJ30;ortholog	
Q38872	AT2G17290	Calcium-dependent protein kinase 6;CPK6;ortholog	
Q9FJ47	AT5G45890	Senescence-specific cysteine protease SAG12;SAG12;ortholog	cysteine protease(PC00081)
Q9SUZ8	AT3G52060	At3g52060;F4F15.170;ortholog	
Q0WP01	AT1G22540	Protein NRT1/ PTR FAMILY 5.10;NPF5.10;ortholog	transporter(PC00227)
Q9FIX7	AT5G43630	Zinc knuckle (CCHC-type) family protein;TZP;ortholog	
F4J152	AT3G03560	Uncharacterized protein;At3g03560;ortholog	
O23212	AT4G36690	Splicing factor U2af large subunit A;U2AF65A;ortholog	
Q9C9W9	AT1G68050	Adagio protein 3;ADO3;ortholog	
Q9FN11	AT5G67420	LOB domain-containing protein 37;LBD37;ortholog	
Q9SU35	AT4G12470	pEARLI1-like lipid transfer protein 1;AZI1;ortholog	
Q9LV52	AT3G24520	Heat stress transcription factor C-1;HSFC1;ortholog	winged helix/forkhead transcription factor(PC00246)
Q9LW12	AT3G15670	Late embryogenesis abundant protein 29;LEA29;ortholog	
Q39100	AT5G46900	Bifunctional inhibitor/lipid-transfer protein/seed storage 2S albumin superfamily protein;extA;ortholog	
Q39204	AT1G32640	Transcription factor MYC2;MYC2;ortholog	
Q93VT9	AT1G14320	60S ribosomal protein L10-1;RPL10A;ortholog	ribosomal protein(PC00202)
P25860	AT3G09390	Metallothionein-like protein 2A;MT2A;ortholog	
Q96262	AT4G20260	Plasma membrane-associated cation-binding protein 1;PCAP1;ortholog	
Q93Z79	AT5G24910	Cytochrome P450 714A1;CYP714A1;ortholog	oxygenase(PC00177)
O82388	AT2G29670	At2g29670/T27A16.23;At2g29670;ortholog	
Q9FUS9	AT1G10360	Glutathione S-transferase U18;GSTU18;ortholog	

P92961	AT2G39890	Proline transporter 1;PROT1;ortholog	amino acid transporter(PC00046)
Q84WU2	AT3G11910	Ubiquitin carboxyl-terminal hydrolase 13;UBP13;ortholog	cysteine protease(PC00081)
Q93ZH7	AT5G03040	AT5g03040/F15A17_70;iqd2;ortholog	
A0A1P8BG25	AT5G20950	Glycosyl hydrolase family protein;At5g20950;ortholog	glucosidase(PC00108)
F4IF36	AT1G79350	Protein FORGETTER 1;FGT1;ortholog	helicase(PC00115);nuclease(PC00170)
Q8L836	AT1G14690	65-kDa microtubule-associated protein 7;MAP65-7;ortholog	non-motor microtubule binding protein(PC00166)
Q9FY94	AT5G13170	Bidirectional sugar transporter SWEET15;SWEET15;ortholog	
P19172	AT5G24090	Acidic endochitinase;CHIB1;ortholog	
Q9T074	AT4G37870	Phosphoenolpyruvate carboxykinase (ATP);PCKA;ortholog	lyase(PC00144)
Q94F39	AT3G29575	Ninja-family protein AFP3;AFP3;ortholog	
P10795	AT1G67090	Ribulose bisphosphate carboxylase small chain 1A, chloroplastic;RBCS-1A;ortholog	
Q8S9J6	AT5G10770	Aspartyl protease family protein At5g10770;At5g10770;ortholog	aspartic protease(PC00053)
Q8RWG2	AT3G17040	Protein high chlorophyll fluorescent 107;HCF107;ortholog	
Q9LJ45	AT3G21870	Cyclin-U1-1;CYCU1-1;ortholog	
P38605	AT2G07050	Cycloartenol synthase;CAS1;ortholog	
Q8W4J2	AT5G19010	Mitogen-activated protein kinase 16;MPK16;ortholog	non-receptor serine/threonine protein kinase(PC00167)
Q9LY31	AT3G60340	AT3G60340 protein;F27H5_130;ortholog	esterase(PC00097)
Q5EAF6	AT5G04010	Probable F-box protein At5g04010;NSFBx;ortholog	
Q67YC0	AT1G73010	Inorganic pyrophosphatase 1;PS2;ortholog	hydrolase(PC00121)
Q9S840	AT5G43270	Squamosa promoter-binding-like protein 2;SPL2;ortholog	
Q9FGL2	AT5G47450	Aquaporin TIP2-3;TIP2-3;ortholog	
Q9SZZ8	AT4G25700	Beta-carotene 3-hydroxylase 1, chloroplastic;BETA-OHASE 1;ortholog	
Q9SD85	AT5G07990	Flavonoid 3'-monooxygenase;CYP75B1;ortholog	oxygenase(PC00177)
Q8S8P4	AT2G38465	Expressed protein;At2g38465;ortholog	
Q94F16	AT3G05510	Phospholipid/glycerol acyltransferase family protein;At3g05510;ortholog	acyltransferase(PC00042)
Q8GRN0	AT1G74940	Cyclin-dependent kinase, putative (DUF581);At1g74940;ortholog	
Q9SIS3	AT2G01910	65-kDa microtubule-associated protein 6;MAP65-6;ortholog	non-motor microtubule binding protein(PC00166)

Q8H0S9	AT1G63770	Puromycin-sensitive aminopeptidase;MPA1;ortholog	
Q96282	AT5G49890	Chloride channel protein CLC-c;CLC-C;ortholog	
Q9FMF1	AT5G64380	AT5g64380/MSJ1_22;MSJ1.22;ortholog	carbohydrate phosphatase(PC00066)
Q9LS71	AT3G29240	AT3g29240/MXO21_9;At3g29240;ortholog	
Q9T0D3	AT4G11660	Heat stress transcription factor B-2b;HSFB2B;ortholog	winged helix/forkhead transcription factor(PC00246)
Q94AB2	AT3G58640	AT3g58640/F14P22_230;At3g58640;ortholog	
Q9SGA2	AT3G02040	Glycerophosphodiester phosphodiesterase GDPD1, chloroplastic;GDPD1;ortholog	phosphodiesterase(PC00185);phospholipase(PC00186)
Q9LZD0	AT5G03555	Purine-uracil permease NCS1;NCS1;ortholog	transporter(PC00227)
Q94C25	AT5G20050	Probable receptor-like protein kinase At5g20050;At5g20050;ortholog	
O22914	AT2G47400	Calvin cycle protein CP12-1, chloroplastic;CP12-1;ortholog	
P46032	AT2G02040	Protein NRT1/ PTR FAMILY 8.3;NPF8.3;ortholog	transporter(PC00227)
P54888	AT3G55610	Delta-1-pyrroline-5-carboxylate synthase B;P5CSB;ortholog	amino acid kinase(PC00045);dehydrogenase(PC00092)
Q9FY46	AT5G13550	Sulfate transporter 4.1, chloroplastic;SULTR4;1;ortholog	
P42777	AT1G03970	G-box-binding factor 4;GBF4;ortholog	basic leucine zipper transcription factor(PC00056)
Q9FKE6	AT5G45190	Cyclin-T1-5;CYCT1-5;ortholog	kinase activator(PC00138);mRNA processing factor(PC00147);transcription cofactor(PC00217)
Q38814	AT5G54770	Thiamine thiazole synthase, chloroplastic;THI1;ortholog	oxidoreductase(PC00176)
Q9SR22	AT3G09410	Pectin acetylesterase 5;PAE5;ortholog	
Q94AP0	AT4G04955	Allantoinase;ALN;ortholog	hydrolase(PC00121)

CHAPTER V

OVERAL CONCLUSIONS

Seashore paspalum has been studied as a turfgrass for decades, and its high salt tolerance has been heavily focused on. Mechanisms including osmolyte production, sodium exclusion, and ion homeostasis have been reported as vital for seashore paspalum to cope with salt stress [1-3]. However, these mechanisms have only been studied when treating seashore paspalum as a trimmed turf. To the best of our knowledge, its salt tolerance has never been studied without trimming vital photosynthetic tissue throughout experiments. By directly comparing salt tolerance in seashore paspalum with *Paspalum distichum*, a glycophytic sister species, our work in Chapters II-IV provides the groundwork to study this species pair as a model glycophyte-halophyte system. Collectively, our results provide a unique look into how seashore paspalum likely copes with high salinity in its natural habitat and suggests new and fascinating research paths to follow.

Chapter II

Our results in Chapter II illustrate that by utilizing node-grown, untrimmed seashore paspalum ramets, we can get novel insights into seashore paspalum's growth habit under salt stress. Importantly, though our growth methods significantly differ from established methods treating seashore paspalum as a trimmed turf, our results can be directly compared. Untrimmed growth averaged across replicated ramets per accession was significantly negatively correlated

with trimmed turf quality measurements, confirming that accessions that are slow-growing under freshwater or low salt when treated as ramets tended to have higher turf quality scores under high salt stress. Slow growth might be associated with an enhanced biosynthesis of proline, which is one of the dominant osmolytes in seashore paspalum [2]. We show that, in contrast to *P. distichum*, several seashore paspalum genotypes enhance growth under low salt stress, illustrative of typical halophytic behavior. This has also been observed in some accessions when treated as turf [4]. Finally, we show that seashore paspalum is highly tolerant of salt shock in our experimental conditions. Our suggested methodology of fast salt level augmentation increases the throughput with which seashore paspalum can be screened for salt tolerance. Furthermore, this chapter showed significant differences in growth and ion uptake/sequestration behavior between *P. vaginatum* accession 'HI10' and *P. distichum* accession 'Spence', which led us to further investigate these two species for leaf anatomy (Chapter III) and gene expression under freshwater, low salt (10 dS/m) and high salt (30 dS/m) (Chapter IV).

Future directions

Though our growth methods are rapid compared with traditional salt screens, comparisons of untrimmed growth and turf quality measures using a larger number of accessions grown under the same environmental conditions are required to confirm our findings. As we have only examined genotypic differences in proline accumulation in five accessions, it will also be fascinating to determine whether the plasticity seen for this trait in our study holds true in a higher number of seashore paspalum accessions. Consequently, screening a larger number of accessions via our rapid methods and measuring proline will provide further insight into the

coping mechanisms used by slow-growing and fast-growing seashore paspalum accessions under salt stress.

Chapter III

Our results in Chapter III illustrate that seashore paspalum utilizes leaf papillae atop costal ridges for sodium sequestration under salt stress. This is a novel mechanism of sequestration not previously reported in seashore paspalum nor in any grass species. Large papillae on the surface of seashore paspalum were first noted in 1974 by Ellis [5], who also observed differences in papilla size between *P. vaginatum* and *P. distichum*. However, their function has remained unknown for nearly 50 years. Though also not characterized in any other species to the best of our knowledge, our results are reminiscent of differences in costal ridge structure observed in *Spartina* species, in which freshwater species have much smaller ridges compared with those native to high salt habitats [6]. The increased boundary layer in saltwater species is thought to help prevent water loss from adaxial stomata, which in contrast to abaxial stomata, are the most active. Though stomata are also present on the adaxial surface in seashore paspalum in the intercostal grooves, more work is required to determine the utilization of stomata on adaxial and abaxial surfaces in seashore paspalum.

Furthermore, our study is the first to examine sodium distribution in the cells making up these costal ridges, and our results raise the possibility of storing sodium in enlarged epidermal cells atop costal ridges in grasses as a possible mechanism of salt tolerance. As the only other unicellular structures used for sodium sequestration in grasses are the unicellular hairs found in *Porteresia coarctata* [7], more work is required to see whether this mechanism is present in other salt tolerant grasses.

Future directions

The mechanism behind sodium-loading into unicellular structures has only been elucidated in dicots, where an HKT-1 type transporter is responsible for one-way sodium transport into unicellular epidermal bladder cells in quinoa [8]. The mechanism used for sodium transport into the unicellular, sodium-sequestering cells of *P. coarctata* is currently unknown, and these are the only other unicellular structures known to sequester sodium in grasses. Thus, we plan to examine cell type-specific patterns of sodium accumulation in seashore paspalum and other glycophytic grasses, which will be vital in determining whether unicellular epidermal cells act as sodium sinks in other species. Consequently, we will determine if simply enlarging these epidermal cells is a beneficial approach to enhancing salt tolerance, though our results illustrate that in addition to papilla size, sodium loading into papilla cells is likely an important determinant of sequestering ability. Additionally, cell type-specific transcriptomic work will determine the genetic mechanisms used for sodium loading into papillae. Considering the ease and utility of studying seashore paspalum as a model halophyte, studying the mechanisms of sodium-loading into papillae is an excellent approach to better understand sodium sequestration.

Chapter IV

Results in Chapter IV illustrate that the seashore paspalum accession ‘HI10’ constitutively utilizes many vital salt response regulators, as opposed to the *P. distichum* accession ‘Spence’, which induces these regulators under salt stress. We provide evidence for several pathways that are used by seashore paspalum accession ‘HI10’ to enhance growth under low salt stress not used by ‘Spence’. Furthermore, our results demonstrate that, while 10 dS/m salt represents a stress for ‘Spence’, this is not the case for ‘HI10’. Though some attempts have

been made to compare transcriptomic responses of halophytic grasses with glycophytic relatives [9], this has only been conducted in grasses belonging to different grass subfamilies. To the best of our knowledge, there are no transcriptomic studies directly comparing grass glycophyte-halophyte species pairs under salt stress. Thus, our results provide much needed insight into the genetic differences separating glycophytic and halophytic patterns of growth under salt stress. Our dataset will thus benefit the research community interested in improving salt tolerance in glycophytic grasses, which includes most cereal crops we rely on for food production.

Future directions

A more detailed examination of our RNA-seq dataset will provide insight into pathways that differ between seashore paspalum and *P. distichum*. Our results only represent transcriptomic responses to salt stress in above-ground tissue, and thus analyzing genotypic differences at the root level at the three salt concentrations tested will help further discern genetic differences between seashore paspalum and *P. distichum*. We have sequenced libraries from root tissue for all samples discussed in this chapter, and analysis of these samples is currently underway.

Major overall conclusions

Collectively, our results illustrate novel mechanisms of salt tolerance in seashore paspalum. Seashore paspalum's high tolerance stems from its ability to modulate growth rate and proline concentration under salt stress, sequester sodium in specialized papilla cells, and modify major regulators of sodium/potassium transport, osmolyte biosynthesis/transport, gibberellin homeostasis, and senescence under salt stress. Future work will focus on comparisons between

node-grown ramets and trimmed turf studies, an investigation into the mechanisms of sodium loading into papillae, and a more in-depth analysis of our RNA-seq dataset. Consequently, our results provide the foundation for studying seashore paspalum and *P. distichum* as a beneficial halophyte-glycophyte species pair, which will ultimately help improve salt sensitive glycophytic crop species.

References

1. Guo, H.L., et al., *Growth response and ion regulation of seashore paspalum accessions to increasing salinity.* Environmental and Experimental Botany, 2016. **131**: p. 137-145.
2. Lee, G., et al., *Synthesis of organic osmolytes and salt tolerance mechanisms in Paspalum vaginatum.* Environmental and Experimental Botany, 2008. **63**(1-3): p. 19-27.
3. Peacock, C.H. and A.E. Dudeck, *PHYSIOLOGICAL AND GROWTH-RESPONSES OF SEASHORE PASPALUM TO SALINITY.* Hortscience, 1985. **20**(1): p. 111-112.
4. Lee, G., R.R. Duncan, and R.N. Carrow, *Salinity tolerance of seashore paspalum ecotypes: Shoot growth responses and criteria.* Hortscience, 2004. **39**(5): p. 1138-1142.
5. Ellis, R.P., *Comparative leaf anatomy of Paspalum paspalodes and P. vaginatum.* Bothalia, 1974. **11**(3): p. 235-241.
6. Maricle, B.R., et al., *Diversity in leaf anatomy, and stomatal distribution and conductance, between salt marsh and freshwater species in the C-4 genus Spartina (Poaceae).* New Phytologist, 2009. **184**(1): p. 216-233.
7. Bal, A.R. and S.K. Dutt, *MECHANISM OF SALT TOLERANCE IN WILD-RICE (ORYZA-COARCTATA-ROXB).* Plant and Soil, 1986. **92**(3): p. 399-404.
8. Bohm, J., et al., *Understanding the Molecular Basis of Salt Sequestration in Epidermal Bladder Cells of Chenopodium quinoa.* Current Biology, 2018. **28**(19): p. 3075-+.
9. Yamamoto, N., et al., *Comprehensive analysis of transcriptome response to salinity stress in the halophytic turf grass Sporobolus virginicus.* Frontiers in Plant Science, 2015. **6**: p. 14.